Development of luminescent lanthanide-based supramolecular and interlocked architectures

Supplementary Information

Gabriela Sansom

Student ID: [redacted]

6. Supplementary Information

General Experimental

All chemicals used for synthesis were purchased from Sigma-Aldrich or Carbosynth. The glassware used for synthesis was washed with acetone, run through a laboratory glass washer and dried in an oven. For UV/Vis and photophysical measurements, HPLC grade solvents (MeOH or ACN) were used and the solutions were made using clean vials. UV/Vis characterisation measurements were carried out on Perkin Elmer Lambda 265 spectrophotometer. UV/Vis titrations were carried out on a Shimadzu UV-1800 spectrophotometer and data was processed using UVProbe. UV/Vis measurements were carried out using quartz cuvettes with a total volume of 3 mL and a path length of 1 cm. Melting point measurements were carried out using an Electrothermal IA9000 Series Melting Point Apparatus. Fourier transfer infrared (FTIR) spectra were collected using the Bruker ALPHA Platinum-ATR and processed using OPUS. All NMR spectra was collected from the Bruker Ultrashield 300 and data was processed using TopSpin 3.6.2. For all NMR analysis, deuterated solvents (either DMSO-d_6 or $CDCl_3$) were used. All NMR spectra were collected using the Bruker Ultrashield 300. NMR tubes were cleaned using acetone. All chemical shifts have been reported in parts per million (ppm) and are referenced according to a standard. NMR peaks are indicated as s (singlet), d (doublet), m (multiplet), br (broad) or quintet. High resolution mass spectrometry (HRMS) was performed on a ThermoFisher QExactive Focus coupled to an Ultimate™ 3000 RSLC. Solutions for HPLC were made using HPLC grade solvents (H_2O, MeOH or ACN). The HRMS for $\mathbf{R_2}$ – $\mathbf{R_4}$ was collected using a direct injection method (*i.e.* bypassing the RSLC) in positive mode whereas complexes were collected using direct injection in negative mode. Fluorescence excitation and emission spectra were collected using the Shimadzu RF-6000 Spectrofluorometer with a 340 nm UV filter whereas lifetime and phosphorescence data was collected using the Aligent Technologies Cary Eclipse spectrophotometer. All phosphorescence data was collected after a 0.2 ms time delay. 1931 2˚ CIE plots were generated using the ColorCalculator v7.77 software. For fluorescence measurements, all excitation slit widths were 3.0 nm however the emission slit widths ranged

from 1.0 to 5.0 nm, hence no comparisons regarding the emission intensities between different samples as well as the emission intensities between the same samples at different excitation wavelengths were made. For phosphorescence measurements, the excitation and emission slit widths were both either 5.0 nm or 10.0 nm. Single crystal X-ray data was collected at 150 K on a Bruker D8 QUEST ECO which contained a CuKα ($\lambda = 1.54178$) X-ray source. The structure was solved using direct methods in OLEX2 version 1.2.7.[283] Mercury 2020.3.0 was used to generate images of the crystallographic structures. For dialysis, the Pur-A-Lyzer™ Mega 1000 Dialysis Kit and the Pur-A-Lyzer™ Mega Floating Rack for Dialysis was purchased from Sigma-Aldrich.

Dimethyl 4-hydroxypyridine-2,6-dicarboxylate (1)

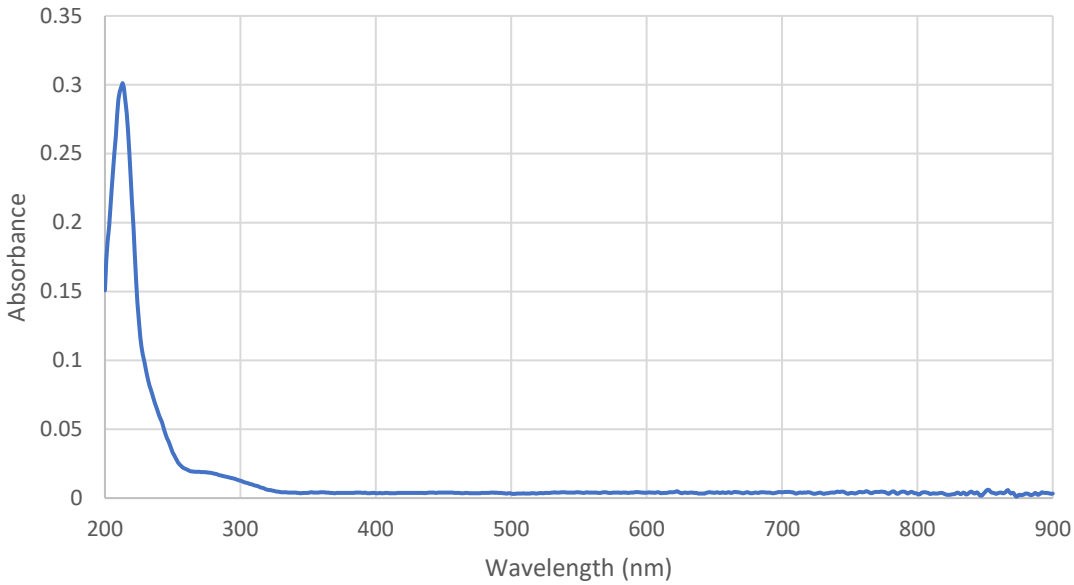

*Figure S1. UV/Vis spectrum of **1** (1 x 10^{-5} M) in MeOH*

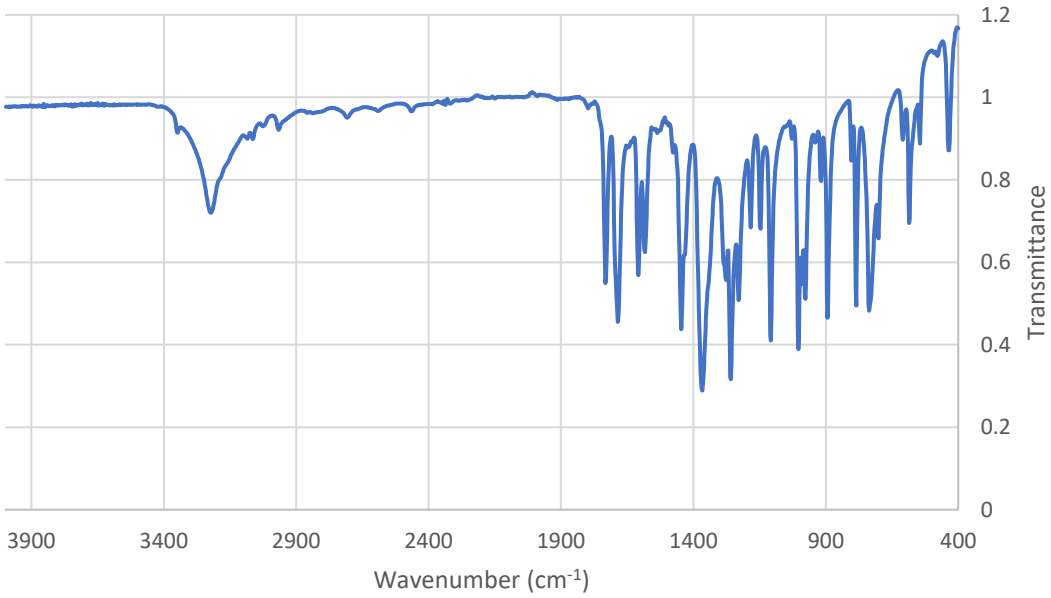

*Figure S2. FTIR spectrum of **1***

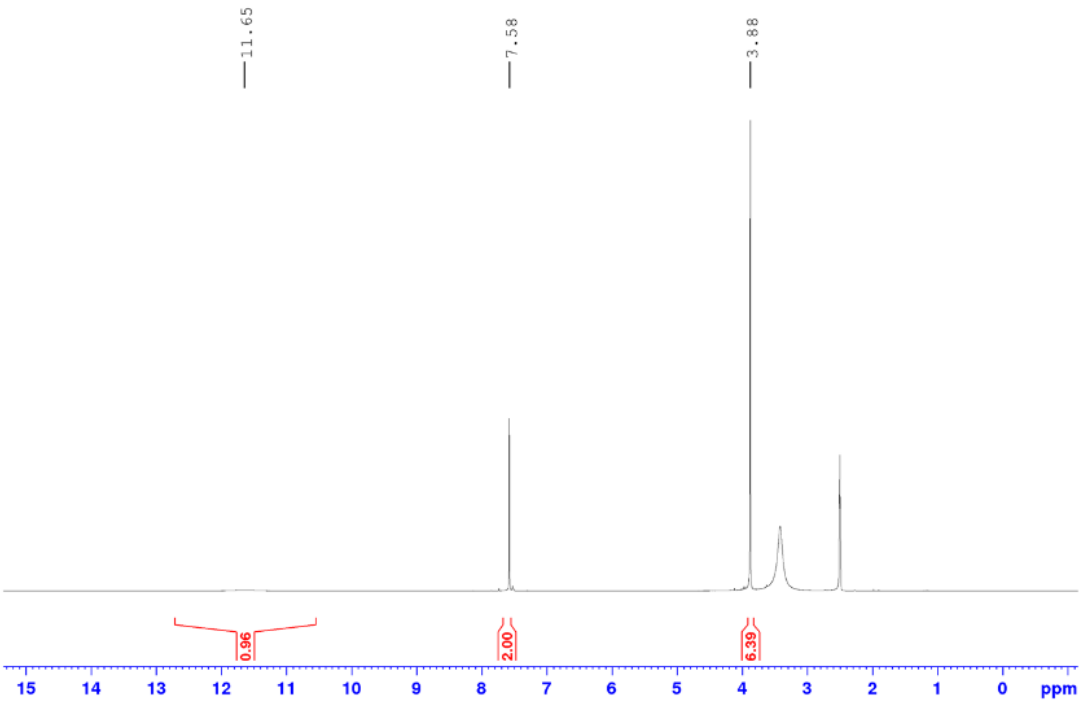

*Figure S3. ^{1}H NMR spectrum of **1** in DMSO-d_6*

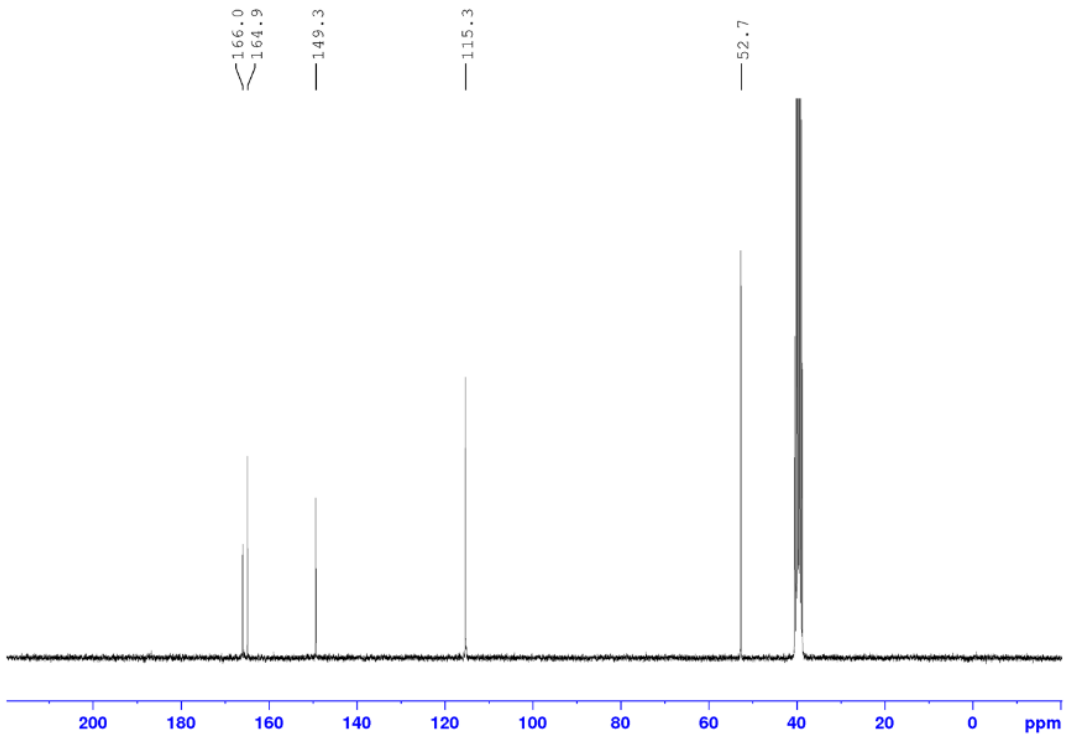

*Figure S4. ^{13}C NMR spectrum of **1** in DMSO-d_6*

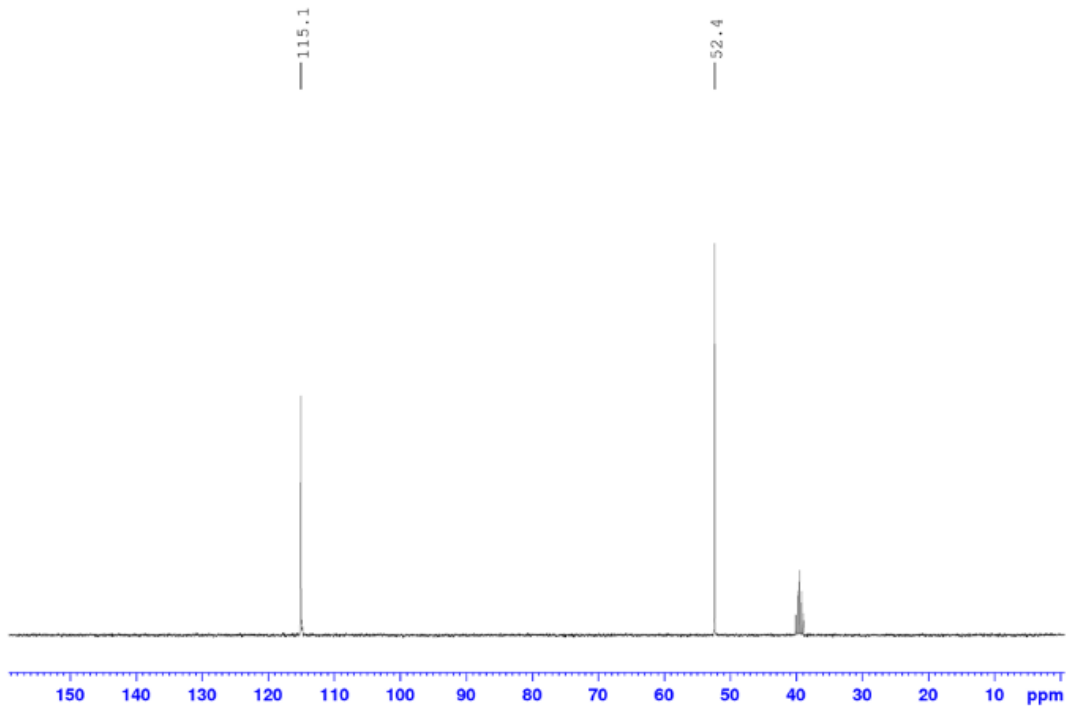

*Figure S5. ^{13}C DEPT spectrum of **1** in DMSO-d_6*

Dimethyl 4-[(prop-2-yn-1-yl)oxy]pyridine-2,6-dicarboxylate (2)

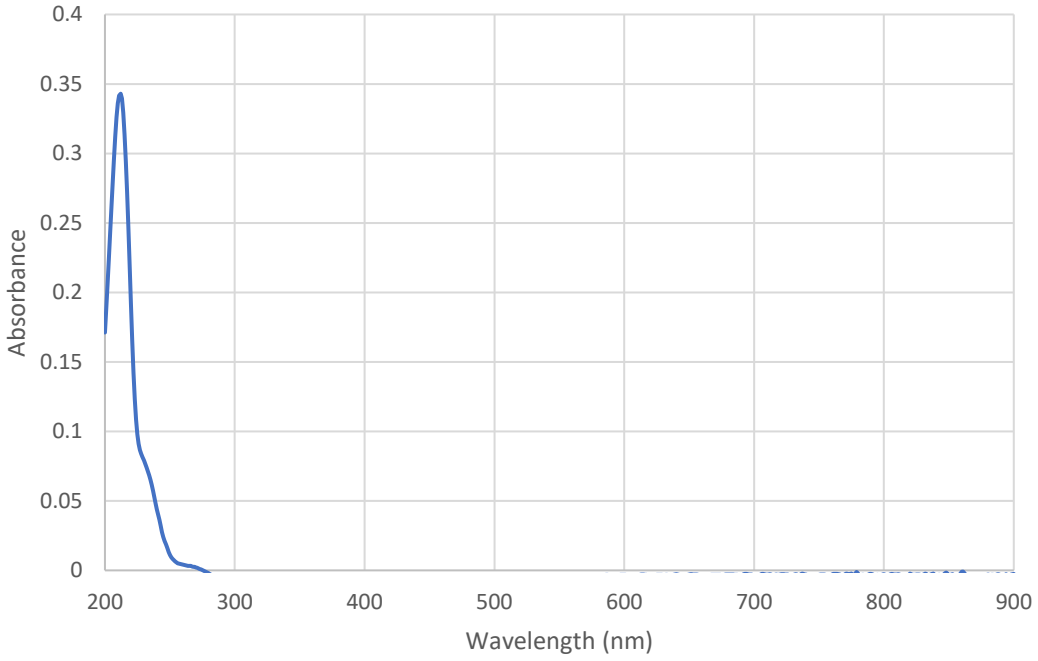

*Figure S6. UV/Vis spectrum of **2** (1 x 10^{-5} M) in ACN*

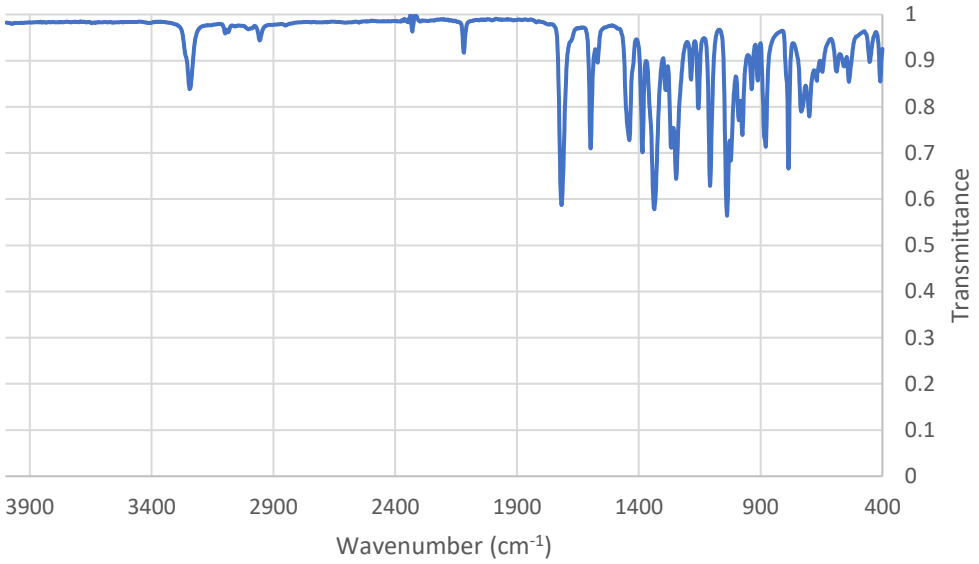

*Figure S7. FTIR spectrum of **2***

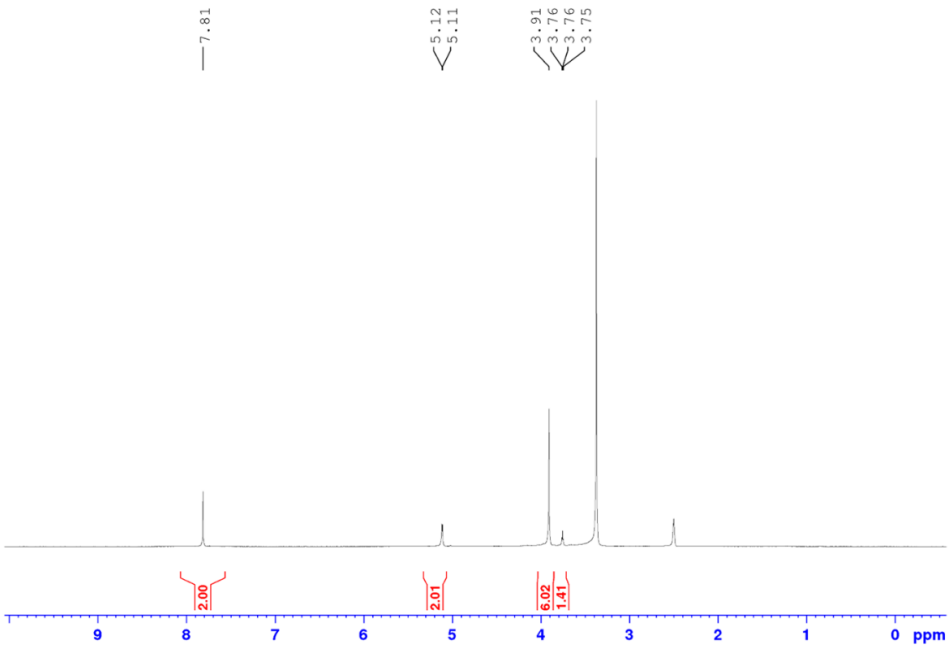

*Figure S8. ^{1}H NMR spectrum of **2** in DMSO-d_6*

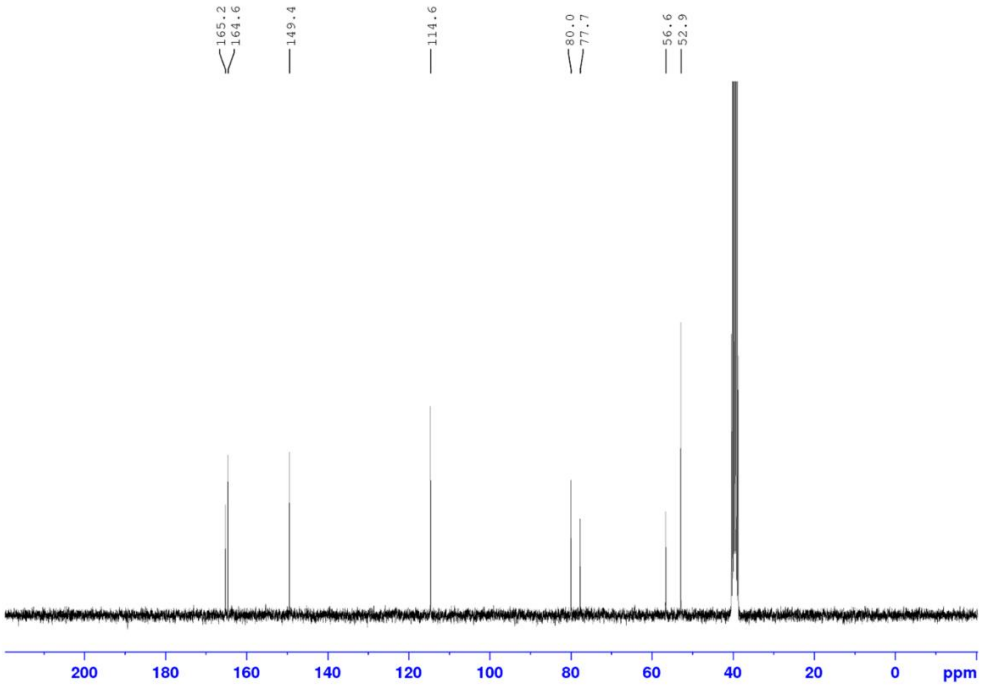

*Figure S9. ^{13}C NMR spectrum of **2** in DMSO-d_6*

4-[(prop-2-yn-1-yl)oxy]pyridine-2,6-dicarboxylic acid (L_1)

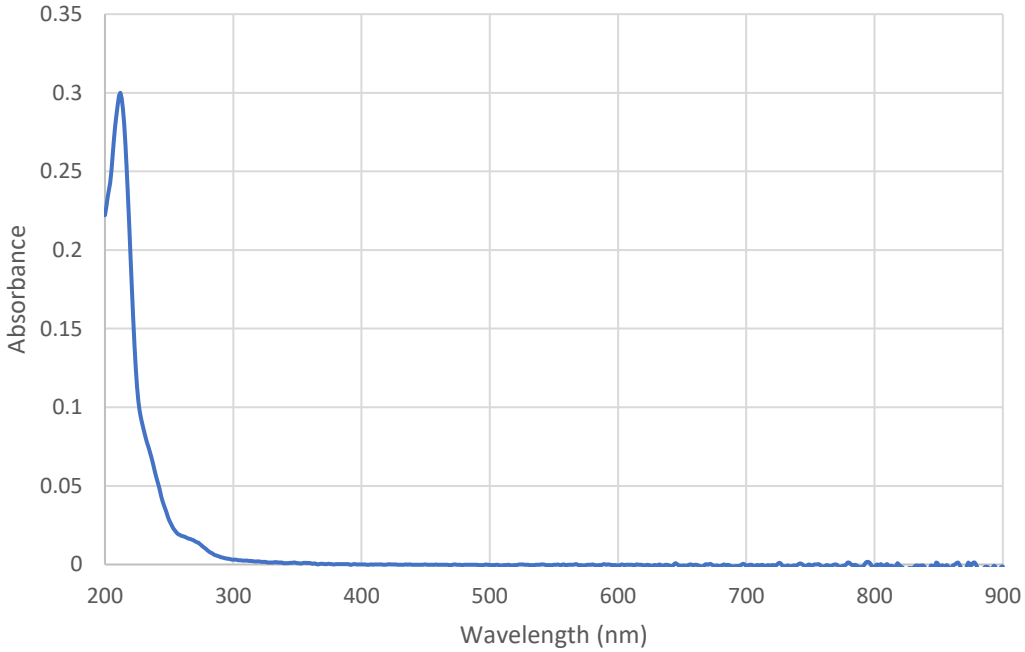

*Figure S10. UV/Vis spectrum of **L_1** (1 x 10^{-5}) in MeOH*

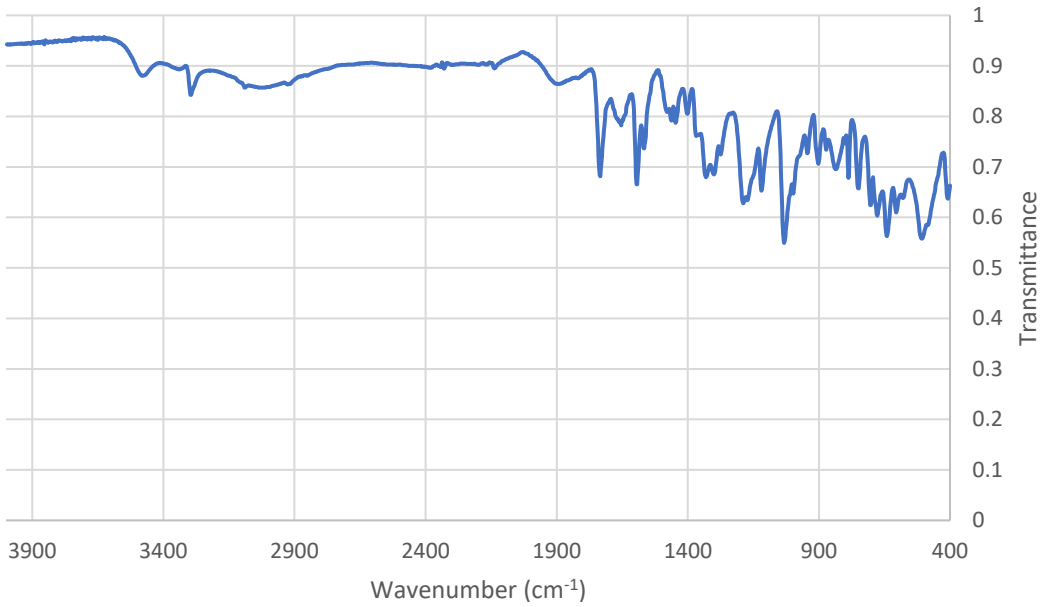

Figure S11. FTIR spectrum of $\boldsymbol{L_1}$

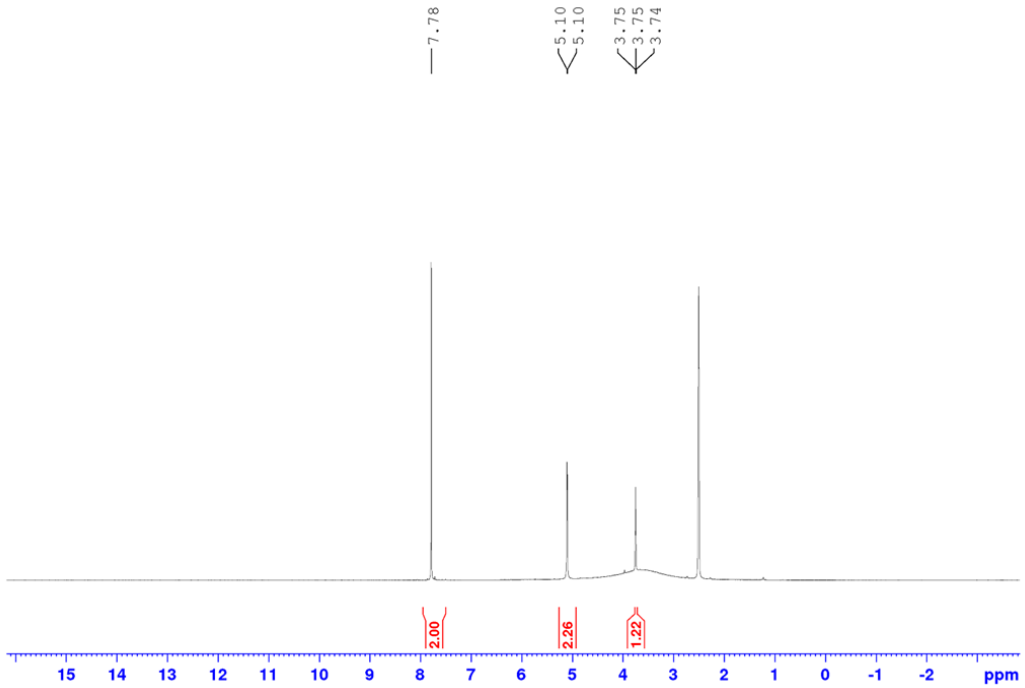

Figure S12. ^{1}*H NMR spectrum of* $\boldsymbol{L_1}$ *in DMSO-*d_6

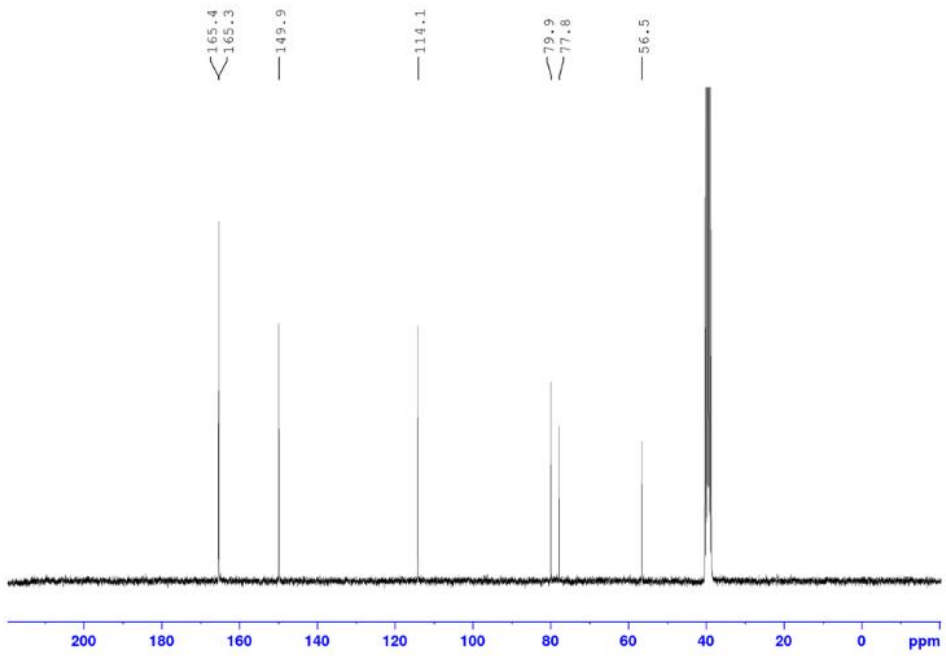

*Figure S13. ^{13}C NMR spectrum of **L₁** in DMSO-d_6*

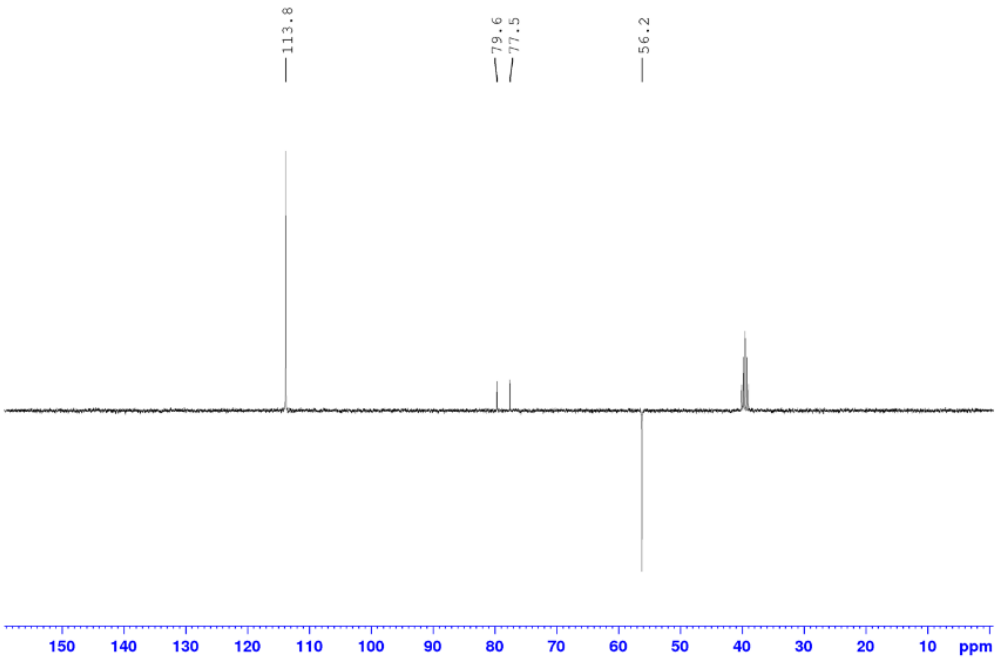

*Figure S14. ^{13}C DEPT spectrum of **L₁** in $DMSO_6$*

$[La(L_1)_3]^{3-}$

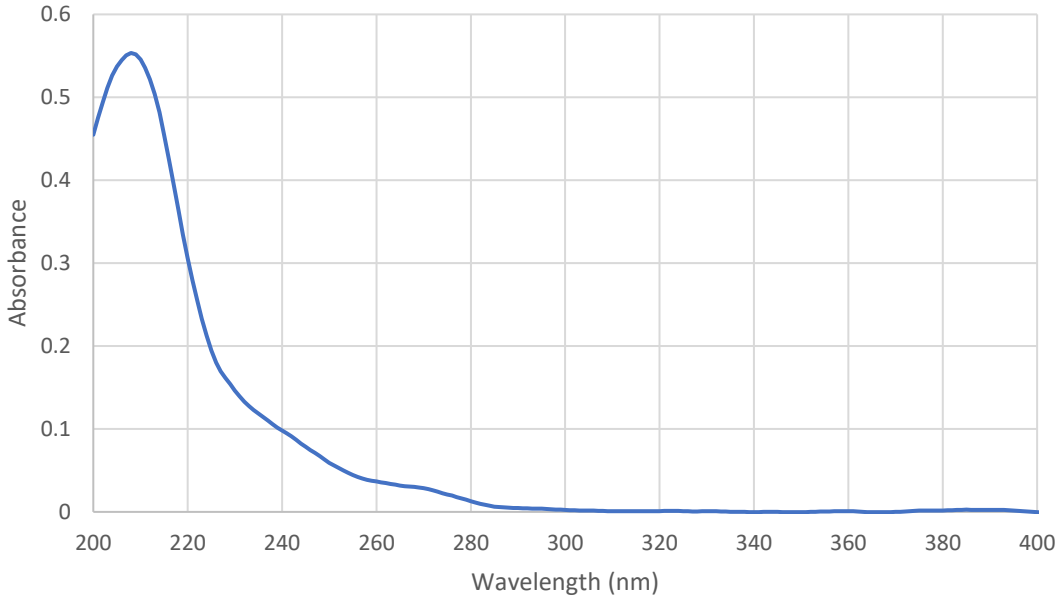

Figure S15. UV/Vis spectrum of ***$[La(L_1)_3]^{3-}$*** *(1 x 10^{-5}) in H_2O*

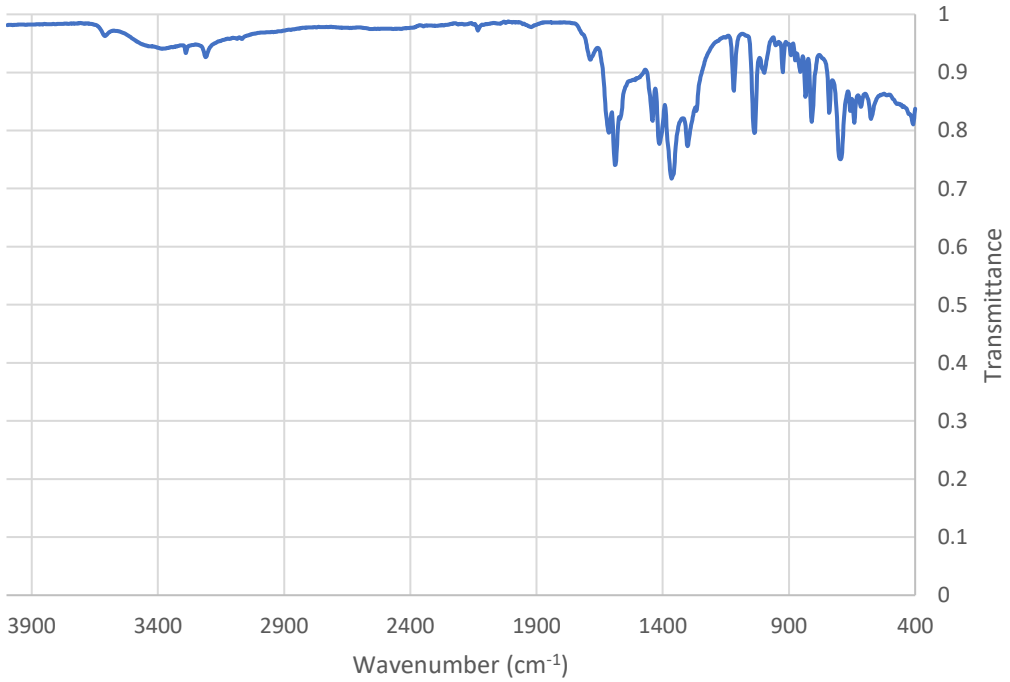

Figure S16. FTIR spectrum of ***$[La(L_1)_3]^{3-}$***

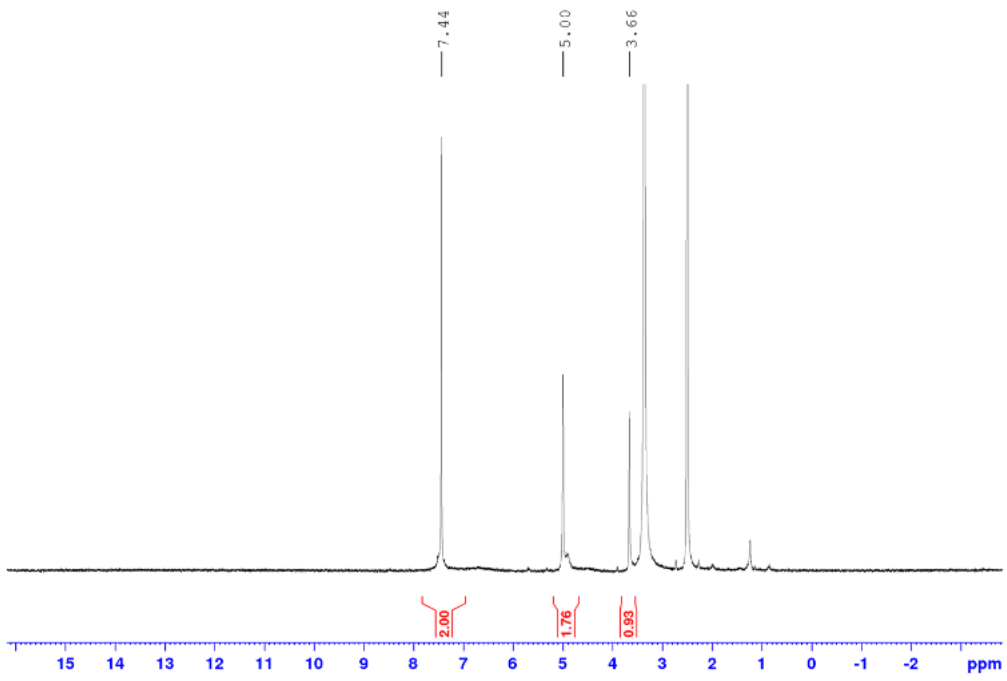

Figure S17. ^{1}H NMR spectrum of ***[La(L$_1$)$_3$]$^{3-}$*** *in DMSO-d$_6$*

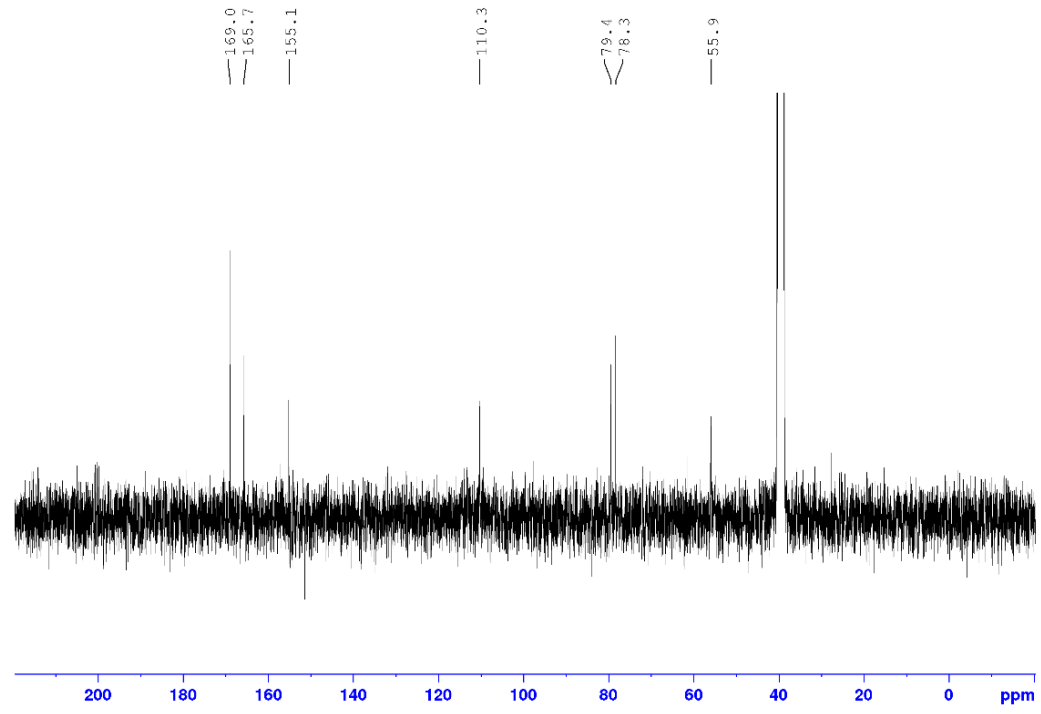

Figure S18. ^{13}C NMR spectrum of ***[La(L$_1$)$_3$]$^{3-}$*** *in DMSO-d$_6$*

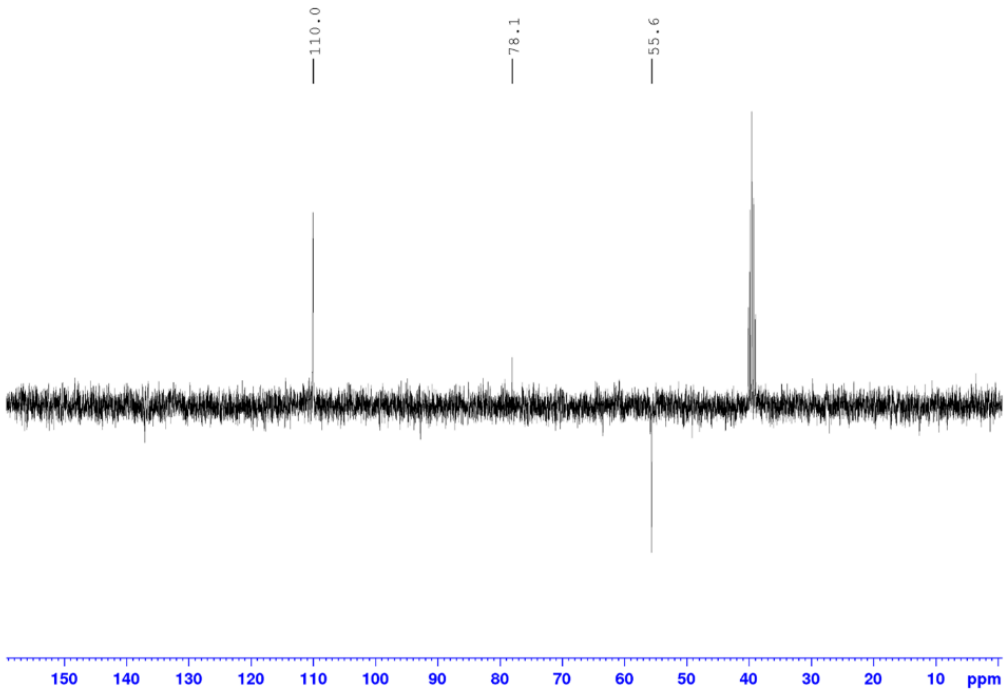

Figure S19. ^{13}C DEPT spectrum of ***$[La(L_1)_3]^{3-}$*** *in DMSO-d_6*

$[Eu(L_1)_3]^{3-}$

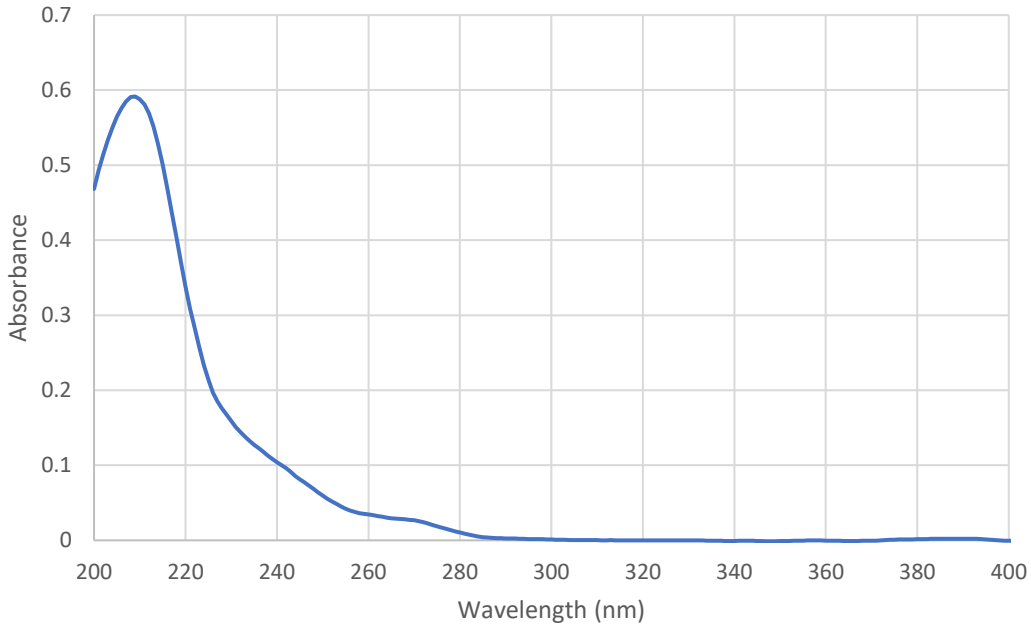

Figure S20. UV/Vis spectrum of ***$[Eu(L_1)_3]^{3-}$*** *(1 x 10^{-5} M) in H_2O*

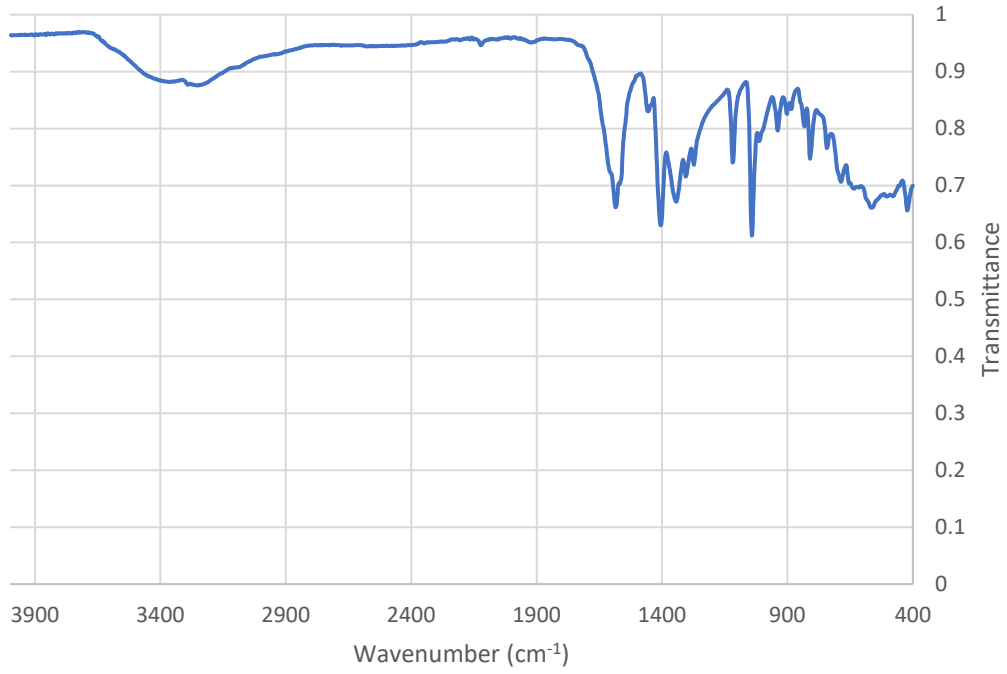

Figure S21. FTIR spectrum of ***[Eu(L$_1$)$_3$]$^{3-}$***

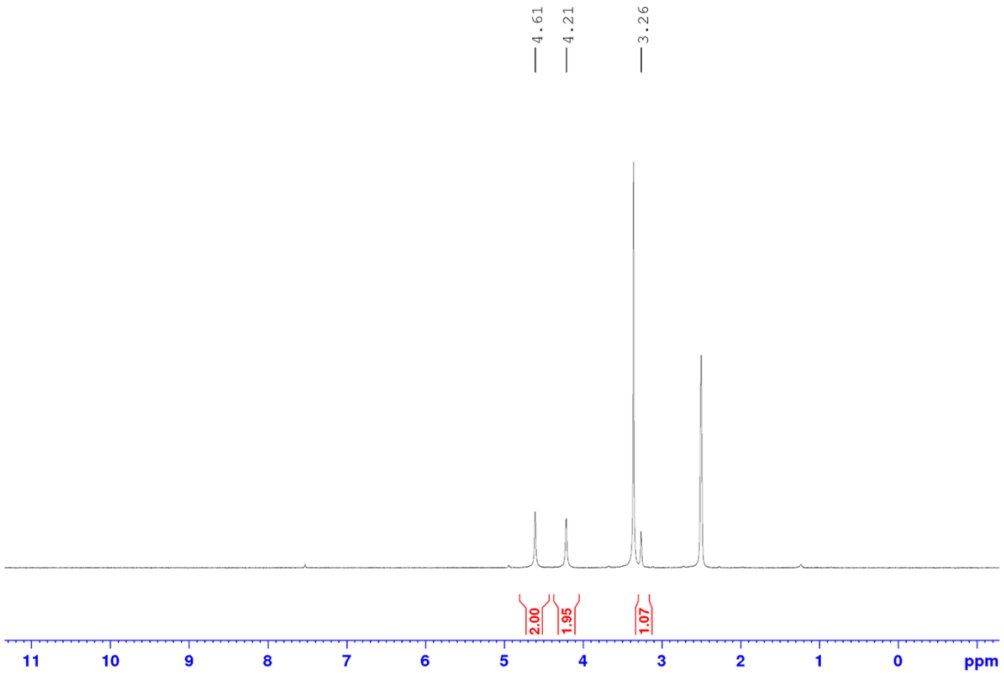

Figure S22. ^{1}H NMR spectrum of ***[Eu(L$_1$)$_3$]$^{3-}$*** *in DMSO-d$_6$*

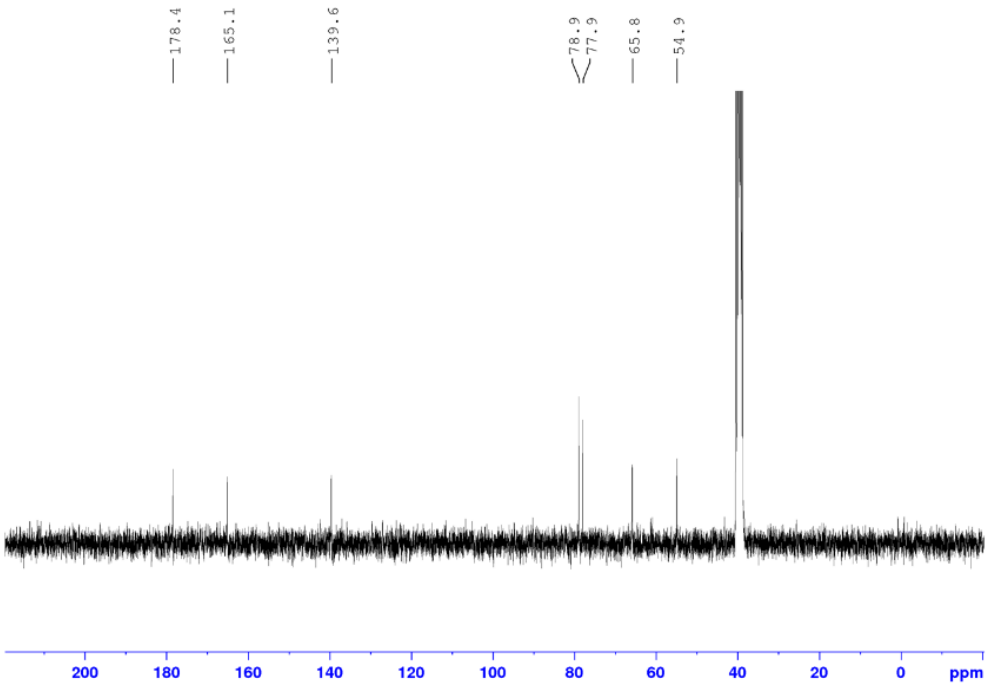

Figure S23. ^{13}C NMR spectrum of ***[Eu(L1)3]3-*** *in DMSO-d6*

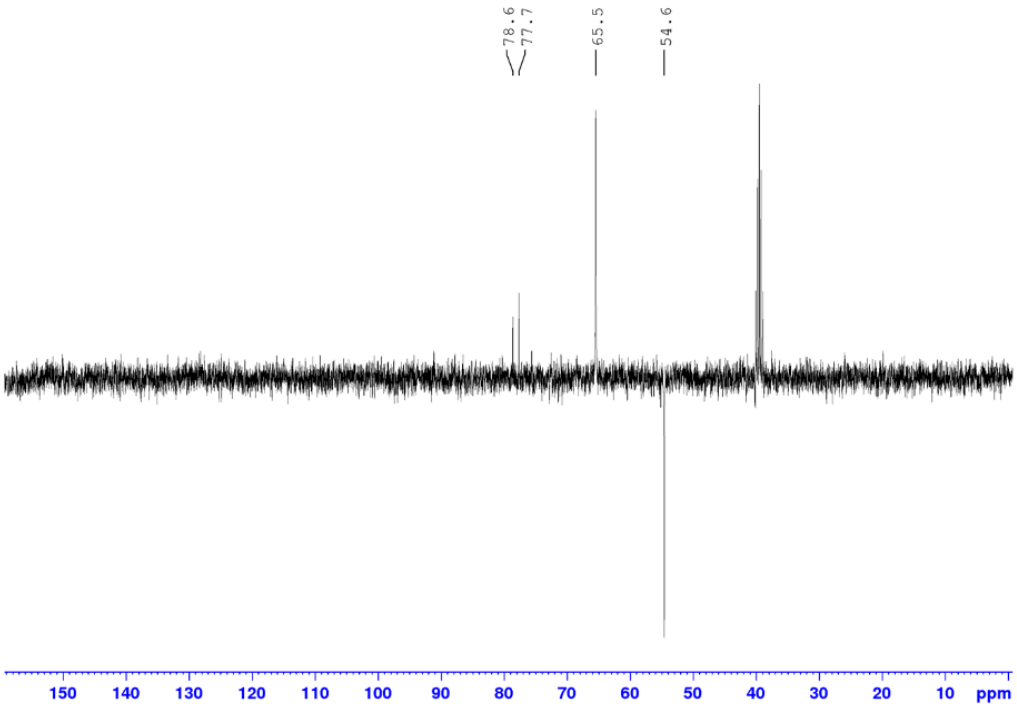

Figure S24. ^{13}C DEPT spectrum of ***[Eu(L1)3]3-*** *in DMSO-d6*

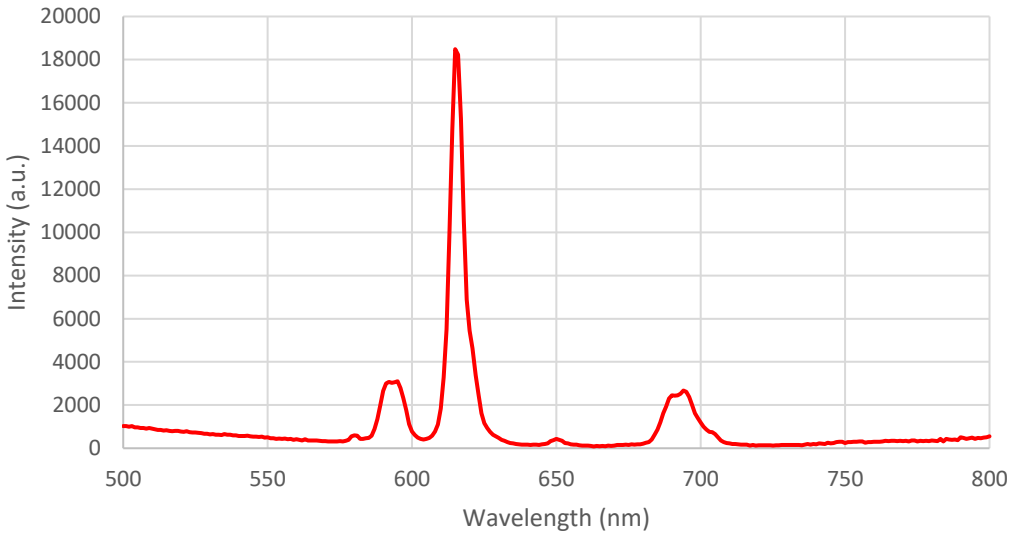

Figure S25. Fluorescence emission spectrum (λ_{ex} = 274 nm) of ***[Eu(L1)3]3-*** *(1 x 10^{-5} M) in H_2O*

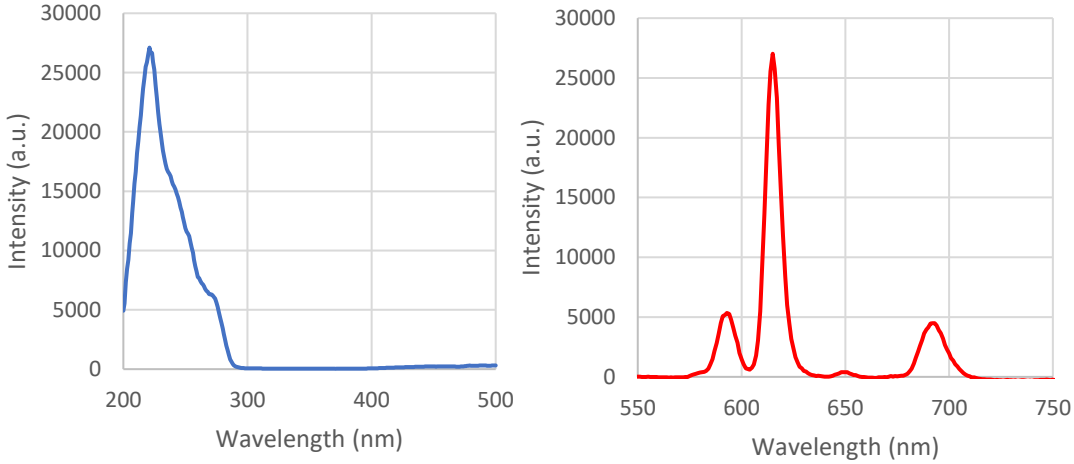

Figure S26. (Left) Fluorescence excitation spectrum (λ_{em} = 615 nm) of ***[Eu(L1)3]3-*** *(1 x 10^{-5} M) in H_2O. (Right) Fluorescence emission spectrum (λ_{ex} = 221 nm) of* ***[Eu(L1)3]3-*** *(1 x 10^{-5} M) in H_2O*

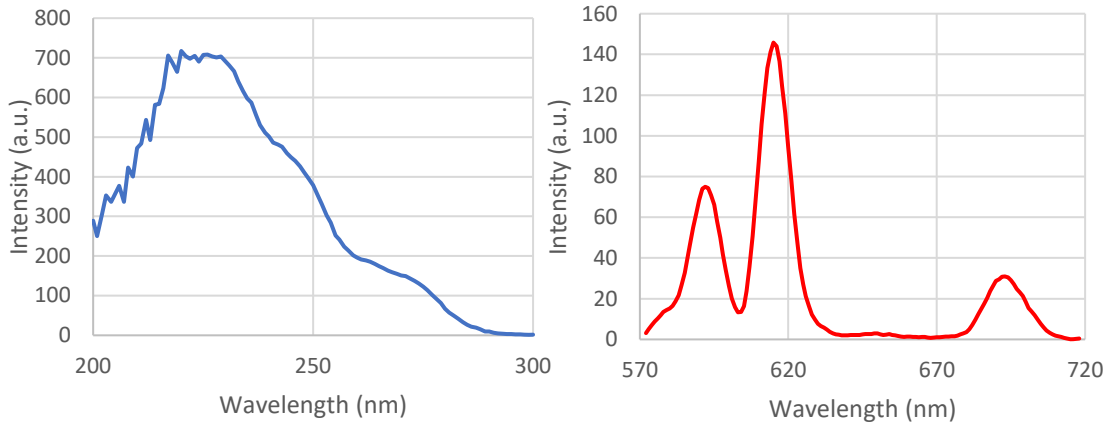

*Figure S27. (Left) Phosphorescence excitation spectrum (λ_{em} = 615 nm) of **$[Eu(L_1)_3]^{3-}$** (1 x 10^{-5} M) in H_2O. (Right) Phosphorescence emission spectrum (λ_{ex} = 274 nm) of **$[Eu(L_1)_3]^{3-}$** (1 x 10^{-5} M) in H_2O. For both the phosphorescence excitation and emission measurements, excitation and emission slit widths were 10.0 nm.*

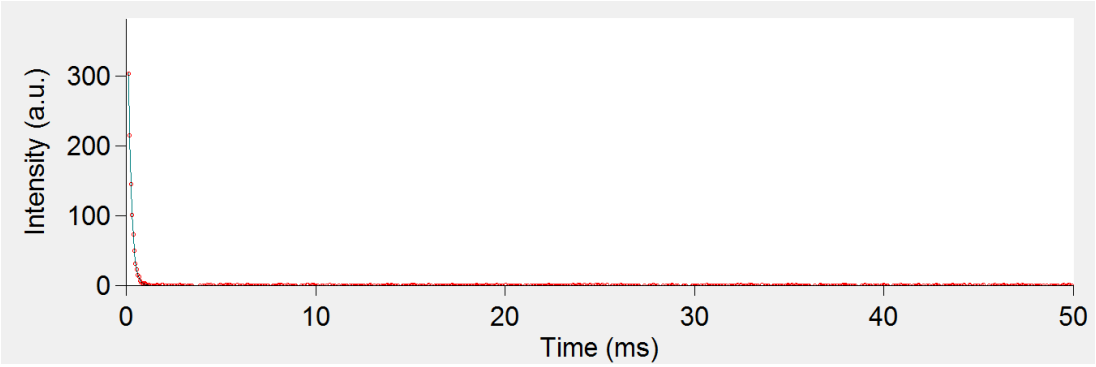

*Figure S28. **$[Eu(L_1)_3]^{3-}$** lifetime (λ_{ex} = 226 nm) (1 x 10^{-5} M) in H_2O tracking emission at 615 nm with a single exponential fit*

*Table S1. **$[Eu(L_1)_3]^{3-}$** lifetimes (λ_{ex} = 226 nm) (1 x 10^{-5} M) in H_2O tracking emission at 615 nm showing values obtained for each run and the average lifetime*

Run number	Lifetime (ms)	Average lifetime (ms)
1	0.164	
2	0.176	0.171
3	0.172	

$[Tb(L_1)_3]^{3-}$

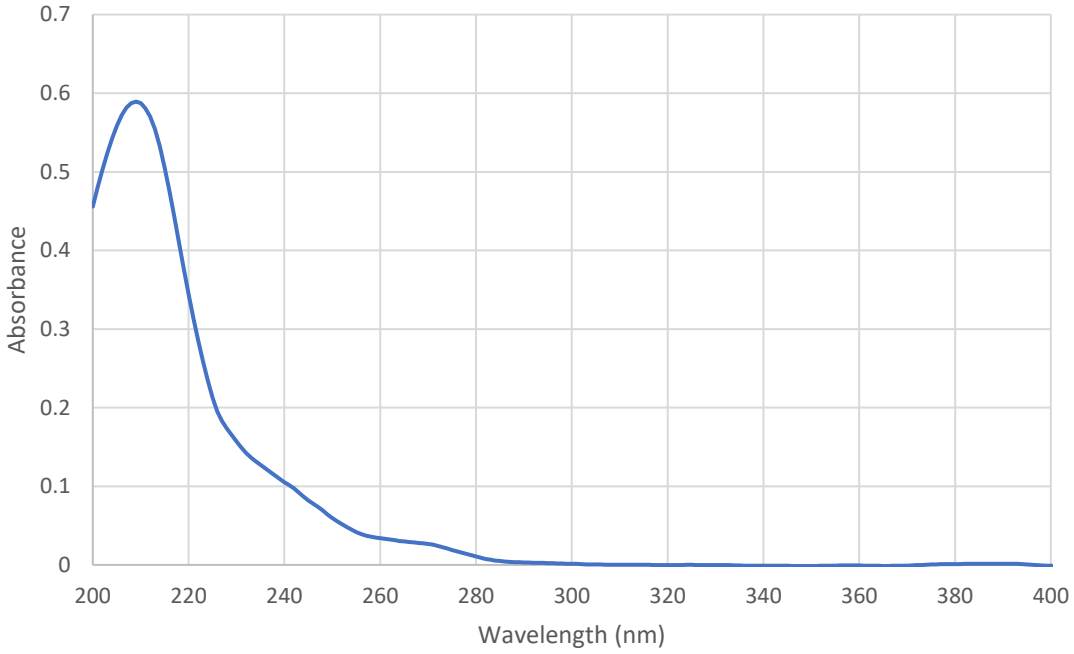

Figure S29. UV/Vis spectrum of ***$[Tb(L_1)_3]^{3-}$*** *(1 x 10^{-5} M) in H_2O*

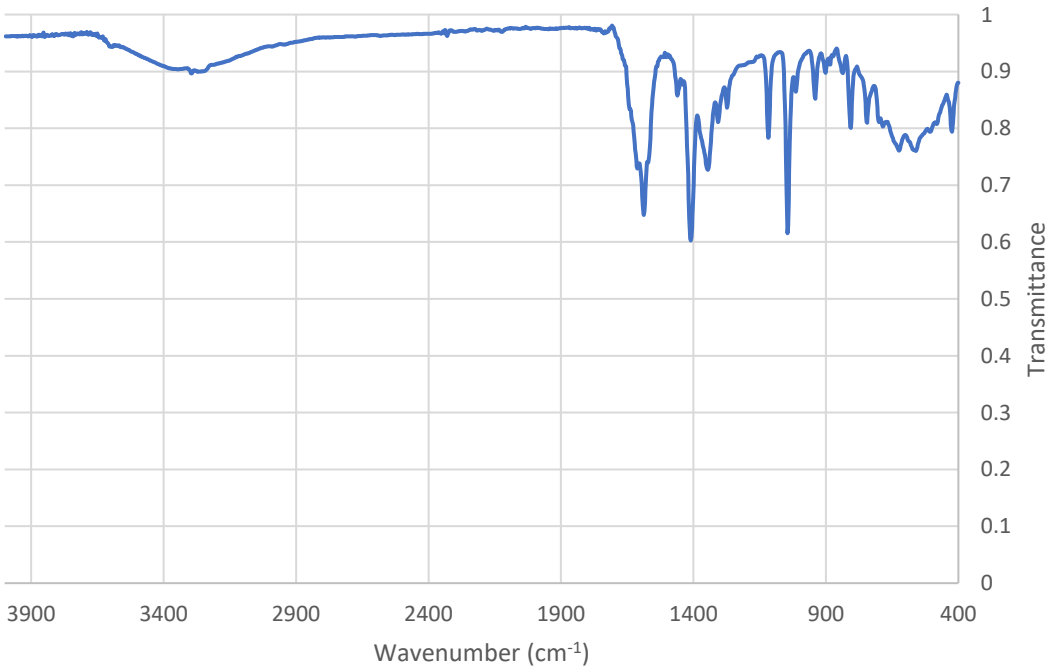

Figure S30. FTIR spectrum of ***$[Tb(L_1)_3]^{3-}$***

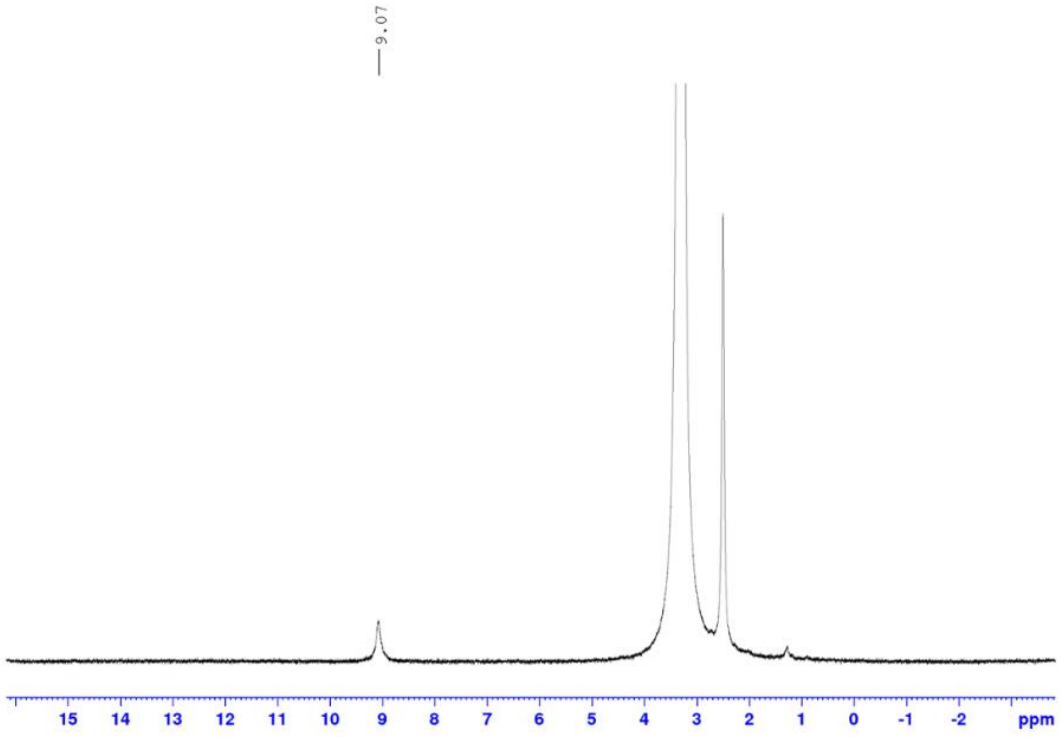

Figure S31. ^{1}H NMR spectrum of $\boldsymbol{[Tb(L_1)_3]^{3-}}$ *in DMSO-d_6*

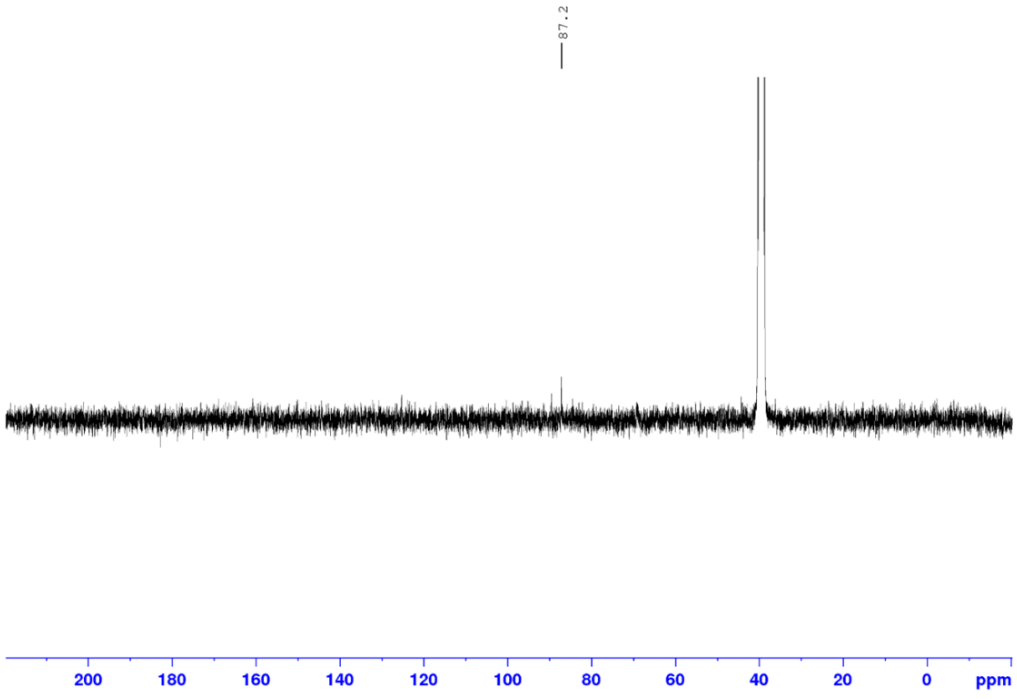

Figure S32. ^{13}C NMR spectrum of $\boldsymbol{[Tb(L_1)_3]^{3-}}$ *in DMSO-d_6*

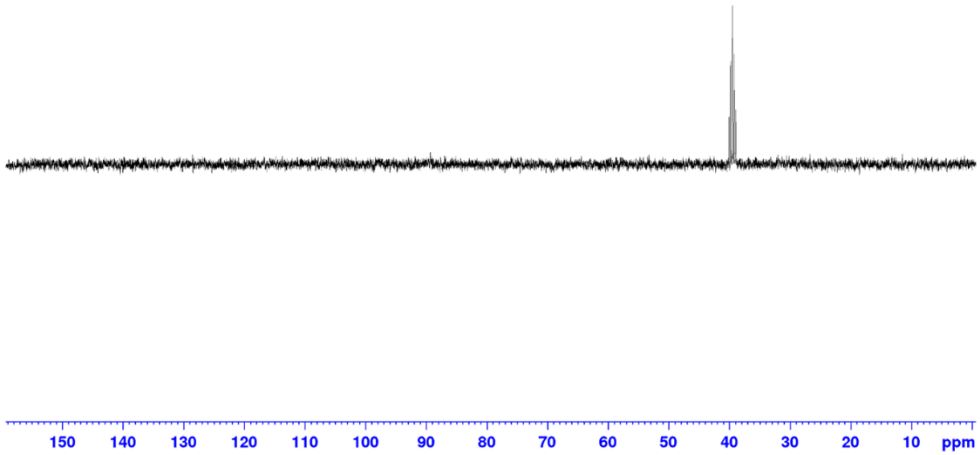

Figure S33. ^{13}C DEPT spectrum of ***[Tb(L$_1$)$_3$]$^{3-}$*** *in DMSO-d_6*

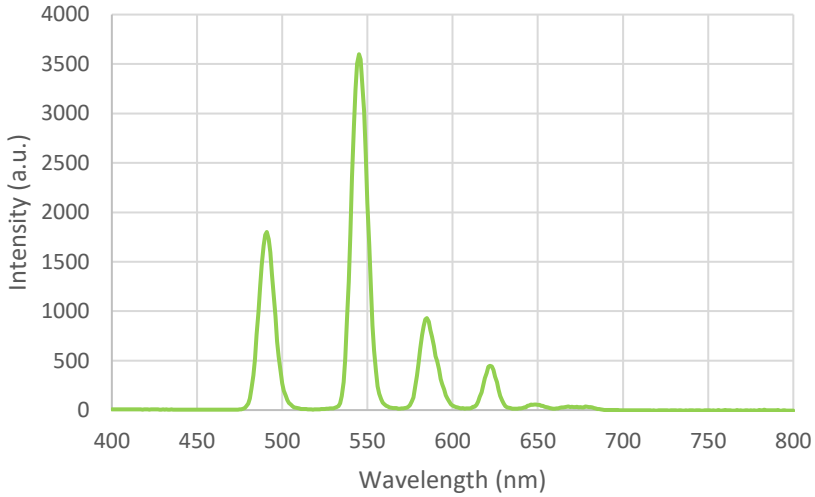

Figure S34. Fluorescence emission spectrum (λ_{ex} = 274 nm) of ***[Tb(L$_1$)$_3$]$^{3-}$*** *(1 x 10^{-5} M) in H_2O. Excitation and emission slit widths were 3.0 and 5.0 nm (respectively)*

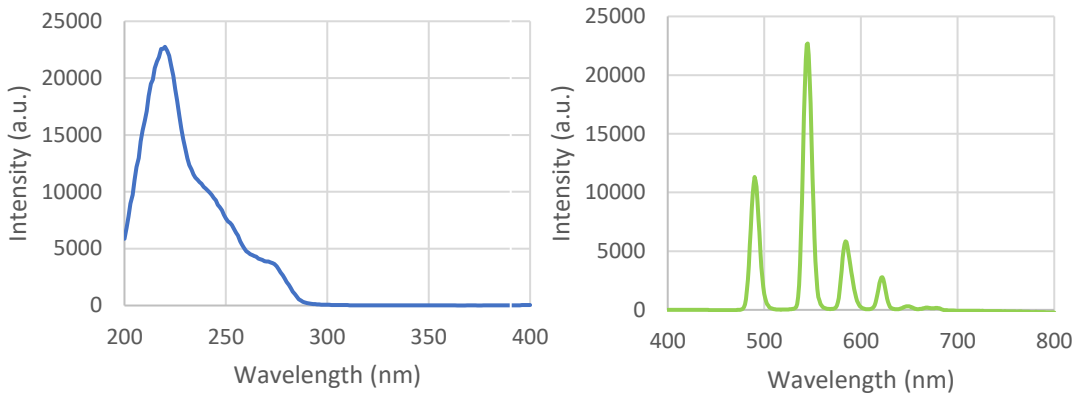

Figure S35. (Left) Fluorescence excitation spectrum (λ_{em} = 545 nm) of ***[Tb(L1)3]3-*** *(1 x 10^{-5} M) in H_2O. (Right) Fluorescence emission spectrum (λ_{ex} = 220 nm) of* ***[Tb(L1)3]3-*** *(1 x 10^{-5} M) in H_2O. For both the fluorescence excitation and emission measurements, excitation and emission slit widths were 3.0 and 5.0 nm (respectively)*

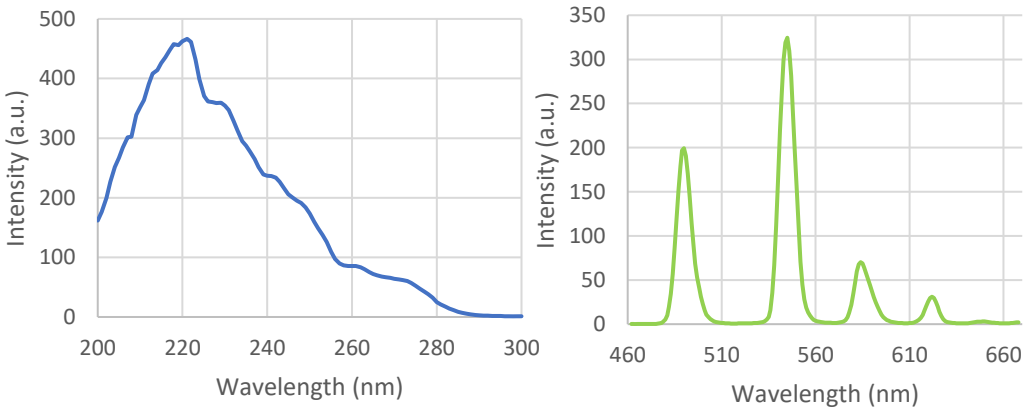

Figure S36. (Left) Phosphorescence excitation spectrum (λ_{em} = 545 nm) of ***[Tb(L1)3]3-*** *(1 x 10^{-5} M) in H_2O. (Right) Phosphorescence emission spectrum (λ_{ex} = 274 nm) of* ***[Tb(L1)3]3-*** *(1 x 10^{-5} M) in H_2O. For both the phosphorescence excitation and emission measurements, excitation and emission slit widths were 5.0 nm*

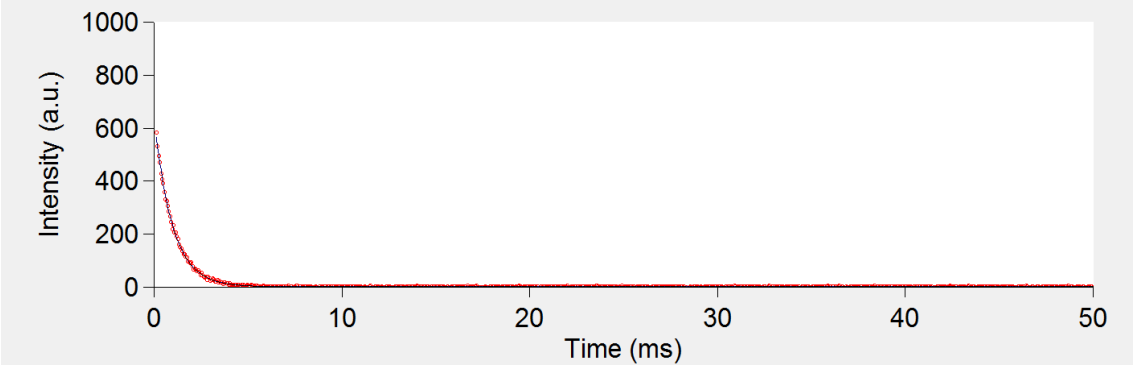

Figure S37. ***[Tb(L1)3]3-*** *lifetime (λ_{ex} = 220 nm) (1 x 10^{-5} M) in H_2O tracking emission at 545 nm with a single exponential fit*

Table S2. ***[Tb(L$_1$)$_3$]$^{3-}$*** *lifetimes (λ_{ex} = 220 nm) (1 x 10^{-5} M) in H_2O tracking emission at 545 nm showing values obtained for each run and the average lifetime*

Run number	Lifetime (ms)	Average (ms)
1	0.990	
2	0.995	0.983
3	0.964	

2-(3-hydroxypropyl)-1*H*-benzo[*de*]isoquinoline-1,3(*2H*)-dione

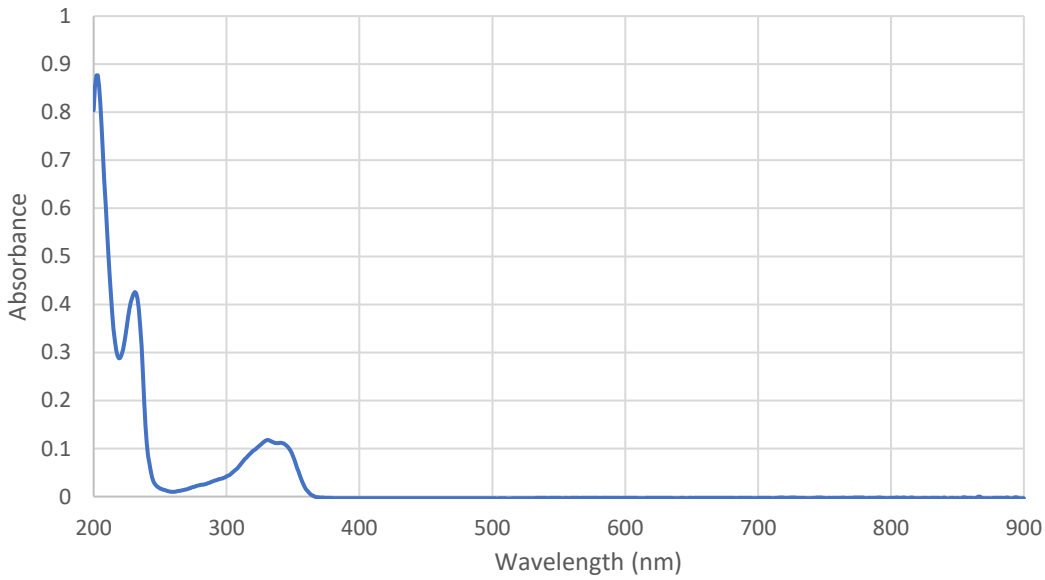

Figure S38. UV/Vis spectrum of ***2-(3-hydroxypropyl)-1H-benzo[de]isoquinoline-1,3(2H)-dione*** *(1 x 10^{-5} M) in MeOH*

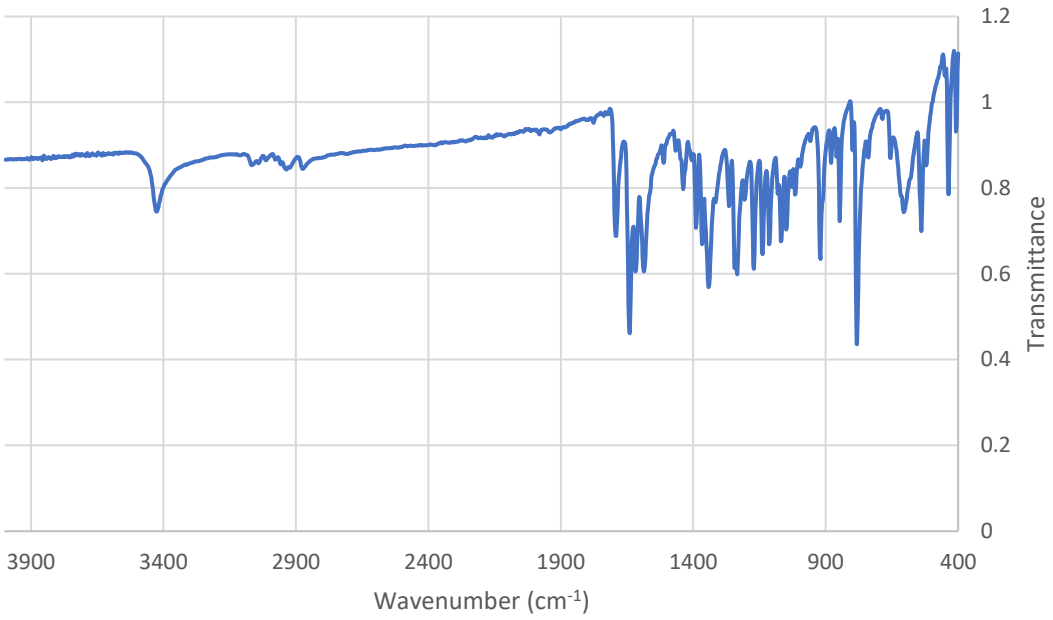

Figure S39. FTIR spectrum of ***2-(3-hydroxypropyl)-1H-benzo[de]isoquinoline-1,3(2H)-dione***

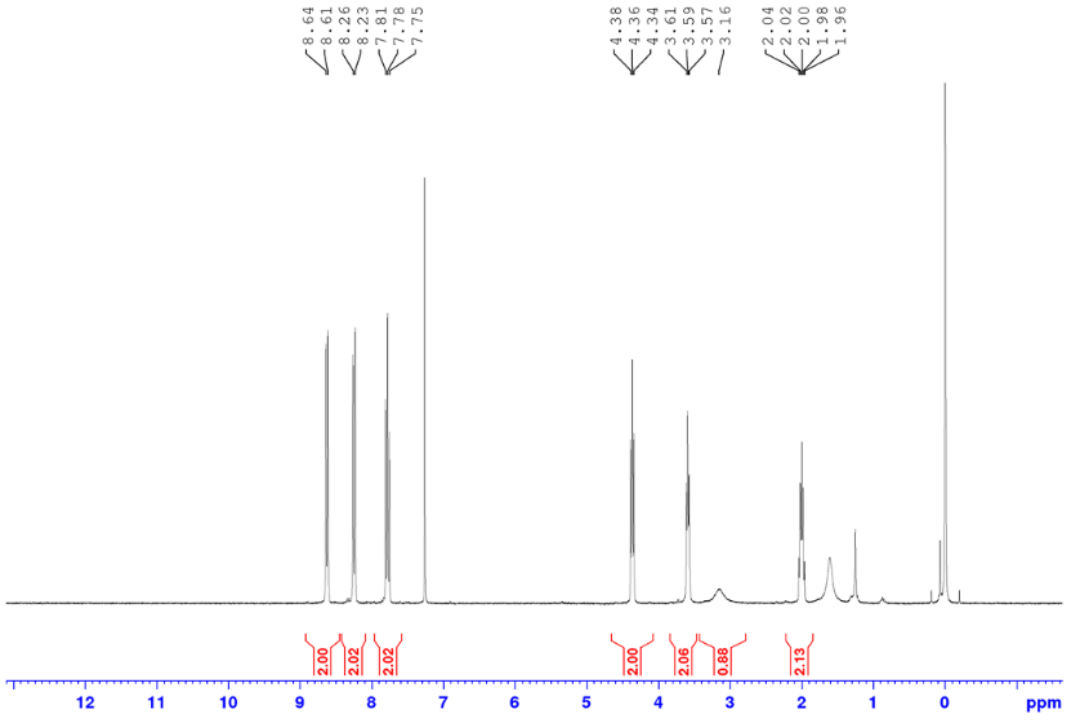

Figure S40. ^{1}H *NMR spectrum of* ***2-(3-hydroxypropyl)-1H-benzo[de]isoquinoline-1,3(2H)-dione*** *in* $CDCl_3$

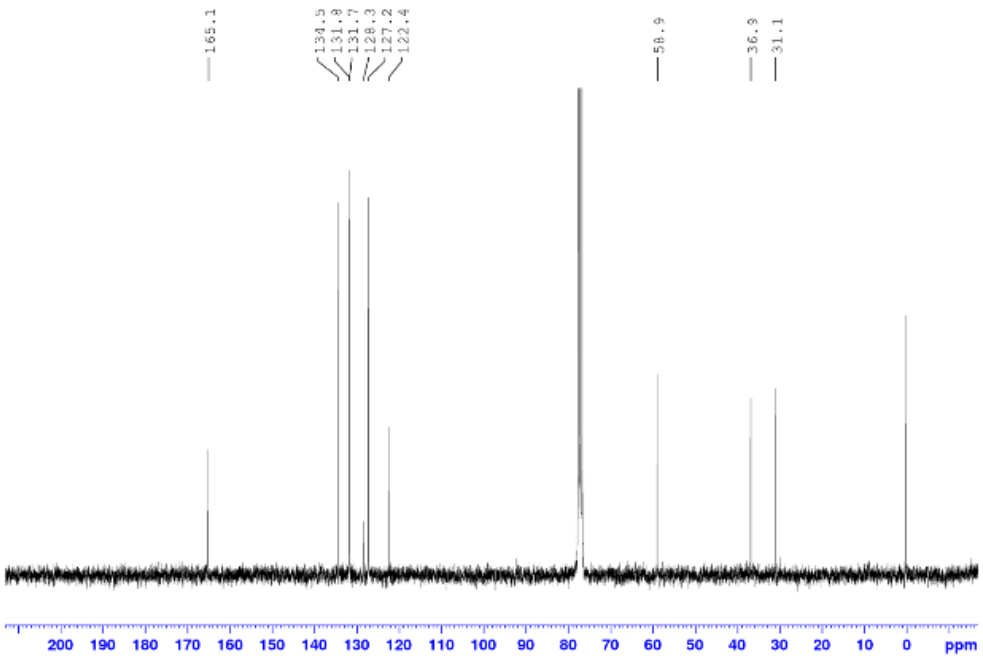

Figure S41. ^{13}C NMR spectrum of ***2-(3-hydroxypropyl)-1H-benzo[de]isoquinoline-1,3(2H)-dione*** *in $CDCl_3$*

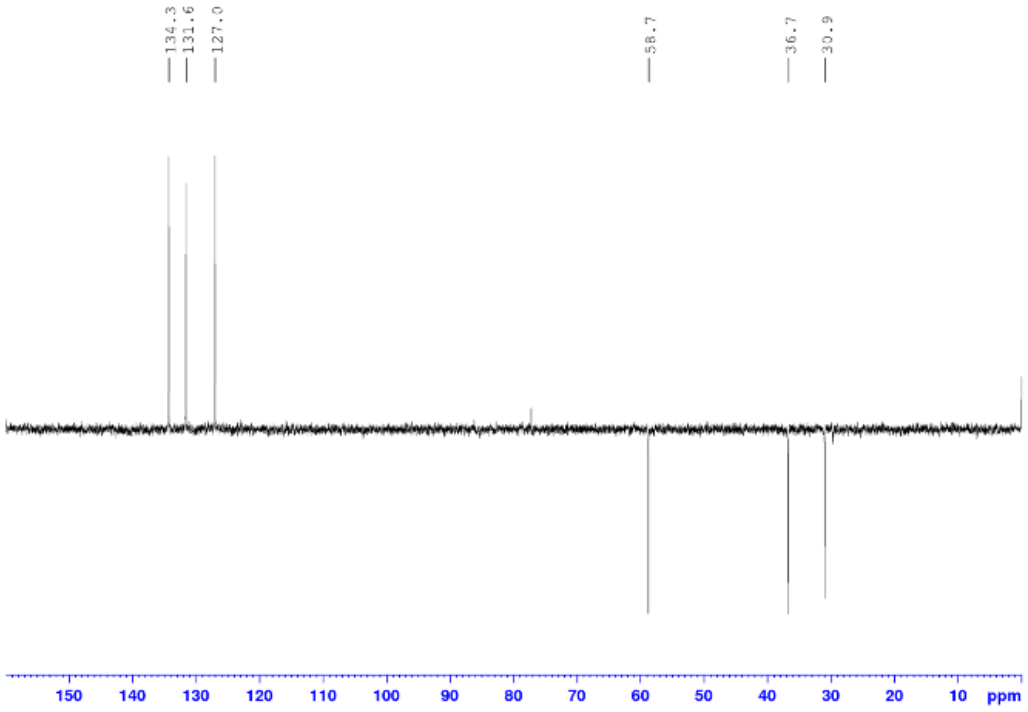

Figure S42. ^{13}C DEPT spectrum of ***2-(3-hydroxypropyl)-1H-benzo[de]isoquinoline-1,3(2H)-dione*** *in $CDCl_3$*

2-(3-bromopropyl)-1*H*-benzo[*de*]isoquinoline-1,3(*2H*)-dione

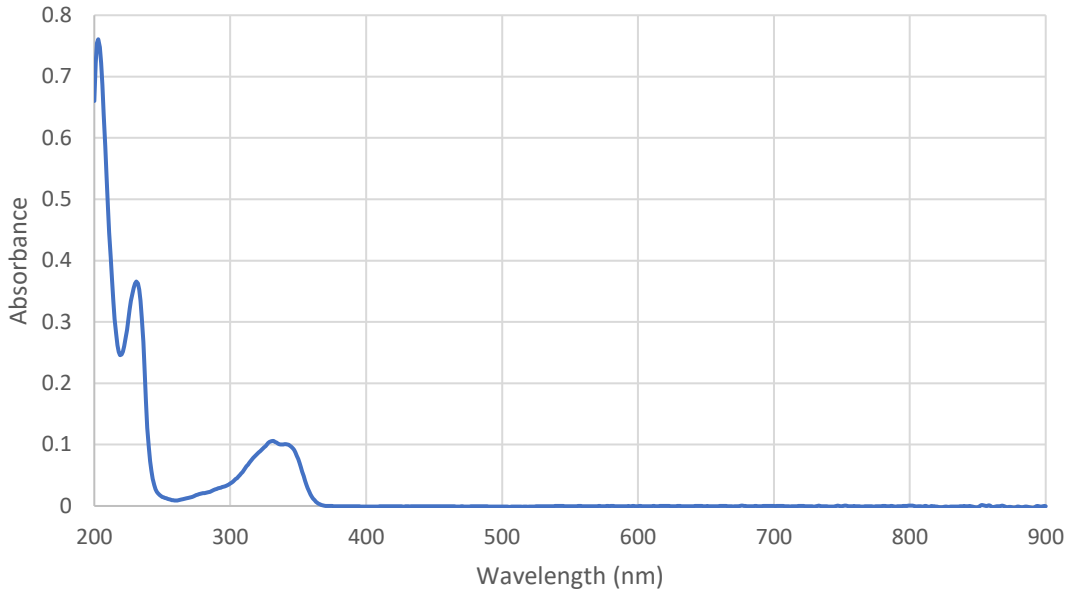

Figure S43. UV/Vis spectrum of ***2-(3-bromopropyl)-1H-benzo[de]isoquinoline-1,3(2H)-dione*** *(1 x 10^{-5} M) in MeOH*

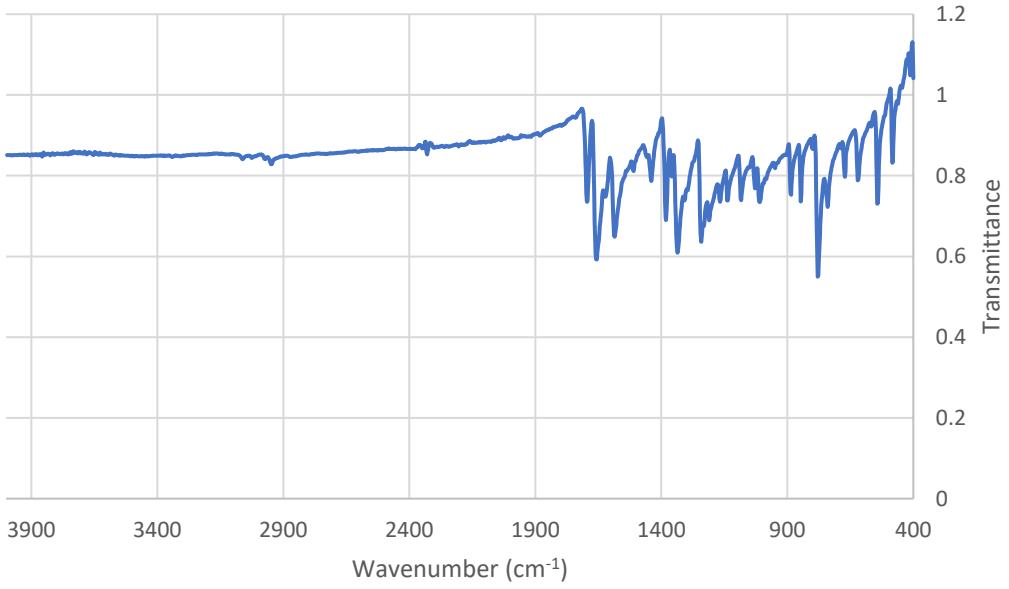

Figure S44. FTIR spectrum of ***2-(3-bromopropyl)-1H-benzo[de]isoquinoline-1,3(2H)-dione***

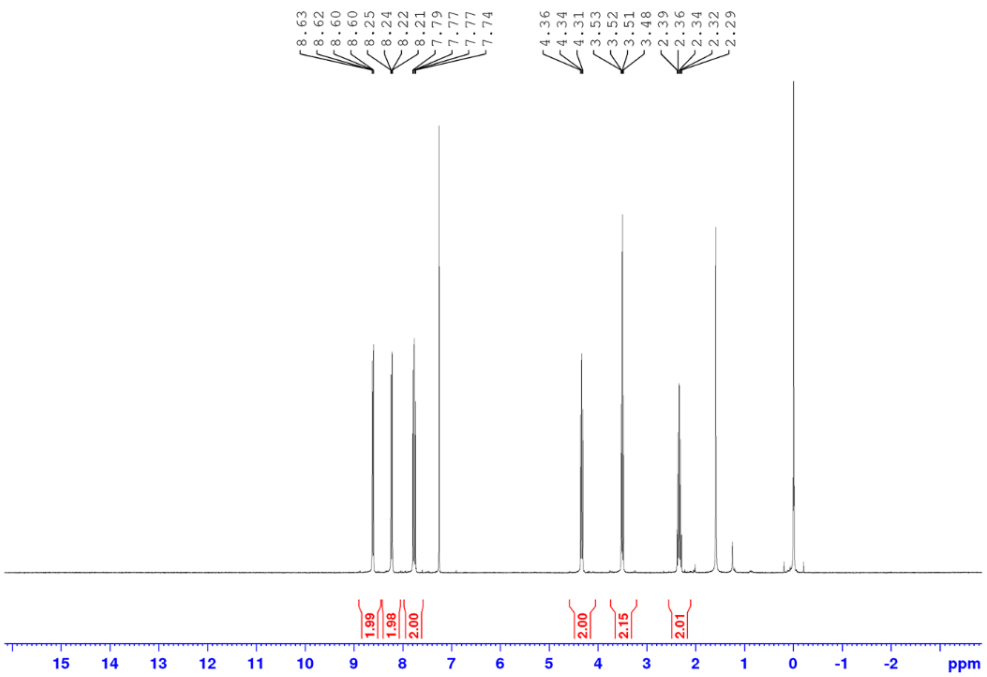

Figure S45. [1]H NMR spectrum of ***2-(3-bromopropyl)-1H-benzo[de]isoquinoline-1,3(2H)-dione*** *in* $CDCl_3$

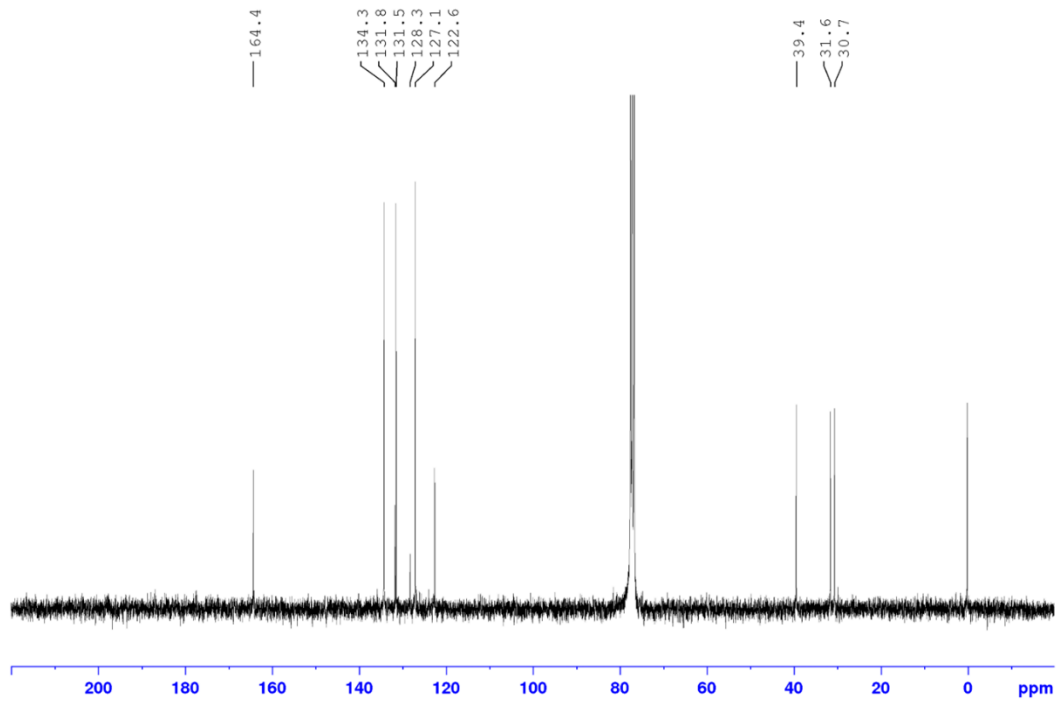

Figure S46. [13]C NMR spectrum of ***2-(3-bromopropyl)-1H-benzo[de]isoquinoline-1,3(2H)-dione*** *in* $CDCl_3$

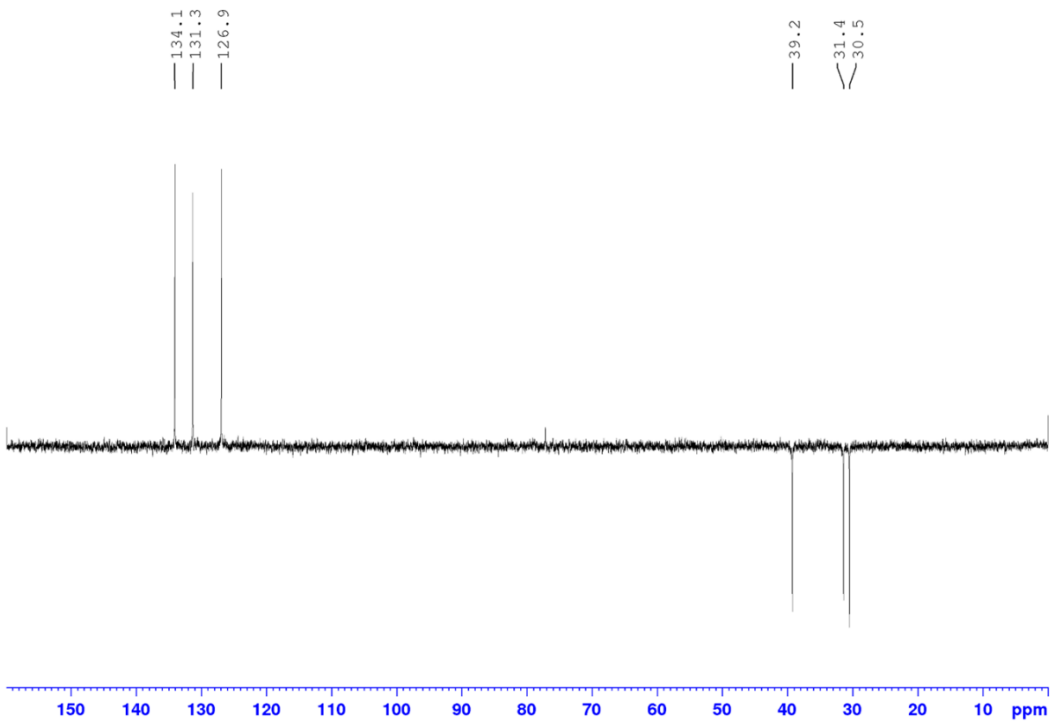

Figure S47. ^{13}C DEPT spectrum of ***2-(3-bromopropyl)-1H-benzo[de]isoquinoline-1,3(2H)-dione*** *in* $CDCl_3$

2-(3-azidopropyl)-1*H*-benzo[*de*]isoquinoline-1,3(*2H*)-dione (2N_3)

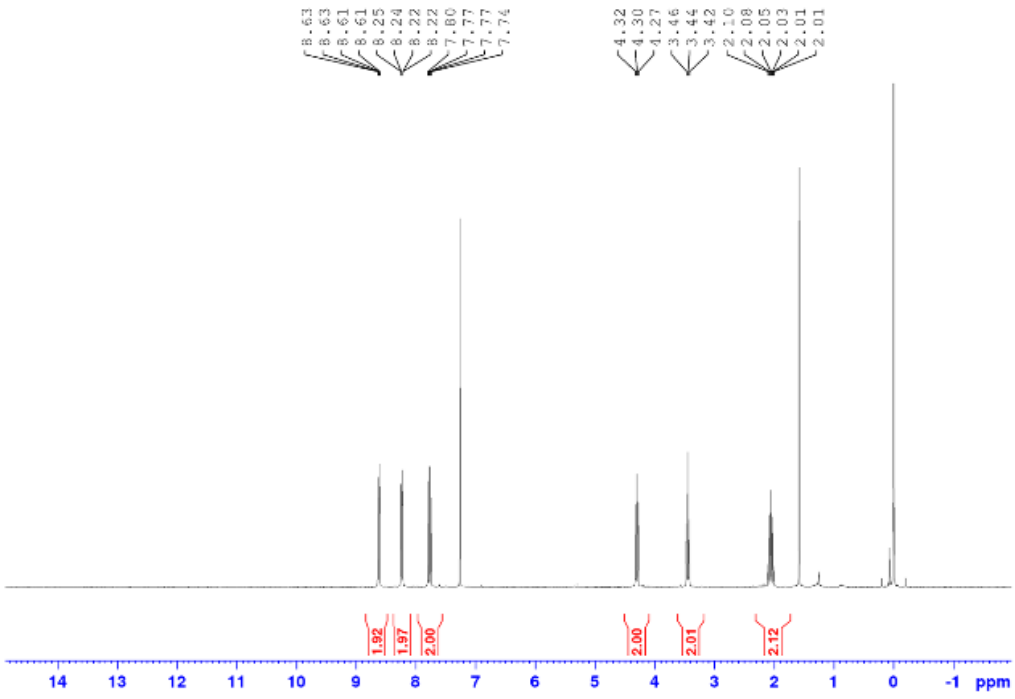

Figure S48. ^{1}H NMR spectrum of ***2N_3*** *in* $CDCl_3$

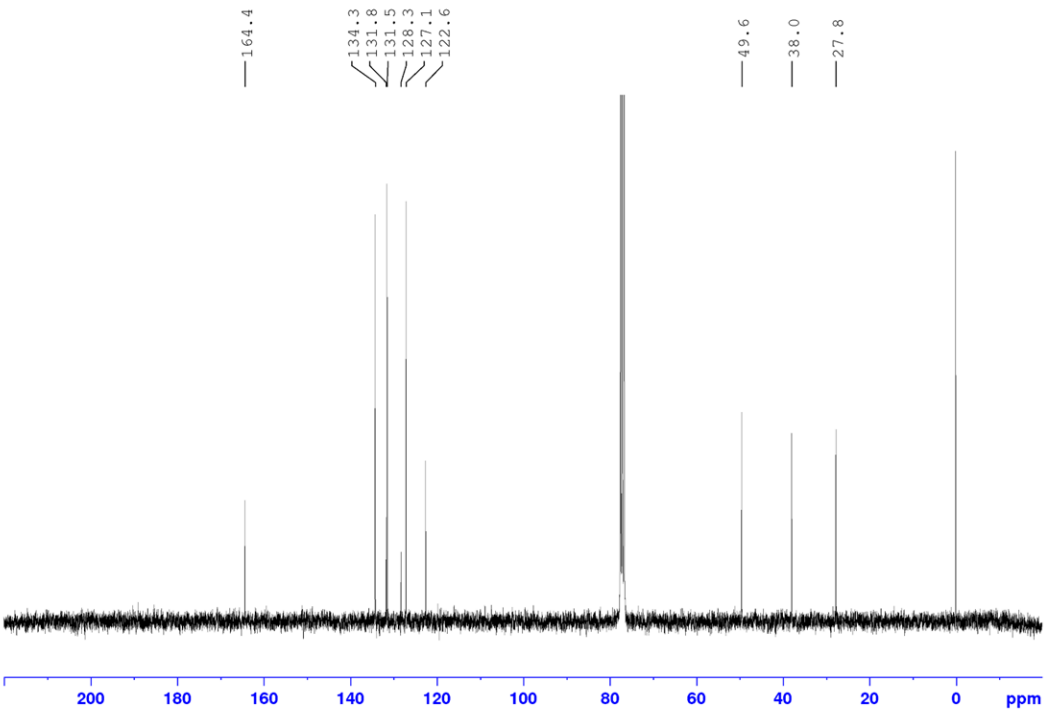

*Figure S49. ^{13}C NMR spectrum of **2N₃** in $CDCl_3$*

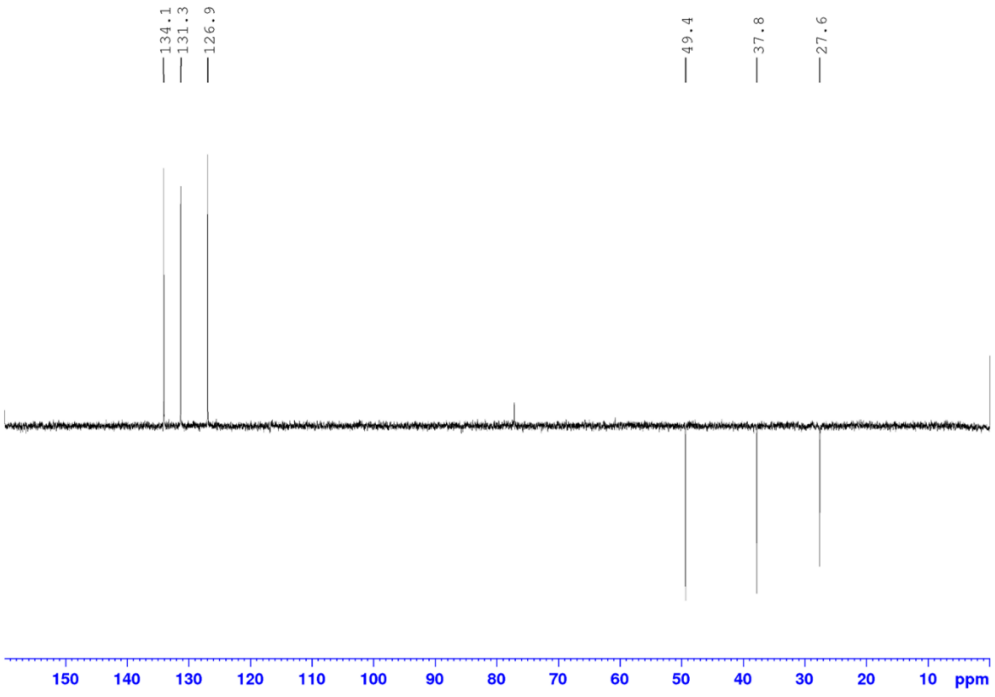

*Figure S50. ^{13}C DEPT spectrum of **2N₃** in $CDCl_3$*

$MeOL_2$

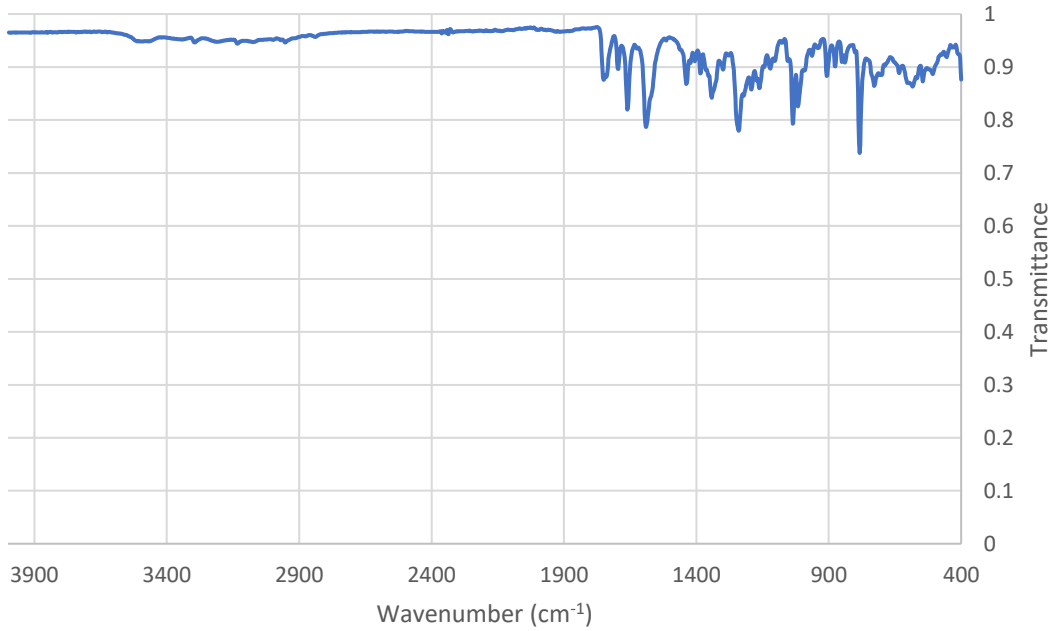

Figure S51. FTIR spectrum of ***$MeOL_2$***

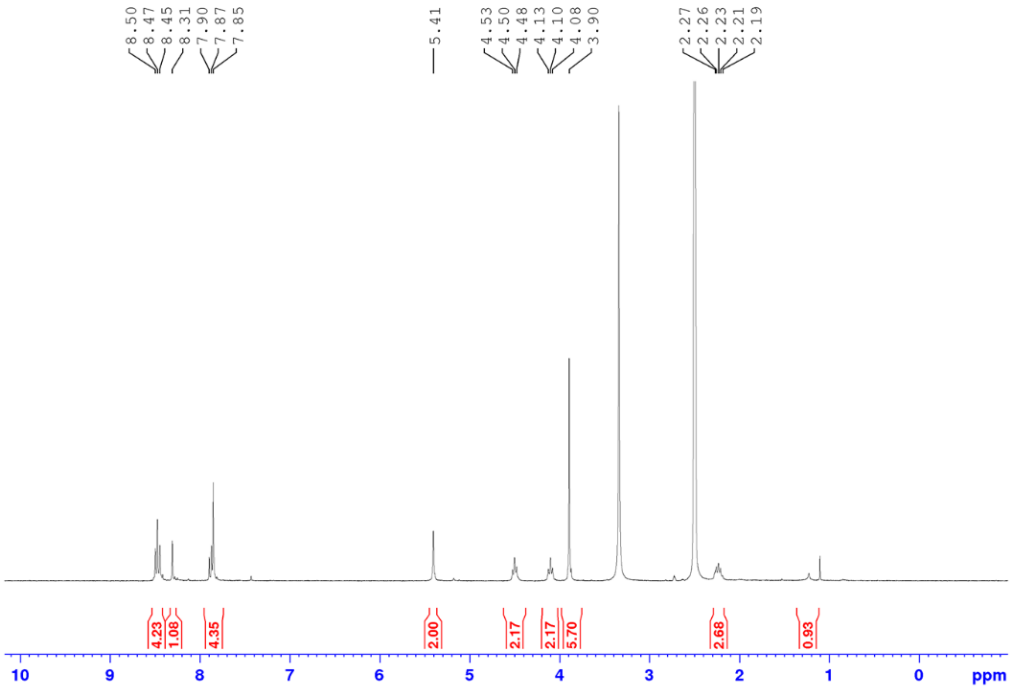

Figure S52. ^1H NMR spectrum of ***$MeOL_2$*** *in DMSO-d_6*

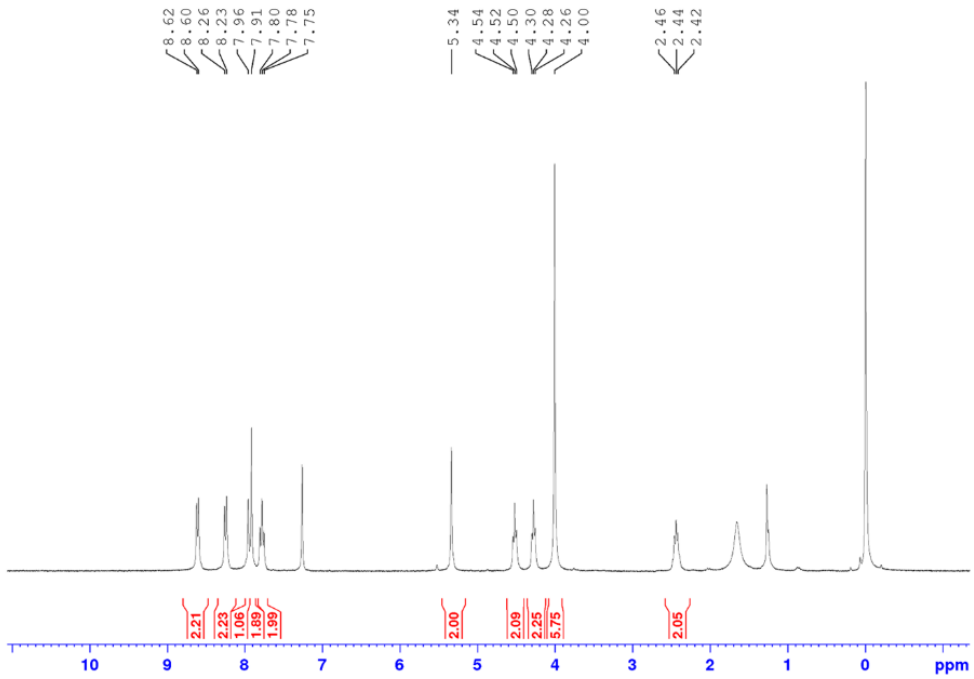

*Figure S53. [1]H NMR spectrum of **MeOL$_2$** in $CDCl_3$*

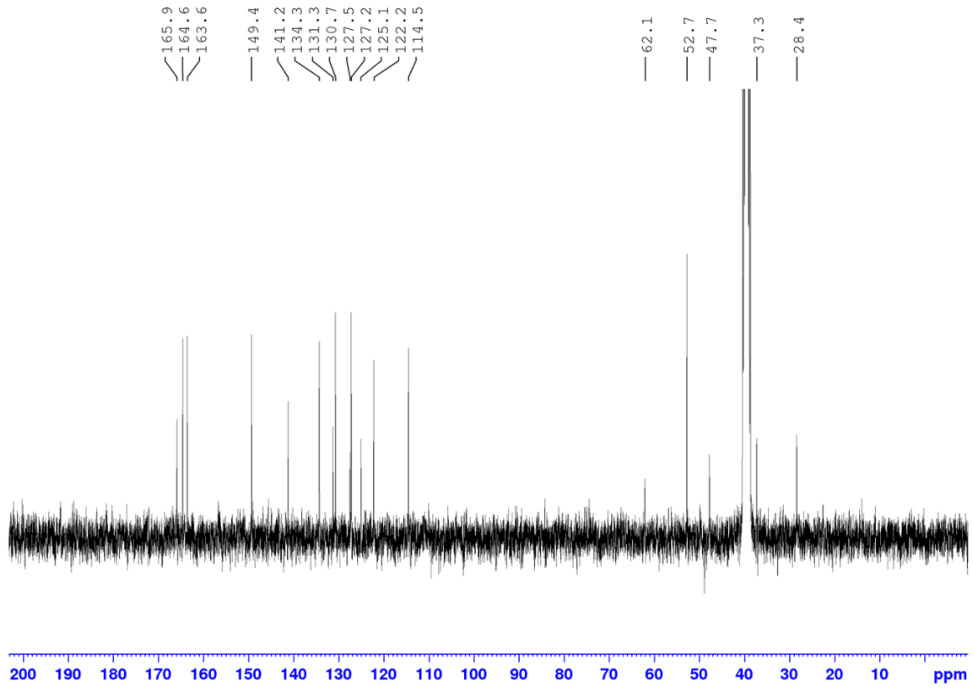

*Figure S54. [13]C NMR spectrum of **MeOL$_2$** in DMSO-d_6*

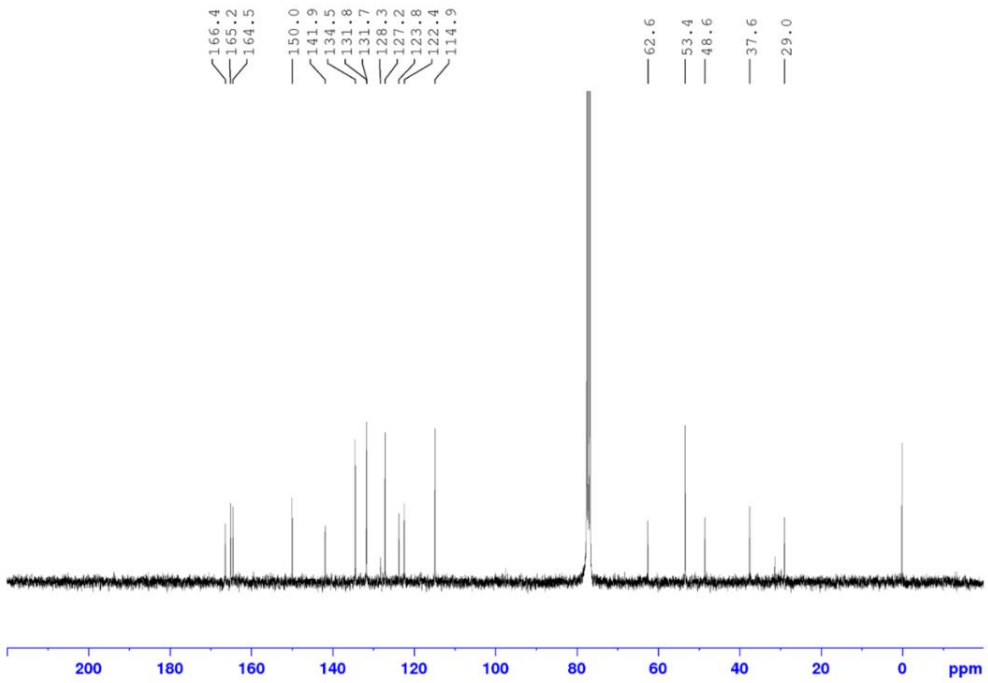

*Figure S55. ^{13}C NMR spectrum of **MeOL$_2$** in $CDCl_3$*

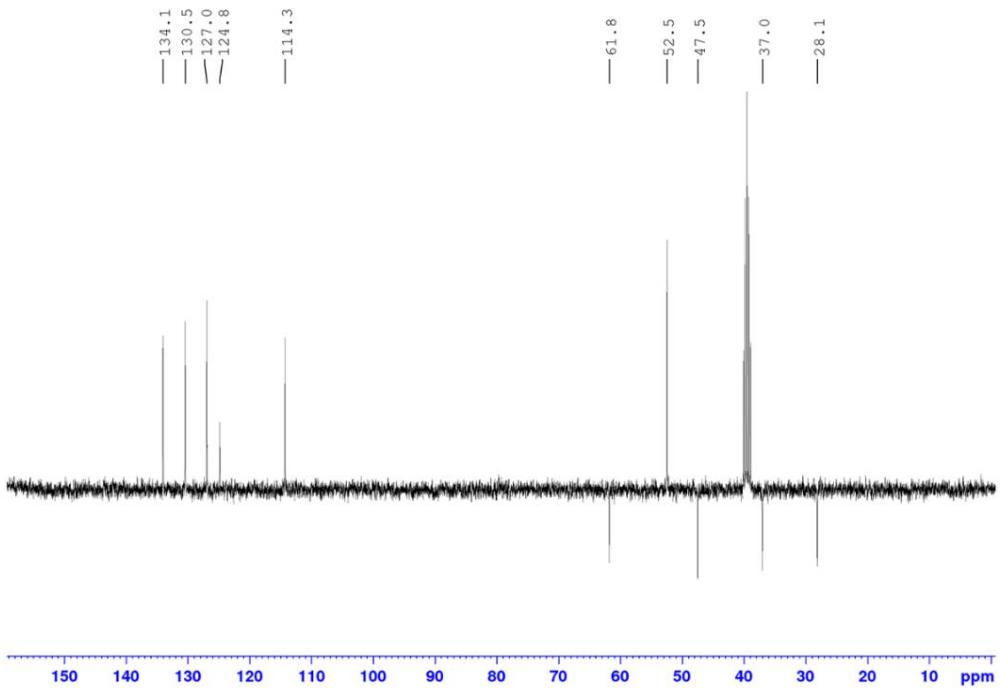

*Figure S56. ^{13}C DEPT spectrum of **MeOL$_2$** in DMSO-d_6*

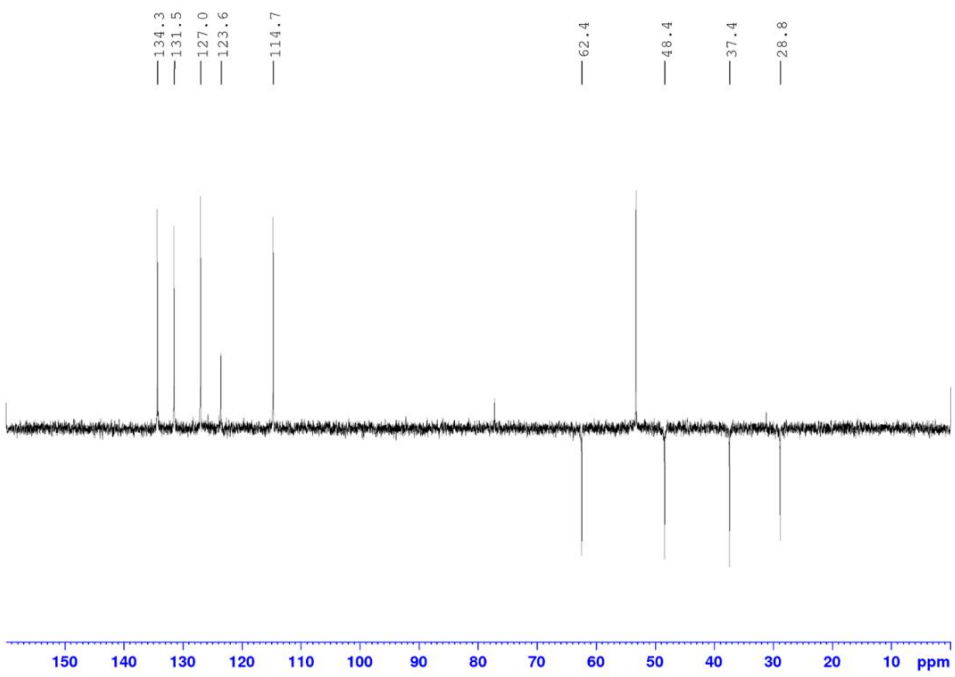

*Figure S57. ^{13}C DEPT spectrum of **MeOL$_2$** in $CDCl_3$*

L$_2$

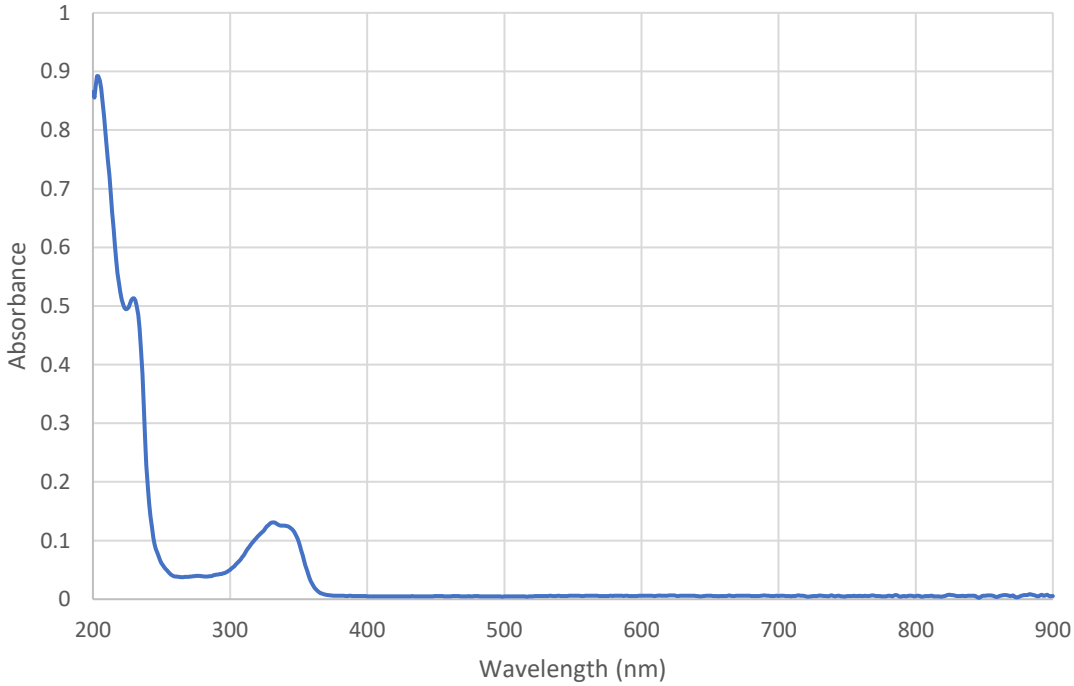

*Figure S58. UV/Vis spectrum of **L$_1$** (1 x 10^{-5} M) in MeOH (made from a 2:1 $CHCl_3$:MeOH stock solution)*

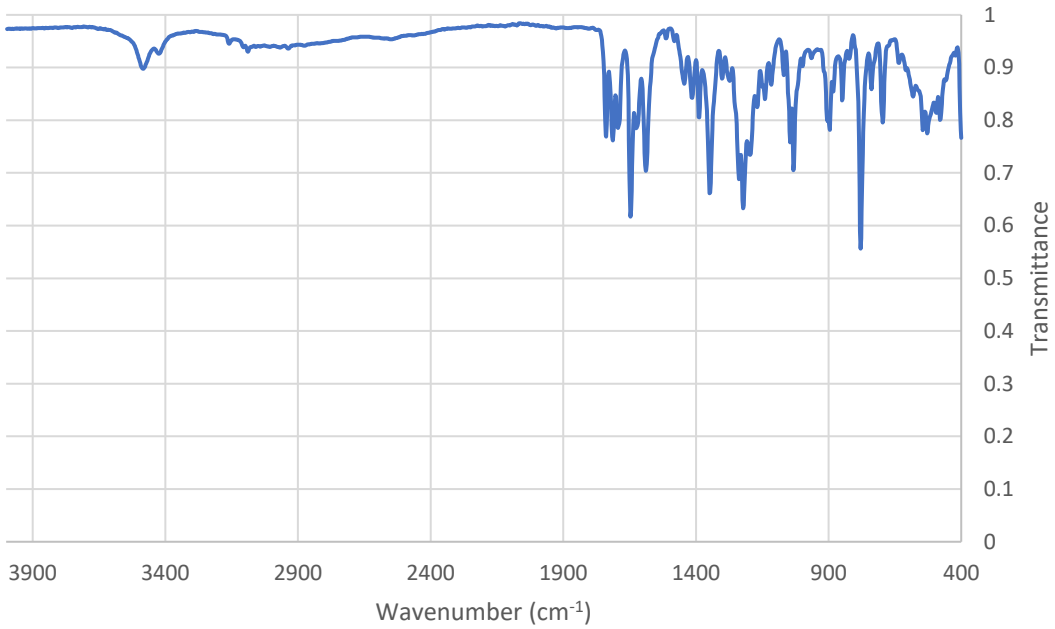

Figure S59. FTIR spectrum of ***L₁***

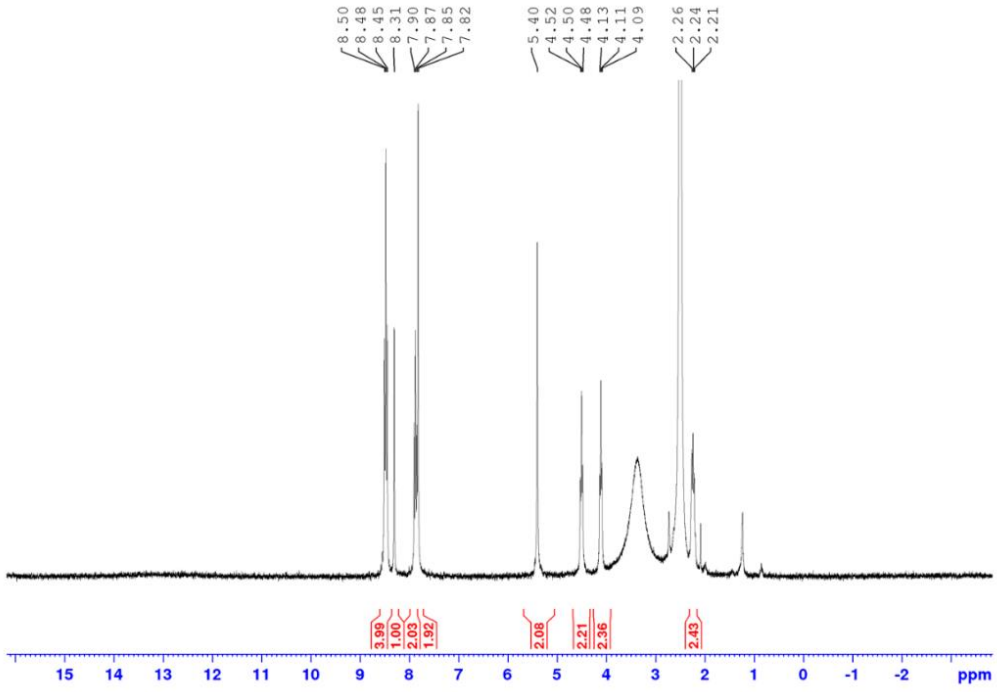

Figure S60. ^{1}H NMR spectrum of ***L₁*** *in DMSO-d_6*

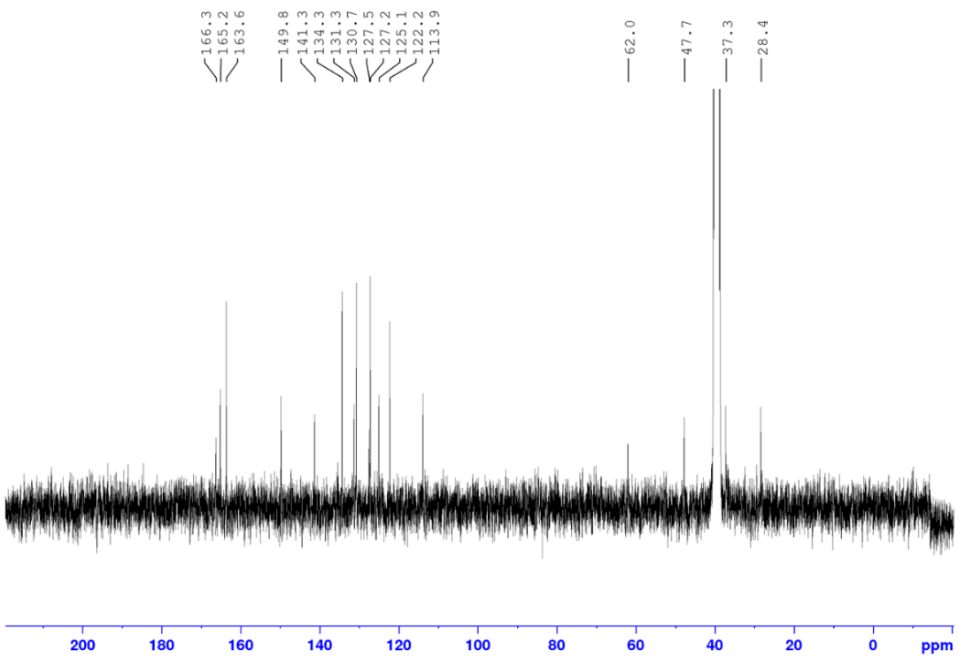

Figure S61. ^{13}C NMR spectrum of ***L*****1**

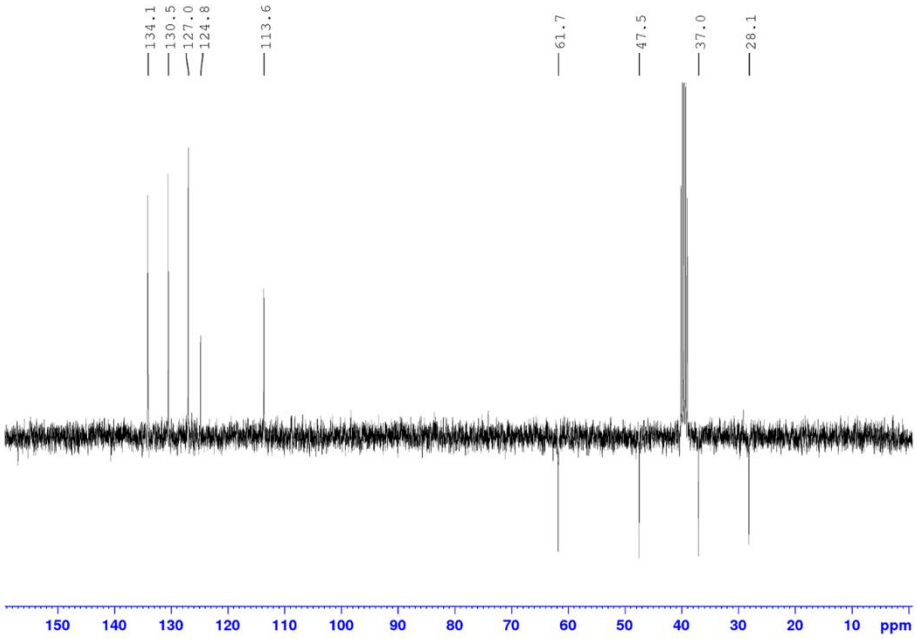

Figure S62. ^{13}C DEPT spectrum of ***L*****1**

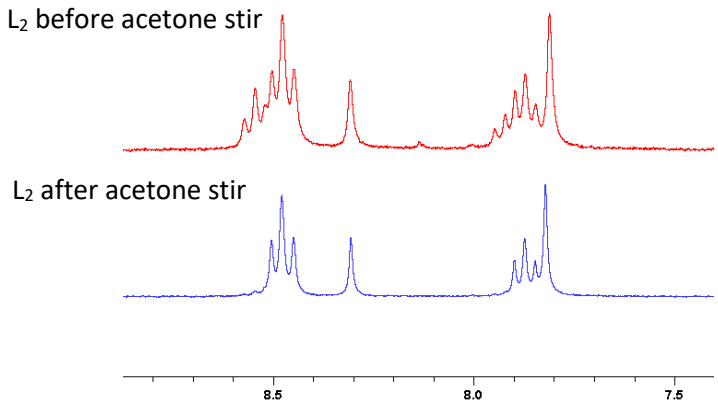

Figure S63. L_2 before stirring in acetone (top) and after stirring in acetone (bottom) showing the removal of the overlapping triplet peaks at approximately 8.55 and 7.95 ppm

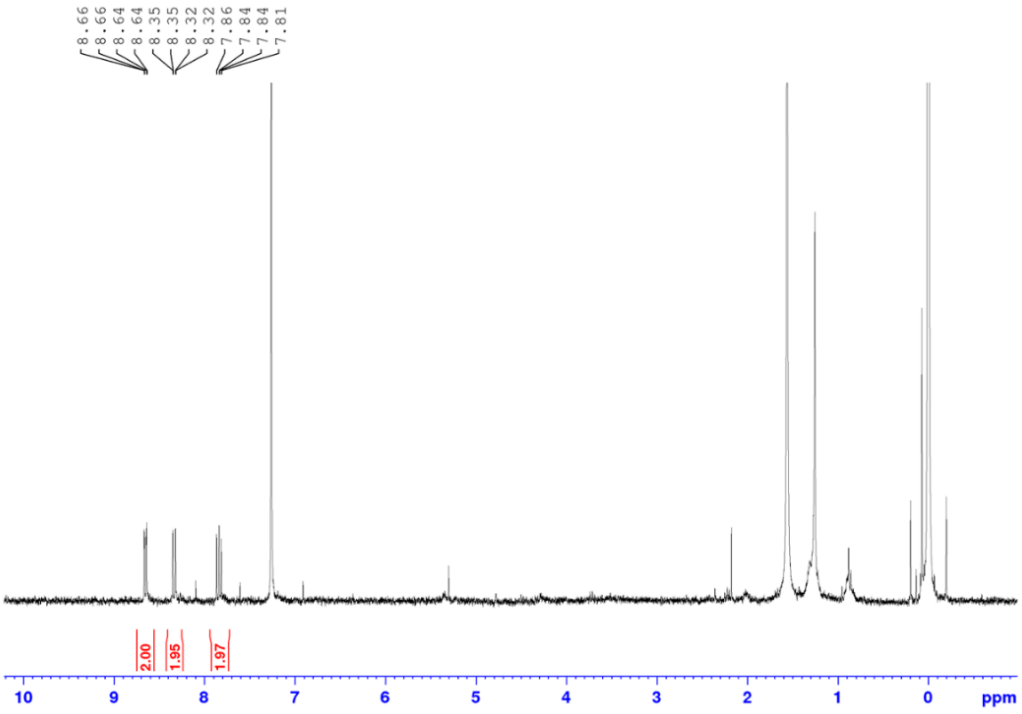

Figure S64. ^1H NMR of acetone soluble impurities in DMSO-d_6

$[La(L_2)_3]^{3-}$

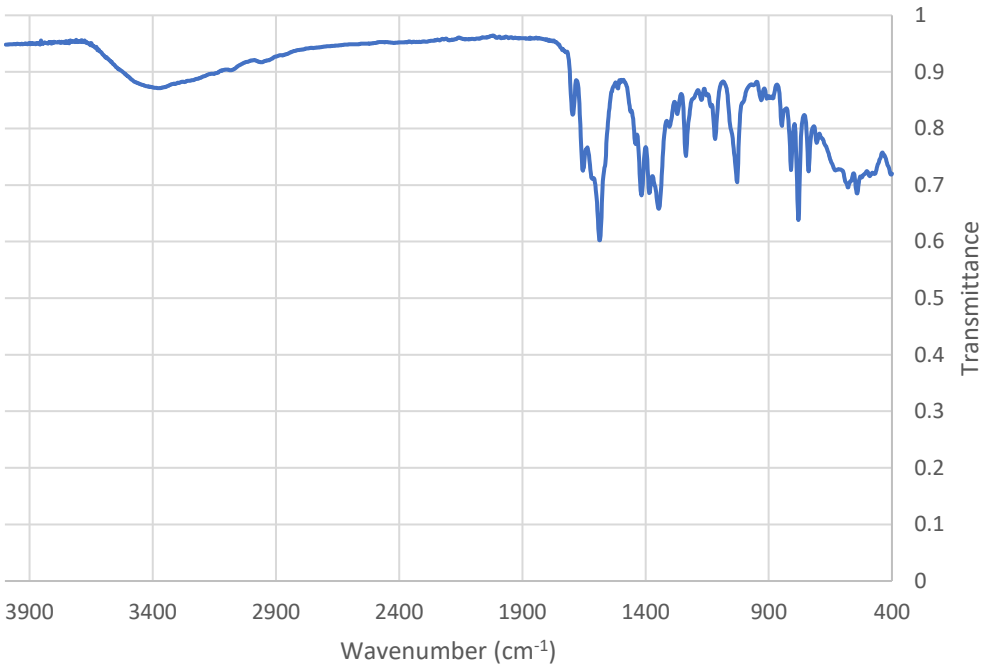

Figure S65. FTIR spectrum of ***$[La(L_2)_3]^{3-}$***

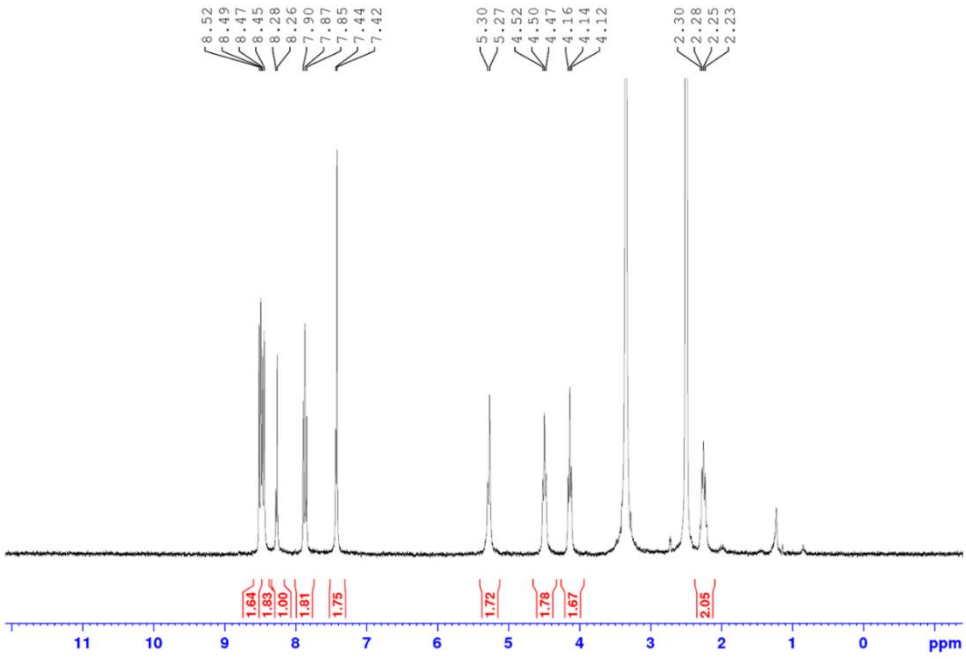

Figure S66. ^1H NMR spectrum of ***$[La(L_2)_3]^{3-}$*** *in DMSO-d_6*

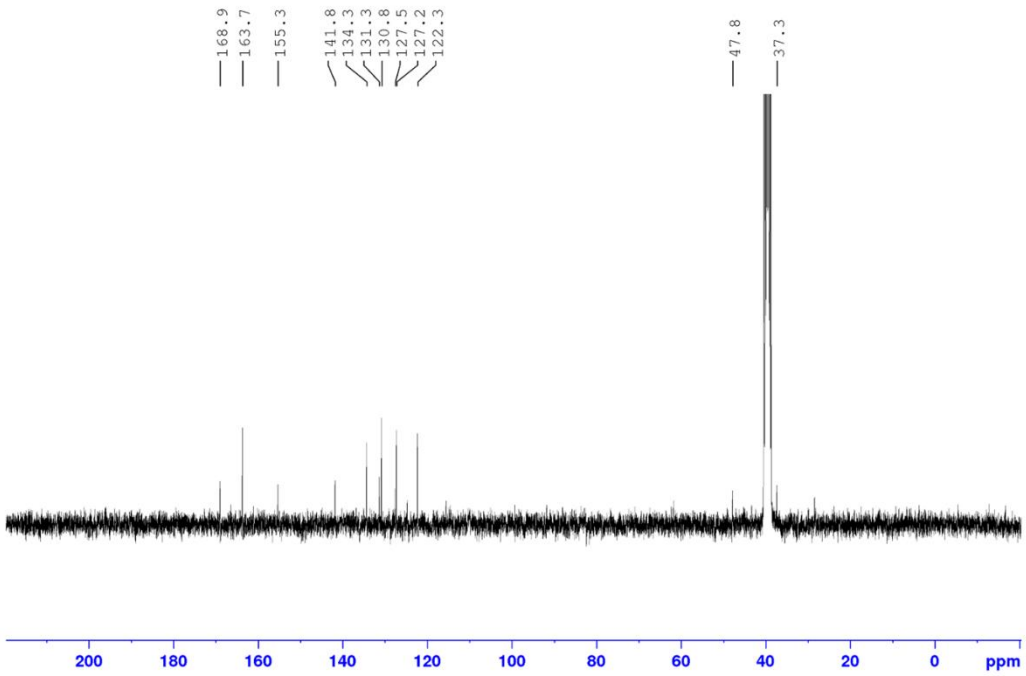

Figure S67. ^{13}C NMR spectrum of ***[La(L$_2$)$_3$]$^{3-}$*** *in DMSO-d$_6$*

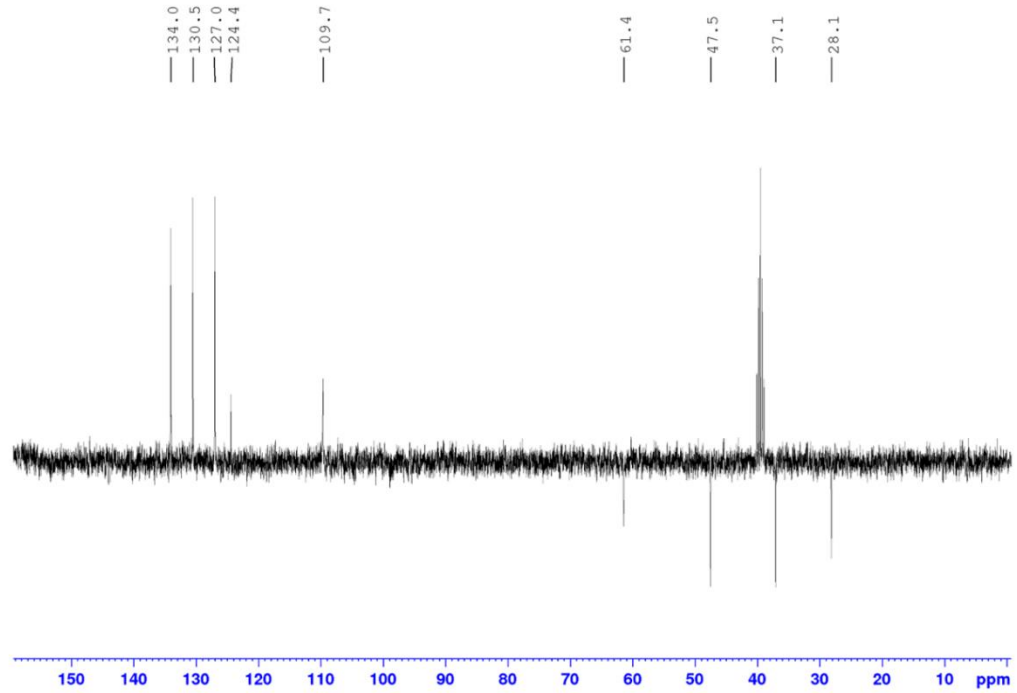

Figure S68. ^{13}C DEPT spectrum of ***[La(L$_2$)$_3$]$^{3-}$*** *in DMSO-d$_6$*

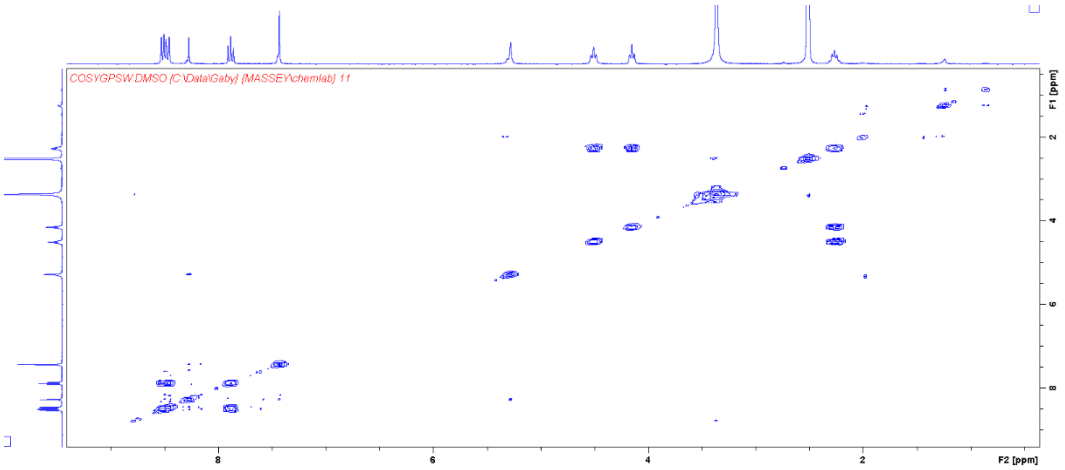

Figure 69. COSY spectrum of ***[La(L2)3]3-*** *in DMSO-d6*

$[Eu(L_2)_3]^{3-}$

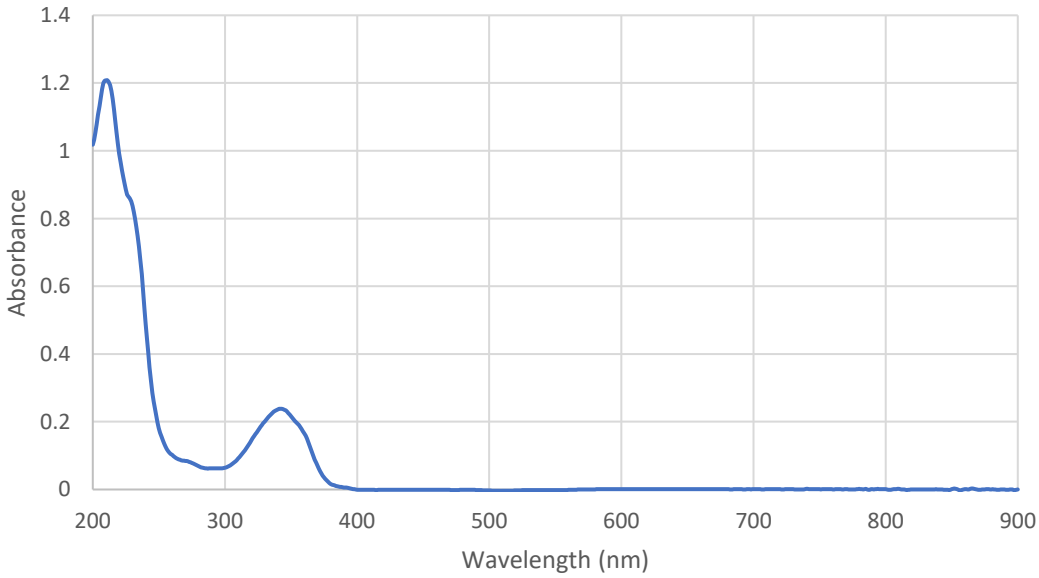

Figure S70. UV/Vis spectrum of ***[Eu(L2)3]3-*** *(1 x 10-5 M) in H2O*

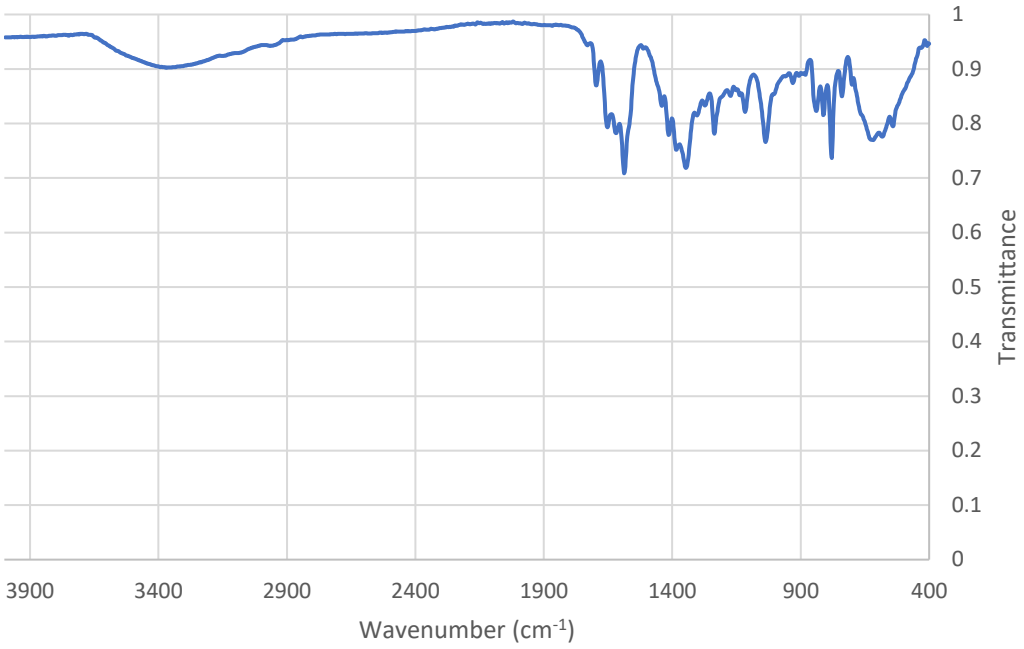

Figure S71. FTIR spectrum of ***[Eu(L$_2$)$_3$]$^{3-}$***

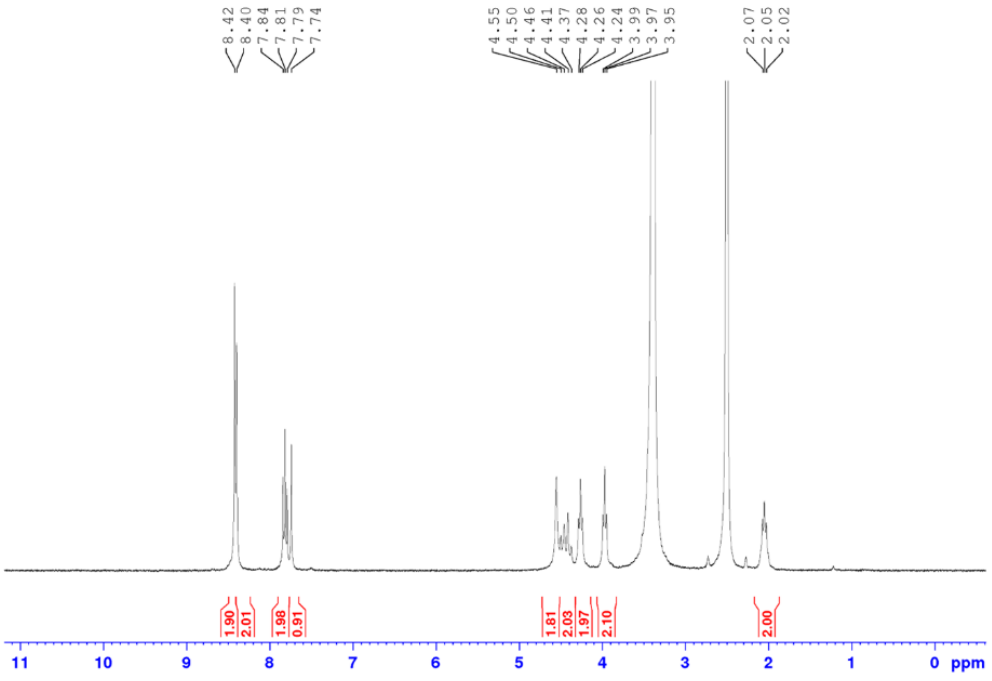

Figure S72. ^{1}H NMR spectrum of ***[Eu(L$_2$)$_3$]$^{3-}$*** *in DMSO-d$_6$*

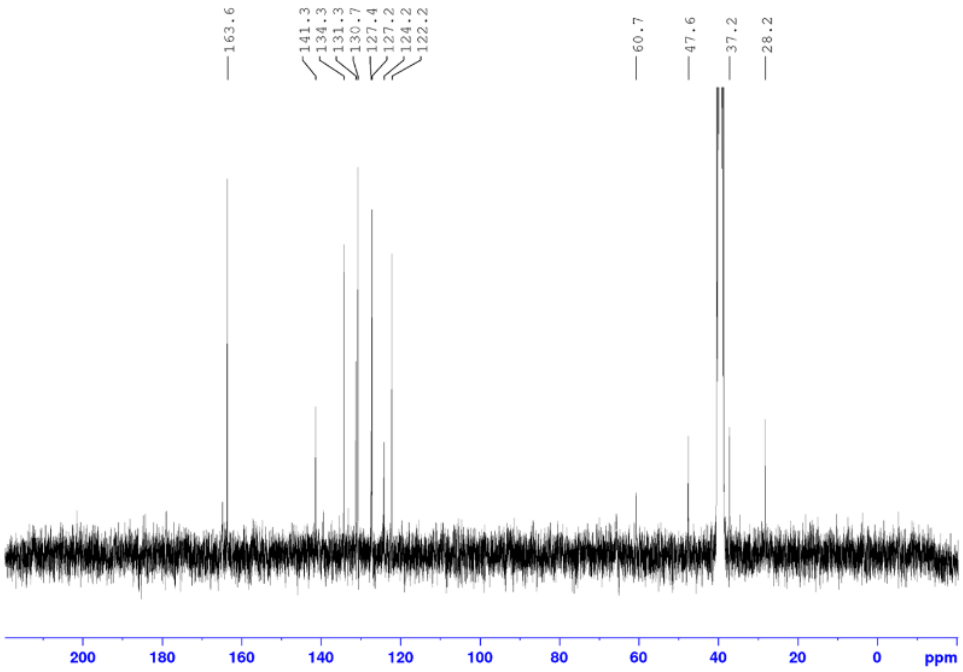

Figure S73. ^{13}C NMR spectrum of ***[Eu(L$_2$)$_3$]$^{3-}$*** *in DMSO-d$_6$*

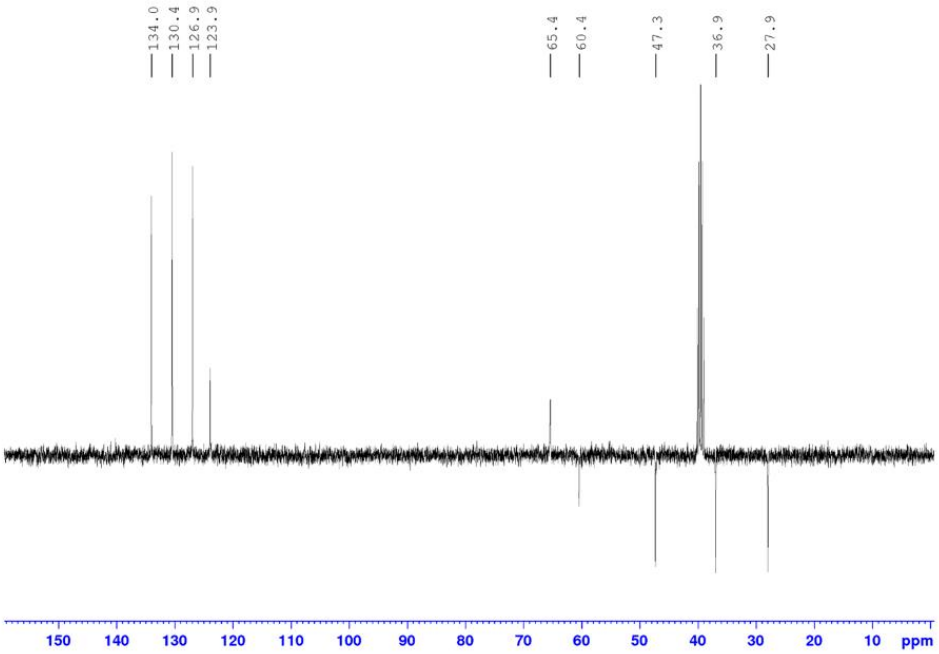

Figure S74. ^{13}C DEPT spectrum of ***[Eu(L$_2$)$_3$]$^{3-}$*** *in DMSO-d$_6$*

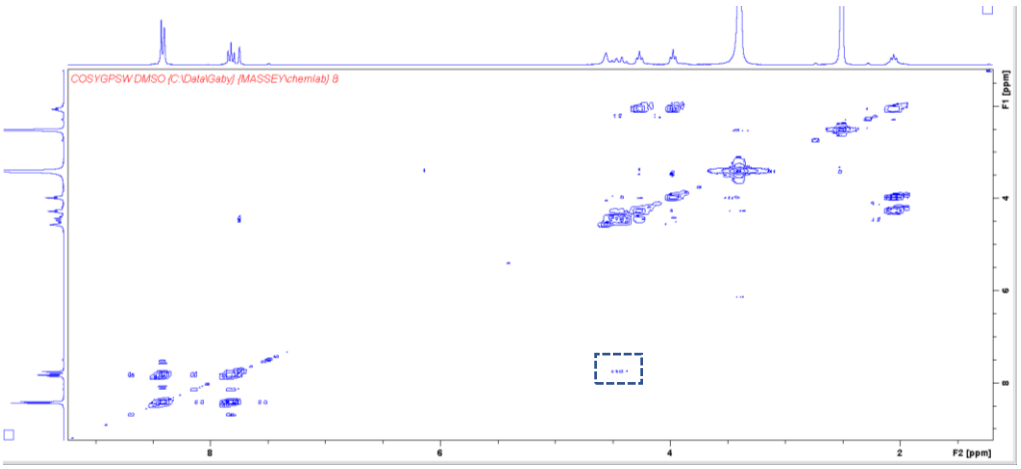

Figure S75. COSY spectrum of $[Eu(L_2)_3]^{3-}$ *in DMSO-*d_6

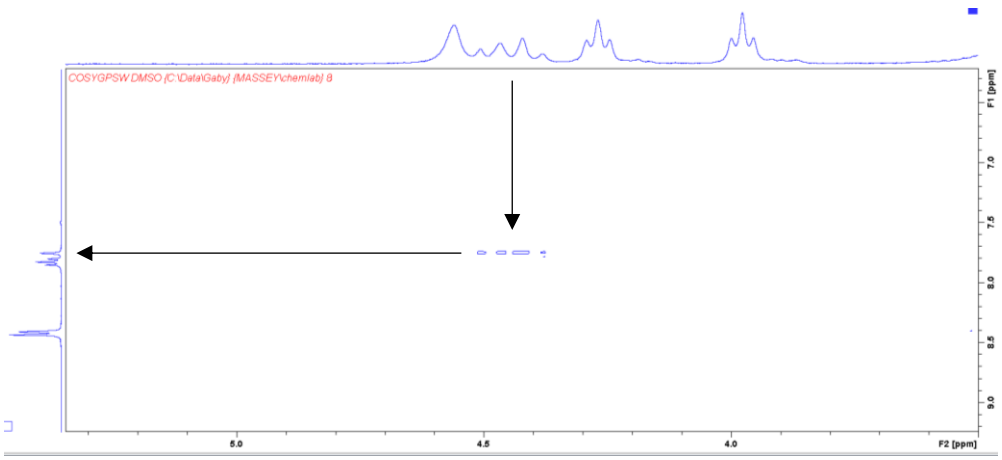

Figure S76. COSY spectrum of $[Eu(L_2)_3]^{3-}$ *in DMSO-*d_6 *showing the interaction of the multiplet at 4.44 ppm with the Tz-H*

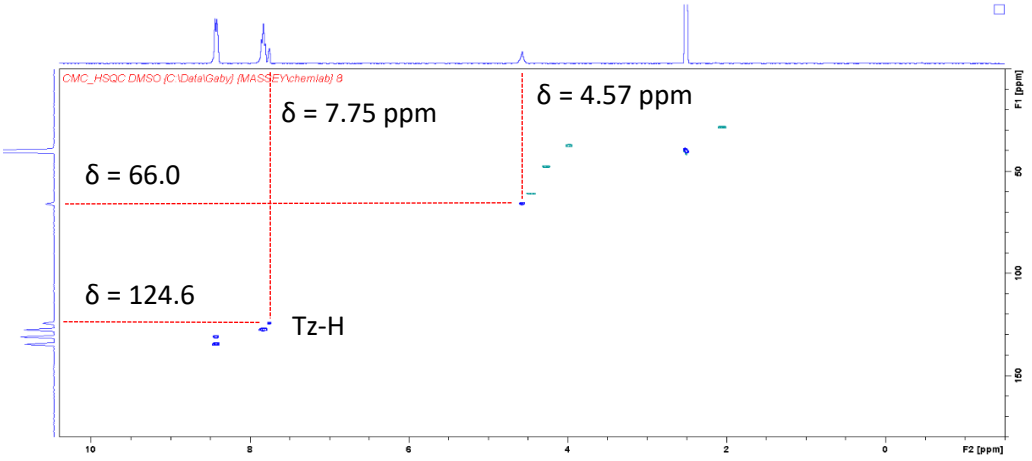

Figure S77. HSQC spectrum of $[Eu(L_2)_3]^{3-}$ *in DMSO-*d_6 *showing the interaction of the pyridyl-H singlet at 4.57 ppm with the pyridyl carbon at 66.0 ppm*

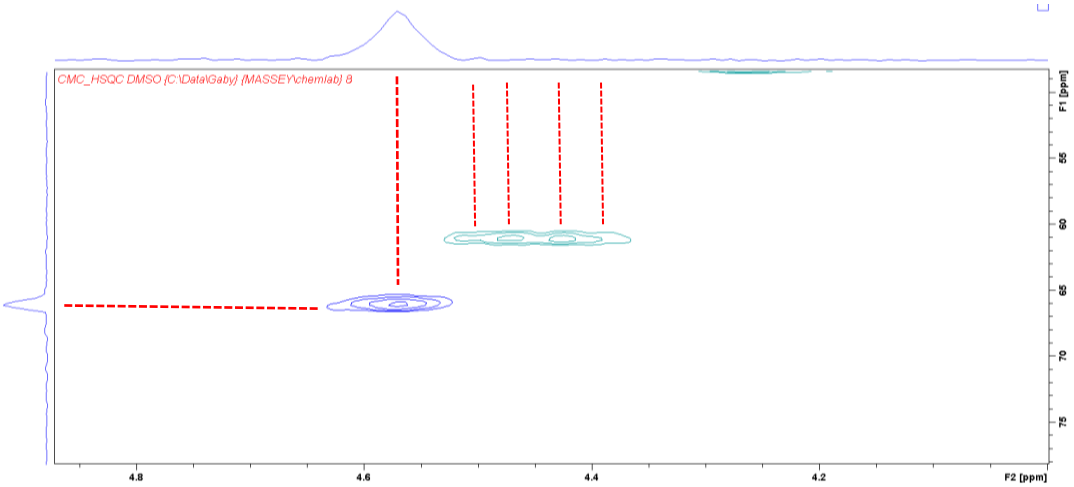

Figure S78. Zoom in on the COSY spectrum of ***[Eu(L$_2$)$_3$]$^{3-}$*** *in DMSO-d$_6$ showing the singlet pyridyl peak interacting with the pyridyl carbon peak and the superimposed multiplet interactions with a peak at a lower ppm when compared to the pyridyl carbon*

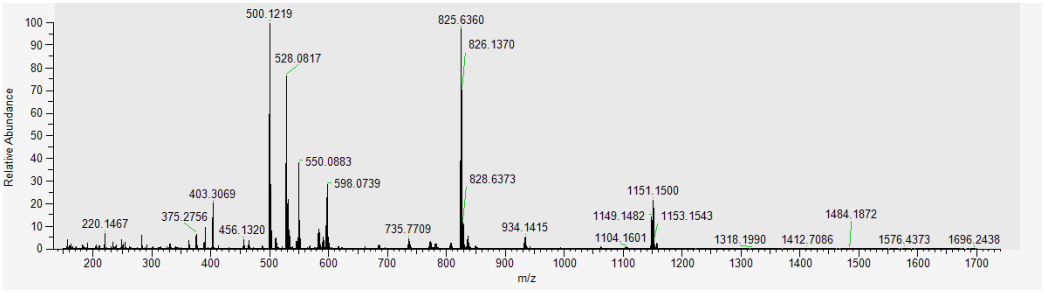

Figure S79. Full HRMS spectrum of ***[Eu(L$_2$)$_3$]$^{3-}$***

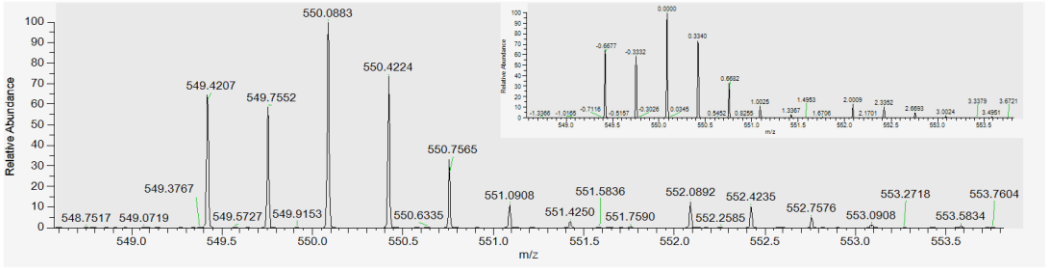

Figure S80. HRMS m/z = 550.0883 [Eu(L$_2$)$_3$]$^{3-}$ (calc. for [C$_{75}$H$_{51}$N$_{15}$O$_{21}$Eu]$^{3-}$, 550.0867 g mol^{-1}). (Insert) m/z labelled relative to the [Eu(L$_2$)$_3$]$^{3-}$ peak confirming the -3 charge

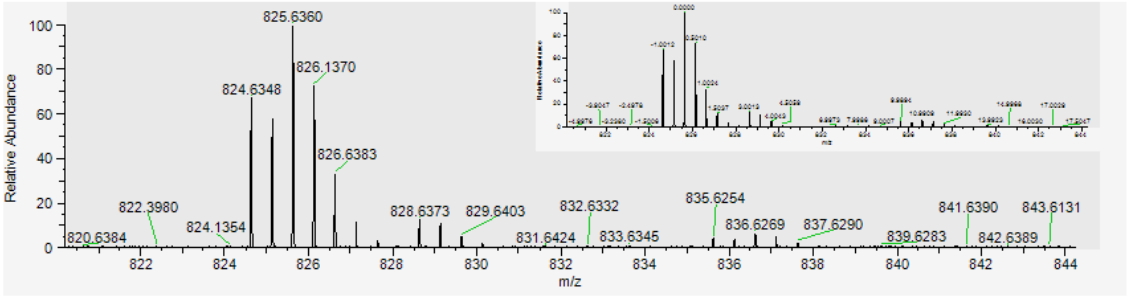

Figure S81. HRMS m/z = 825.6360 $\{[Eu(L_2)_3]^{3-} + H^+\}^{2-}$ (calc. for $\{[C_{75}H_{51}N_{15}O_{21}Eu]^{3-} + H^+\}^{2-}$, 825.6335 g mol^{-1}). (Insert) m/z labelled relative to the $\{[Eu(L_2)_3]^{3-} + H^+\}^{2-}$ peak confirming the -2 charge

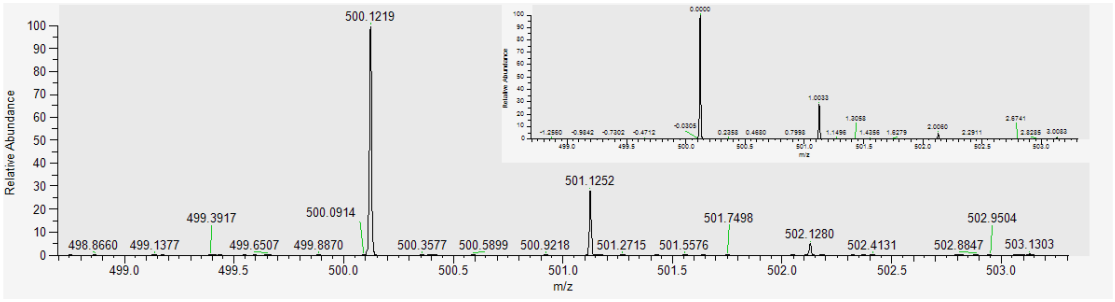

Figure S82. HRMS m/z = 500.1219 $\{(L_2)^{2-} + H^+\}^-$ (calc. for $\{(C_{25}H_{17}N_5O_7)^{2-} + H^+\}^-$, 500.1206 g mol^{-1}). (Insert) m/z labelled relative to the $\{(L_2)^{2-} + H^+\}^-$ peak confirming the -1 charge

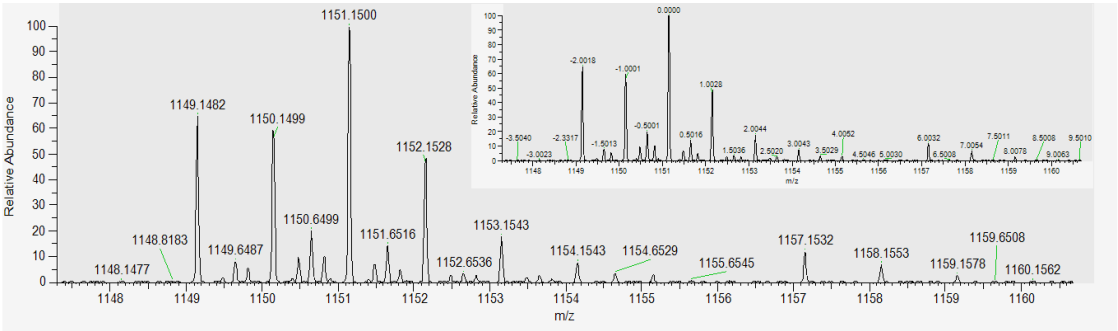

Figure S83. HRMS m/z = 1151.1500 $[Eu(L_2)_2]^-$ (calc. for $[C_{50}H_{34}N_{10}O_{14}Eu]^-$, 1151.147 g mol^{-1}). (Insert) m/z labelled relative to $[Eu(L_2)_2]^-$ peak showing the -1 charge

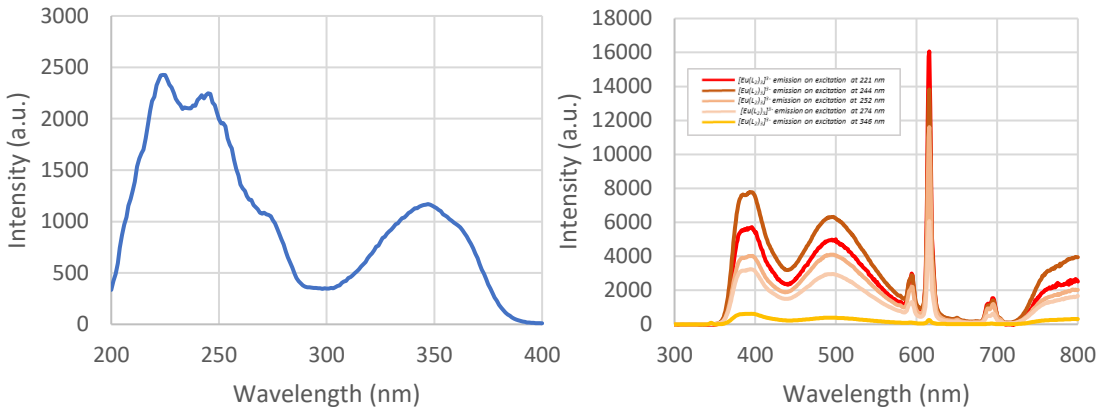

Figure S84. (Left) Fluorescence excitation spectrum (λ_{em} = 616 nm) of ***[Eu(L$_2$)$_3$]$^{3-}$*** *(1 x 10^{-5} M) in H$_2$O. (Right) Fluorescence emission spectrum (λ_{ex} = 221, 244, 252, 274 and 346 nm) of* ***[Eu(L$_2$)$_3$]$^{3-}$*** *(1 x 10^{-5} M) in H$_2$O*

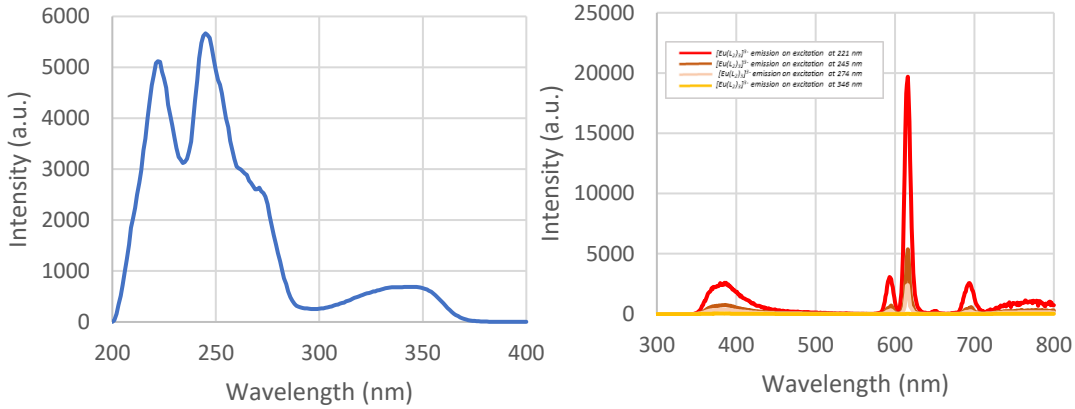

Figure S85. (Left) Fluorescence excitation spectrum (λ_{em} = 616 nm) of ***[Eu(L$_2$)$_3$]$^{3-}$*** *(1 x 10^{-5} M) in MeOH. For the fluorescence excitation measurement, the excitation and emission slit widths were both 3.0 nm. (Right) Fluorescence emission spectrum (λ_{ex} = 221, 245, 274 and 346 nm) of* ***[Eu(L$_2$)$_3$]$^{3-}$*** *(1 x 10^{-5} M) in MeOH. For the fluorescence emission measurements, excitation slit widths were 3.0 nm and emission slit widths ranged from 1.0 – 5.0 nm*

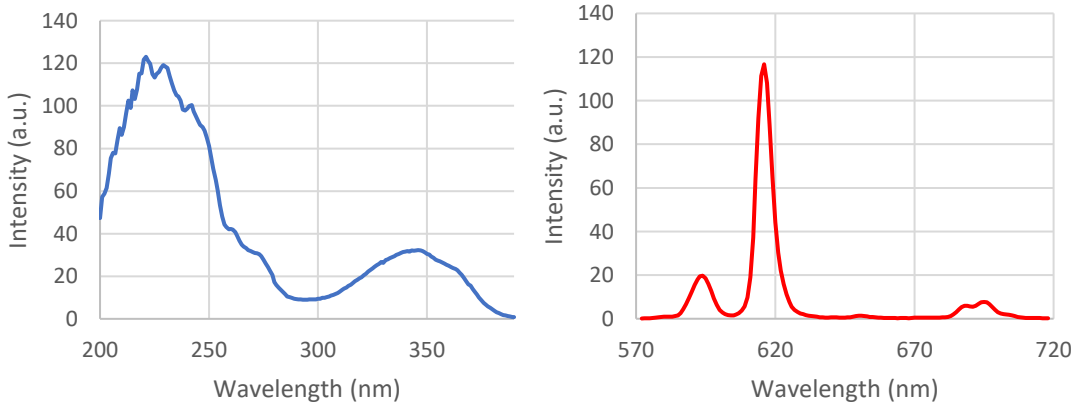

Figure S86. (Left) Phosphorescence excitation spectrum (λ_{em} = 616 nm) of ***[Eu(L$_2$)$_3$]$^{3-}$*** *(1 x 10^{-5} M) in H$_2$O. (Right) Phosphorescence emission spectrum (λ_{ex} = 279 nm) of* ***[Eu(L$_2$)$_3$]$^{3-}$*** *(1 x 10^{-5} M) in H$_2$O. For both the phosphorescence excitation and emission measurements, excitation and emission slit widths were 5.0 nm*

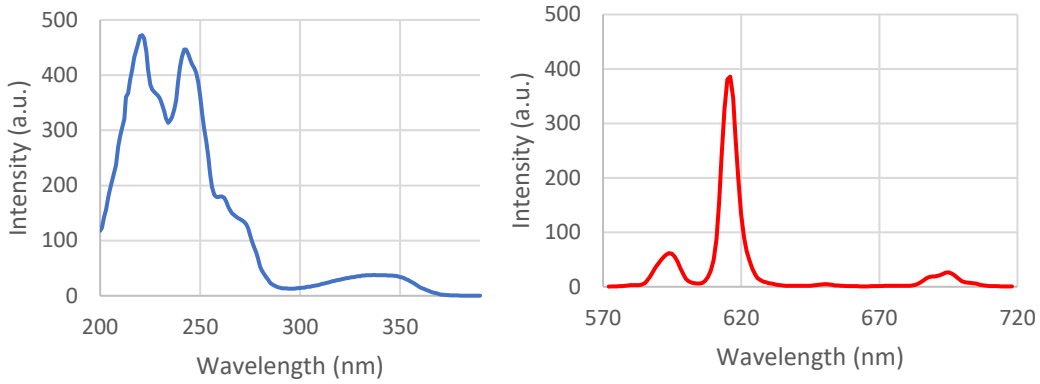

Figure S87. (Left) Phosphorescence excitation spectrum (λ_{em} = 616 nm) of ***[Eu(L$_2$)$_3$]$^{3-}$*** *(1 x 10^{-5} M) in MeOH. (Right) Phosphorescence emission spectrum (λ_{ex} = 279 nm) of* ***[Eu(L$_2$)$_3$]$^{3-}$*** *(1 x 10^{-5} M) in MeOH. For both the phosphorescence excitation and emission measurements, excitation and emission slit widths were 5.0 nm*

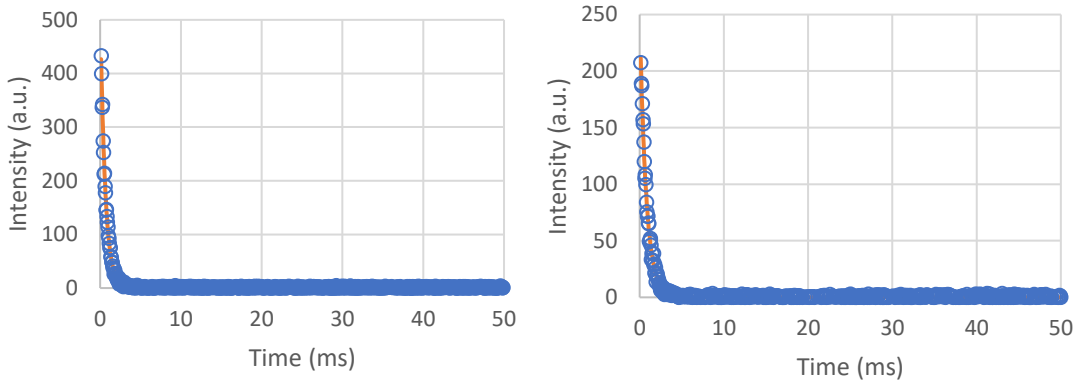

Figure S88. (Left) Intensity of the $^5D_0 \rightarrow {}^7F_2$ transition (λ_{em} = 616 nm) of ***[Eu(L$_2$)$_3$]$^{3-}$*** *(1 x 10^{-5} M) on excitation at 220 nm in H$_2$O (blue spots) with single exponential fit (orange line) for lifetime measurement. (Right). Intensity of the $^5D_0 \rightarrow {}^7F_2$ transition (λ_{em} = 616 nm) of* ***[Eu(L$_2$)$_3$]$^{3-}$*** *(1 x 10^{-5} M) on excitation at 220 nm in D$_2$O (blue spots) with single exponential fit (orange line) for lifetime measurement*

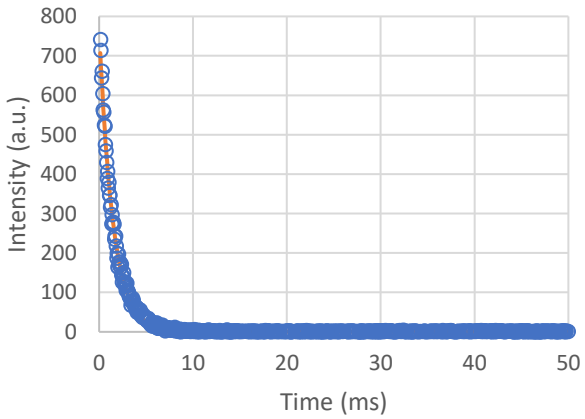

Figure S89. Intensity of the $^5D_0 \rightarrow {}^7F_2$ transition (λ_{em} = 616 nm) of ***[Eu(L$_2$)$_3$]$^{3-}$*** *(1 x 10^{-5} M) on excitation at 220 nm in MeOH (blue spots) with single exponential fit (orange line) for lifetime measurement*

Table S3. Lifetimes of the $^5D_0 \rightarrow {}^7F_2$ transition (λ_{em} = 616 nm) recorded for ***[Eu(L$_2$)$_3$]$^{3-}$*** *on excitation at 220 nm in H_2O, D_2O and MeOH*

Solvent	Lifetime (ms)	Standard deviation
H_2O	0.607 ± 0.0	2.1552
D_2O	0.769 ± 0.0	1.5646
MeOH	1.449 ± 0.0	4.8112

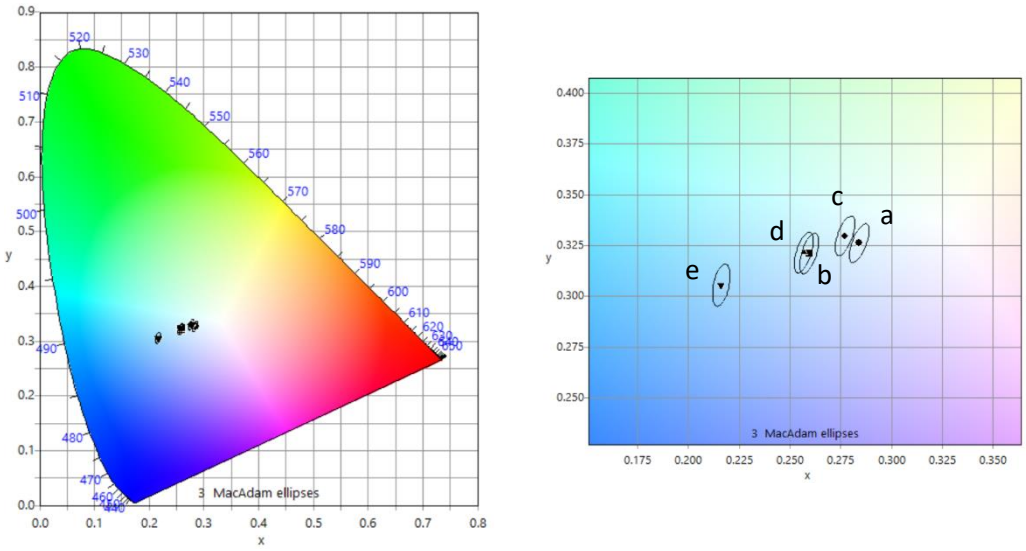

Figure S90. (Left) 1931 CIE plot for ***[Eu(L$_2$)$_3$]$^{3-}$*** *in H_2O. (Right) Zoomed in 1931 CIE plot showing the CIE coordinates calculated for* ***[Eu(L$_2$)$_3$]$^{3-}$*** *in H_2O on excitation at 221 (a), 224 (b), 252 (c), 274 (d) and 346 (e) nm*

Table S4. CIE coordinates calculated for $[Eu(L_2)_3]^{3-}$ *in* H_2O *on excitation at different wavelengths*

Excitation wavelength (nm)	CIE coordinates	
	x	y
221	0.2841	0.3262
224	0.2595	0.3211
252	0.2771	0.3298
274	0.2568	0.3216
346	0.2162	0.3055

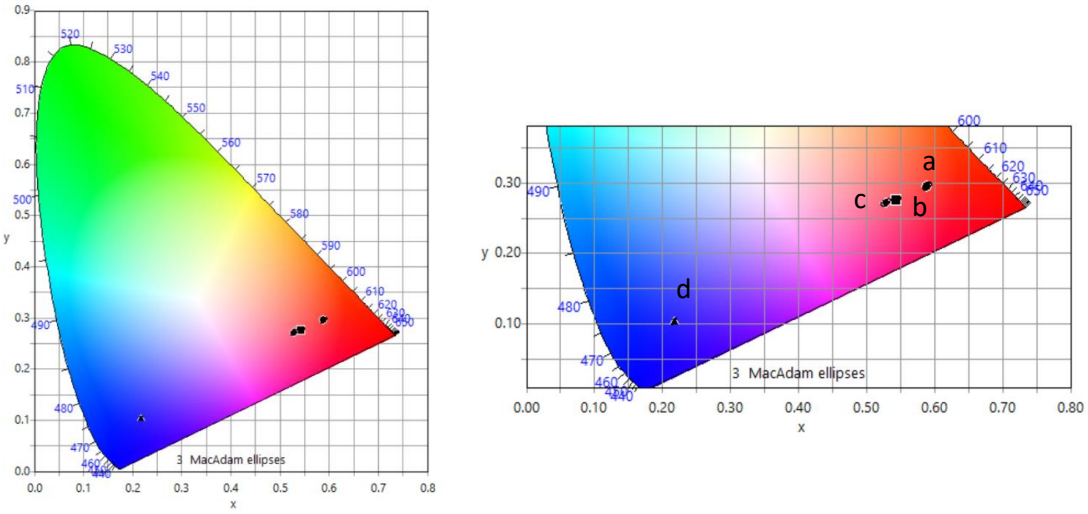

Figure S91. (Left) 1931 CIE plot for $[Eu(L_2)_3]^{3-}$ *in MeOH. (Right) Zoomed in 1931 CIE plot showing the CIE coordinates calculated for* $[Eu(L_2)_3]^{3-}$ *in MeOH on excitation at 221 (a), 245 (b), 274 (c) and 346 (d) nm*

Table S5. CIE coordinates calculated for $[Eu(L_2)_3]^{3-}$ *in MeOH on excitation at different wavelengths*

Excitation wavelength (nm)	CIE coordinates	
	x	y
221	0.5890	0.2955
245	0.5437	0.2756
274	0.5287	0.2722
346	0.2176	0.1032

$[Tb(L_2)_3]^{3-}$

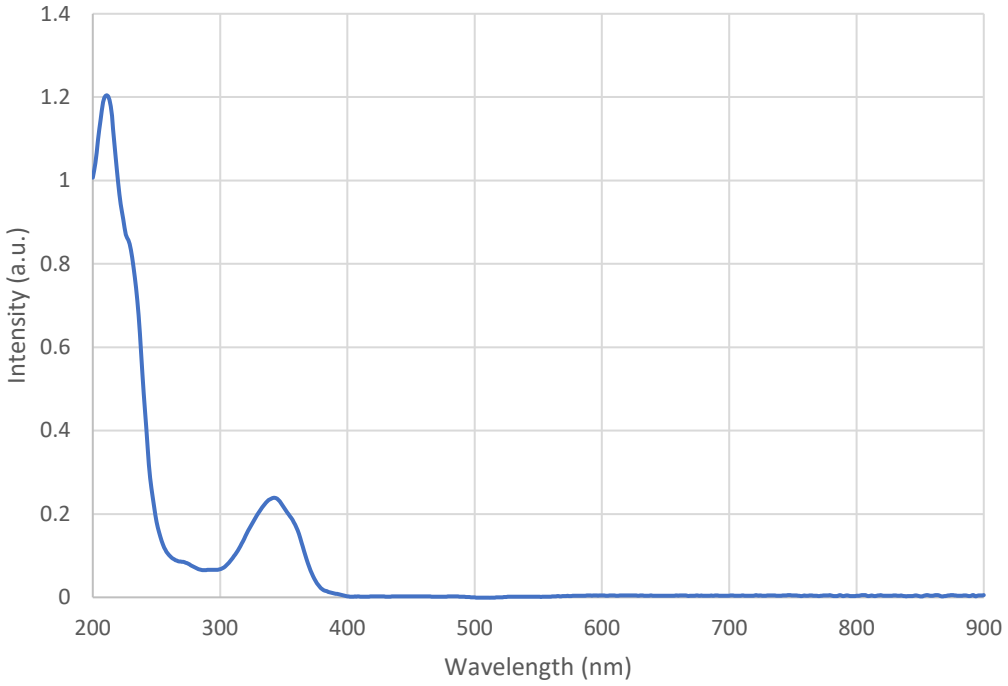

Figure S92. UV/Vis spectrum of ***$[Tb(L_2)_3]^{3-}$*** *(1 x 10^{-5} M) in H_2O*

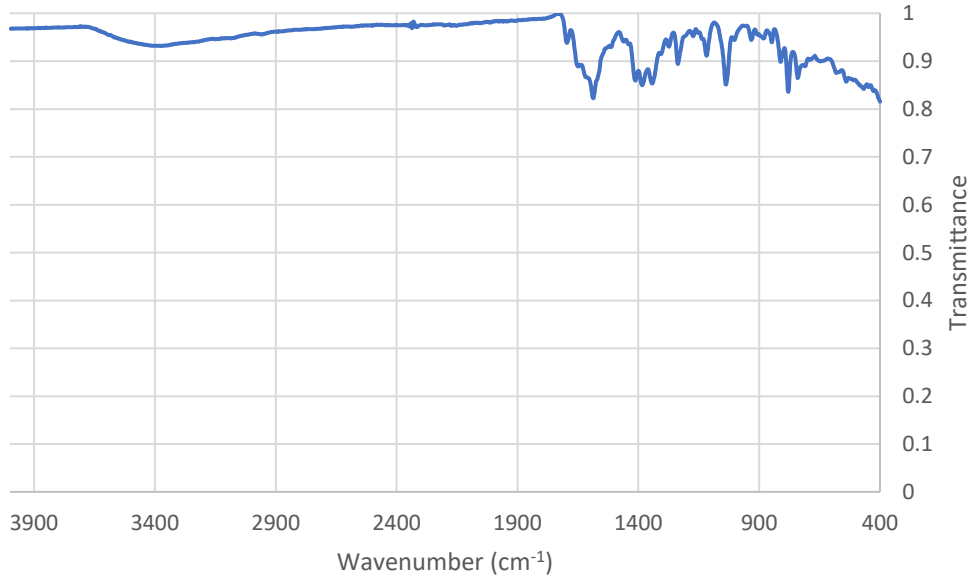

Figure S93. FTIR spectrum of ***$[Tb(L_2)_3]^{3-}$***

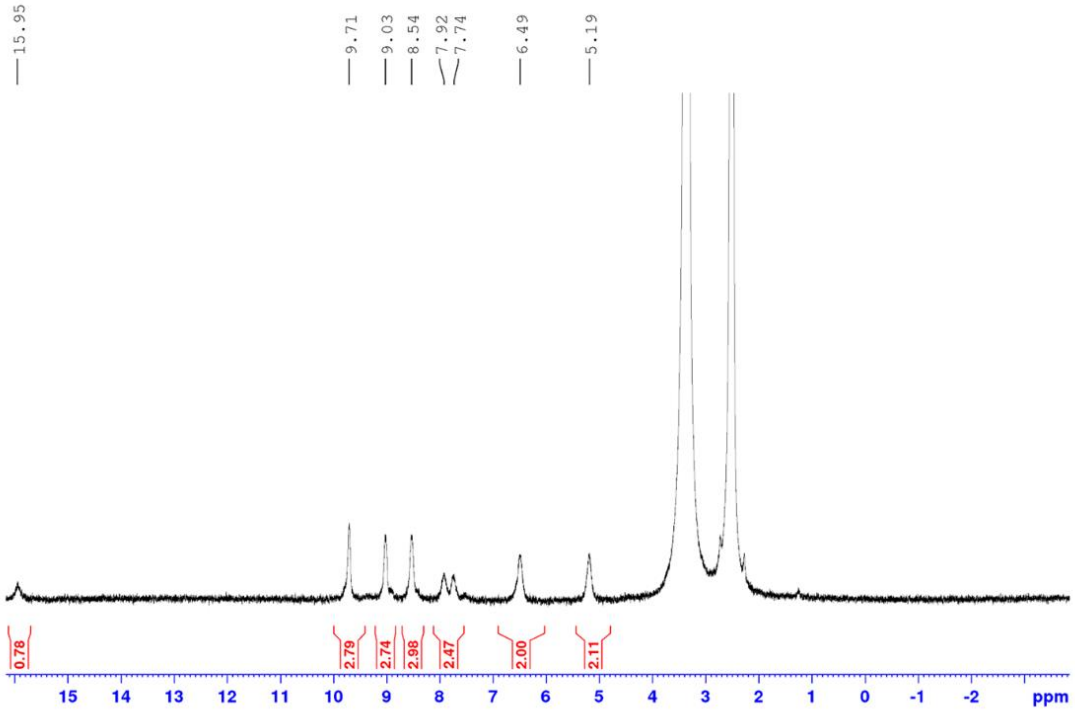

Figure S94. ^{1}H NMR spectrum of $\mathbf{[Tb(L_2)_3]^{3-}}$ *in DMSO-d_6*

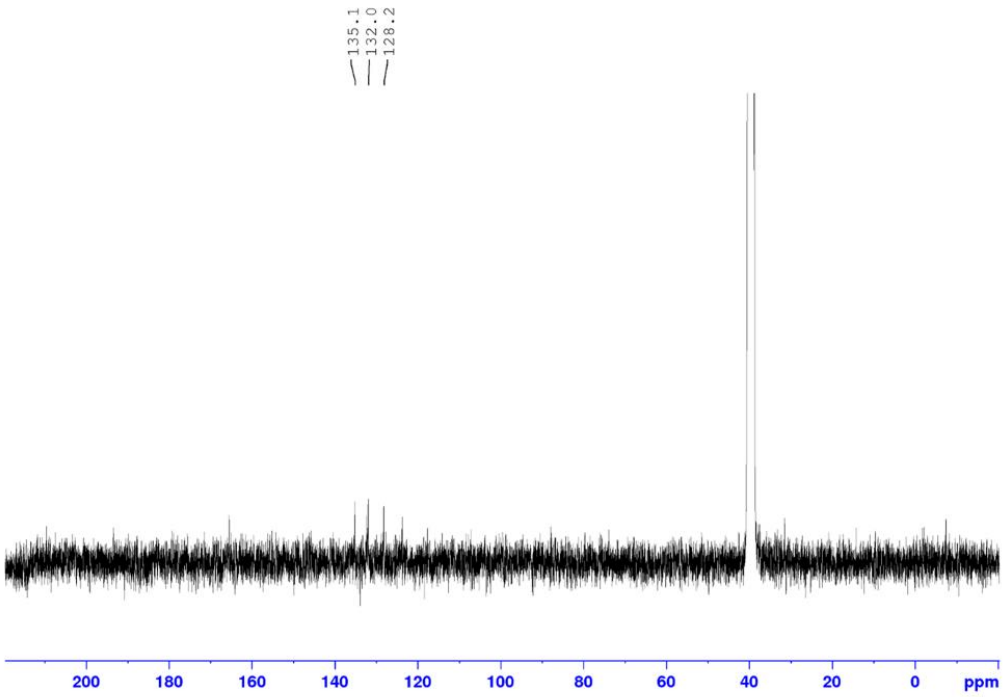

Figure S95. ^{13}C NMR spectrum of $\mathbf{[Tb(L_2)_3]^{3-}}$ *in DMSO-d_6*

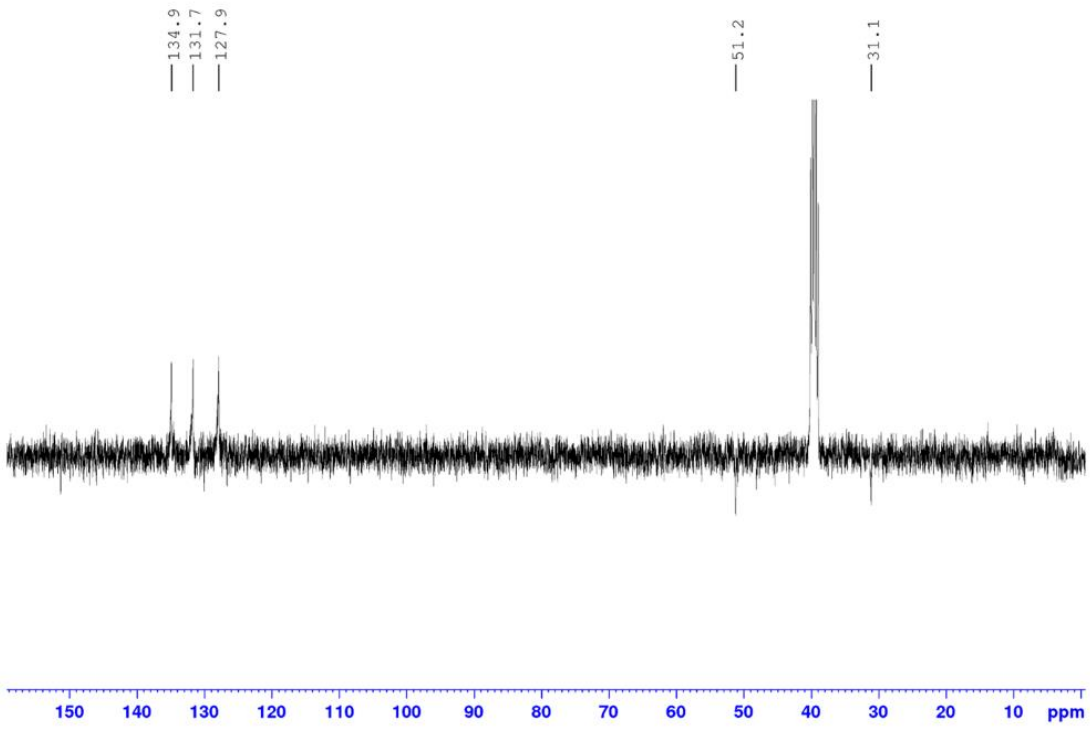

Figure S96. ^{13}C DEPT spectrum of ***[Tb(L$_2$)$_3$]$^{3-}$*** *in DMSO-d$_6$*

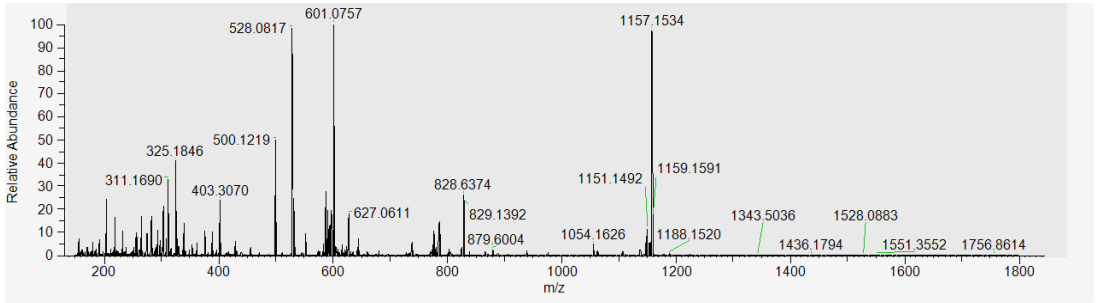

Figure S97. Full HRMS spectrum of ***[Tb(L$_2$)$_3$]$^{3-}$***

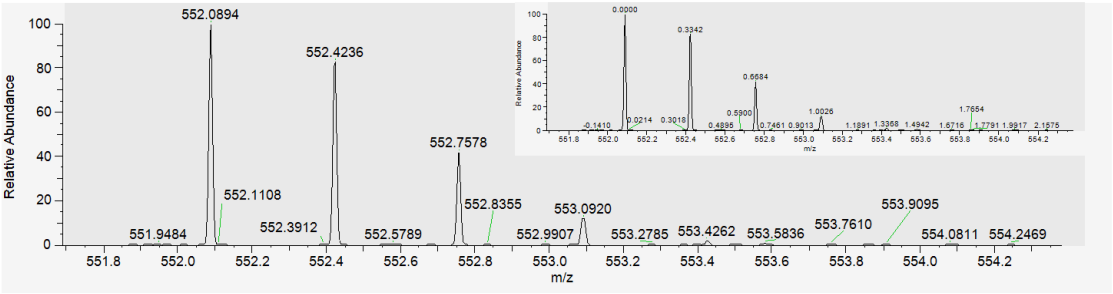

Figure S98. HRMS m/z 552.0894 [Tb(L$_2$)$_3$]$^{3-}$ (calc. for [C$_{75}$H$_{51}$N$_{15}$O$_{21}$Tb]$^{3-}$, 552.0880 g mol^{-1}). (Insert) m/z labelled relative to the [Tb(L$_2$)$_3$]$^{3-}$ peak confirming the -3 charge

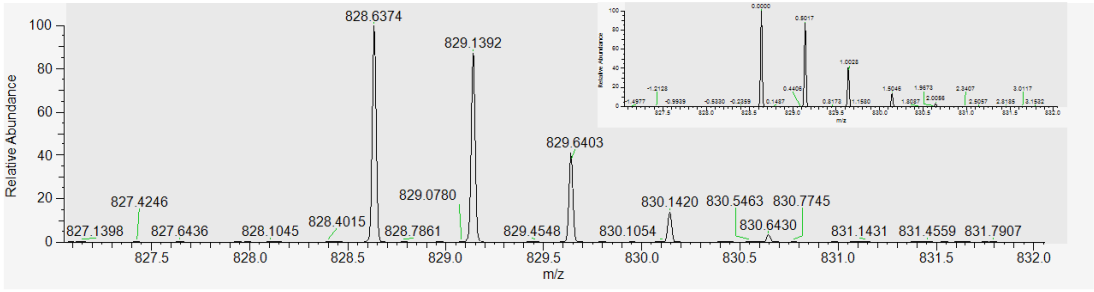

Figure S99. HRMS m/z 828.6374 $\{[Tb(L_2)_3]^{3-} + H^+\}^{2-}$ (calc. for $\{[C_{75}H_{51}N_{15}O_{21}Tb]^{3-} + H^+\}^{2-}$, 828.6360 g mol^{-1}). (Insert) m/z labelled relative to the $\{[Tb(L_2)_3]^{3-} + H^+\}^{2-}$ peak confirming the -2 charge

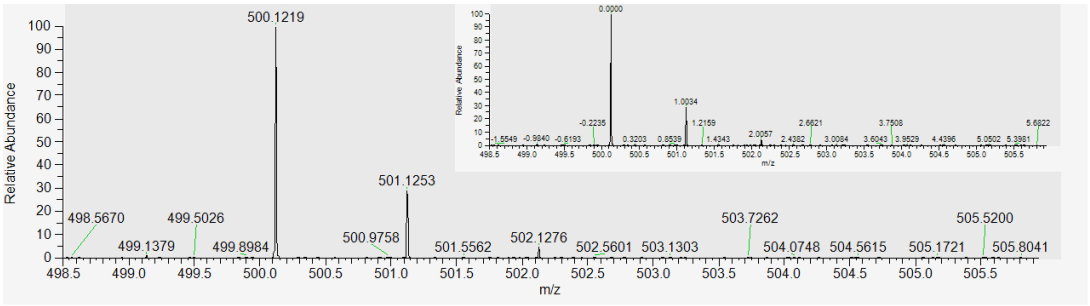

Figure S100. HRMS m/z = 500.1219 $\{(L_2)^{2-} + H^+\}^-$ (calc. for $\{(C_{25}H_{17}N_5O_7)^{2-} + H^+\}^-$, 500.1206 g mol^{-1}). (Insert) m/z labelled relative to the $\{(C_{25}H_{17}N_5O_7)^{2-} + H^+\}^-$ peak confirming the -1 charge

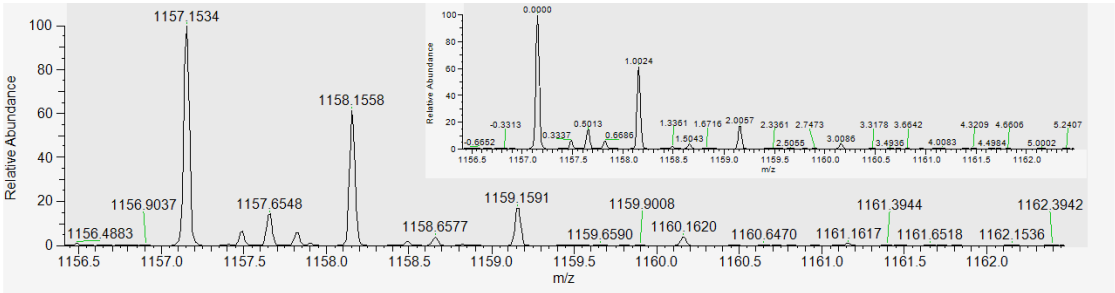

Figure S101. HRMS m/z 1157.1534 $[Tb(L_2)_2]^-$ (calc. for $[C_{50}H_{34}N_{10}O_{14}Tb]^-$, 1157.1510 g mol^{-1}). (Insert) m/z labelled relative to the $[Tb(L_2)_2]^-$ peak confirming the -1 charge

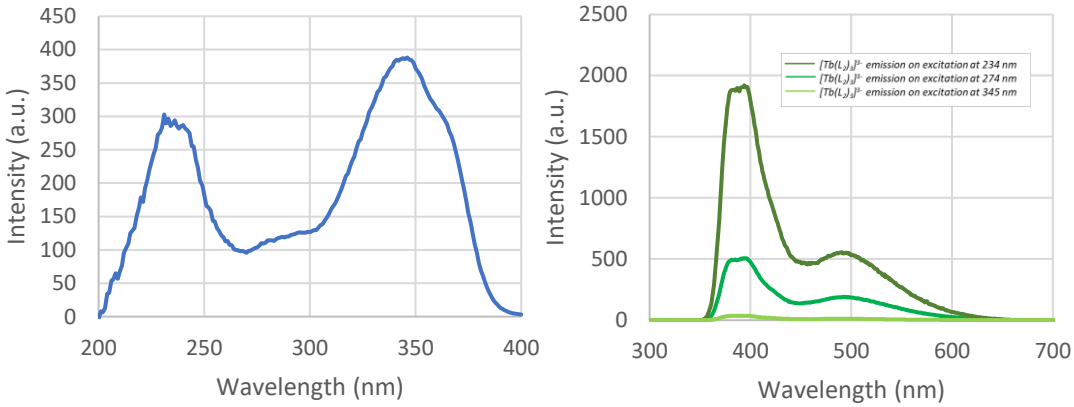

Figure S102. (Left) Fluorescence excitation spectrum (λ_{em} = 545 nm) of ***[Tb(L$_2$)$_3$]$^{3-}$*** *(1 x 10^{-5} M) in H$_2$O. For the fluorescence excitation measurement, excitation and emission slit widths were both 3.0 nm. (Right) Fluorescence emission spectrum (λ_{ex} = 234, 274 and 345 nm) of* ***[Tb(L$_2$)$_3$]$^{3-}$*** *(1 x 10^{-5} M) in H$_2$O. For the fluorescence emission measurements, excitation and emission slit widths were also both 3.0 nm except for the case of* ***[Tb(L$_2$)$_3$]$^{3-}$*** *on excitation at 345 nm whereby the excitation and emission slit widths were 3.0 and 1.0 nm (respectively)*

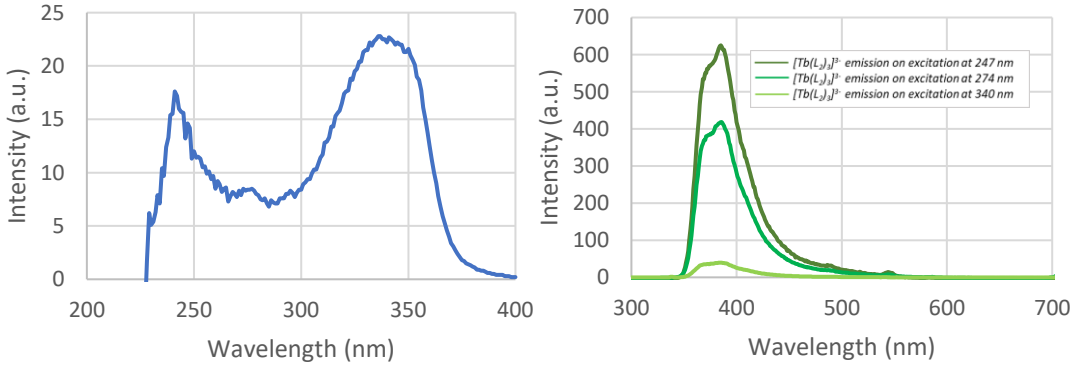

Figure S103. (Left) Fluorescence excitation spectrum (λ_{em} = 545 nm) of ***[Tb(L$_2$)$_3$]$^{3-}$*** *(1 x 10^{-5} M) in MeOH. For the fluorescence excitation measurement, the excitation and emission slit widths were both 3.0 nm. (Right) Fluorescence emission spectrum (λ_{ex} = 247, 274 and 340 nm) of* ***[Tb(L$_2$)$_3$]$^{3-}$*** *(1 x 10^{-5} M) in MeOH. For the fluorescence emission measurements, excitation and emission slit widths were also both 3.0 nm except for the case of* ***[Tb(L$_2$)$_3$]$^{3-}$*** *on excitation at 340 nm whereby the excitation and emission slit widths were 3.0 and 1.0 nm (respectively)*

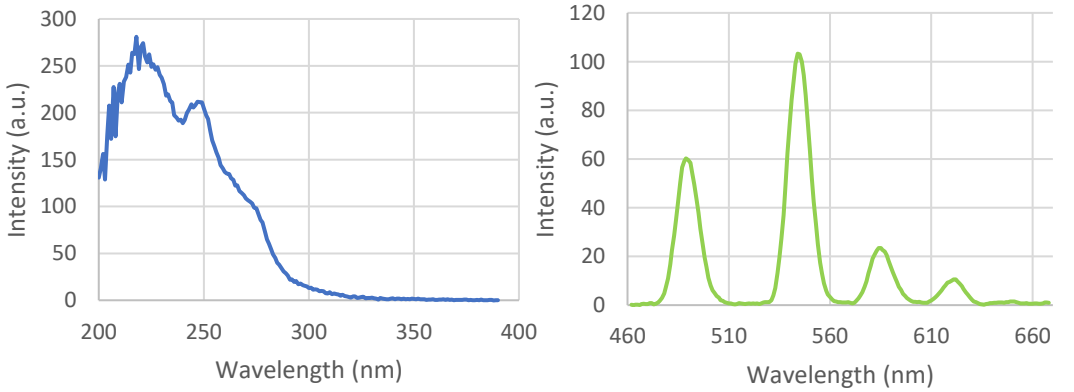

Figure S104. (Left) Phosphorescence excitation spectrum (λ_{em} = 545 nm) of ***[Tb(L$_2$)$_3$]$^{3-}$*** *(1 x 10^{-5} M) in H$_2$O. (Right) Phosphorescence emission spectrum (λ_{ex} = 274 nm) of* ***[Tb(L$_2$)$_3$]$^{3-}$*** *(1 x 10^{-5} M) in H$_2$O. For both the phosphorescence excitation and emission measurements, excitation and emission slit widths were 10.0 nm*

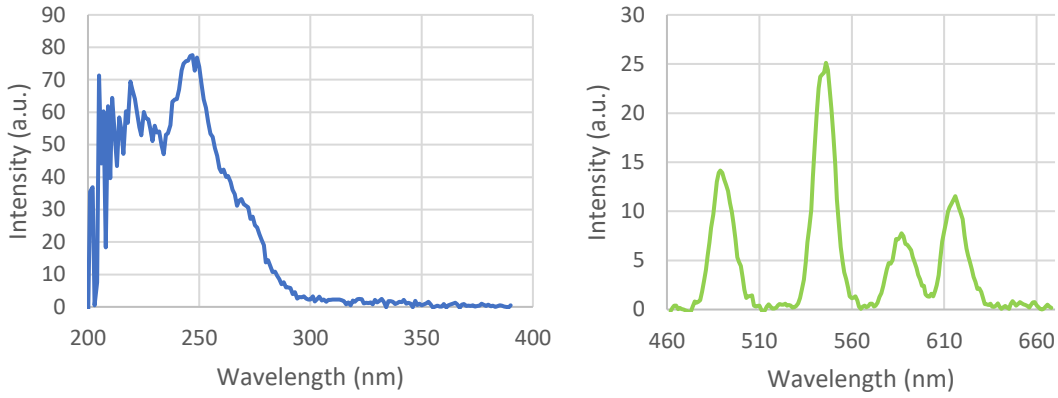

Figure S105. (Left) Phosphorescence excitation spectrum (λ_{em} = 545 nm) of ***[Tb(L$_2$)$_3$]$^{3-}$*** *(1 x 10^{-5} M) in MeOH. (Right) Phosphorescence emission spectrum (λ_{ex} = 274 nm) of* ***[Tb(L$_2$)$_3$]$^{3-}$*** *(1 x 10^{-5} M) in MeOH. For both the phosphorescence excitation and emission measurements, excitation and emission slit widths were 5.0 nm*

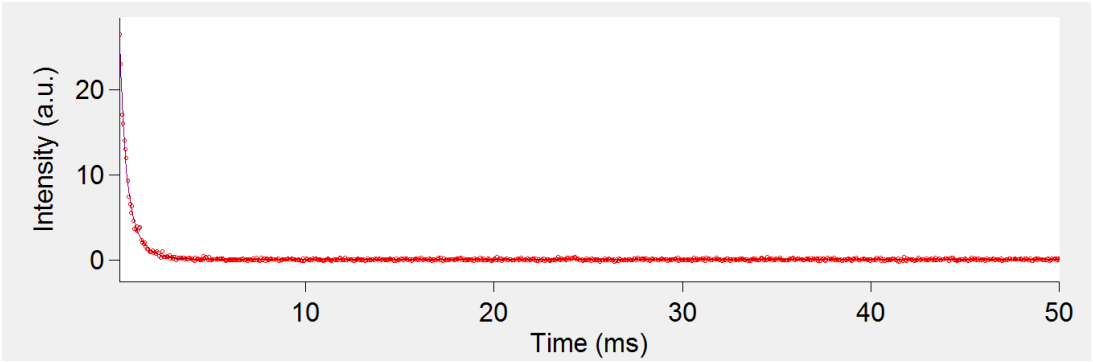

Figure S106. Intensity of the $^5D_4 \rightarrow {}^7F_5$ transition (λ_{em} = 545 nm) of ***[Tb(L$_2$)$_3$]$^{3-}$*** *(1 x 10^{-5} M) on excitation at 247 nm in H2O (red spots) with double exponential fit (purple line) for lifetime measurement*

Table S6. Lifetimes of the $^5D_4 \rightarrow {}^7F_5$ transition (λ_{em} = 545 nm) recorded for ***[Tb(L$_2$)$_3$]$^{3-}$*** *on excitation at 247 nm in H_2O*

Run number	**Lifetime (ms)**	
	Tau1	**Tau2**
1	0.697 ± 0.1	0.257 ± 0.0
2	0.622 ± 0.0	0.206 ± 0.0
3	0.567 ± 0.0	0.161 ± 0.0
Average lifetime	0.629	0.208

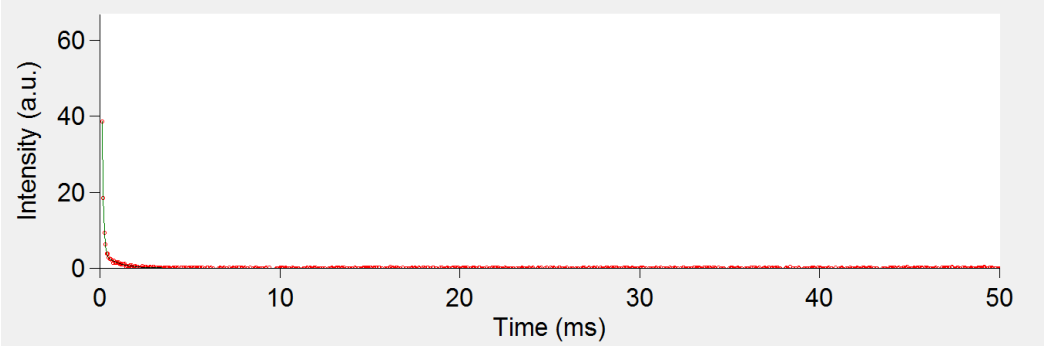

*Figure S107. Intensity of the $^5D_4 \rightarrow {}^7F_5$ transition (λ_{em} = 545 nm) of **$[Tb(L_2)_3]^{3-}$** (1×10^{-5} M) on excitation at 247 nm in MeOH (red spots) with double exponential fit (green line) for lifetime measurement*

*Table S7. Lifetimes of the $^5D_4 \rightarrow {}^7F_5$ transition (λ_{em} = 545 nm) recorded for **$[Tb(L_2)_3]^{3-}$** on excitation at 247 nm in MeOH*

Run number	Lifetime (ms)	
	Tau1	Tau2
1	0.772 ± 0.0	0.070 ± 0.0
2	0.742 ± 0.0	0.068 ± 0.0
3	0.794 ± 0.1	0.073 ± 0.0
Average lifetime	0.769	0.070

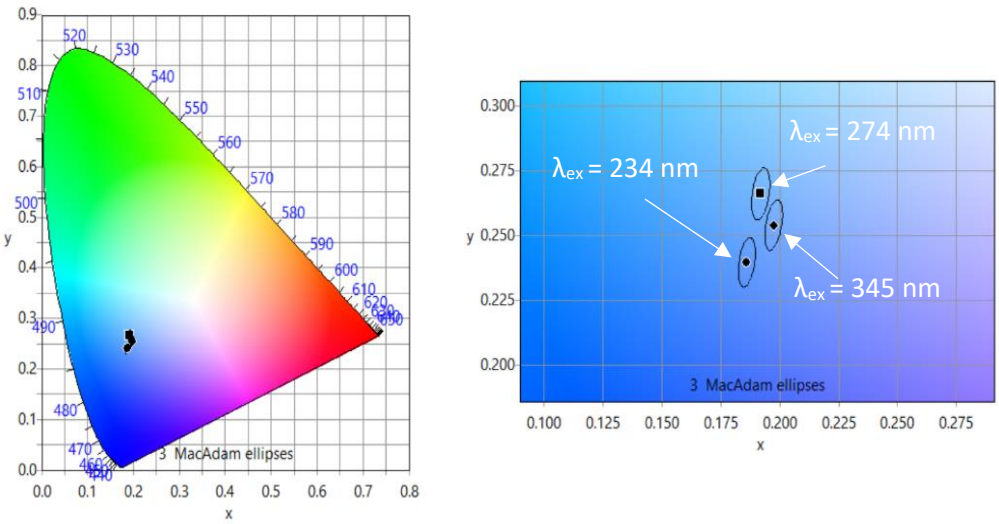

*Figure S108. (Left) 1931 CIE plot for **$[Tb(L_2)_3]^{3-}$** in H_2O. (Right) Zoomed in 1931 CIE plot showing the CIE coordinates calculated for **$[Tb(L_2)_3]^{3-}$** in H_2O on excitation at 234, 274 and 345 nm*

Table S8. CIE coordinates calculated for $[Tb(L_2)_3]^{3-}$ *in* H_2O *on excitation at different wavelengths*

Excitation wavelength (nm)	CIE coordinates	
	x	y
234	0.1861	0.2397
274	0.1920	0.2662
345	0.1975	0.2541

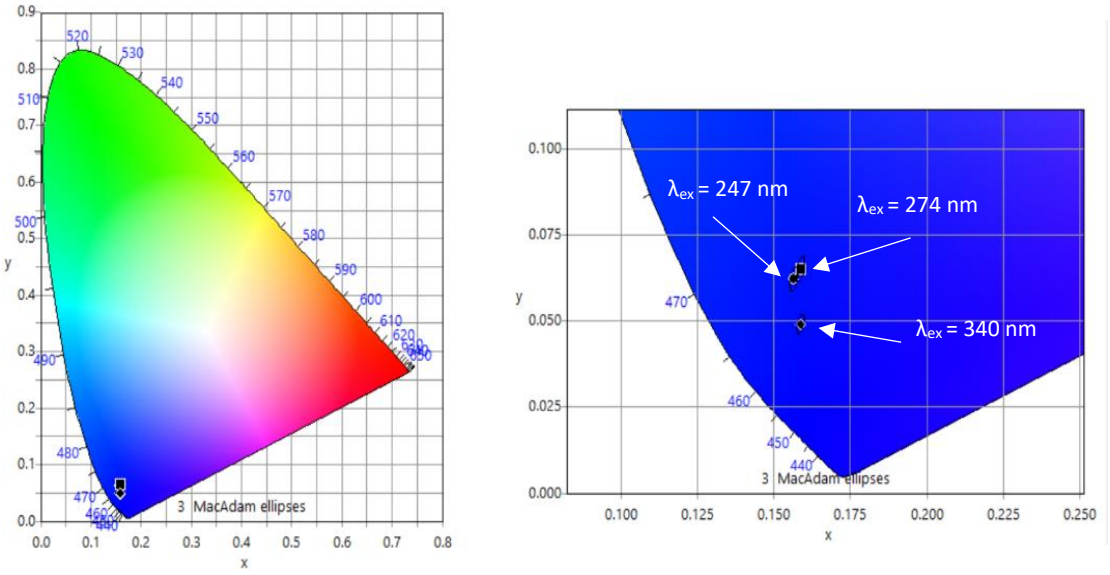

Figure S109. (Left) 1931 CIE plot for $[Tb(L_2)_3]^{3-}$ *in MeOH. (Right) Zoomed in 1931 CIE plot showing the CIE coordinates calculated for* $[Tb(L_2)_3]^{3-}$ *in MeOH on excitation at 247, 274 and 340 nm*

Table S9. CIE coordinates calculated for $[Tb(L_2)_3]^{3-}$ *in MeOH on excitation at different wavelengths*

Excitation wavelength (nm)	CIE coordinates	
	x	y
247	0.1566	0.0623
274	0.1588	0.0651
340	0.1588	0.0491

$[La(L_2*)_3]^{3-}$

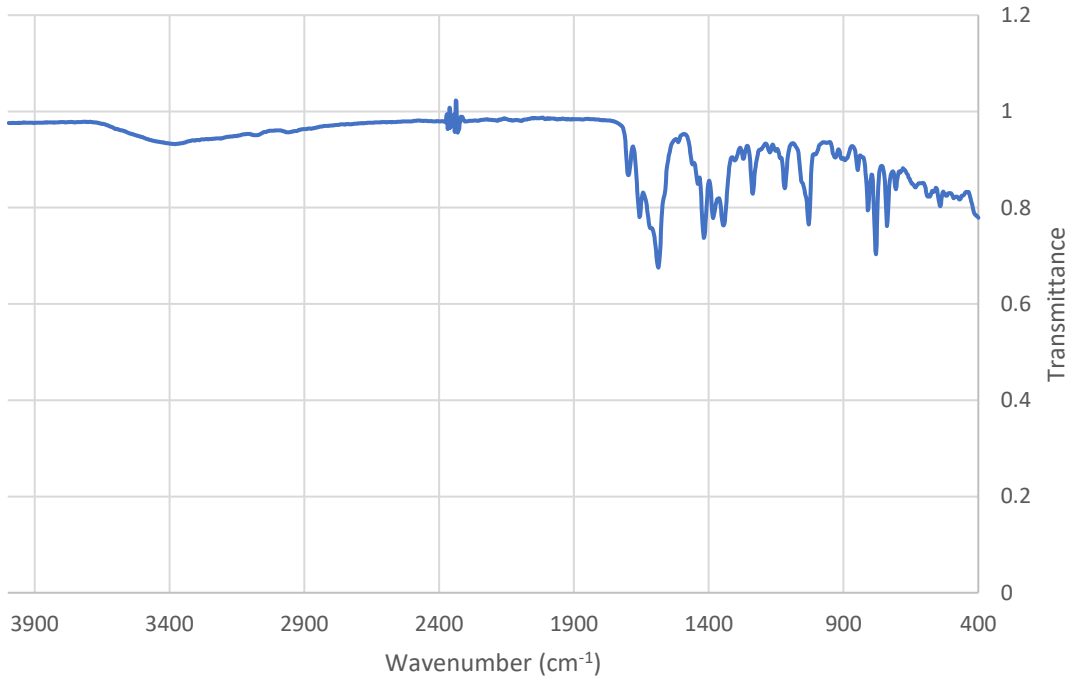

Figure S110. FTIR spectrum of ***$[La(L_2*)_3]^{3-}$***

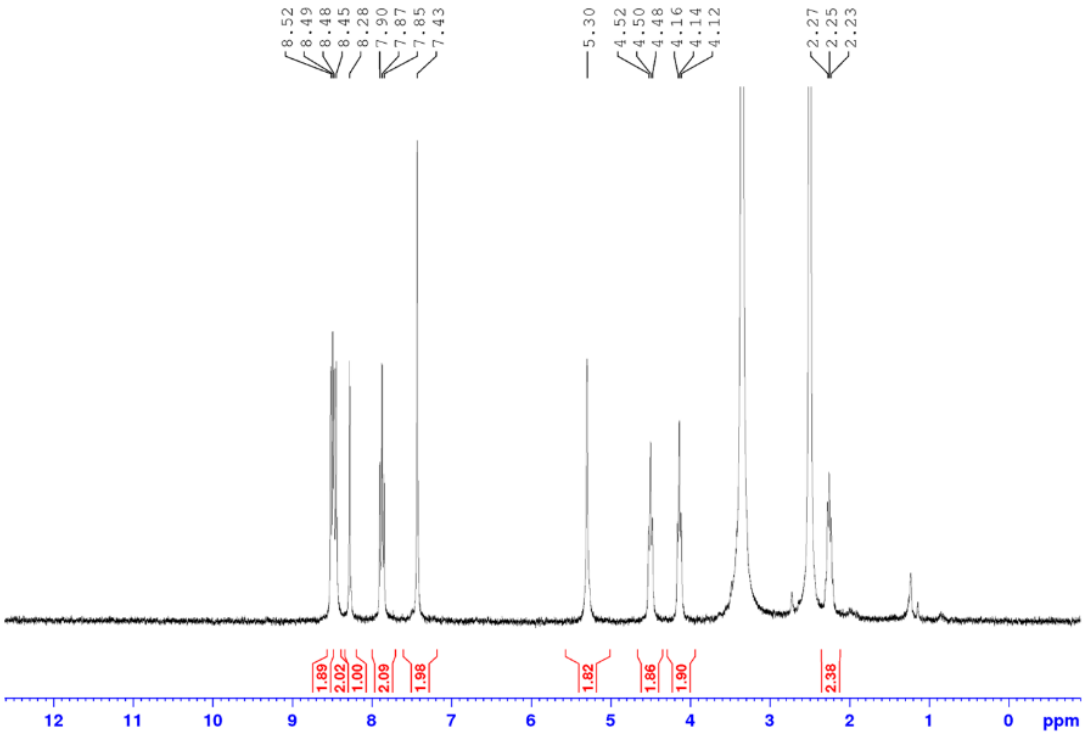

Figure S111. ^1H NMR spectrum of ***$[La(L_2*)_3]^{3-}$*** *in DMSO-d_6*

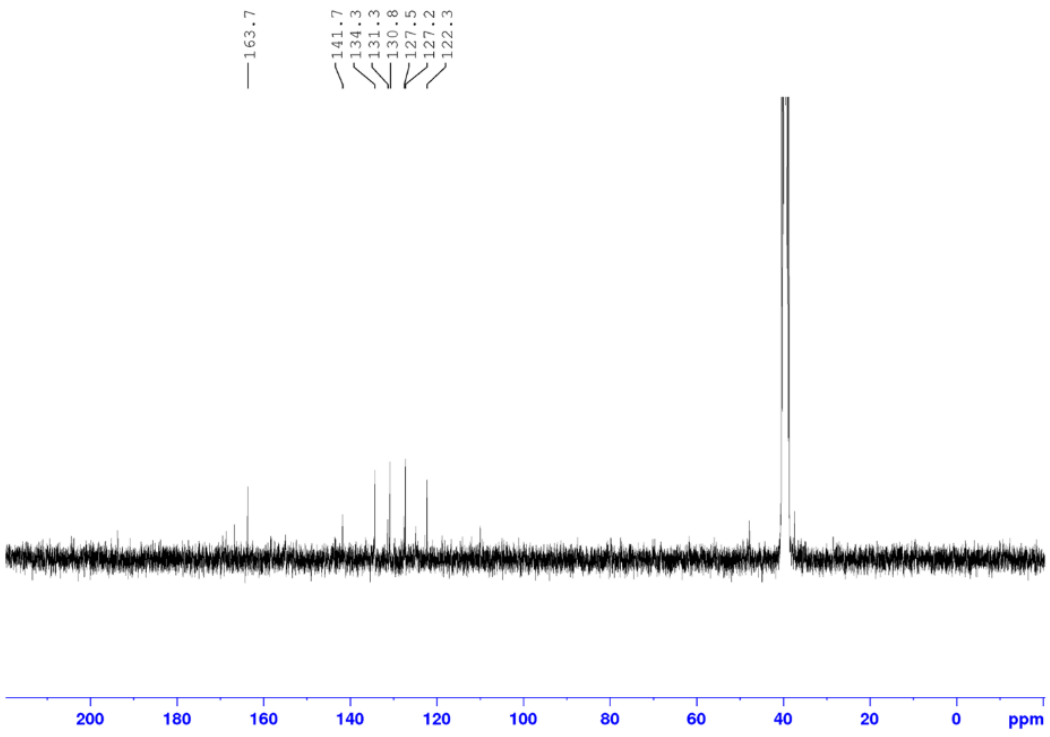

Figure S112. ^{13}C NMR spectrum of ***[La(L$_2$*)$_3$]$^{3-}$*** *in DMSO-d$_6$*

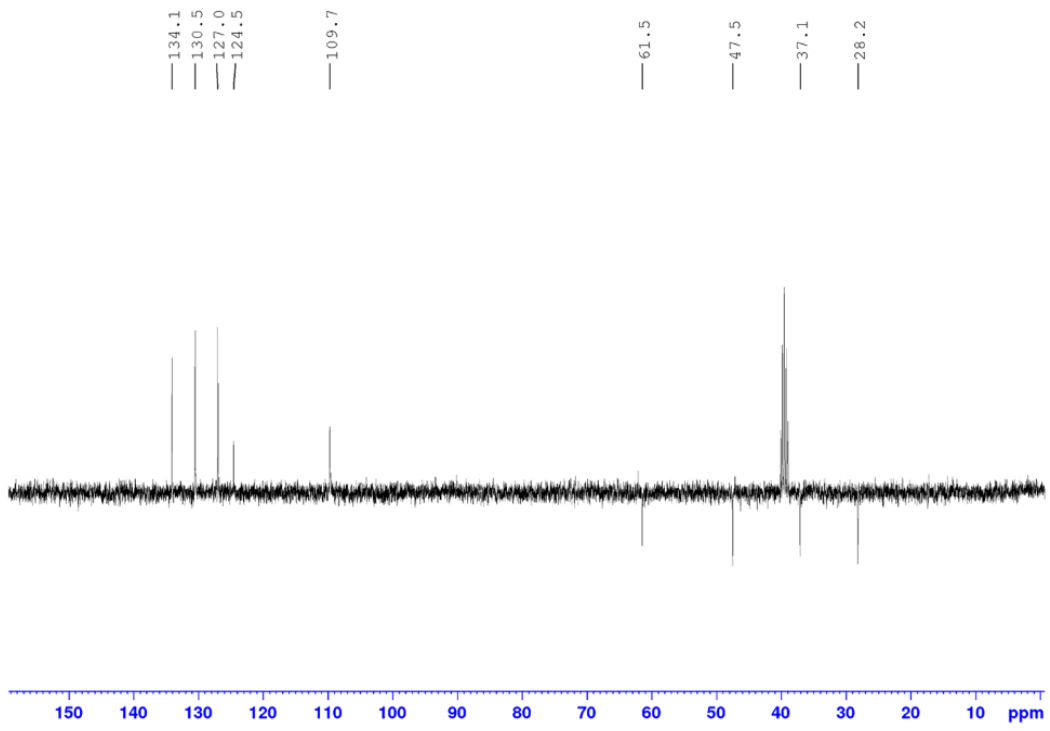

Figure S113. ^{13}C DEPT spectrum of ***[La(L$_2$*)$_3$]$^{3-}$*** *in DMSO-d$_6$*

$[Eu(L_2*)_3]^{3-}$

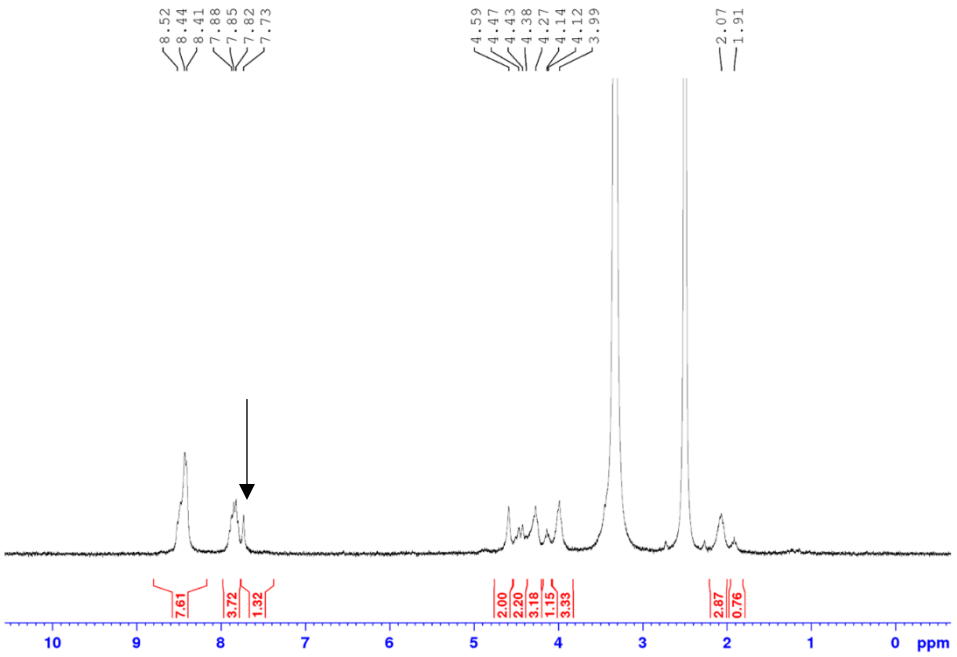

Figure S114. ^{1}H NMR spectrum of crude $[Eu(L_2*)_3]^{3-}$ in DMSO-d_6

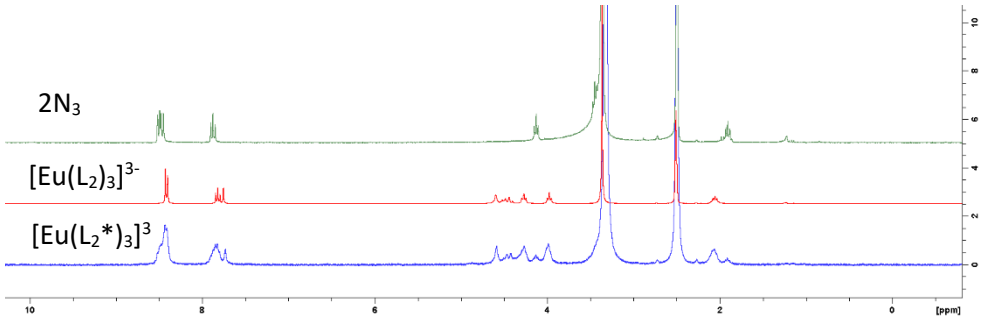

Figure S115. ^{1}H NMR spectrum of crude $[Eu(L_2*)_3]^{3-}$ (blue, bottom) compared to that of $[Eu(L_2)_3]^{3-}$ (red, middle) and $2N_3$ (green, top) in DMSO-d_6 showing that peaks for $[Eu(L_2)_3]^{3-}$ line up with some of those for $[Eu(L_2*)_3]^{3-}$ (although broad). There are also peaks suggestive of $2N_3$ impurities. This suggested that the CuAAC reaction on $[Eu(L_1)_3]^{3-}$ worked but required purification

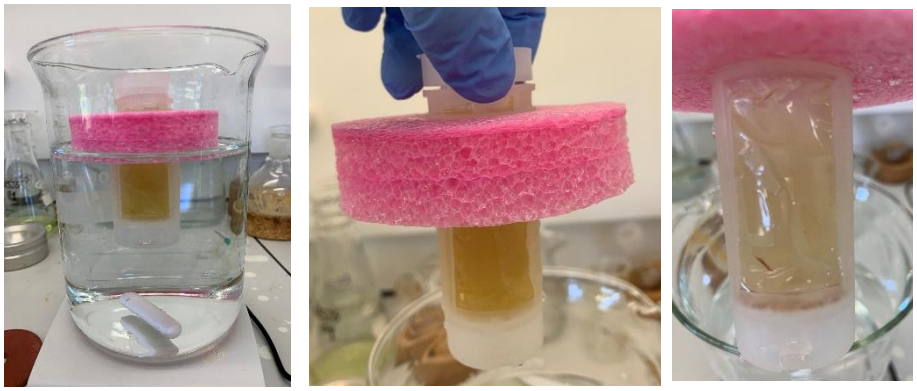

Figure S116. (Left) Dialysis experimental setup. (Middle) Dialysis tube containing crude $[Eu(L_2*)_3]^{3-}$ in 20 mL deionised H_2O before dialysis. (Right) Dialysis tube containing crude $[Eu(L_2*)_3]^{3-}$ in 20 mL deionised H_2O after dialysis

1-(azidomethyl)-3,5-di-*tert*-butylbenzene (3N$_3$)

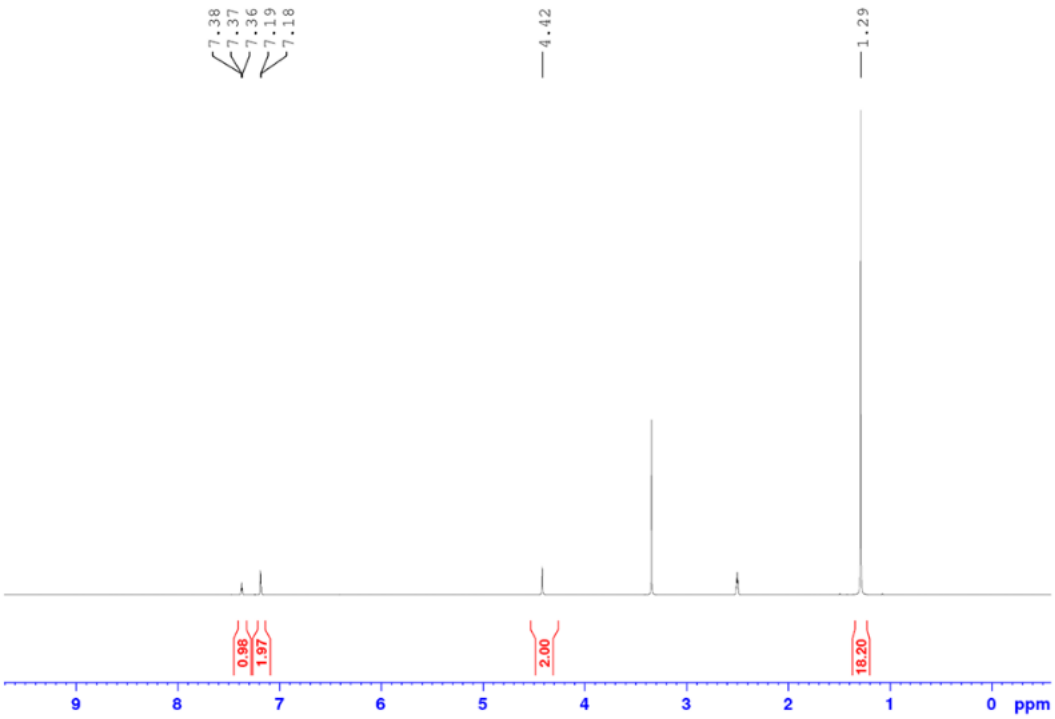

*Figure S117. ^{1}H NMR spectrum of **3N$_3$** in DMSO-d$_6$*

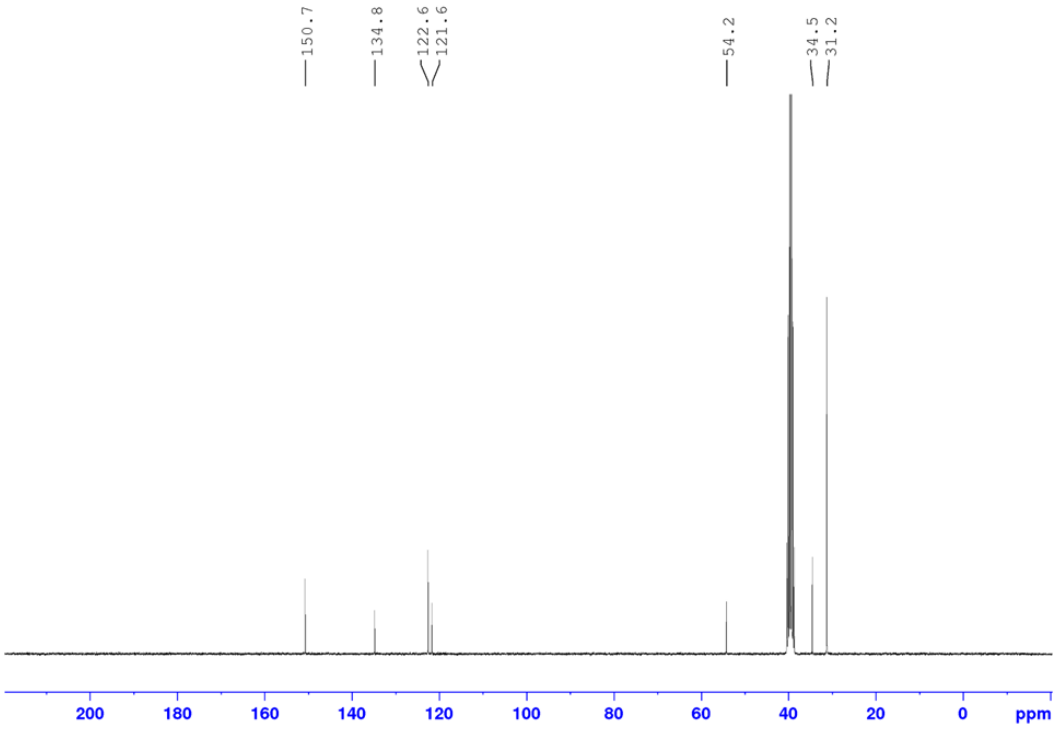

*Figure S118. ^{13}C NMR spectrum of **3N$_3$** in DMSO-d$_6$*

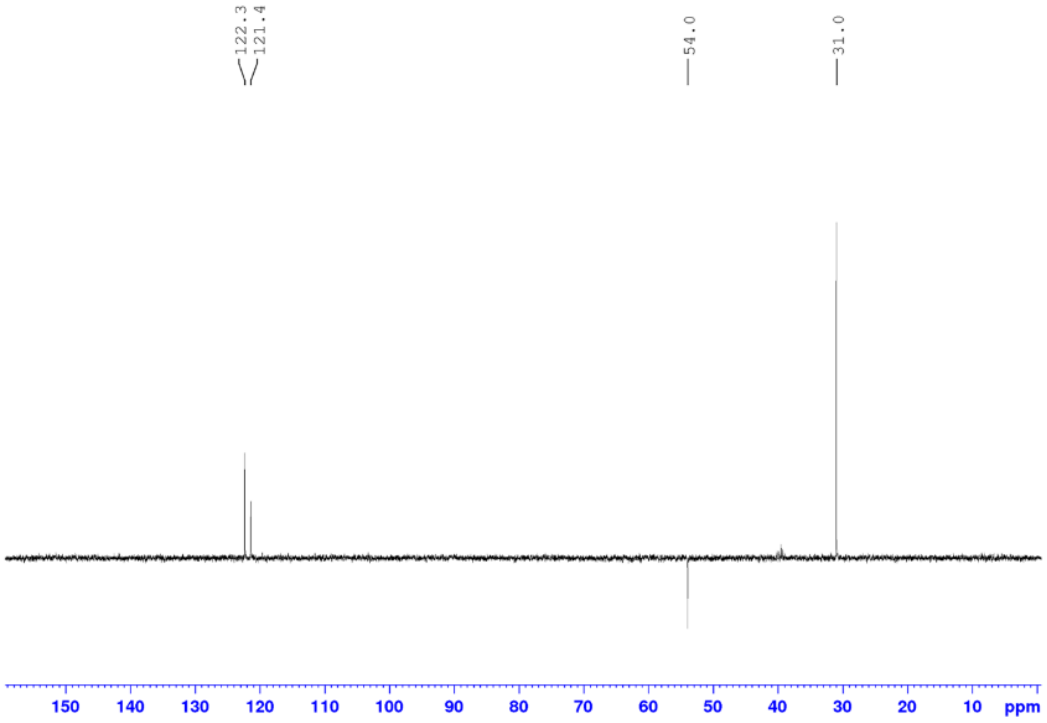

*Figure S119. ^{13}C DEPT spectrum of **3N₃** in DMSO-d_6*

Dimethyl 4-({1-[(3,5-di-*tert*-butylphenyl)methyl]1*H*-1,2,3-triazol-4-yl}methoxy)pyridine-2,6-dicarboxylate (MeOL₃)

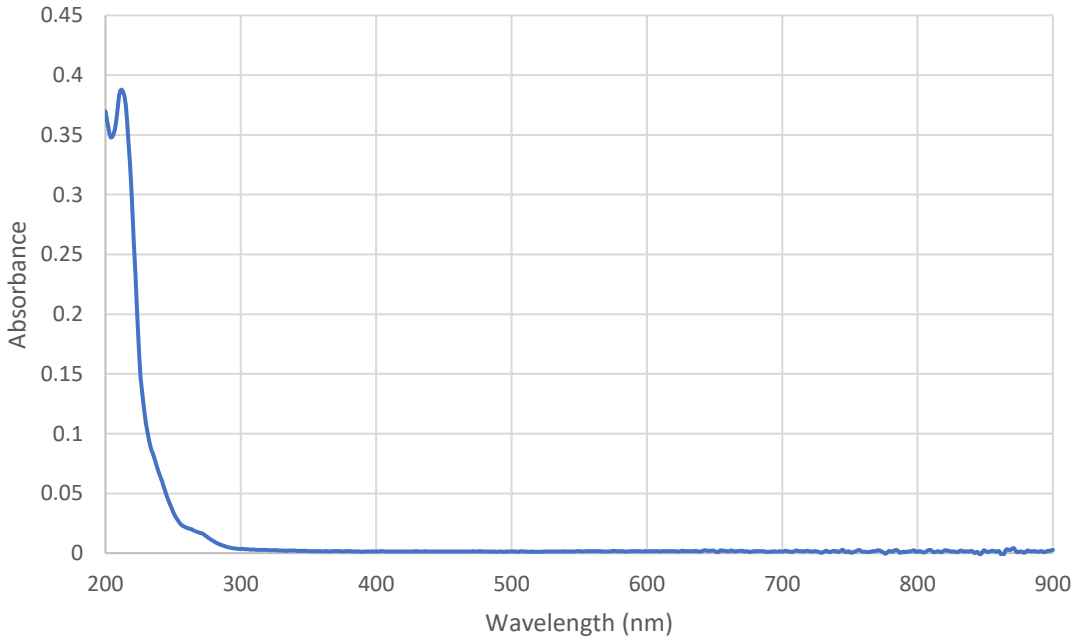

*Figure S120. UV/Vis spectrum of **MeOL₃** (1 x 10^{-5} M) in MeOH*

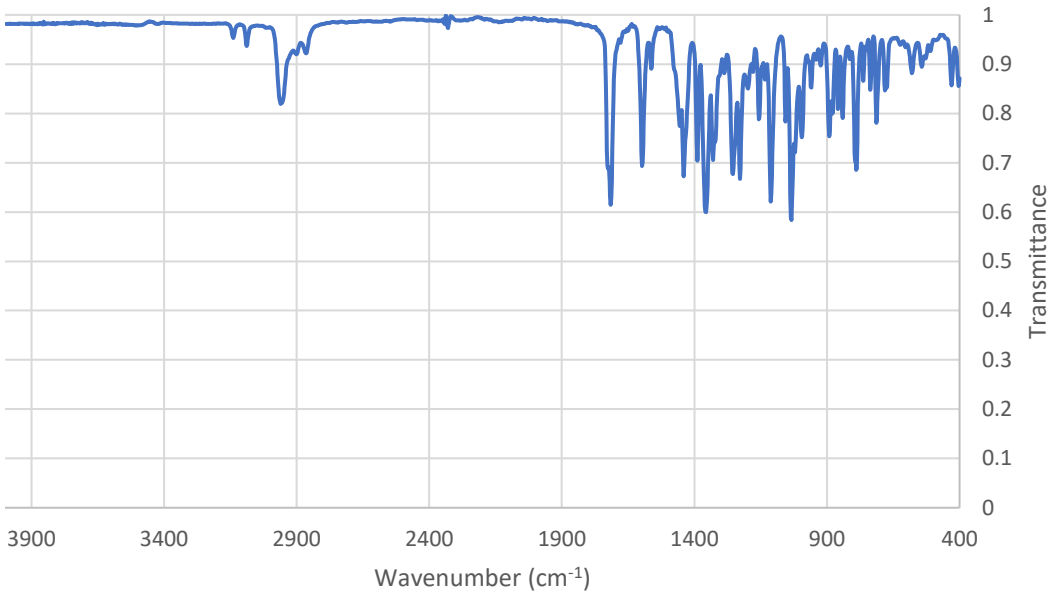

Figure S121. FTIR spectrum of ***MeOL₃***

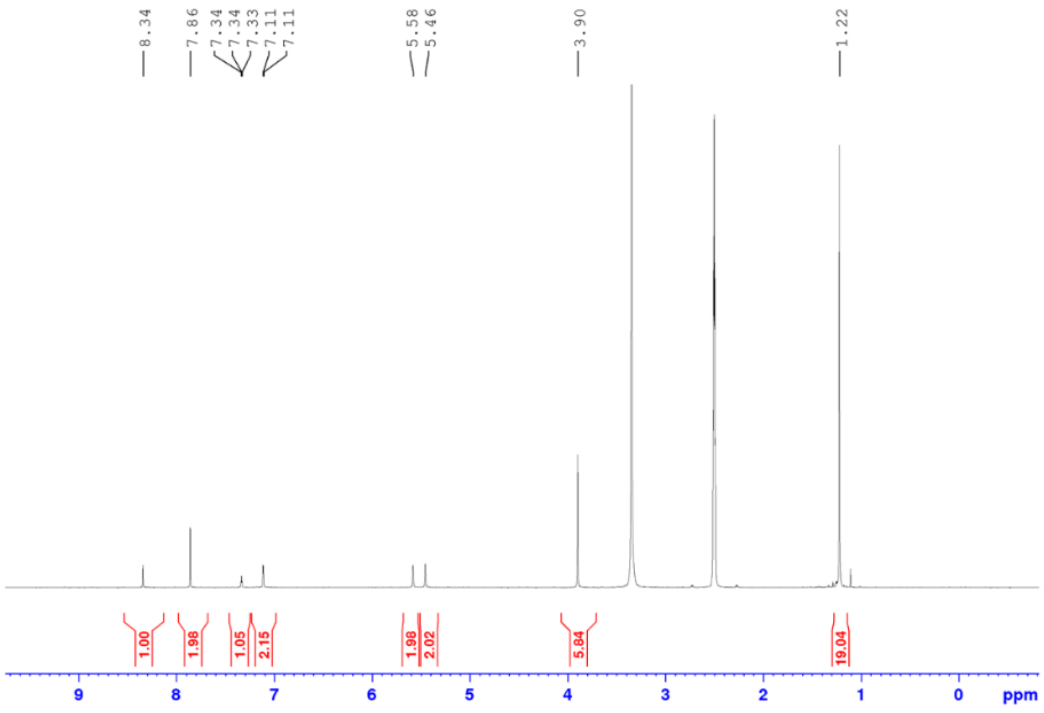

Figure S122. ^{1}H NMR spectrum of ***MeOL₃*** *in DMSO-d_6*

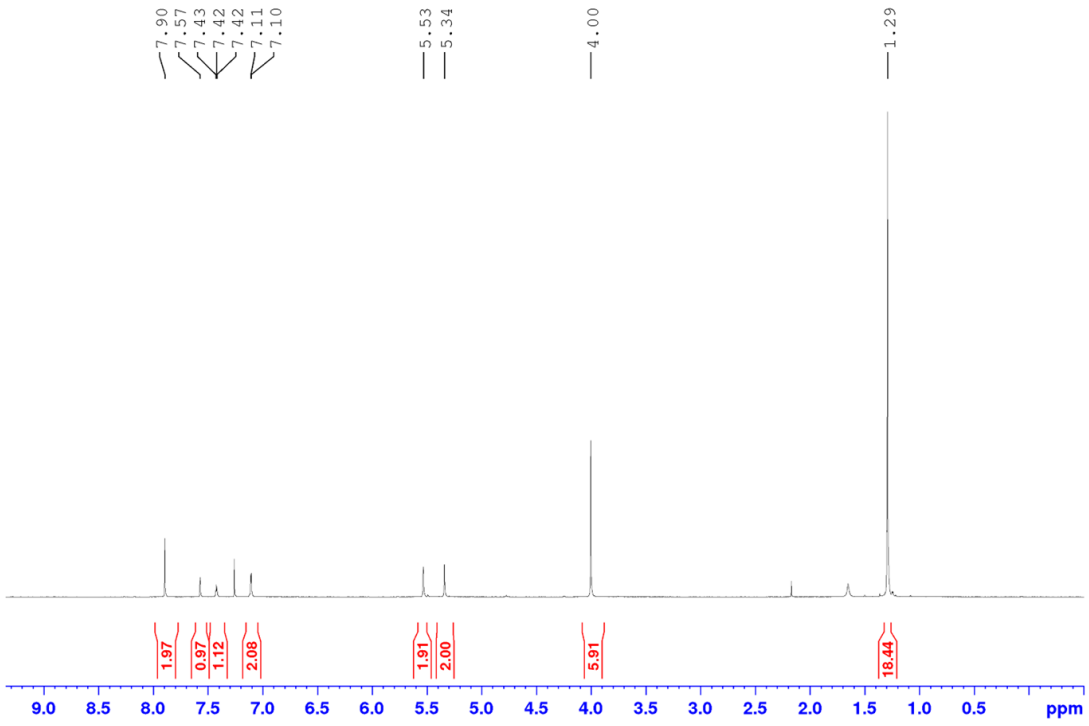

*Figure S123. ^{1}H NMR spectrum of **MeOL$_3$** in $CDCl_3$*

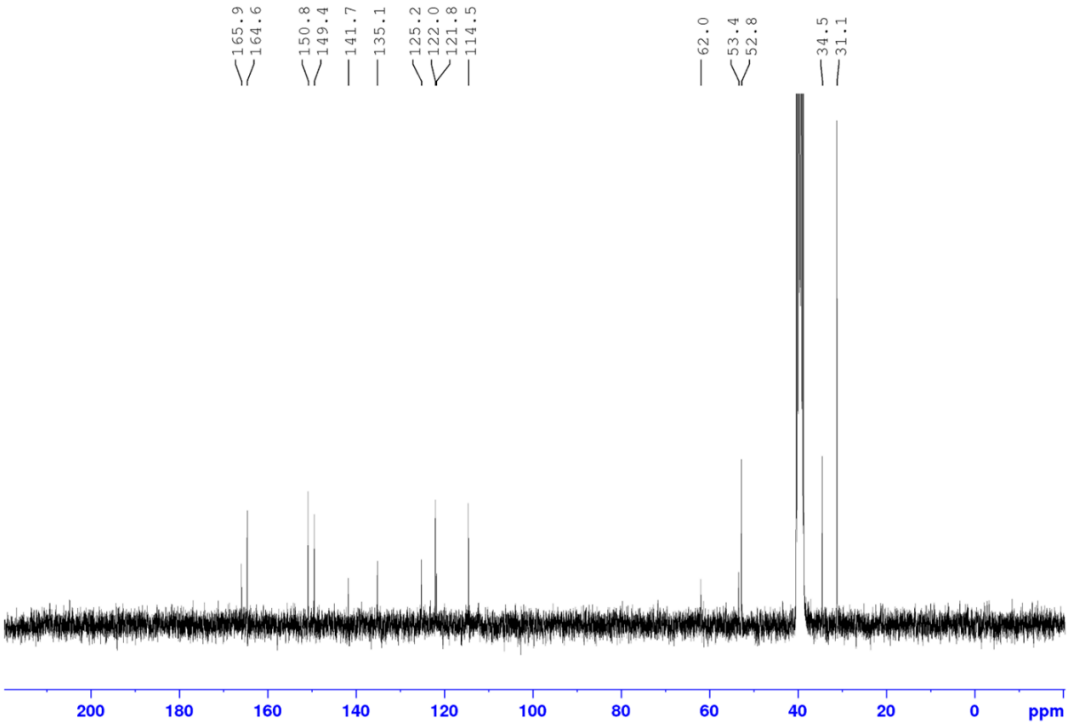

*Figure S124. ^{13}C NMR spectrum of **MeOL$_3$** in DMSO-d_6*

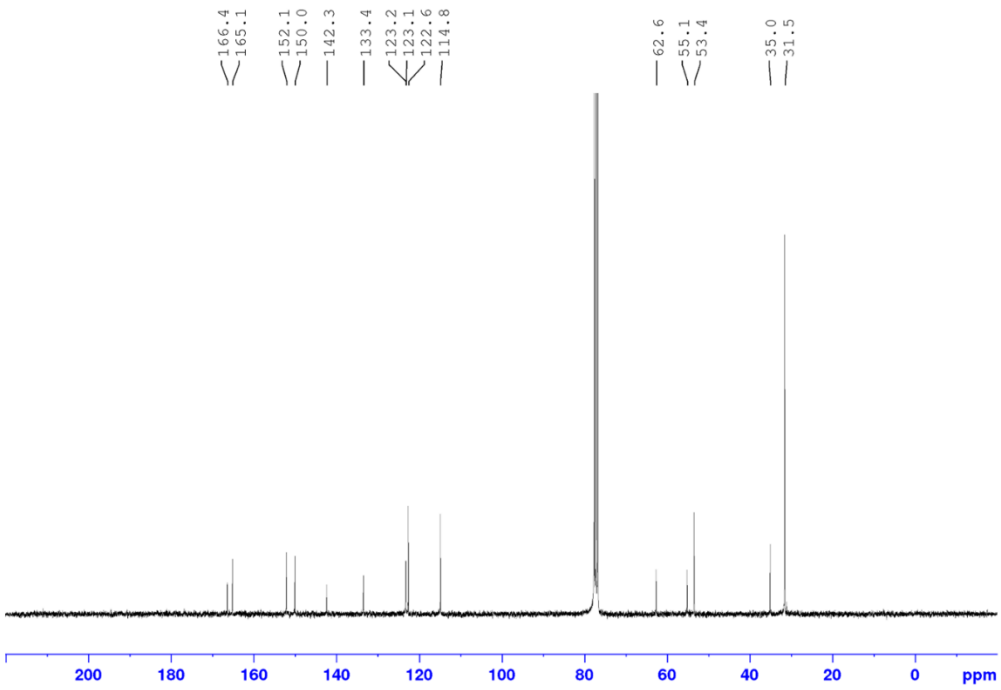

*Figure S125. ^{13}C NMR spectrum of **MeOL$_3$** in $CDCl_3$*

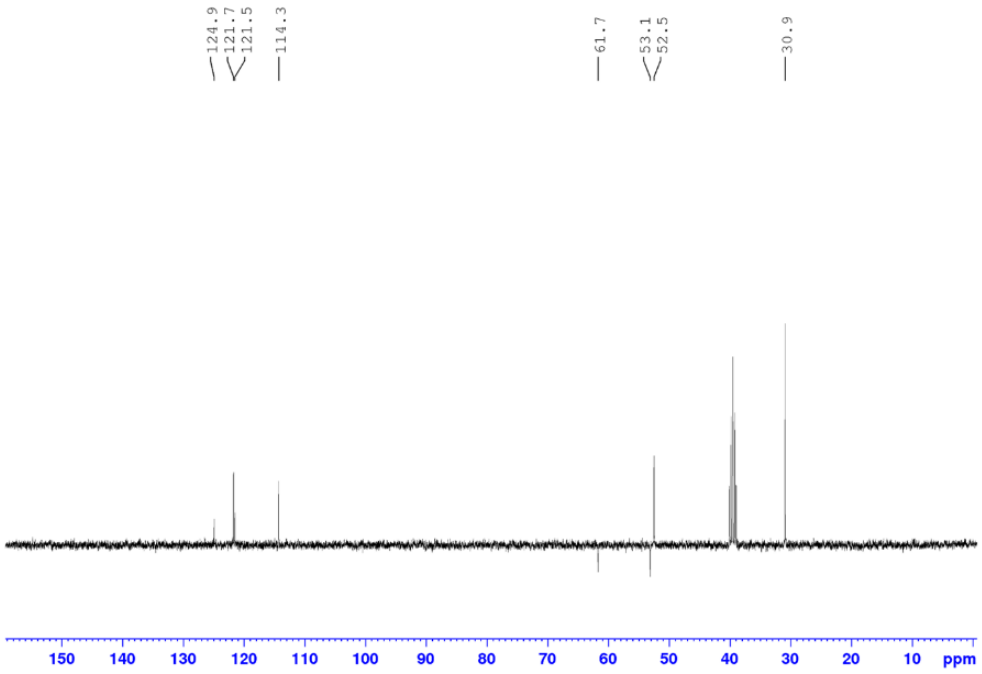

*Figure S126. ^{13}C DEPT spectrum of **MeOL$_3$** in DMSO-d_6*

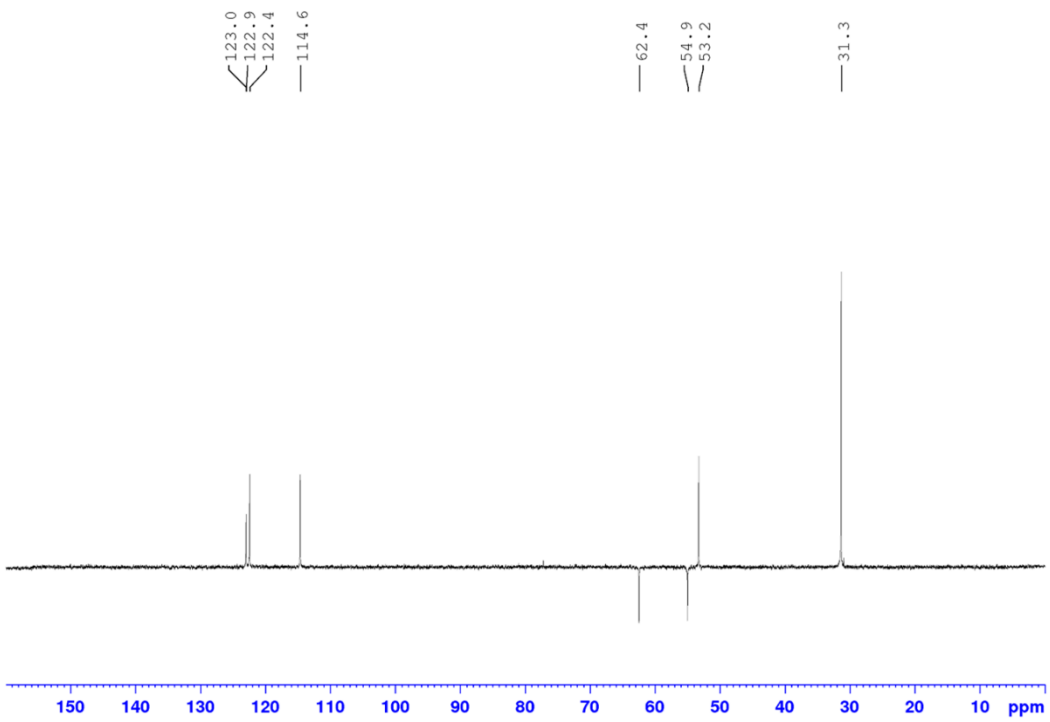

*Figure S127. ^{13}C DEPT spectrum of **MeOL$_3$** in $CDCl_3$*

4-({1-[(3,5-di-*tert*-butylphenyl)methyl]-1*H*-1,2,3-triazol-4-yl}methoxy)pyridine-2,6-dicarboxylic acid (L_3)

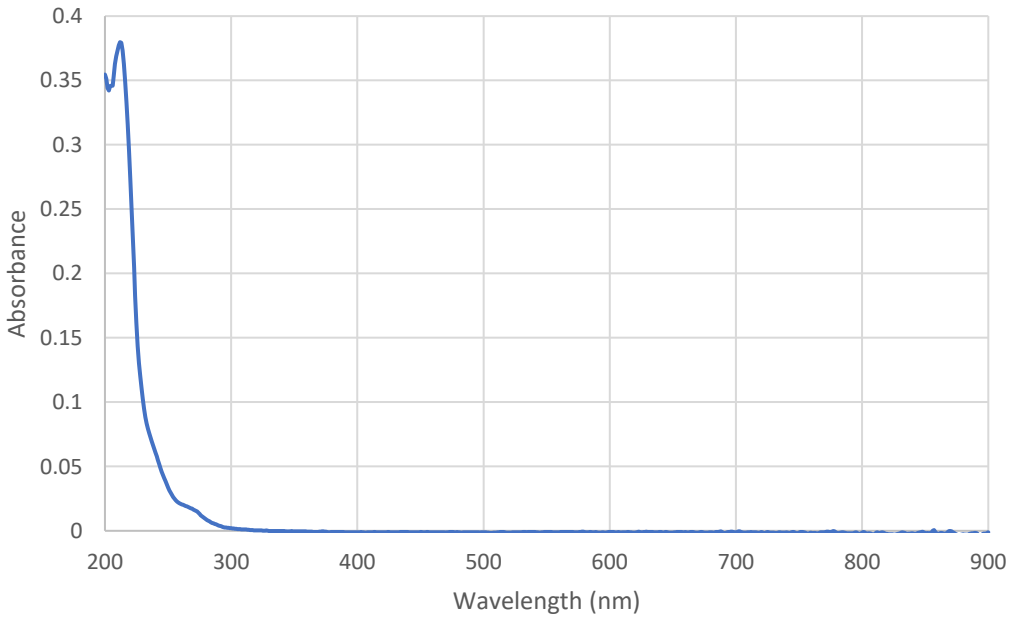

*Figure S128. UV/Vis spectrum of **L$_3$** (1 x 10^{-5} M) in MeOH*

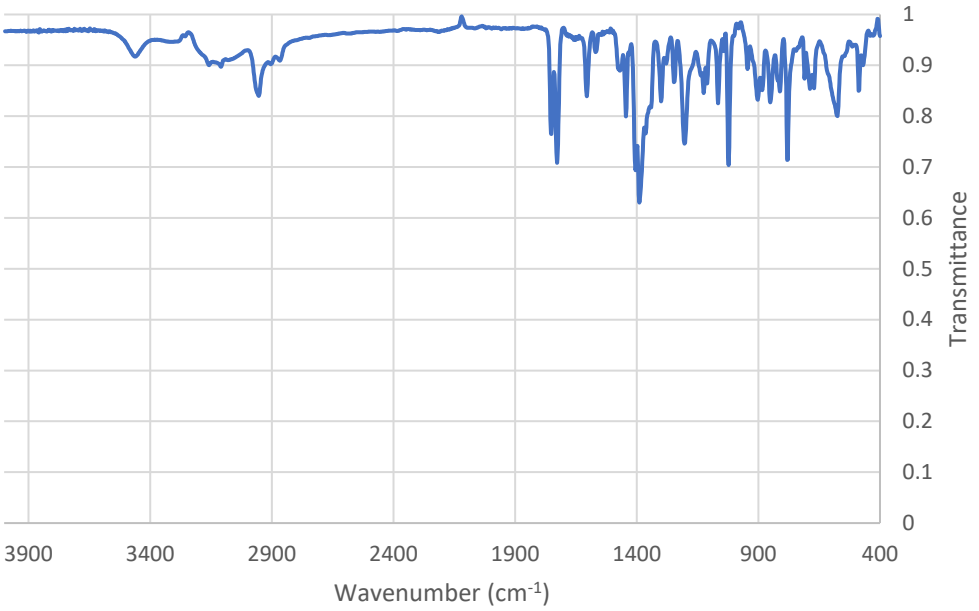

Figure S129. FTIR spectrum of $\boldsymbol{L_3}$

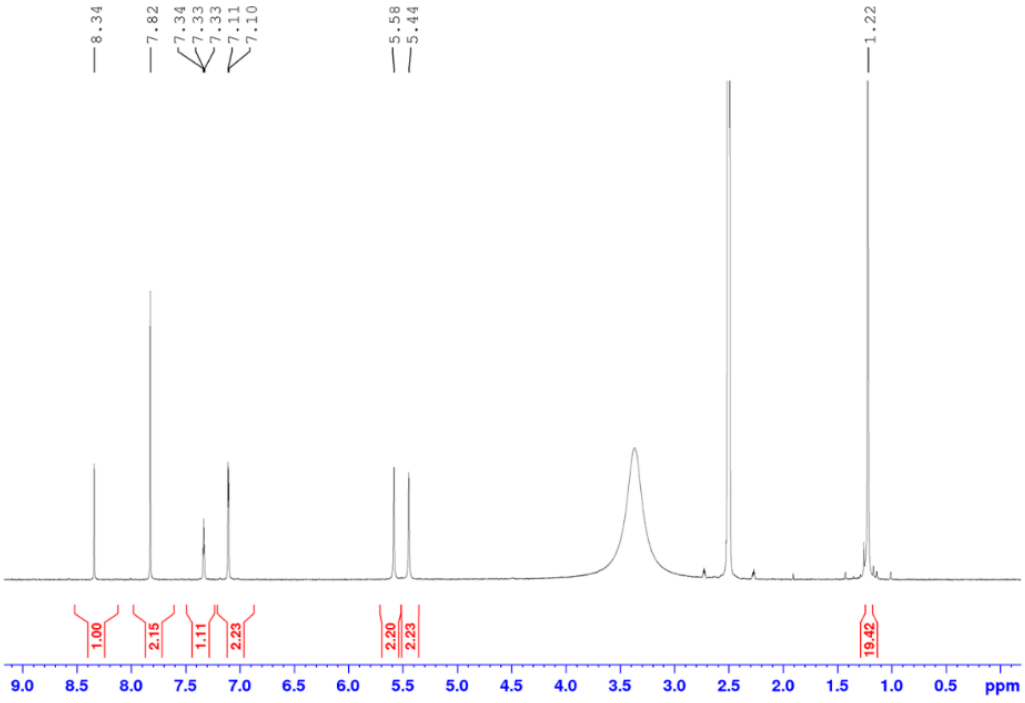

Figure S130. ^1H *NMR spectrum of* $\boldsymbol{L_3}$ *in DMSO-*d_6

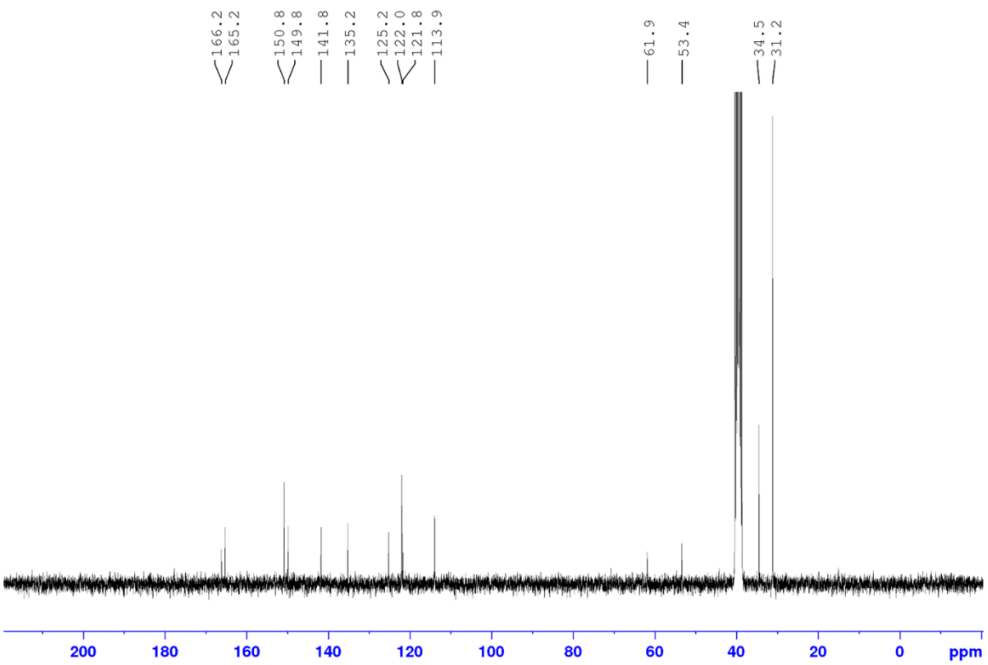

*Figure S131. ^{13}C NMR spectrum of **L₃** in DMSO-d_6*

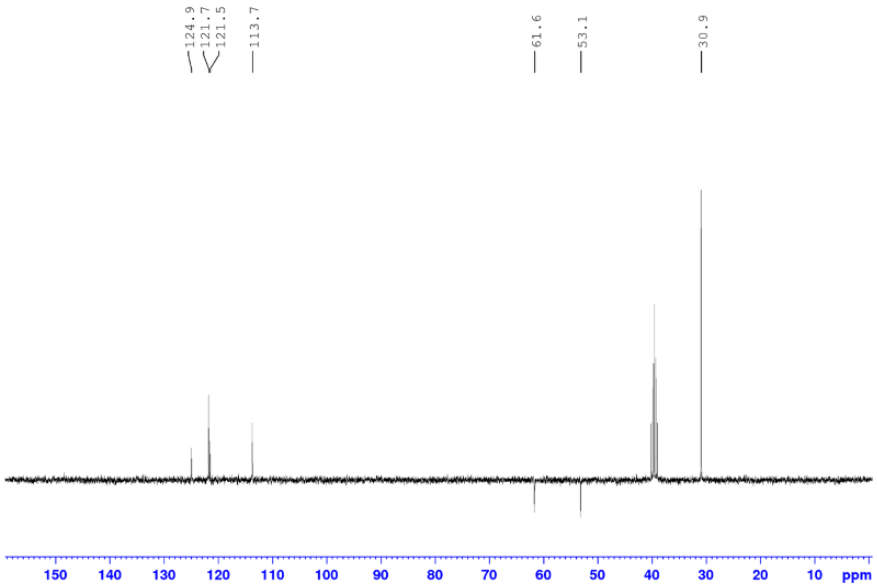

*Figure S132. ^{13}C DEPT spectrum of **L₃** in DMSO-d_6*

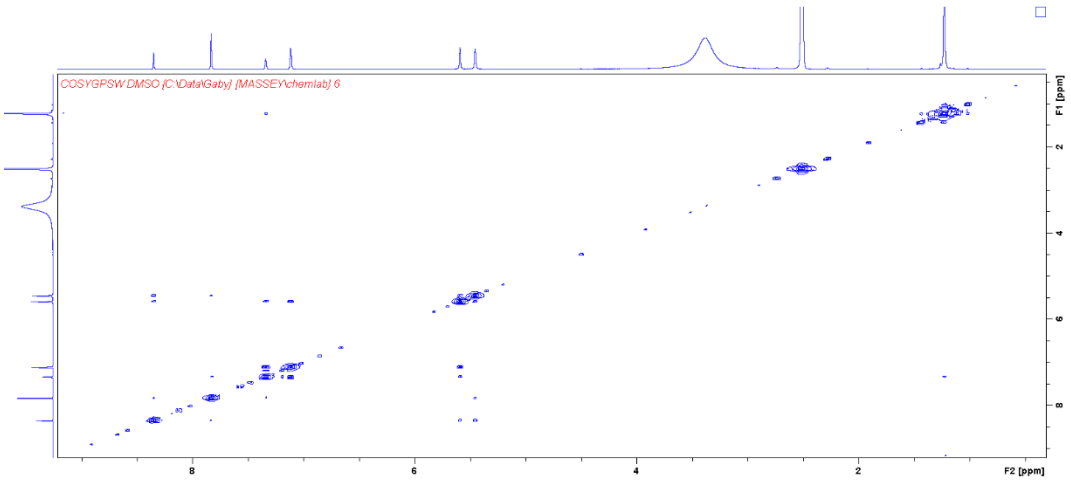

Figure S133. COSY spectrum of ***L*** $_3$ *in DMSO-d* $_6$

[La(L$_3$)$_3$]$^{3-}$

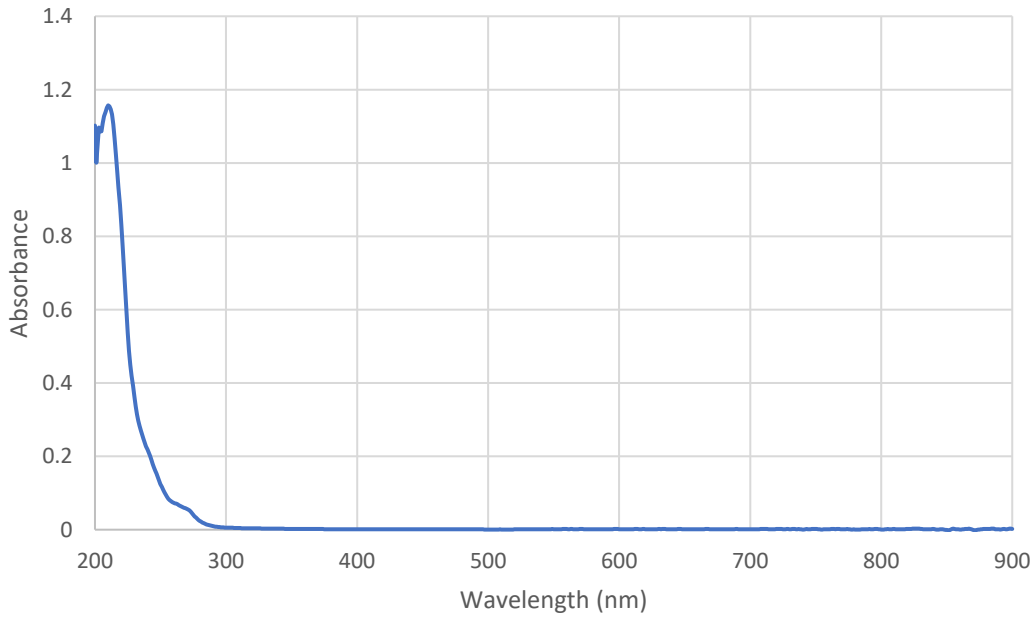

Figure S134. UV/Vis spectrum of ***[La(L*** $_3$***)*** $_3$***]*** $^{3-}$ *(1 x 10* $^{-5}$ *M) in MeOH*

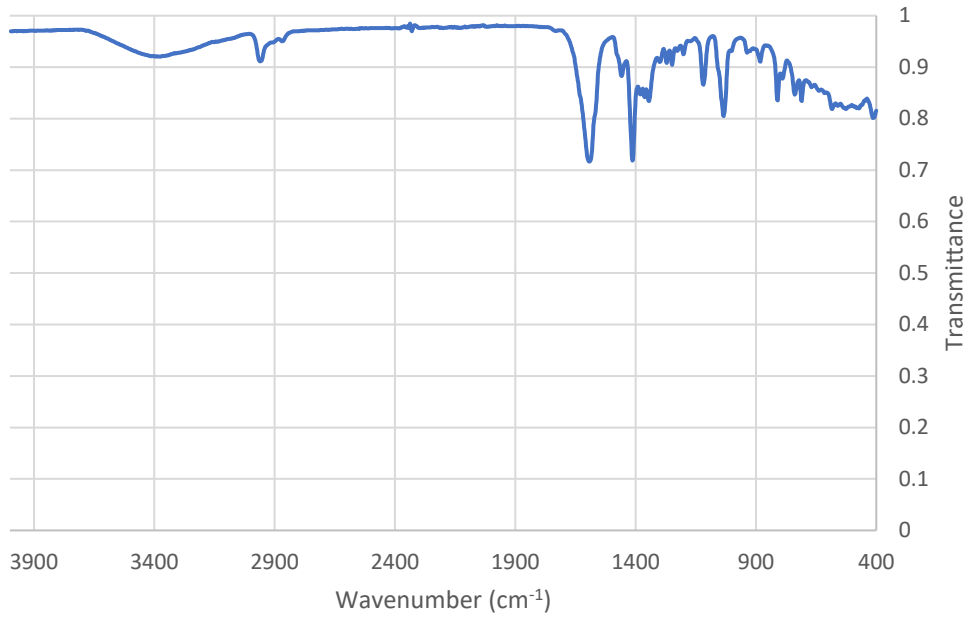

Figure S135. FTIR spectrum of ***[La(L3)3]3-***

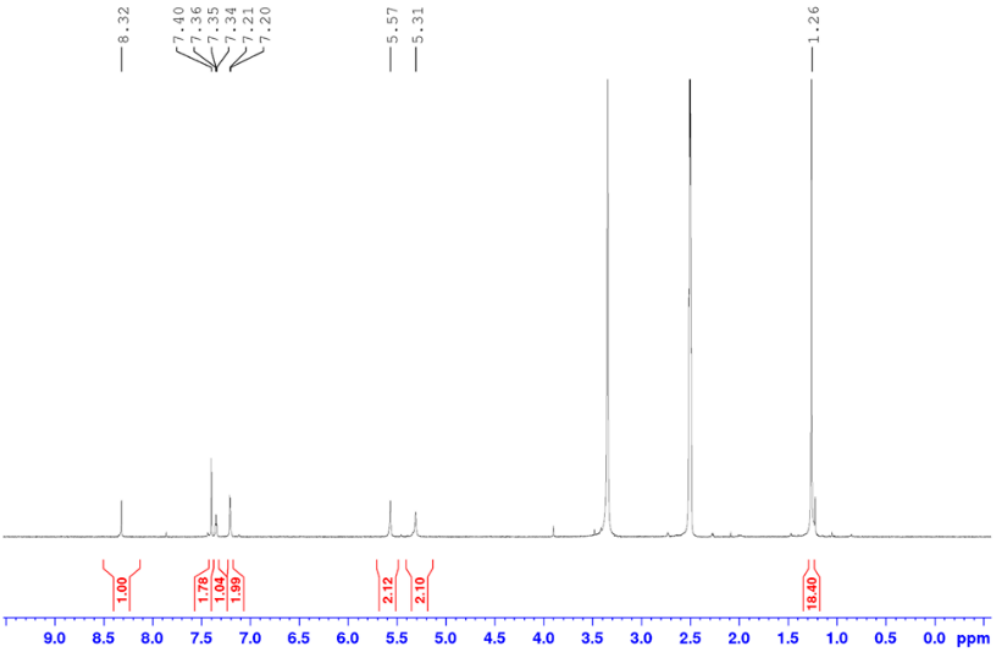

Figure S136. ^{1}H NMR spectrum of ***[La(L3)3]3-*** *in DMSO-d6*

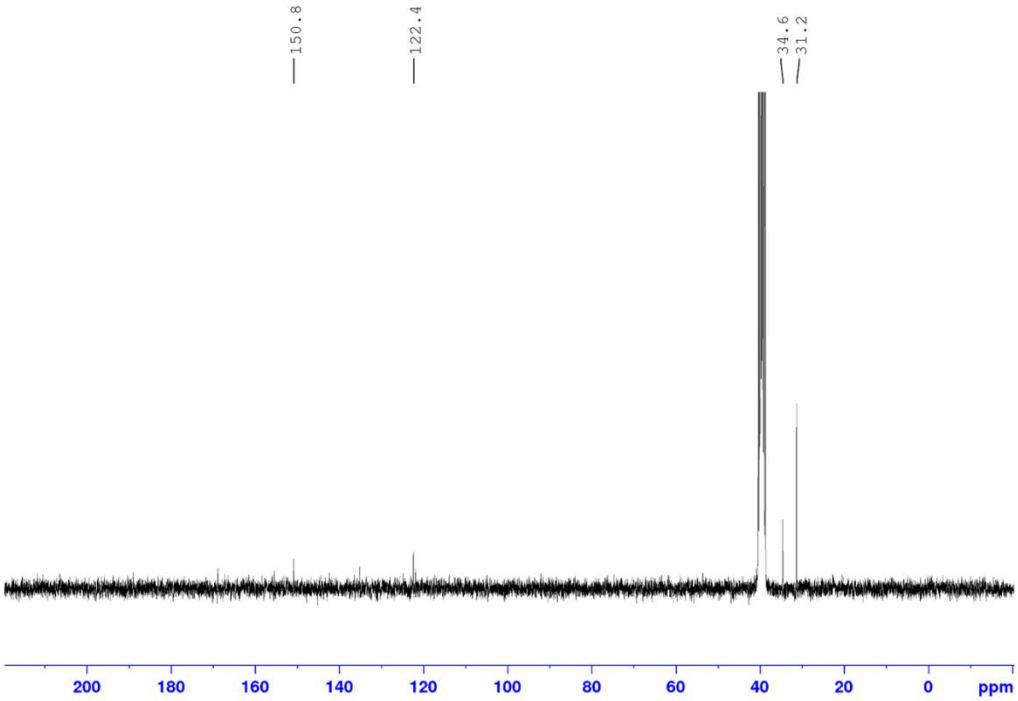

Figure S137. ^{13}C NMR spectrum of ***[La(L$_3$)$_3$]$^{3-}$*** *in DMSO-d$_6$*

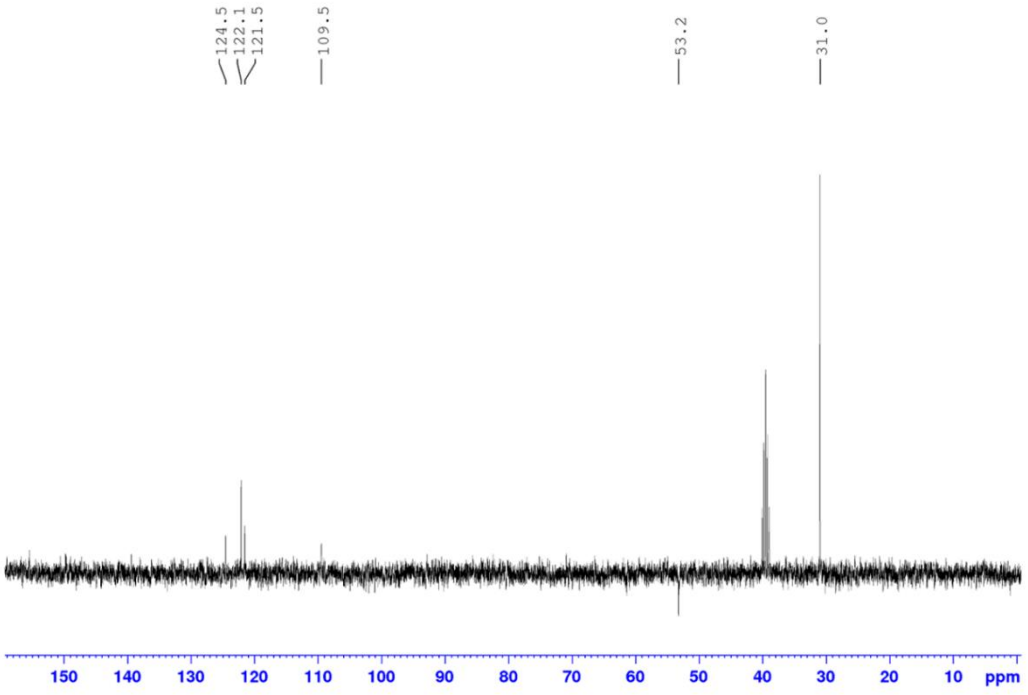

Figure S138. ^{13}C DEPT spectrum of ***[La(L$_3$)$_3$]$^{3-}$*** *in DMSO-d$_6$*

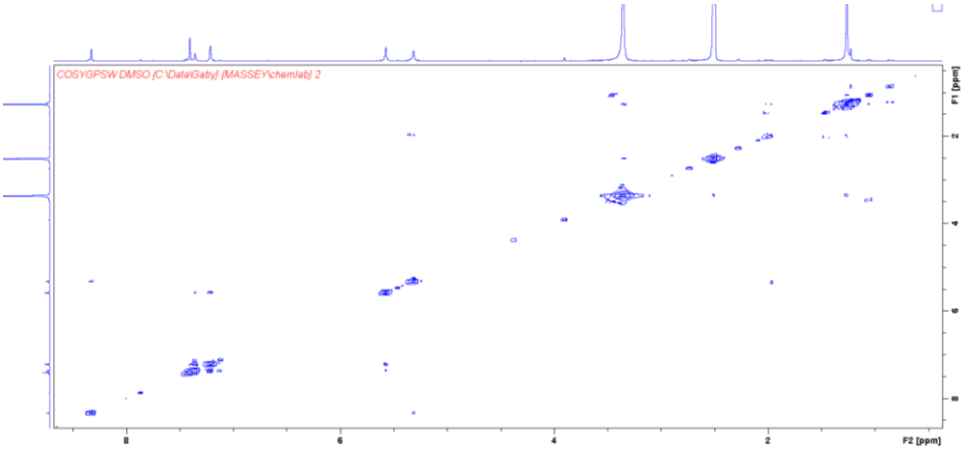

Figure S139. COSY spectrum of ***[La(L3)3]3-*** *in DMSO-d6*

[Eu(L3)3]3-

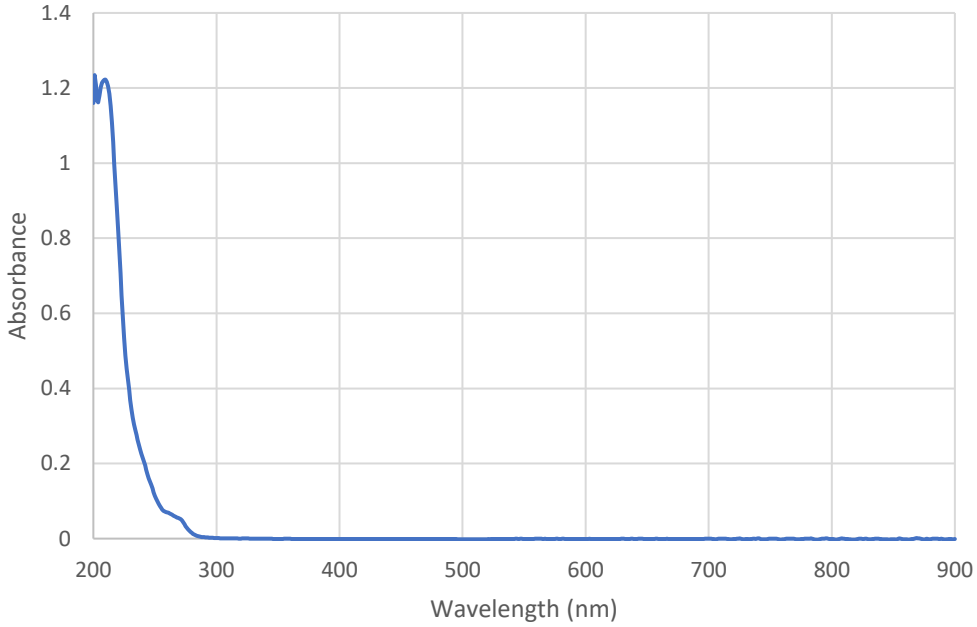

Figure S140. UV/Vis spectrum of ***[Eu(L3)3]3-*** *(1 x 10-5 M) in MeOH*

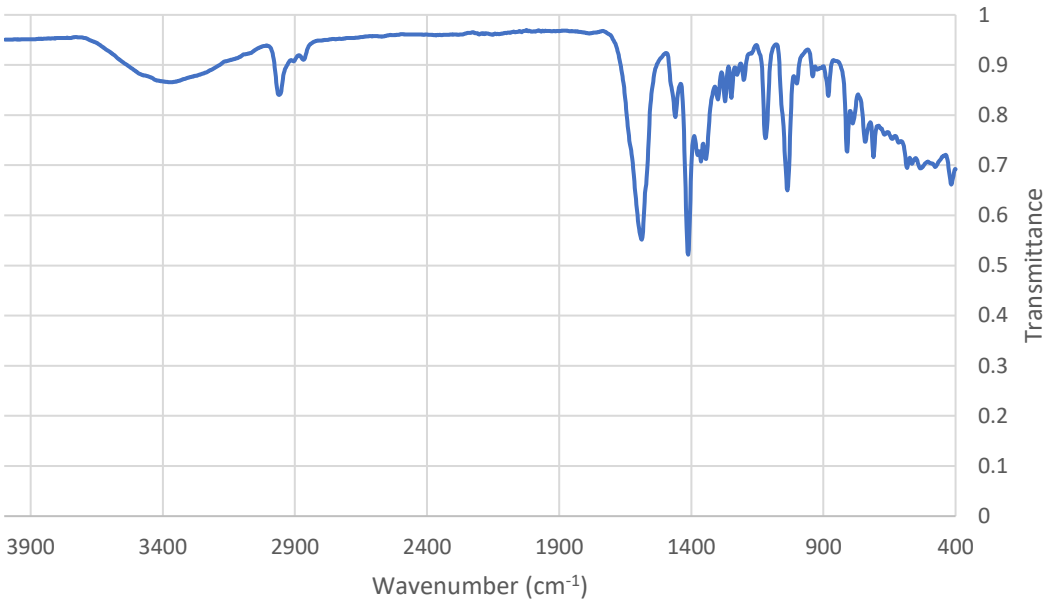

Figure S141. FTIR spectrum of ***[Eu(L3)3]3-***

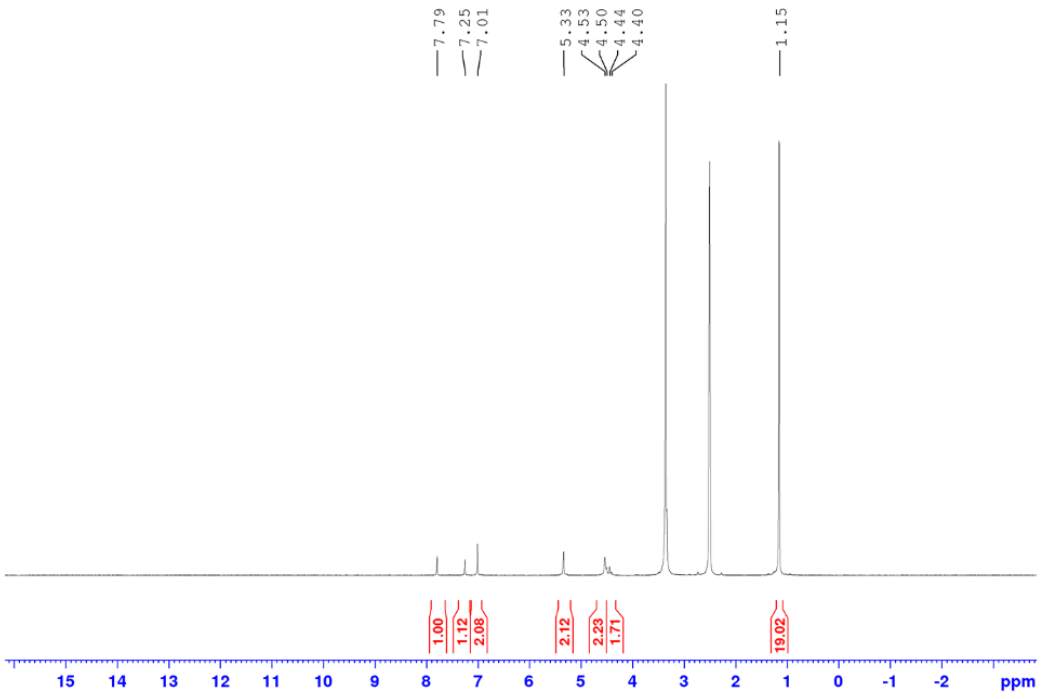

Figure S142. ^{1}H NMR spectrum of ***[Eu(L3)3]3-*** *in DMSO-d6*

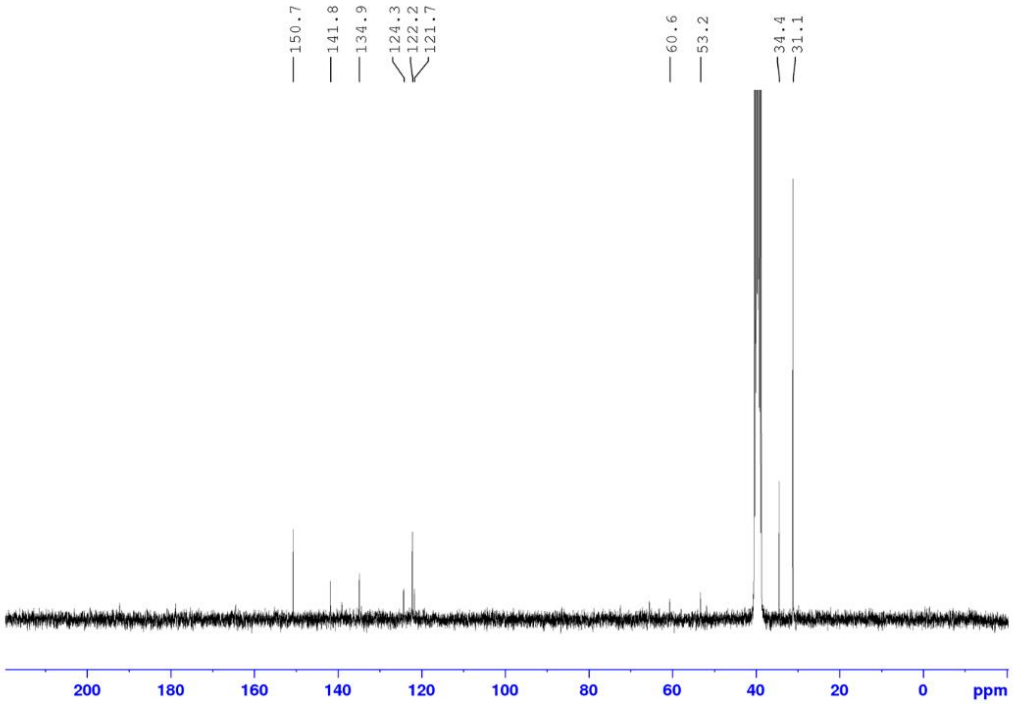

Figure S143. ^{13}C NMR spectrum of ***[Eu(L$_3$)$_3$]$^{3-}$*** *in DMSO-d$_6$*

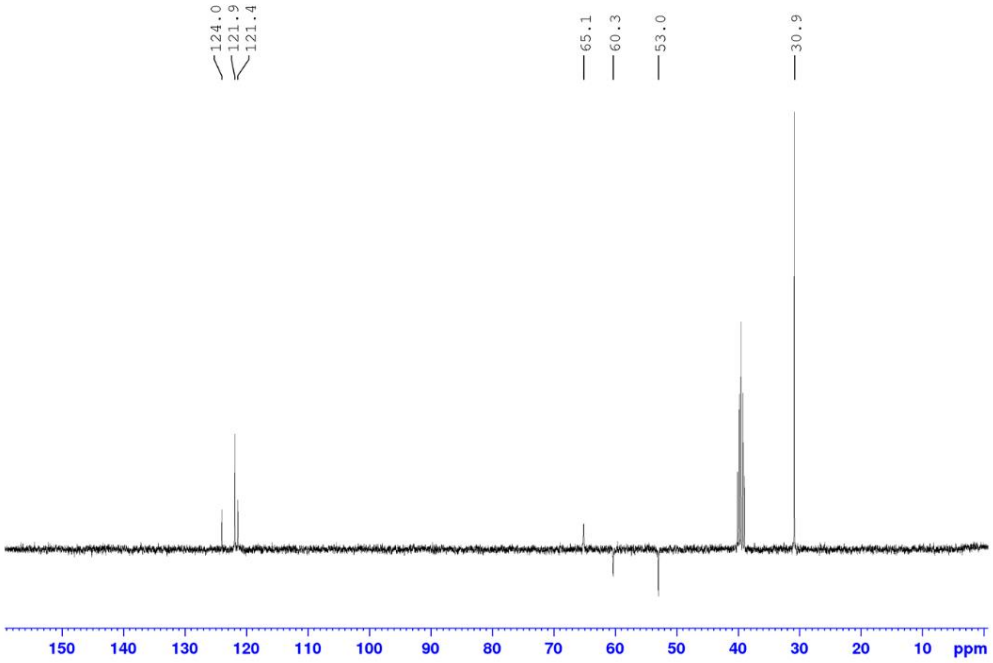

Figure S144. ^{13}C DEPT spectrum of ***[Eu(L$_3$)$_3$]$^{3-}$*** *in DMSO-d$_6$*

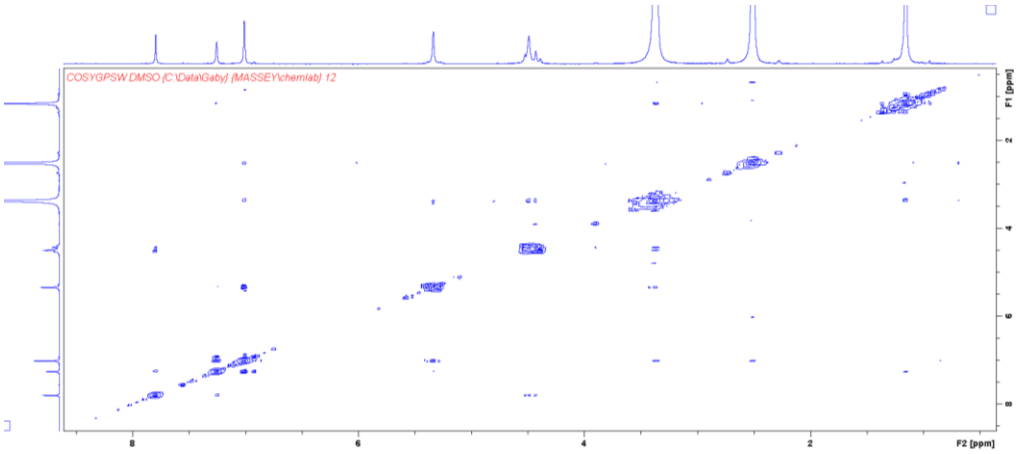

Figure S145. COSY spectrum of $[Eu(L_3)_3]^{3-}$ *in DMSO-d*$_6$

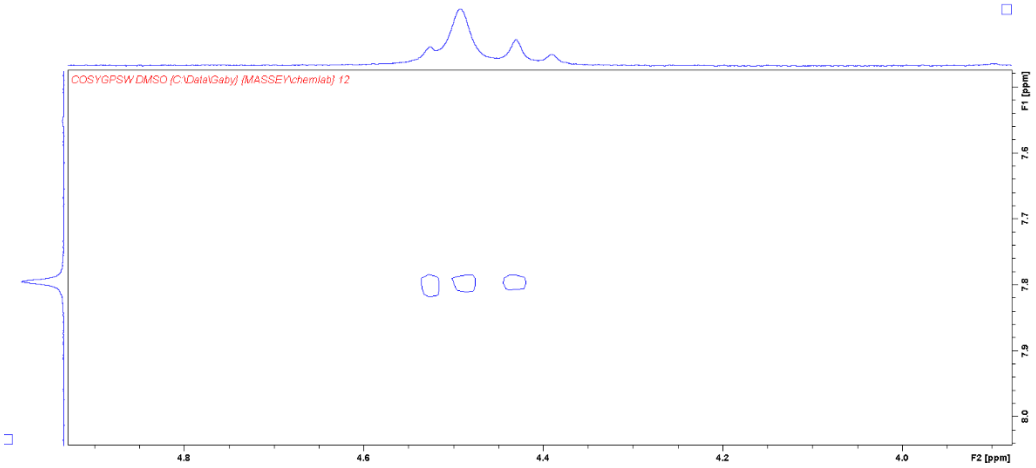

Figure S146. Zoom in of COSY spectrum of $[Eu(L_3)_3]^{3-}$ *in DMSO-d*$_6$ *showing the similar multiplet coupling with the Tz-H as observed in the COSY spectrum of* $[Eu(L_2)_3]^{3-}$

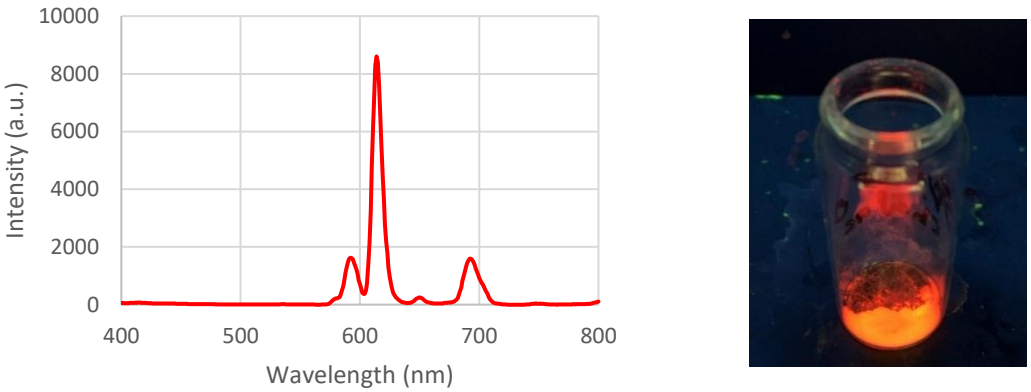

Figure S147. (Left) Fluorescence emission spectrum (λ_{ex} *= 274 nm) of* $[Eu(L_3)_3]^{3-}$ *(1 x 10*$^{-5}$ *M) in MeOH. Excitation and emission slit widths were 3.0 and 5.0 nm (respectively). (Right) Solid-state emission of* $[Eu(L_3)_3]^{3-}$ *under a short-wave UV lamp (254 nm)*

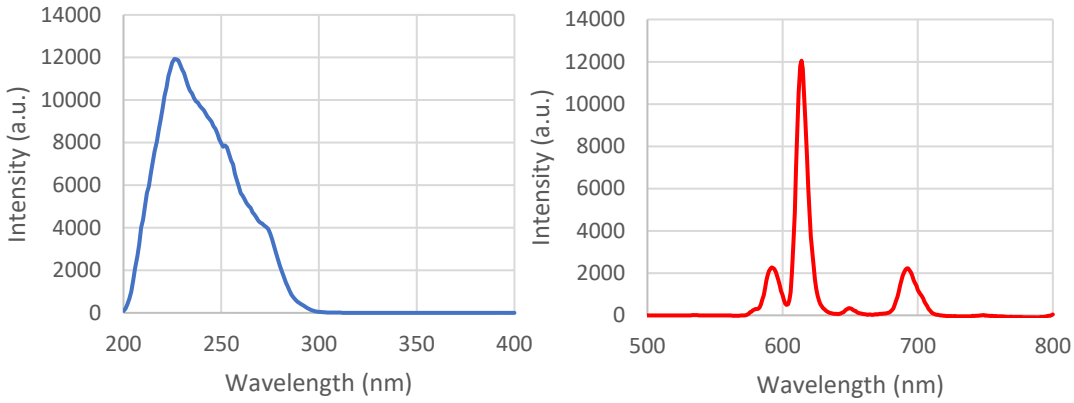

Figure S148. (Left) Fluorescence excitation spectrum (λ_{em} = 614 nm) of ***[Eu(L$_3$)$_3$]$^{3-}$*** *(1 x 10^{-5} M) in MeOH. (Right) Fluorescence emission spectrum (λ_{ex} = 227 nm) of* ***[Eu(L$_3$)$_3$]$^{3-}$*** *(1 x 10^{-5} M) in MeOH. For both the fluorescence excitation and emission measurements, excitation and emission slit widths were 3.0 and 5.0 nm (respectively)*

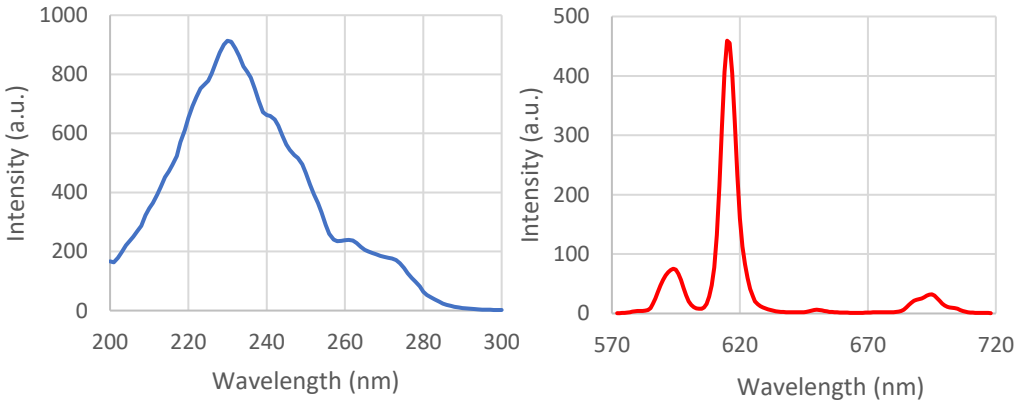

Figure S149. (Left) Phosphorescence excitation spectrum (λ_{em} = 616 nm) of ***[Eu(L$_3$)$_3$]$^{3-}$*** *(1 x 10^{-5} M) in MeOH. (Right) Phosphorescence emission spectrum (λ_{ex} = 274 nm) of* ***[Eu(L$_3$)$_3$]$^{3-}$*** *(1 x 10^{-5} M) in MeOH. For both the phosphorescence excitation and emission measurements, excitation and emission slit widths were 5.0 nm*

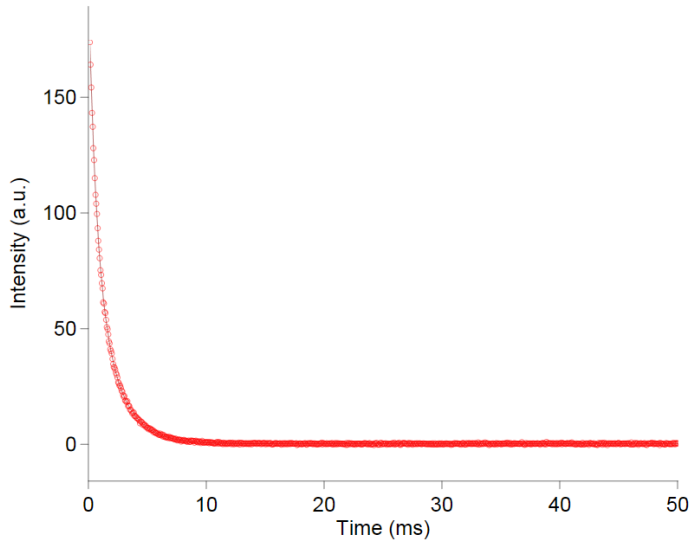

Figure S150. Intensity of the $^5D_0 \rightarrow {}^7F_2$ transition (λ_{em} = 616 nm) of ***[Eu(L$_3$)$_3$]$^{3-}$*** *(1 x 10^{-5} M) on excitation at 230 nm in MeOH (red spots) with double exponential fit (brown line) for lifetime measurement*

Table S10. Lifetimes (λ_{em} = 616 nm) of the long- and short- emitting species recorded for ***[Eu(L3)3]3-*** *on excitation at 230 nm in MeOH*

Lifetime (ms)	
Tau1	**Tau2**
0.631 ± 0.0	1.906 ± 0.0

[Tb(L3)3]3-

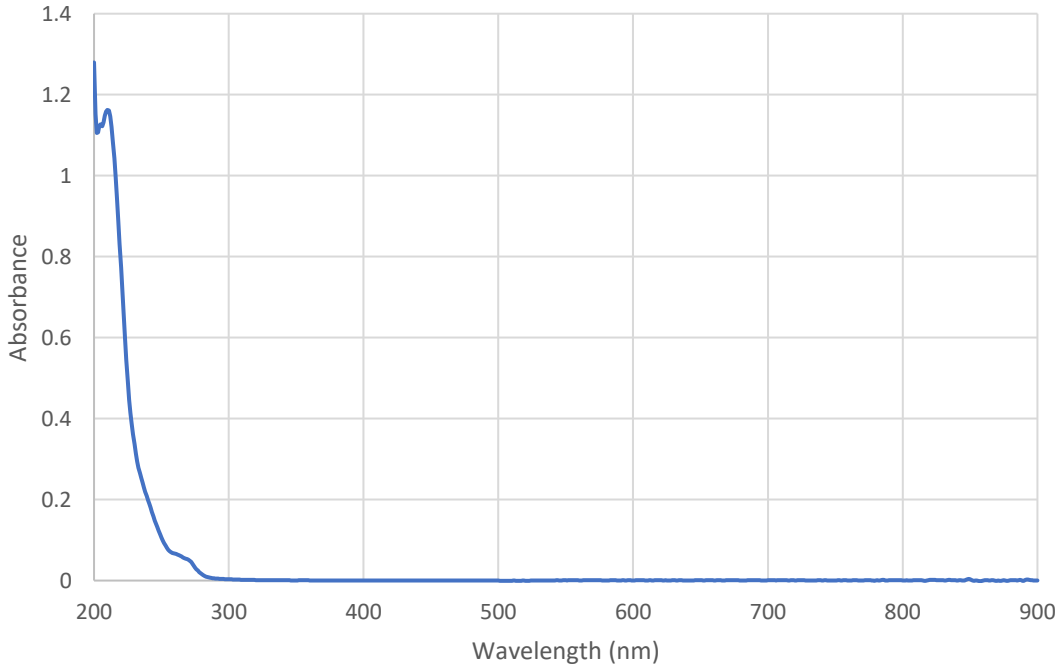

Figure S151. UV/Vis spectrum of ***[Tb(L3)3]3-*** *(1 x 10-5 M) in MeOH*

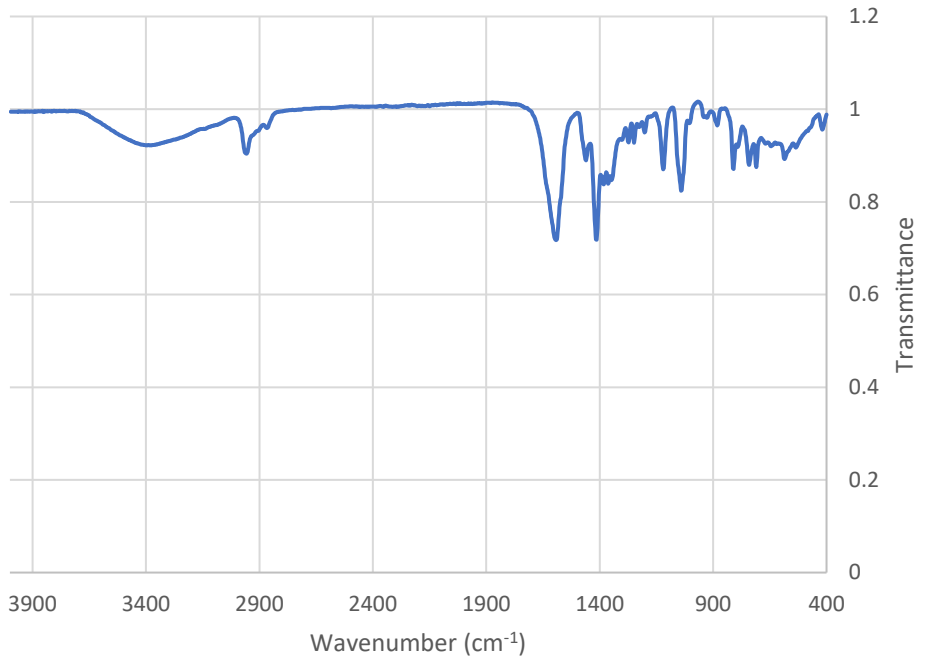

Figure S152. FTIR spectrum of ***[Tb(L3)3]3-***

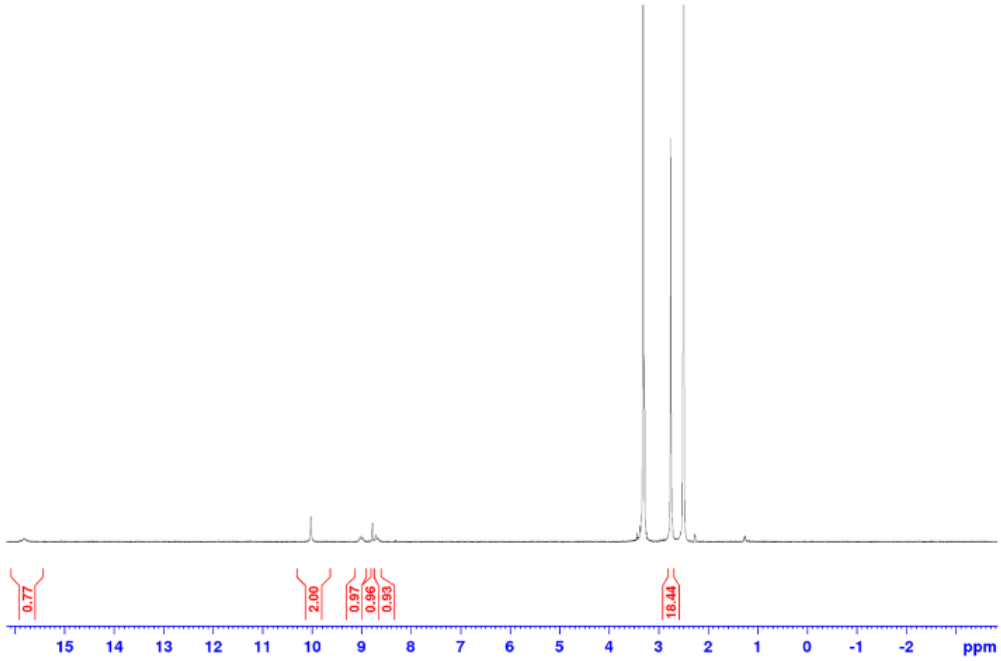

Figure S153. ^{1}H NMR spectrum of ***[Tb(L3)3]3-*** *in DMSO-d_6*

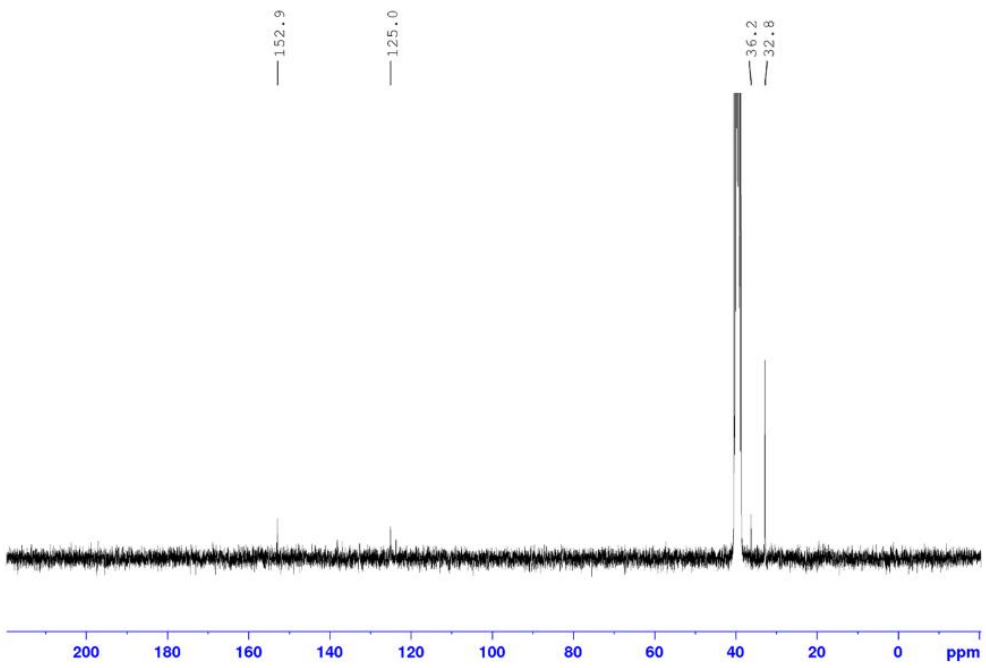

Figure S154. ^{13}C NMR spectrum of ***[Tb(L$_3$)$_3$]$^{3-}$*** *in DMSO-d$_6$*

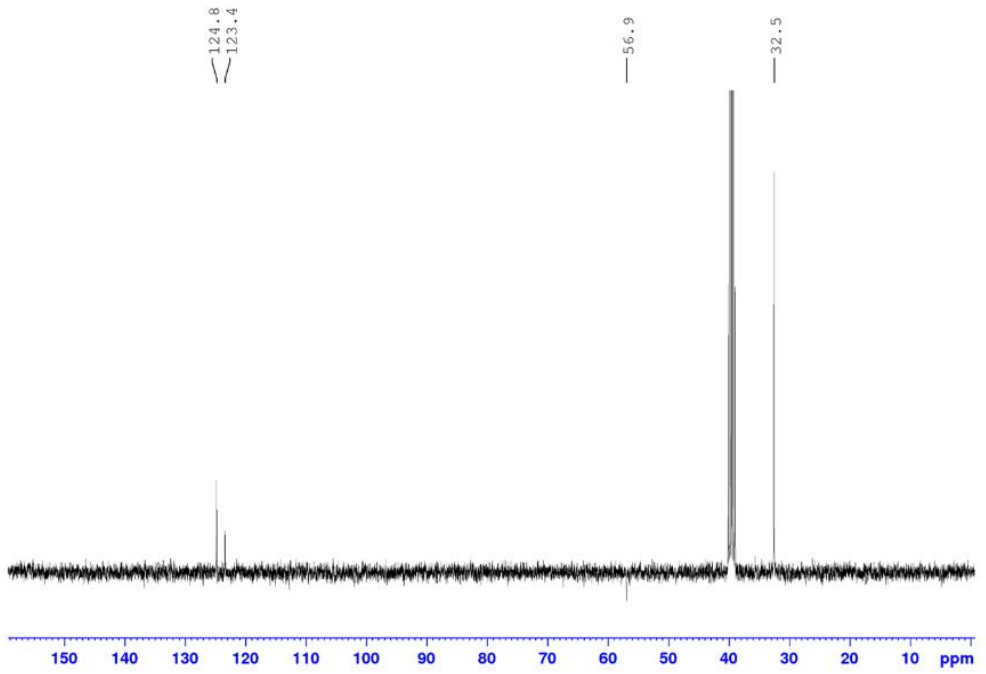

Figure S155. ^{13}C DEPT spectrum of ***[Tb(L$_3$)$_3$]$^{3-}$*** *in DMSO-d$_6$*

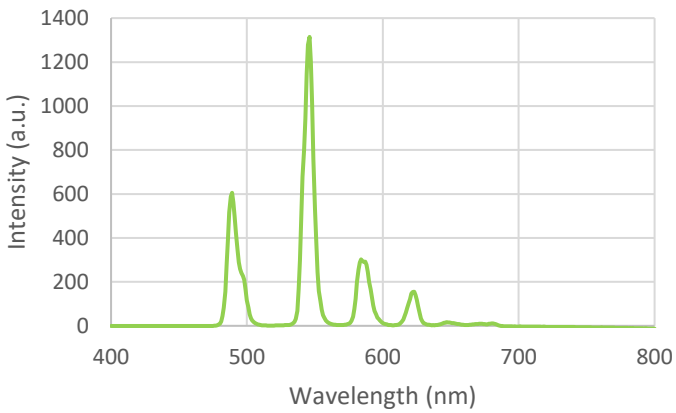

Figure S156. (Left) Fluorescence emission spectrum (λ_{ex} = 274 nm) of ***[Tb(L$_3$)$_3$]$^{3-}$*** *(1 x 10^{-5} M) in MeOH. Emission and excitation slit widths were both 3.0 nm. (Right) Solid-state emission of* ***[Tb(L$_3$)$_3$]$^{3-}$*** *under a short-wave UV lamp (254 nm)*

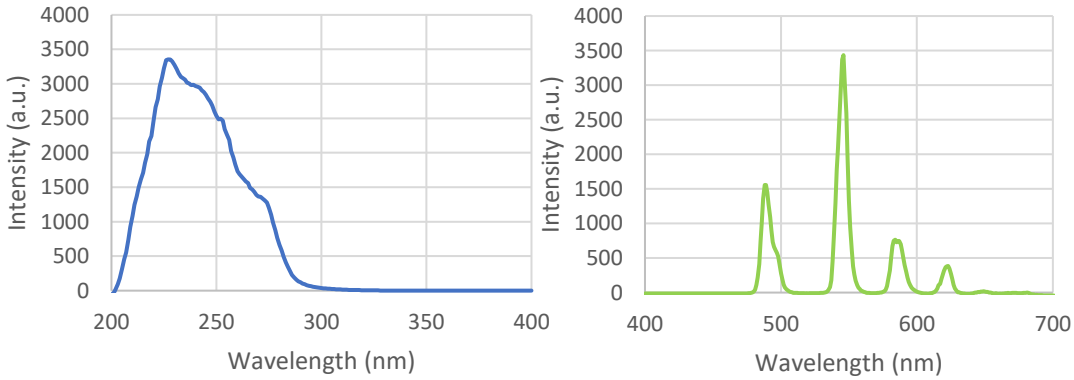

Figure S157. (Left) Fluorescence excitation spectrum (λ_{em} = 545 nm) of ***[Tb(L$_3$)$_3$]$^{3-}$*** *(1 x 10^{-5} M) in MeOH. (Right) Fluorescence emission spectrum (λ_{ex} = 227 nm) of* ***[Tb(L$_3$)$_3$]$^{3-}$*** *(1 x 10^{-5} M) in MeOH. For both the fluorescence excitation and emission measurements, excitation and emission slit widths were 3.0 nm*

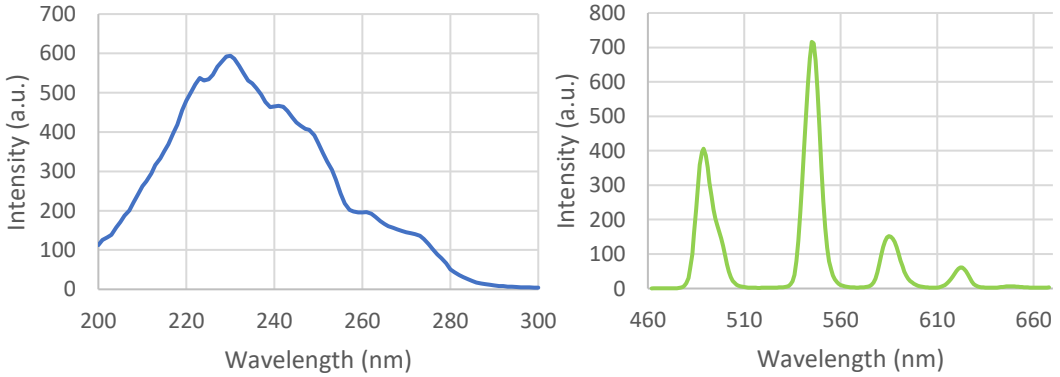

Figure S158. (Left) Phosphorescence excitation spectrum (λ_{em} = 545 nm) of ***[Tb(L$_3$)$_3$]$^{3-}$*** *(1 x 10^{-5} M) in MeOH. (Right) Phosphorescence emission spectrum (λ_{ex} = 274 nm) of* ***[Tb(L$_3$)$_3$]$^{3-}$*** *(1 x 10^{-5} M) in MeOH. For both the phosphorescence excitation and emission measurements, excitation and emission slit widths were 5.0 nm*

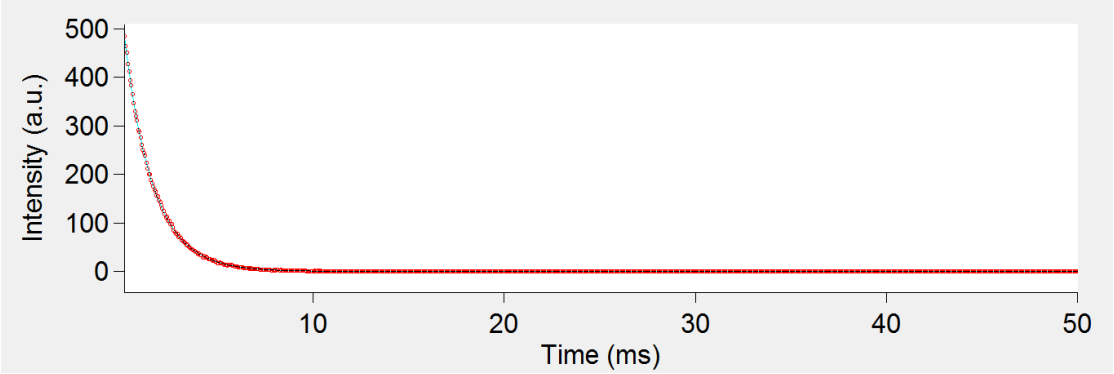

Figure S159. Intensity of the $^5D_4 \rightarrow {}^7F_5$ transition (λ_{em} = 545 nm) of ***[Tb(L$_3$)$_3$]$^{3-}$*** *(1 x 10^{-5} M) on excitation at 229 nm in MeOH (red spots) with double exponential fit (blue line) for lifetime measurement*

Table S11. Lifetimes (λ_{em} = 545 nm) of the long- and short- emitting species recorded for ***[Tb(L$_3$)$_3$]$^{3-}$*** *on excitation at 229 nm in MeOH*

Run number	**Lifetime (ms)**	
	Tau1	**Tau2**
1	0.358 ± 0.1	1.513 ± 0.0
2	1.456 ± 0.1	2.043 ± 2.9
3	0.053 ± 0.0	1.493 ± 0.0
Average	0.622	1.683

9-(bromomethyl)anthracene

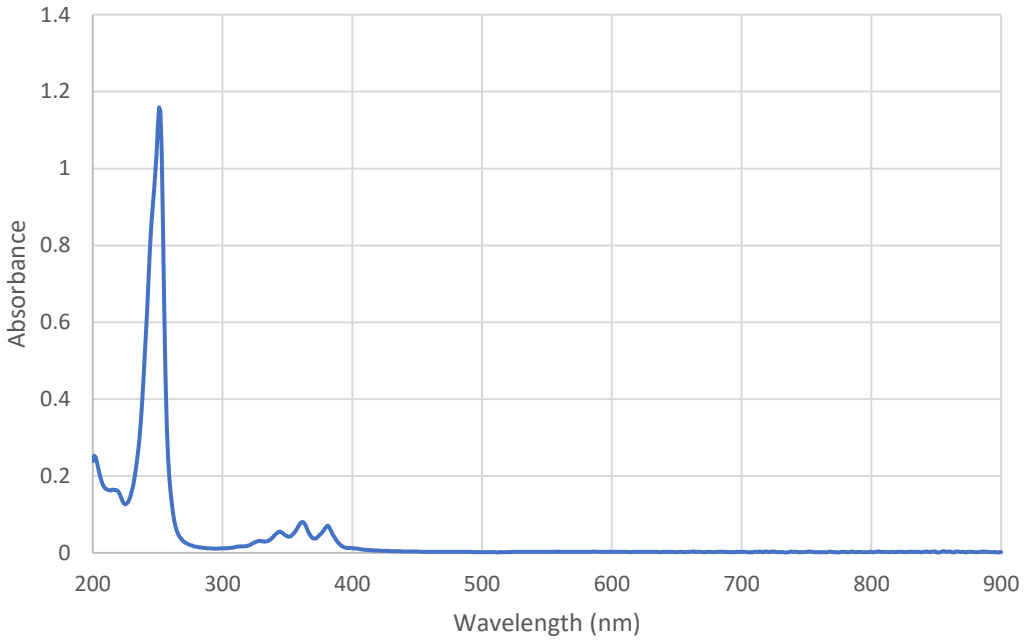

*Figure S160. UV/Vis spectrum of **9-(bromomethyl)anthracene** (1 x 10^{-5} M) in MeOH (made from a 1:1 DCM:MeOH stock solution)*

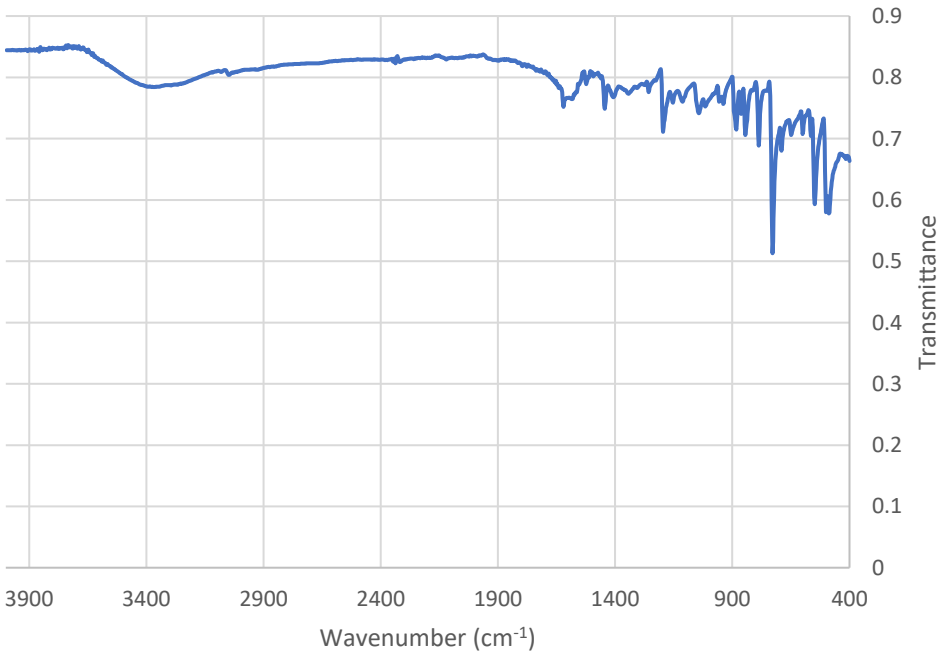

*Figure S161. FTIR spectrum of **9-(bromomethyl)anthracene***

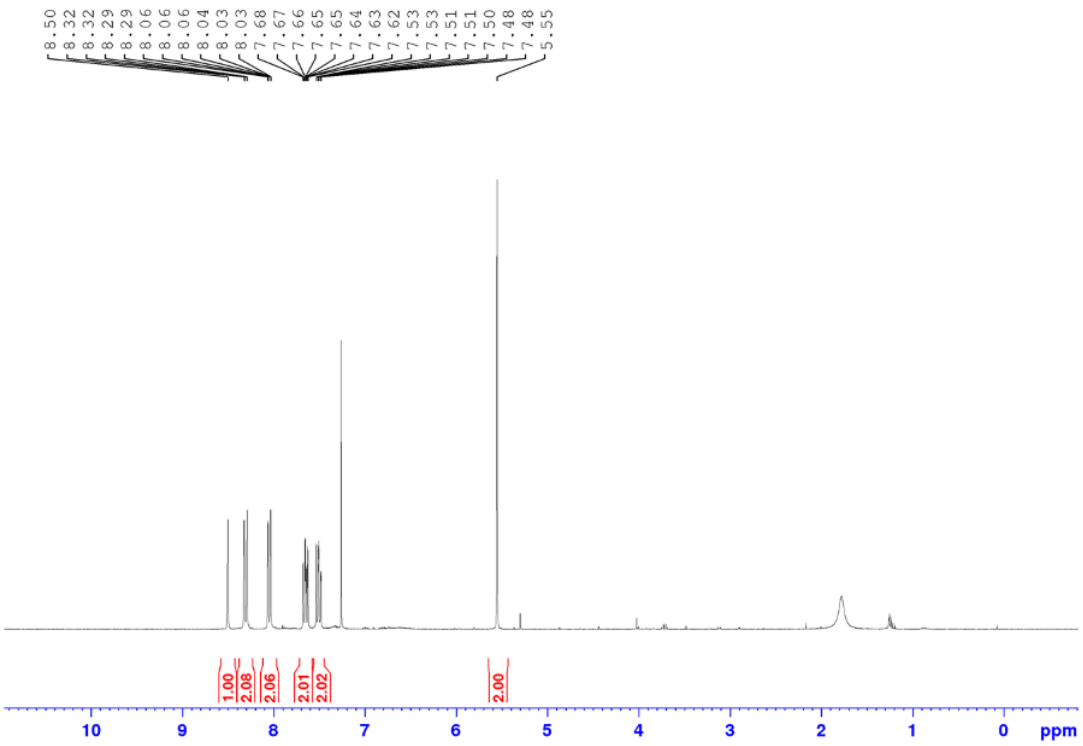

*Figure S162. [1]H NMR spectrum of **9-(bromomethyl)anthracene** in $CDCl_3$*

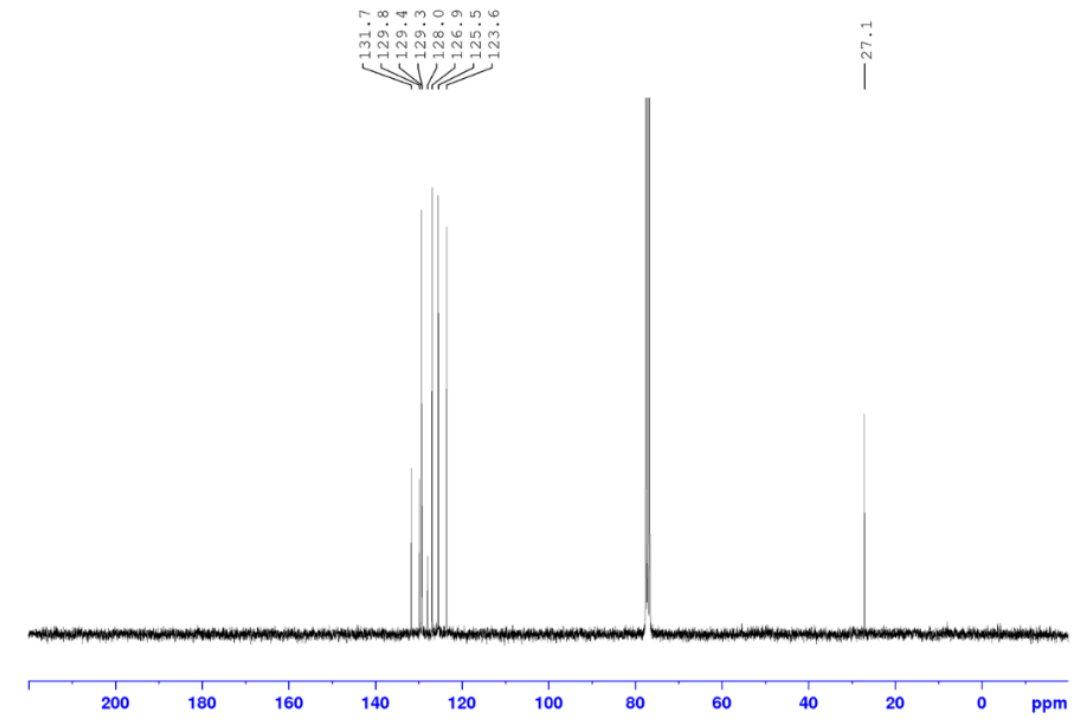

*Figure S163. [13]C NMR spectrum of **9-(bromomethyl)anthracene** in $CDCl_3$*

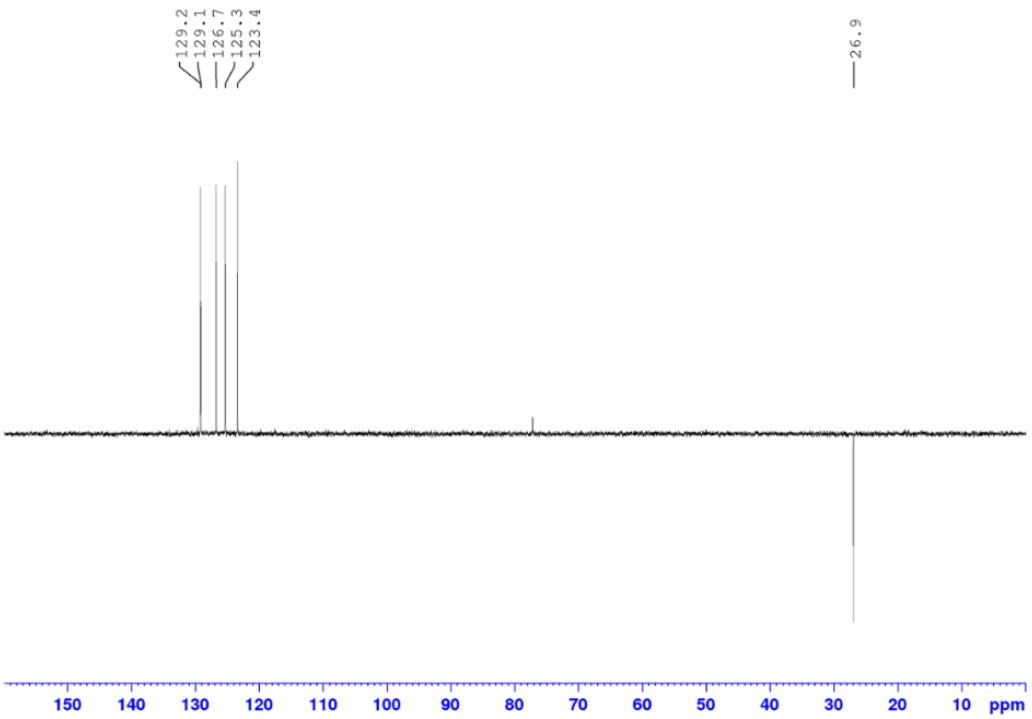

*Figure S164. ^{13}C DEPT spectrum of **9-(bromomethyl)anthracene** in $CDCl_3$*

9-(azidomethyl)anthracene (4N$_3$)

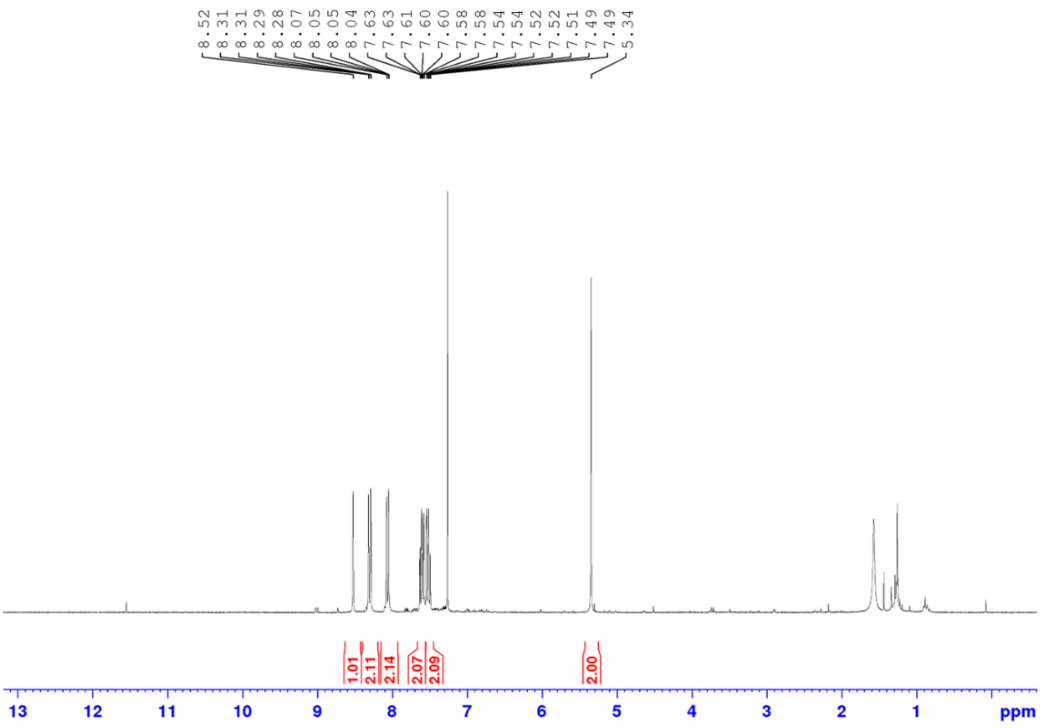

*Figure S165. ^{1}H NMR spectrum of **4N$_3$** in $CDCl_3$*

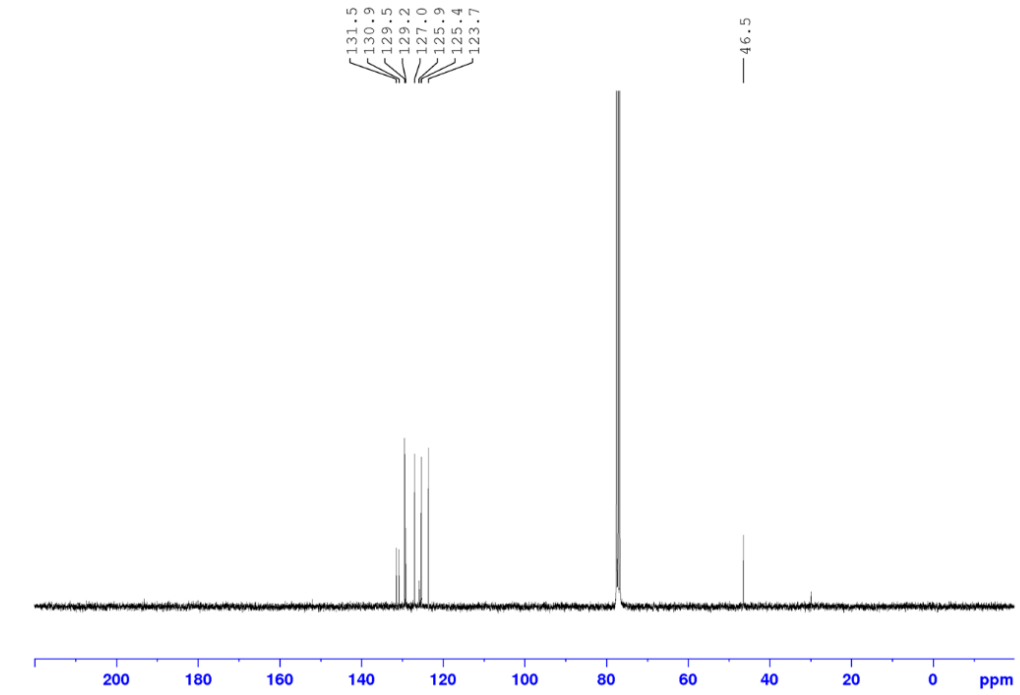

*Figure S166. ^{13}C NMR spectrum of **4N₃** in $CDCl_3$*

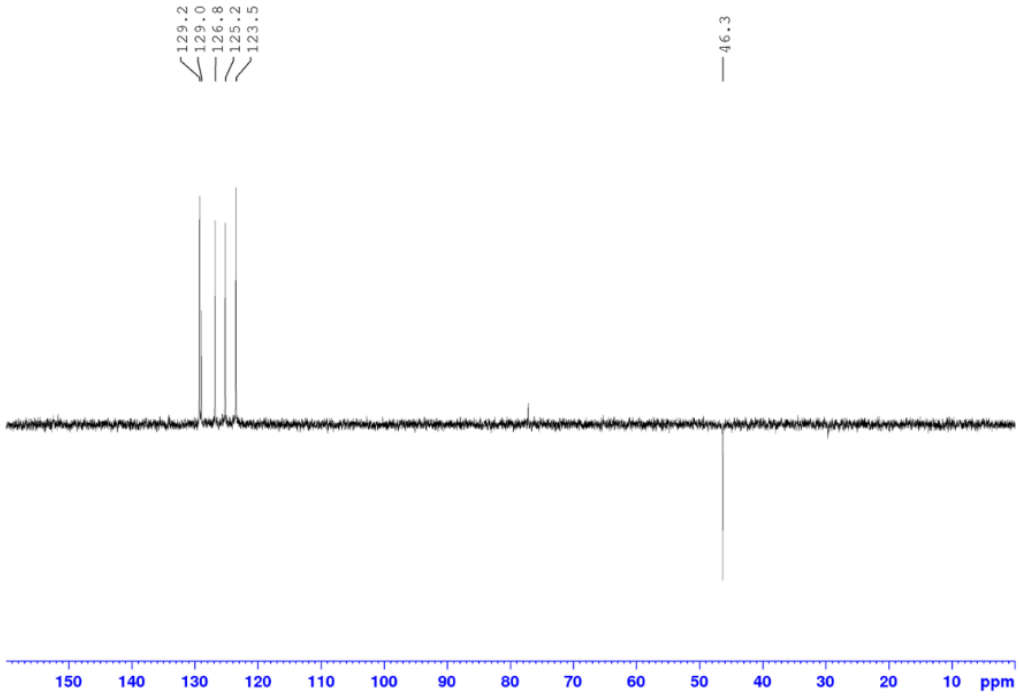

*Figure S167. ^{13}C DEPT spectrum of **4N₃** in $CDCl_3$*

MeOL$_4$

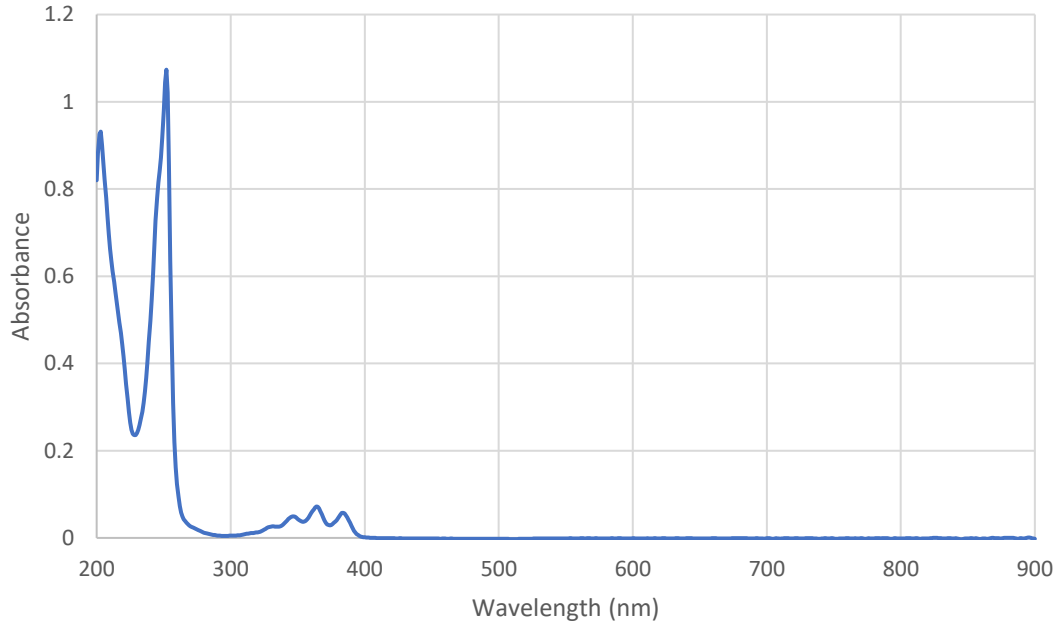

*Figure S168. UV/Vis spectrum of **MeOL$_4$** (1 x 10^{-5} M) in MeOH (made from a 1:1 DCM:MeOH stock solution)*

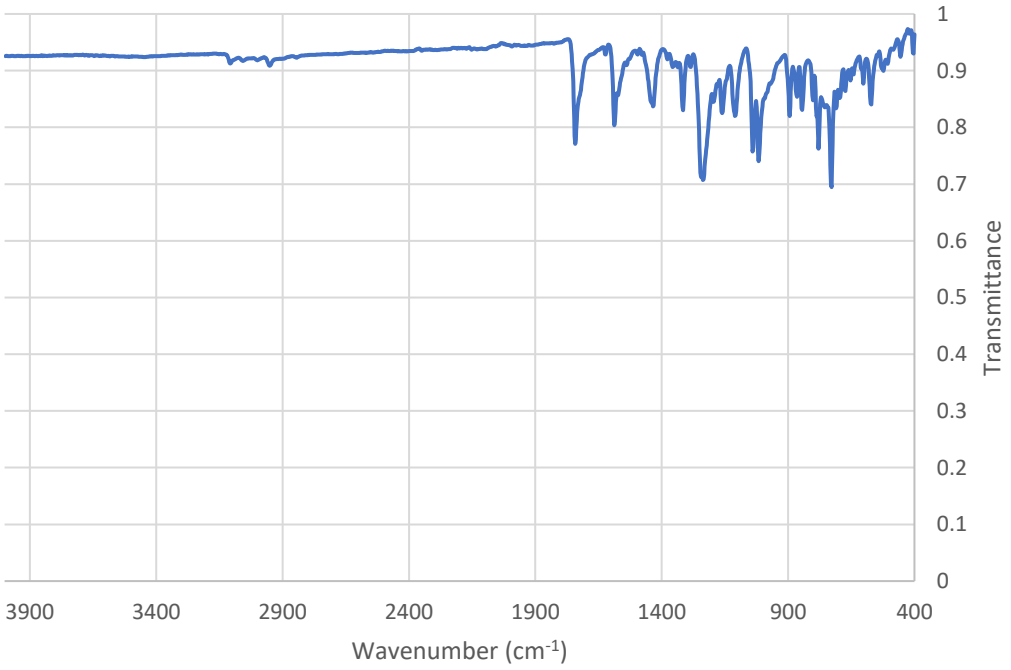

*Figure S169. FTIR spectrum of **MeOL$_4$***

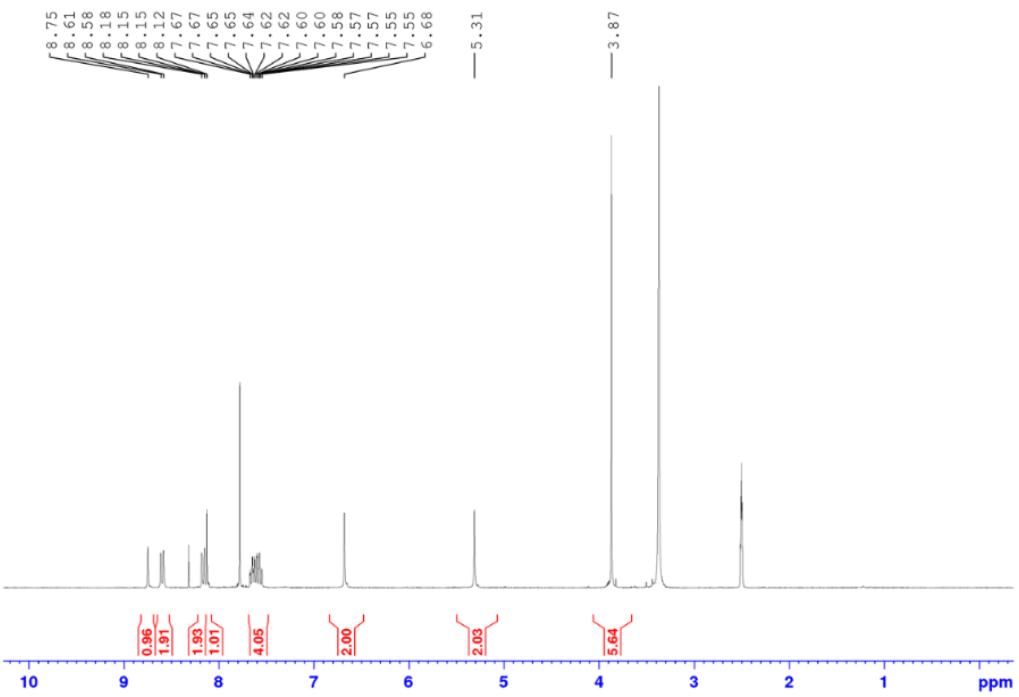

*Figure S170. [1]H NMR spectrum of **MeOL4** in DMSO-d6*

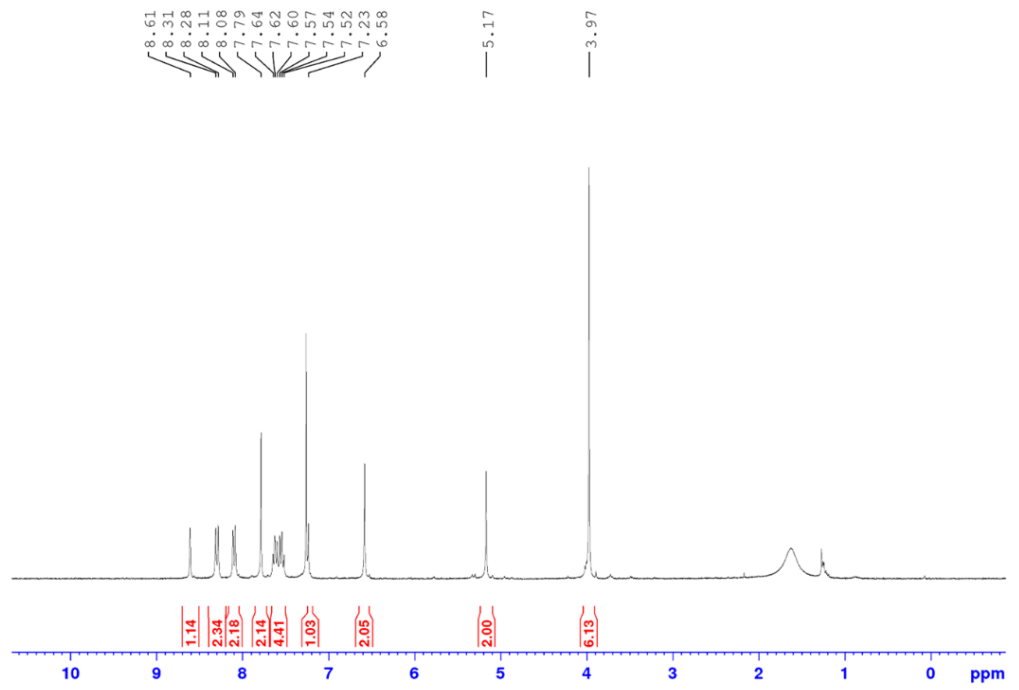

*Figure S171. [1]H NMR spectrum of **MeOL4** in CDCl3*

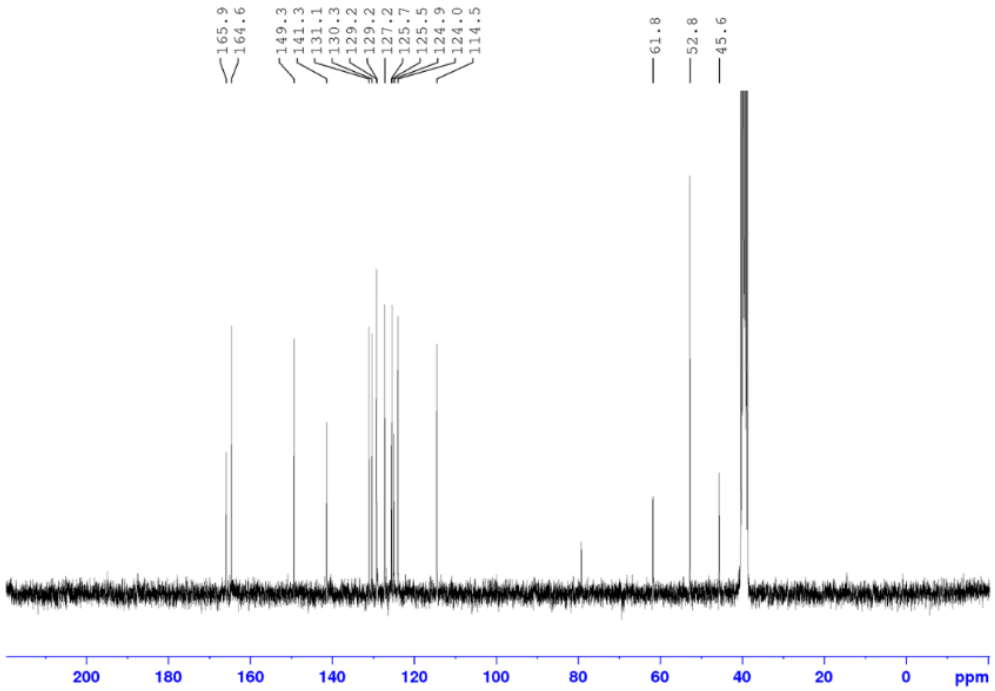

*Figure S172. ^{13}C NMR spectrum of **MeOL4** in DMSO-d_6*

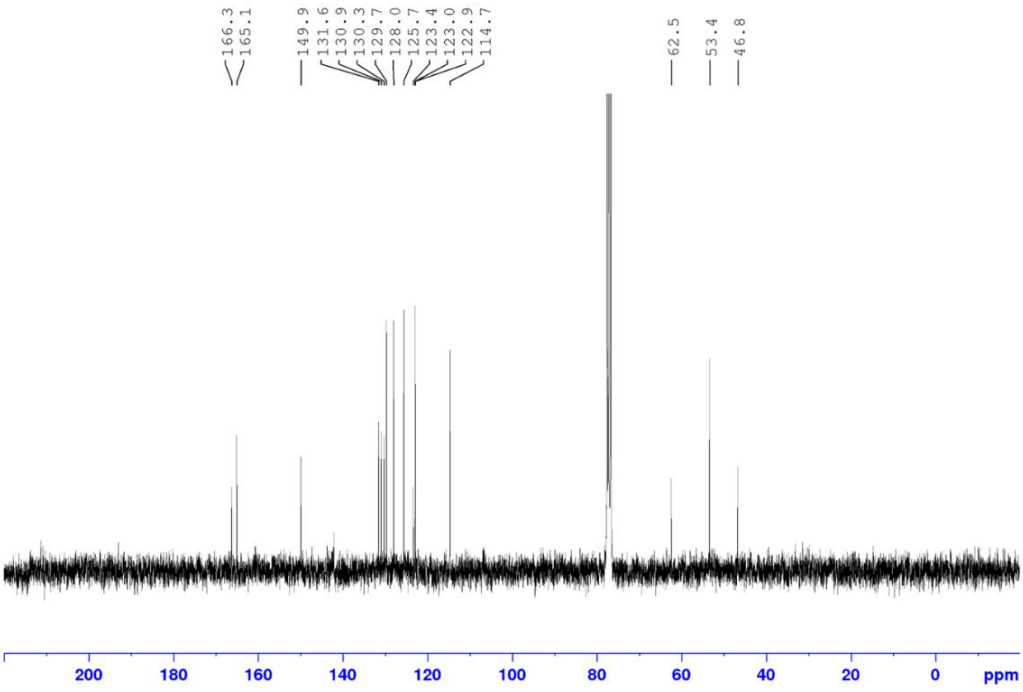

*Figure S173. ^{13}C NMR spectrum of **MeOL4** in DMSO-d_6*

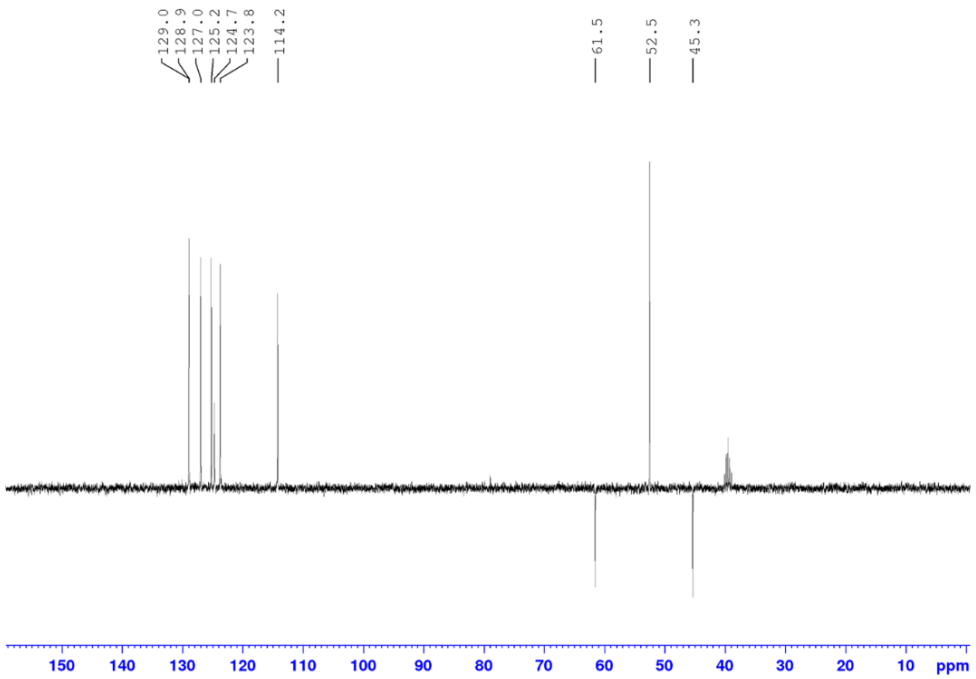

*Figure S174. ^{13}C DEPT spectrum of **MeOL$_4$** in DMSO-d_6*

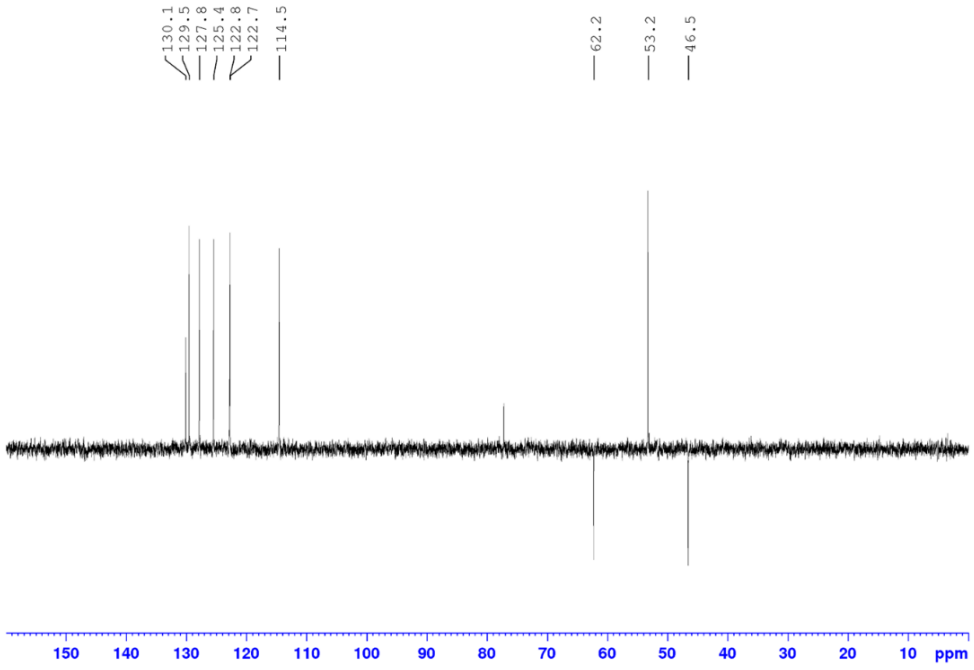

*Figure S175. ^{13}C DEPT spectrum of **MeOL$_4$** in $CDCl_3$*

L4

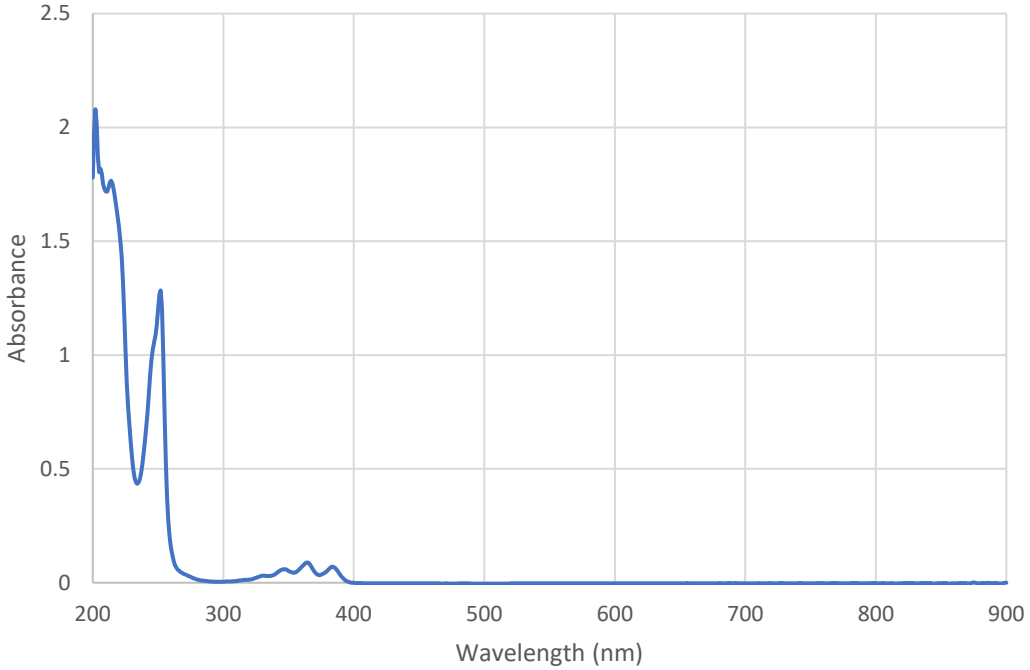

Figure S176. UV/Vis spectrum of ***L4*** *(1 x 10^{-5} M) in MeOH (made from a 1:1 DMSO:MeOH stock solution)*

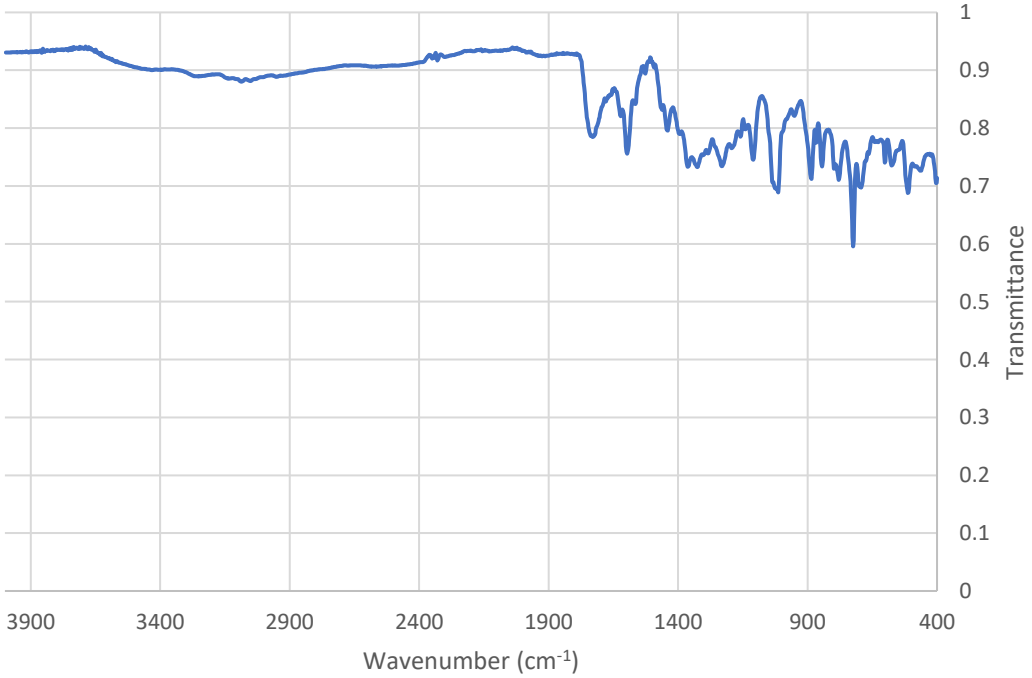

Figure S177. FTIR spectrum of ***L4***

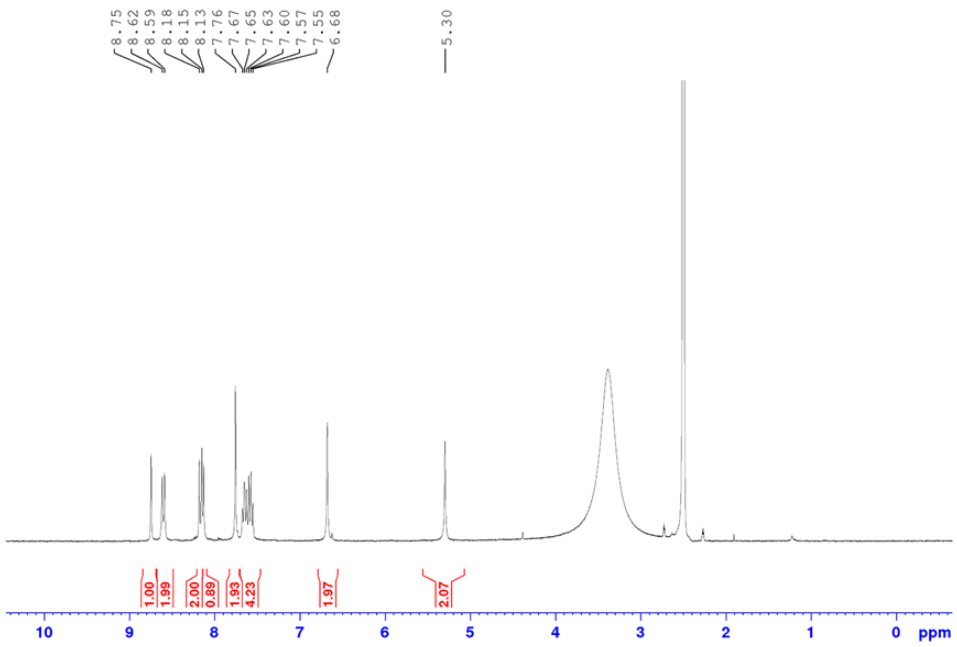

Figure S178. ^{1}H NMR spectrum of ***L*****$_4$** *in DMSO-d_6*

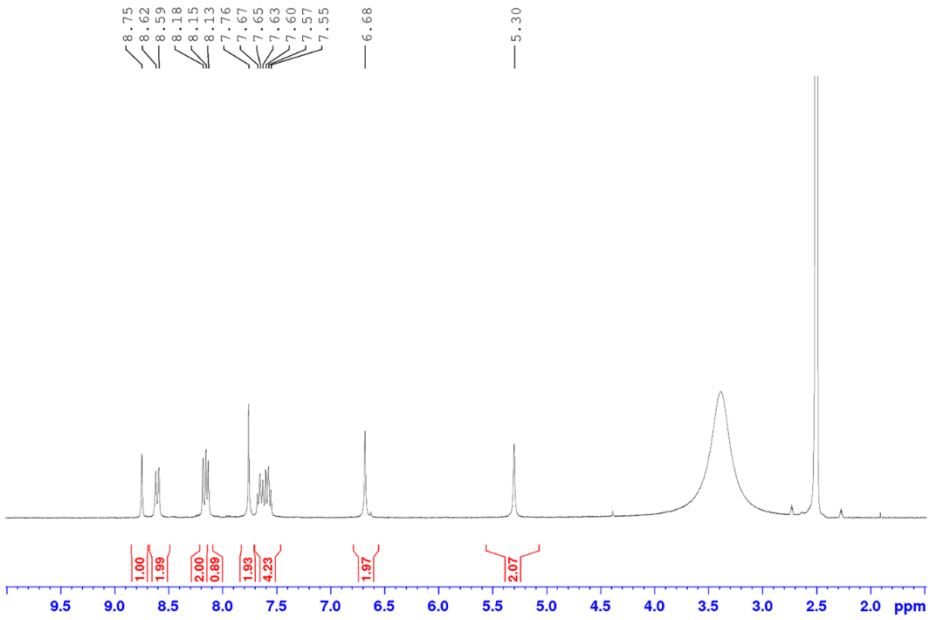

Figure S179. ^{1}H NMR spectrum of ***L*****$_4$** *in DMSO-d_6 zoomed in*

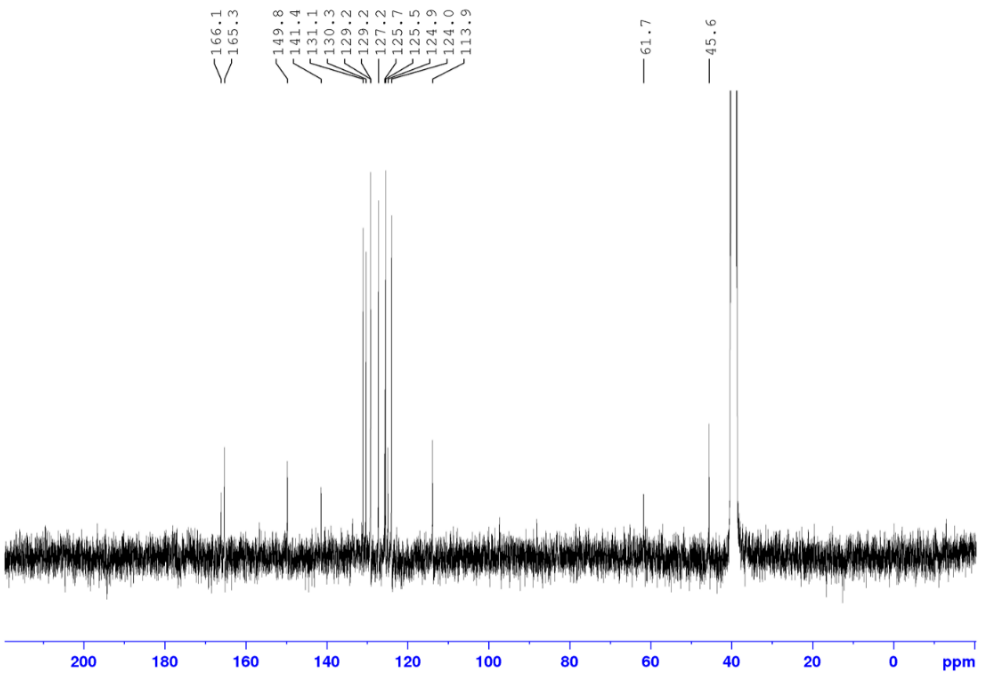

*Figure S180. ^{13}C NMR spectrum of **L4** in DMSO-d_6*

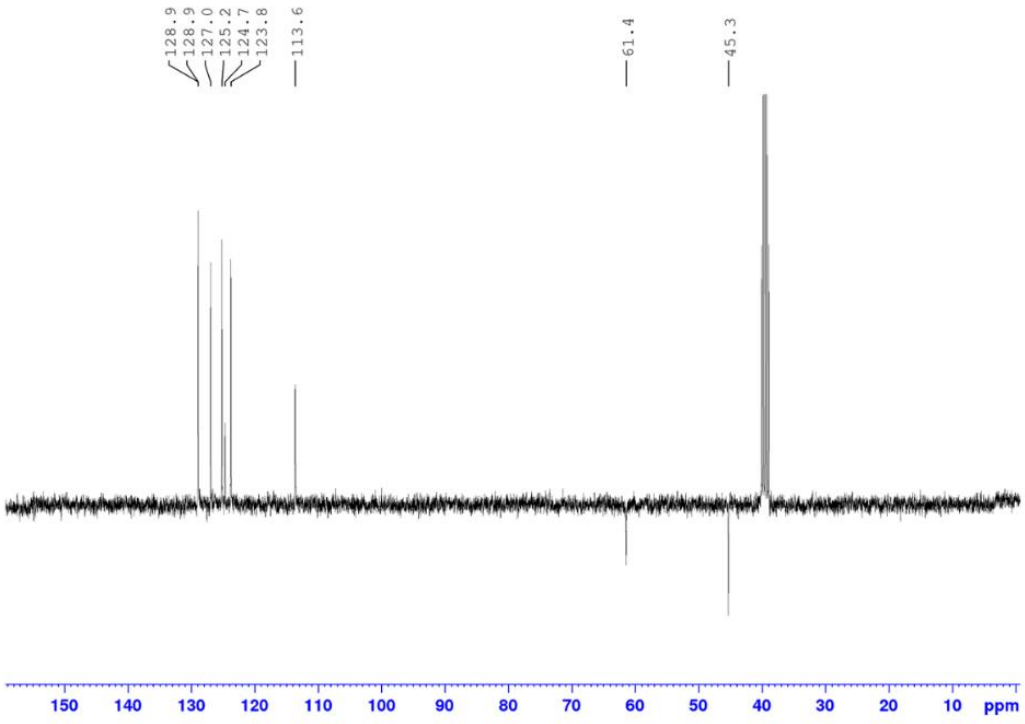

*Figure S181. ^{13}C DEPT spectrum of **L4** in DMSO-d_6*

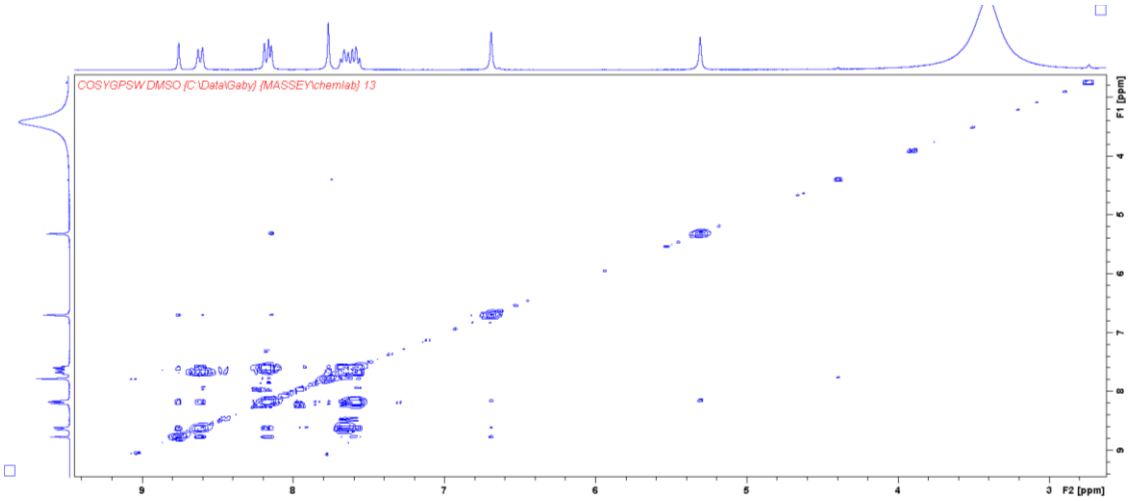

Figure S182. COSY spectrum of ***L4*** *in DMSO-d6*

$[La(L_4)_3]^{3-}$

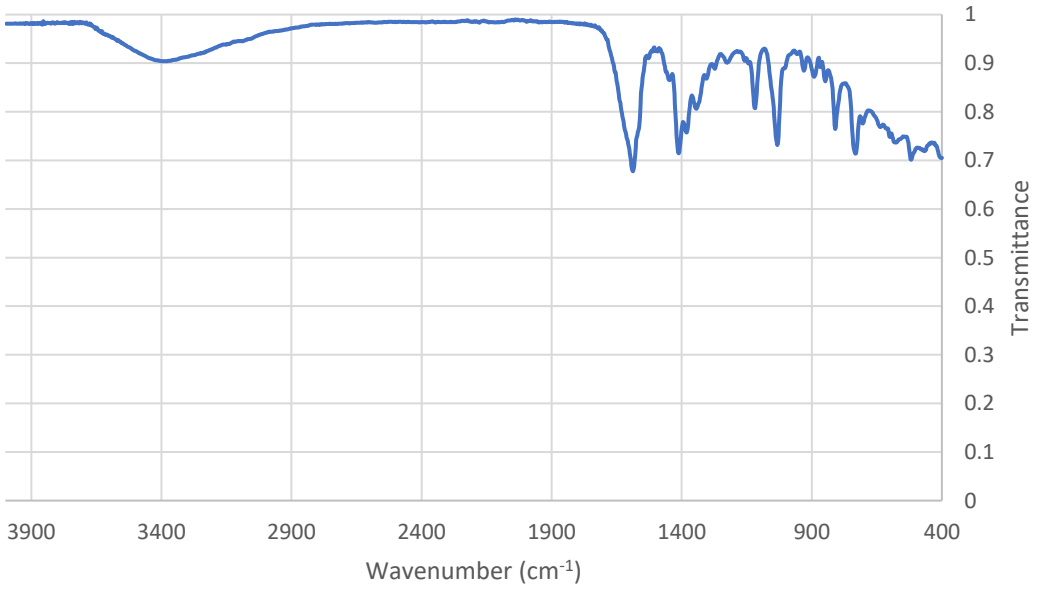

Figure S183. FTIR spectrum of ***$[La(L_4)_3]^{3-}$***

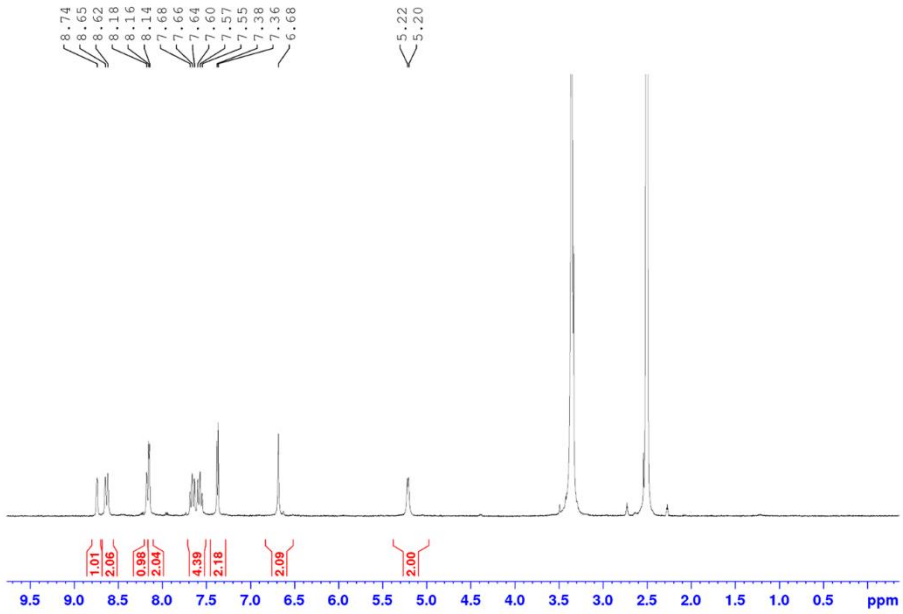

Figure S184. ^{1}H NMR spectrum of ***[La(L4)3]3-*** *in DMSO-d6*

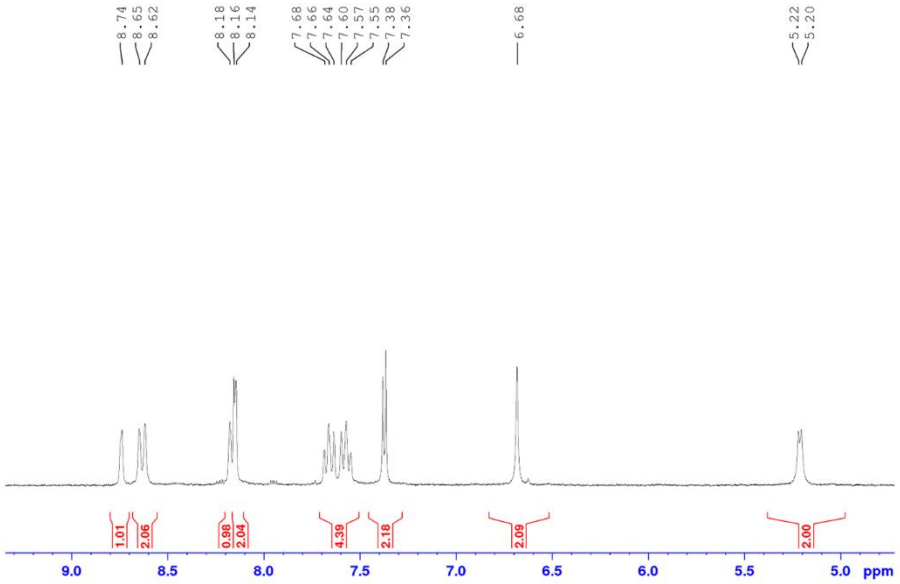

Figure S185. ^{1}H NMR spectrum zoom in of ***[La(L4)3]3-*** *in DMSO-d6*

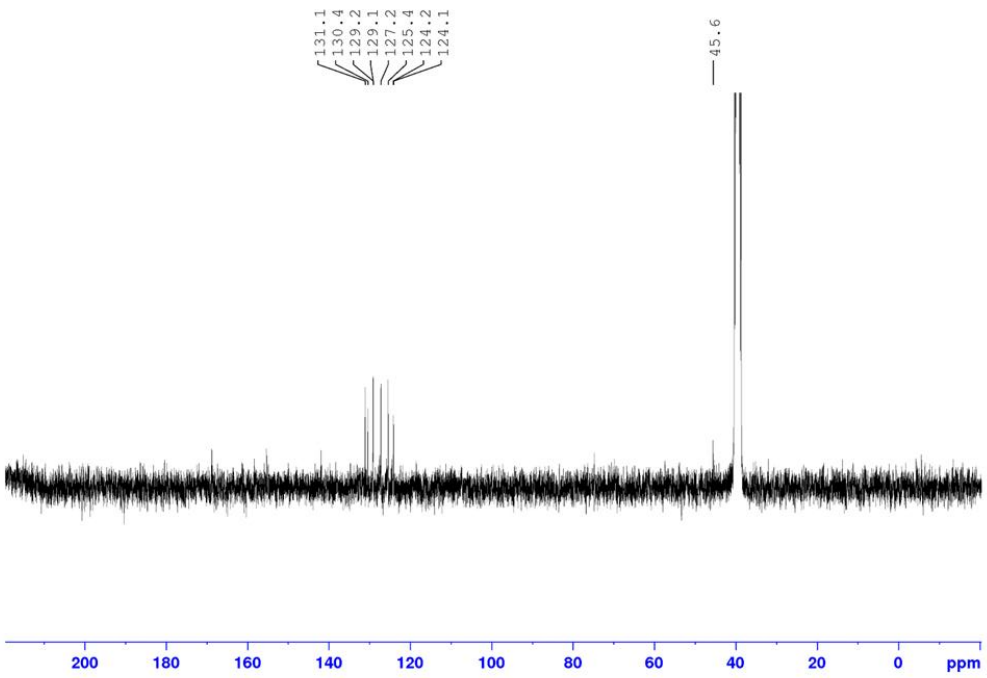

Figure S186. ^{13}C NMR spectrum of ***[La(L4)3]3-*** *in DMSO-d6*

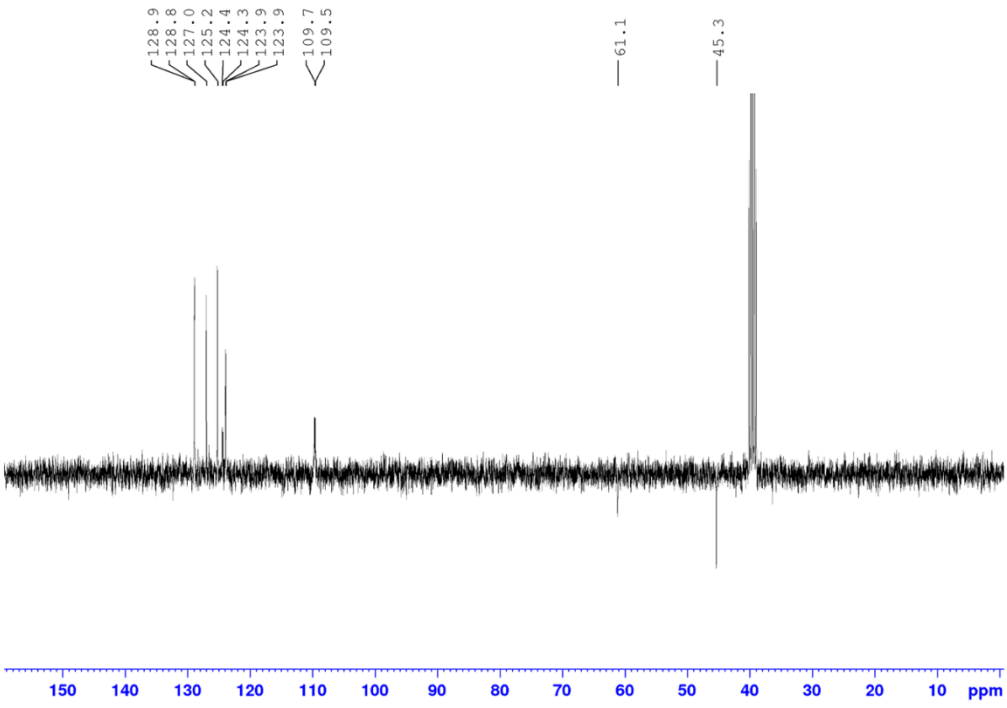

Figure S187. ^{13}C DEPT spectrum of ***[La(L4)3]3-*** *in DMSO-d6*

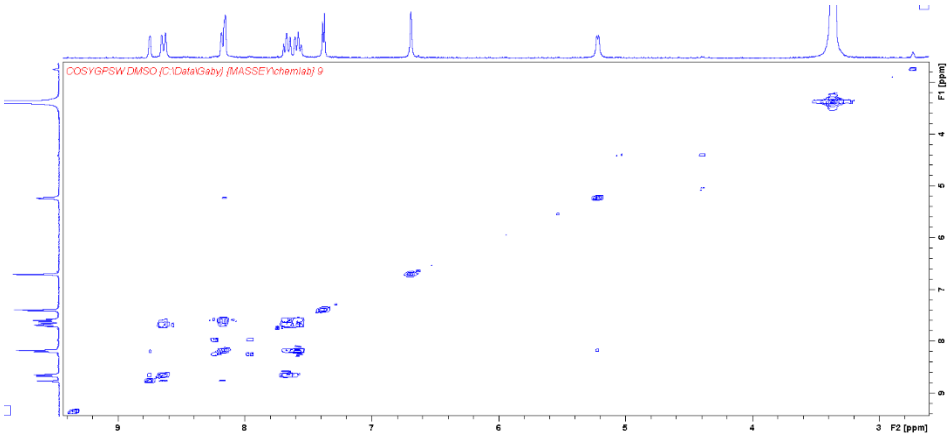

Figure S188. COSY spectrum of ***[La(L4)3]3-*** *in DMSO-d6*

$[Eu(L_4)_3]^{3-}$

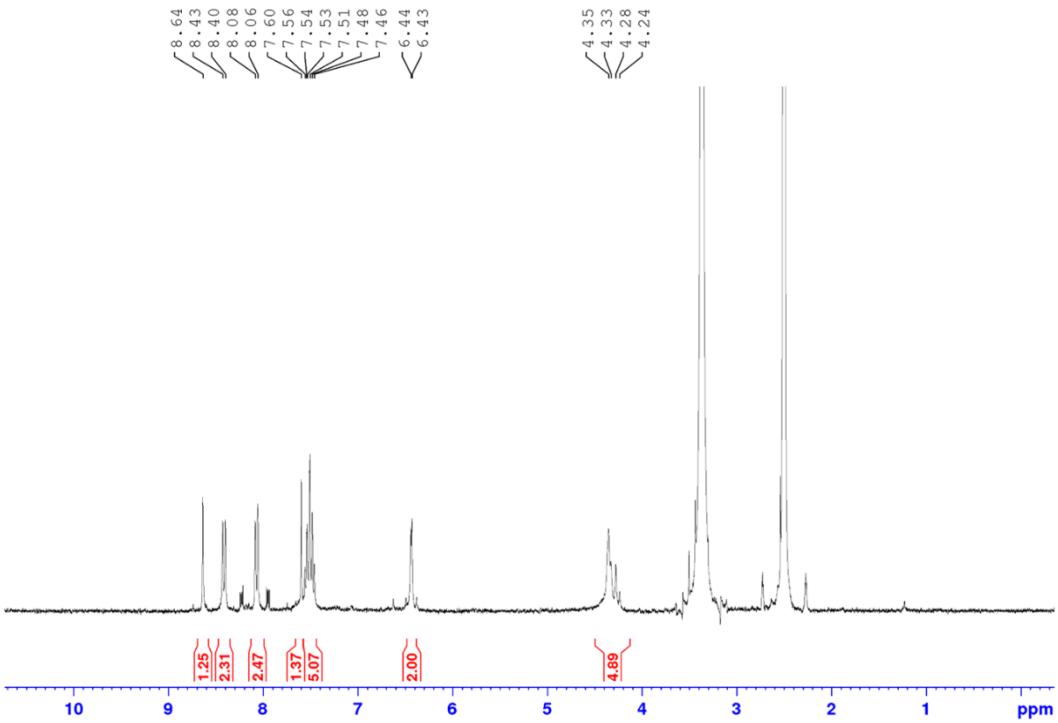

Figure S189. ^{1}*H NMR spectrum of crude* ***[Eu(L4)3]3-*** *in DMSO-d6*

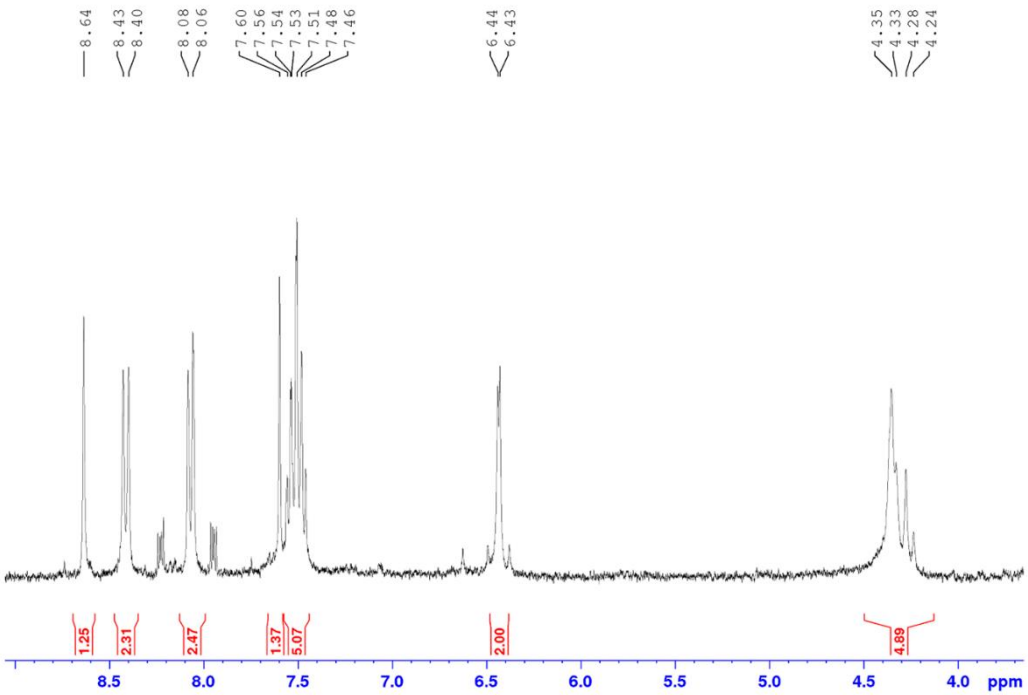

Figure S190. ^{1}H NMR spectrum zoom in of crude ***[Eu(L4)3]3-*** *in DMSO-d_6*

Macrocycle (M_1)

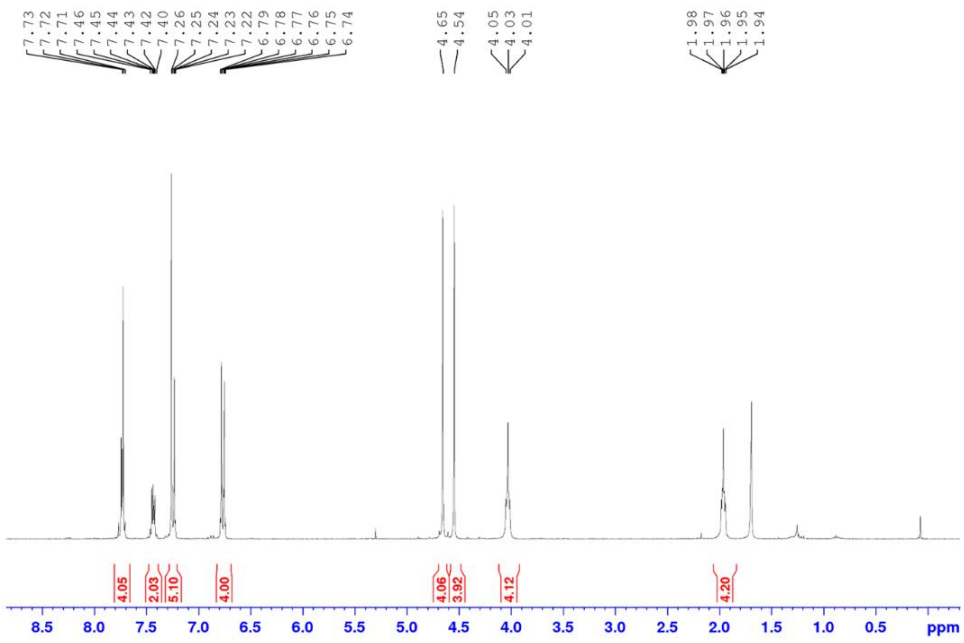

Figure S191. ^{1}H NMR spectrum of ***M_1*** *in $CDCl_3$*

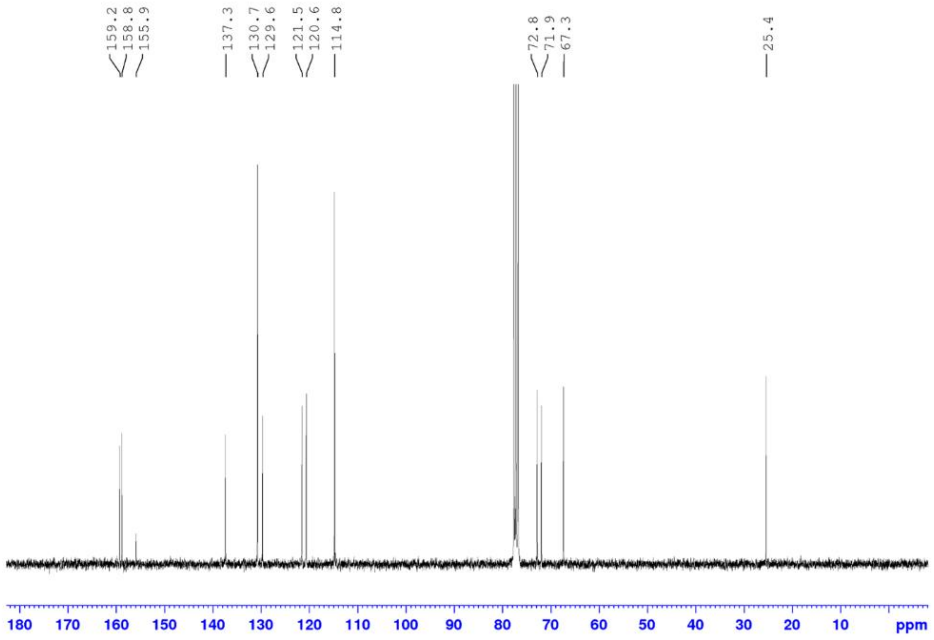

*Figure S192. ^{13}C NMR spectrum of **M₁** in $CDCl_3$*

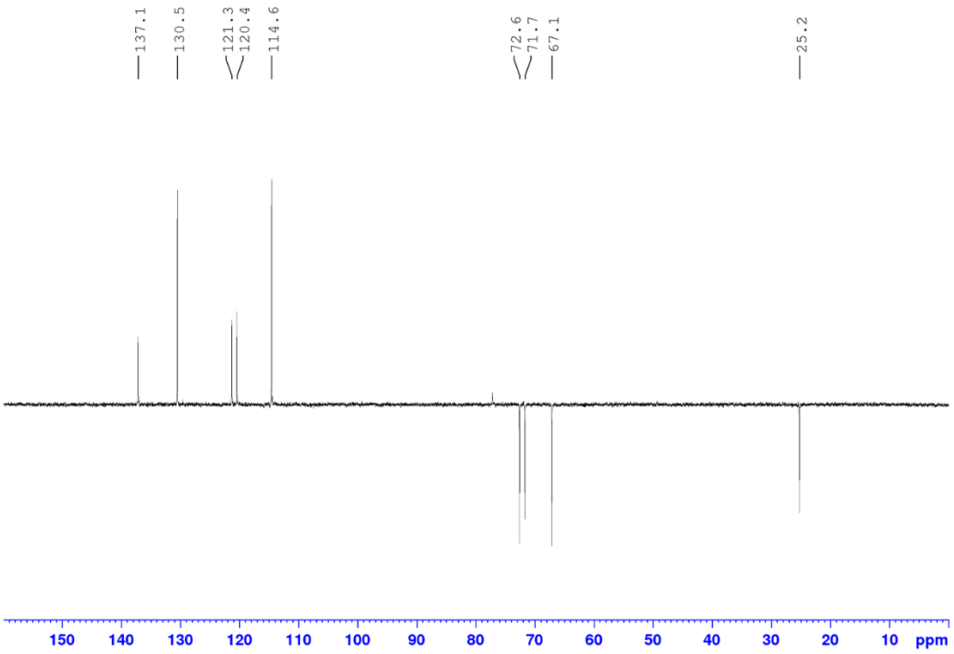

*Figure S193. ^{13}C DEPT spectrum of **M₁** in $CDCl_3$*

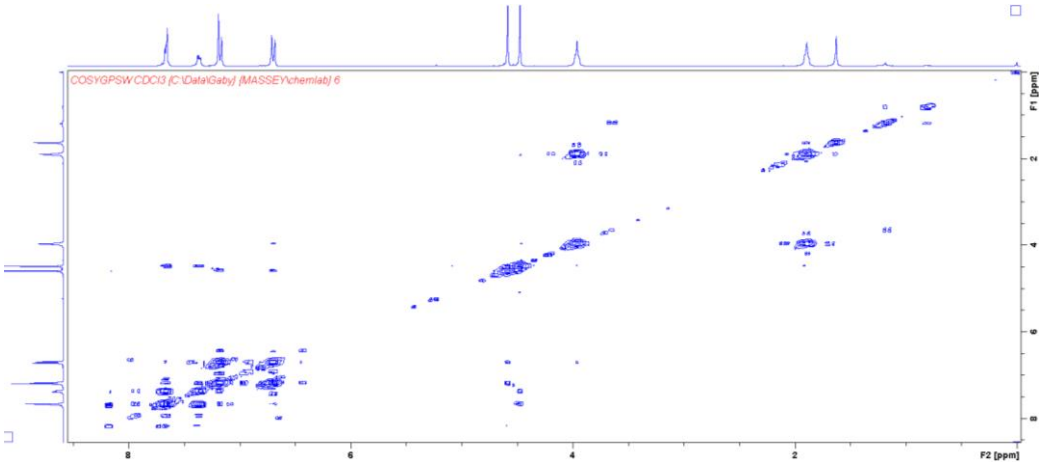

Figure S194. COSY spectrum of ***M₁*** *in* $CDCl_3$

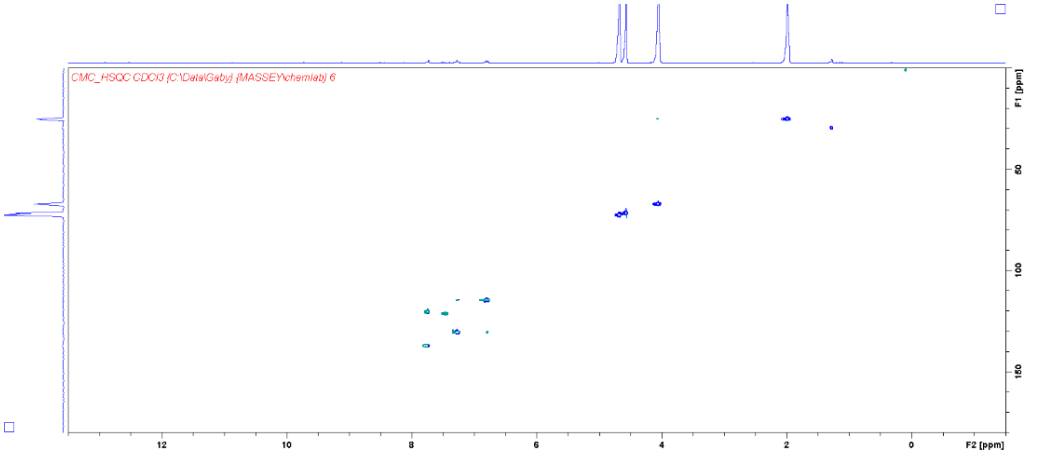

Figure S195. HSQC spectrum of ***M₁*** *in* $CDCl_3$

L_1 titration with $EuCl_3.6H_2O$

The ability of **L_1** to form 3:1 L_1:Eu^{3+} complexes was investigated through UV/Vis and fluorescence titrations. To make the **L_1** and base (1 x 10^{-5} M) solution, **L_1** (1 equivalent) was combined with Na_2CO_3 (2 equivalents) and dissolved in the appropriate amount of deionised H_2O to make a 1 x 10^{-2} M solution after which it was diluted to make the 1 x 10^{-5} M solution. Next, a 7.5 x 10^{-5} M solution of $EuCl_3 \cdot 6H_2O$ in deionised H_2O was made from which appropriate aliquots could be taken and added to the 1 x 10^{-5} M **L_1** and Na_2CO_3 solution depending on the equivalents to be added. Additions from 0 → 4.0 equivalents were carried out. UV/Vis titrations were carried out in triplicate whereas only a single crude fluorescence titrations was carried out.

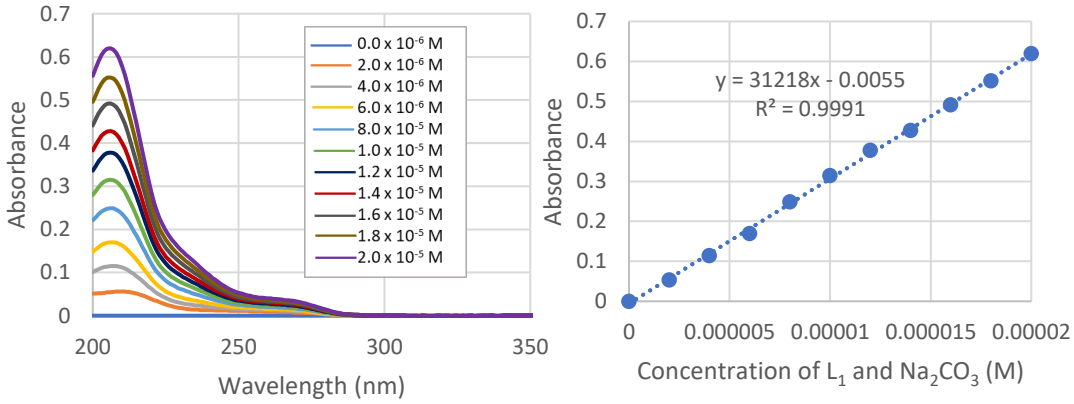

Figure S196. (Left) Absorbance of L_1 and Na_2CO_3 in H_2O at increasing concentrations for molar absorptivity calculation. (Right) Absorbance at 206 nm plotted as a function of concentration of L_1 and Na_2CO_3 in H_2O

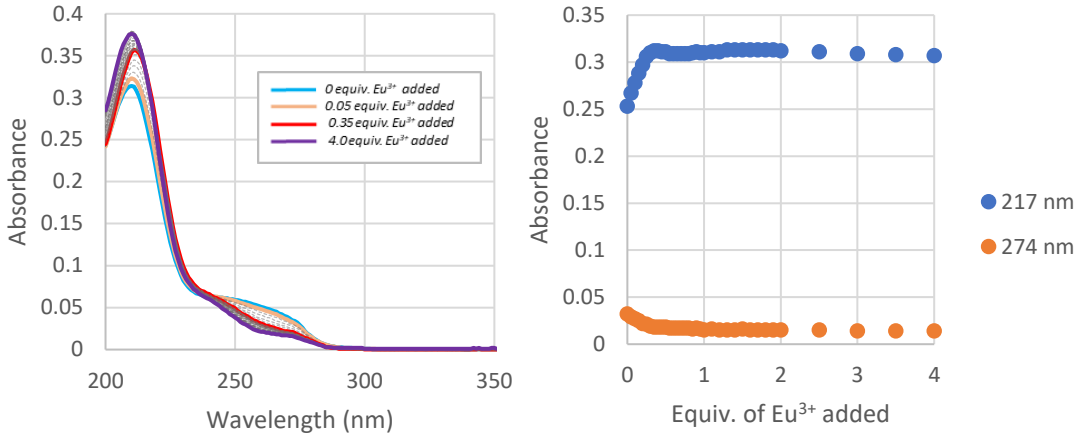

Figure S197. (Left) Run 1: UV/Vis titration of L_1 and Na_2CO_3 on the stepwise addition of $EuCl_3{\cdot}6H_2O$ from 0 → 4.0 equivalents. (Right) Run 1: Changes in absorbance values of L_1 and Na_2CO_3 at 217 nm (blue dots) and 274 nm (orange dots) as a function of equivalents of Eu^{3+} added

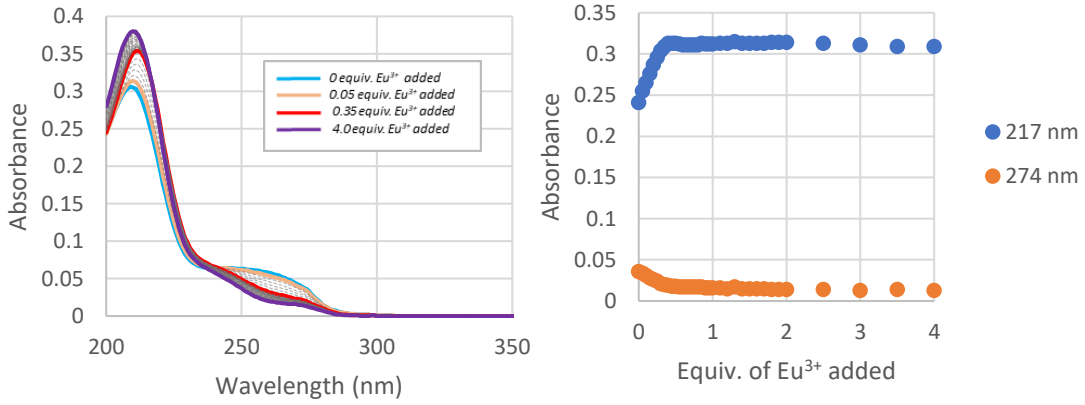

Figure S198. (Left) Run 2: UV/Vis titration of L_1 and Na_2CO_3 on the stepwise addition of $EuCl_3{\cdot}6H_2O$ from 0 → 4.0 equivalents. (Right) Run 2: Changes in absorbance values of L_1 and Na_2CO_3 at 217 nm (blue dots) and 274 nm (orange dots) as a function of equivalents of Eu^{3+} added

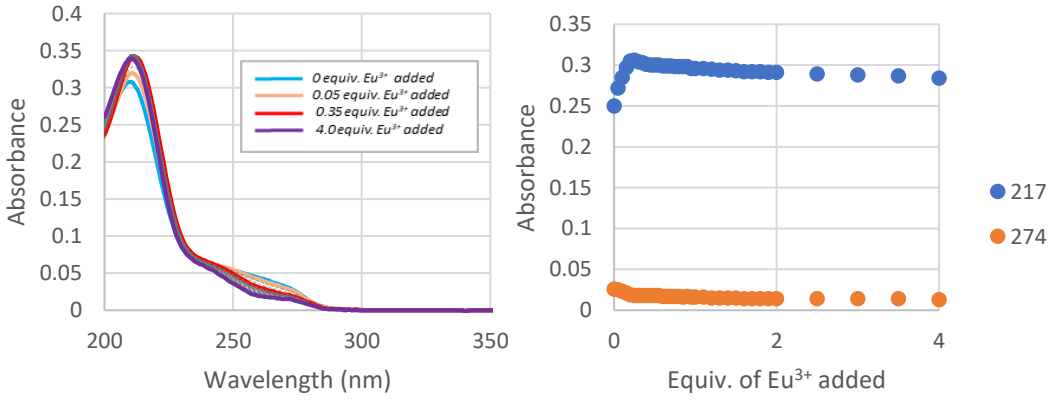

Figure S199. (Left) Run 3: UV/Vis titration of L_1 and Na_2CO_3 on the stepwise addition of $EuCl_3{\cdot}6H_2O$ from 0 → 4.0 equivalents. (Right) Run 3: Changes in absorbance values of L_1 and Na_2CO_3 at 217 nm (blue dots) and 274 nm (orange dots) as a function of equivalents of Eu^{3+} added

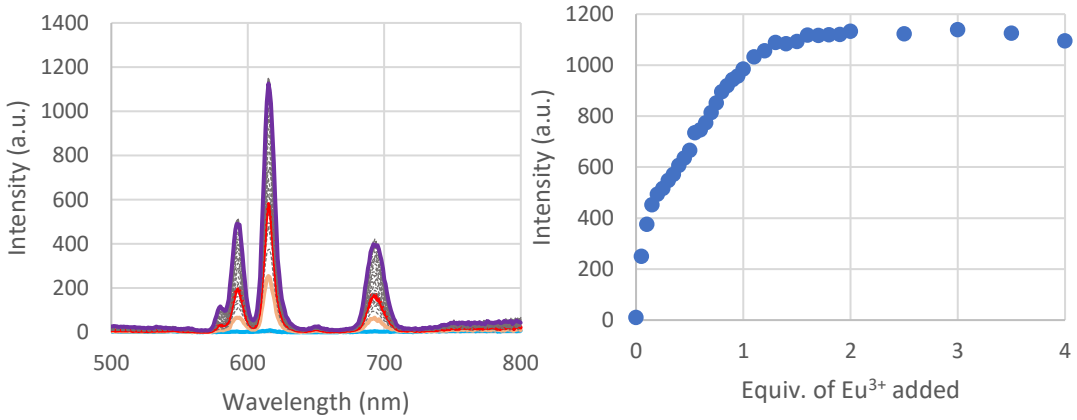

Figure S200. (Left) Fluorescence titration of L_1 and Na_2CO_3 on the stepwise addition of $EuCl_3 \cdot 6H_2O$ from 0 → 4.0 equivalents. (Right). Changes in the intensity of emission corresponding to the $^5D_0 \rightarrow {}^7F_2$ transition (616 nm) as a function of equivalents of Eu^{3+} added

$Na_3[Eu(L_1)_3]\cdot 16H_2O$

Table S12. Crystal and refinement data summary

Empirical formula	$C_{30}H_{39.5}EuN_3Na_{2.75}O_{28.25}$
Formula weight	1109.33
Temperature/K	150.0
Crystal system	Triclinic
Space group	P-1
a/Å	15.6757(7)
b/Å	15.8499(7)
c/Å	17.4545(8)
α/°	94.186(2)
β/°	104.644(2)
γ/°	90.116(2)
Volume/Å^3	4183.7(3)
Z	4
ρ_{calc}g/cm^3	1.761
μ/mm^{-1}	11.948
F(000)	2239.0
Crystal size/mm^3	0.42 x 0.20 x 0.1
Radiation	CuKα (λ = 1.54178)
2Θ range for data collection/°	5.248 to 130.66
Index ranges	$-18 \le h \le 18$, $-16 \le k \le 18$, $-20 \le l \le 20$
Reflections collected	71134
Independent reflections	13937 [R_{int} = 0.0807, R_{sigma} = 0.0587]
Data/restraints/parameters	13937/0/1201
Goodness-of-fit on F^2	1.078
Final R indexes [I>=2σ (I)]	R_1 = 0.0876, wR_2 = 0.2319
Final R indexes [all data]	R_1 = 0.0954, wR_2 = 0.2375
Largest diff. peak/hole / e Å^{-3}	2.54/-2.07

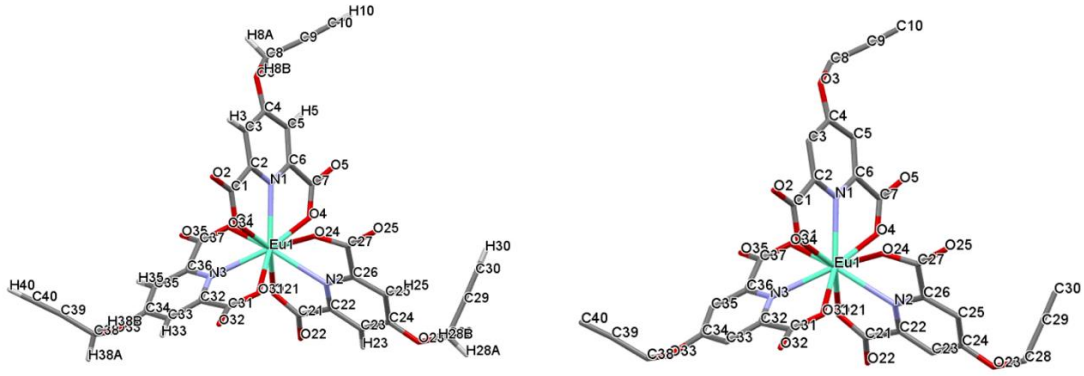

Figure S201. (Left) Capped stick representation of the Eu1 unit with hydrogen atoms. (Right) Capped stick representation of the Eu1 unit without hydrogen atoms

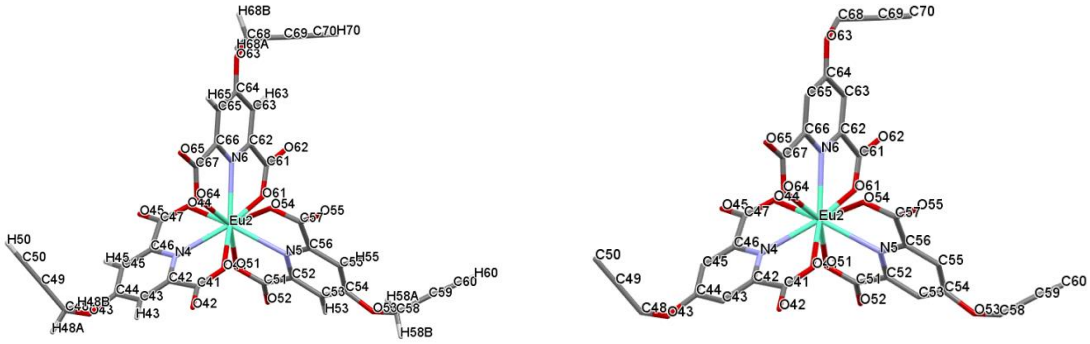

Figure S202. (Left) Capped stick representation of the Eu2 unit with hydrogen atoms. (Right) Capped stick representation of the Eu2 unit without hydrogen atoms

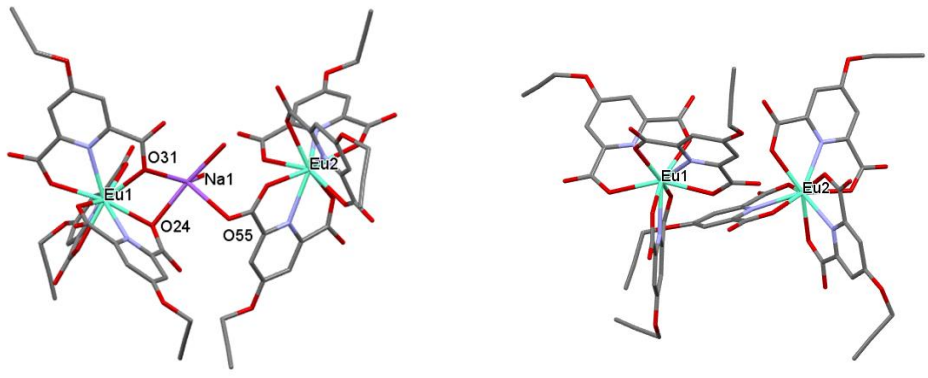

Figure S203. (Left) Capped stick representation showing how the two crystallographically distinct Eu1 and Eu2 complexes are linked together in the asymmetric unit through a sodium (Na1) bridge between O31 and O24 of the Eu1 and O55 of Eu2. (Right). Capped stick representation showing how the two crystallographically distinct Eu1 and Eu2 motifs orientate relative to one-another in the asymmetric unit

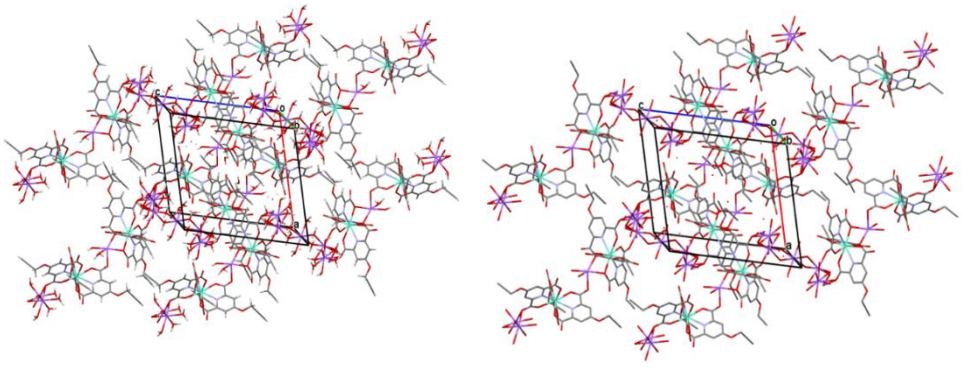

Figure S204. (Left) Packing diagram obtained for $Na_3[Eu(L_1)_3]\cdot 16H_2O$ with hydrogen atoms. (Right) Packing diagram obtained for $Na_3[Eu(L_1)_3]\cdot 16H_2O$ without hydrogen atoms for clarity

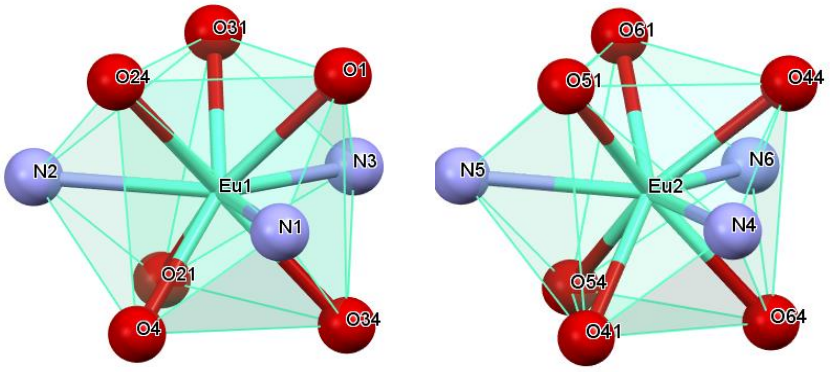

Figure S205. (Left) Coordination polyhedron obtained for the Eu1 motif showing the tricapped trigonal prismatic geometry. (Right) Coordination polyhedron obtained for the Eu2 motif showing the tricapped trigonal prismatic geometry

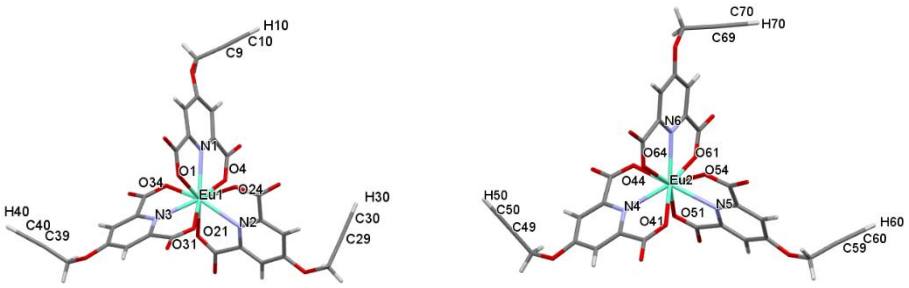

Figure S206. Capped stick representation of the Eu1 motif (left) and the Eu2 motif (right) with simplified labelling

Different conditions used for the AT-CuAAC reactions on $[La(L_1)_3]^{3-}$

Conditions 1:

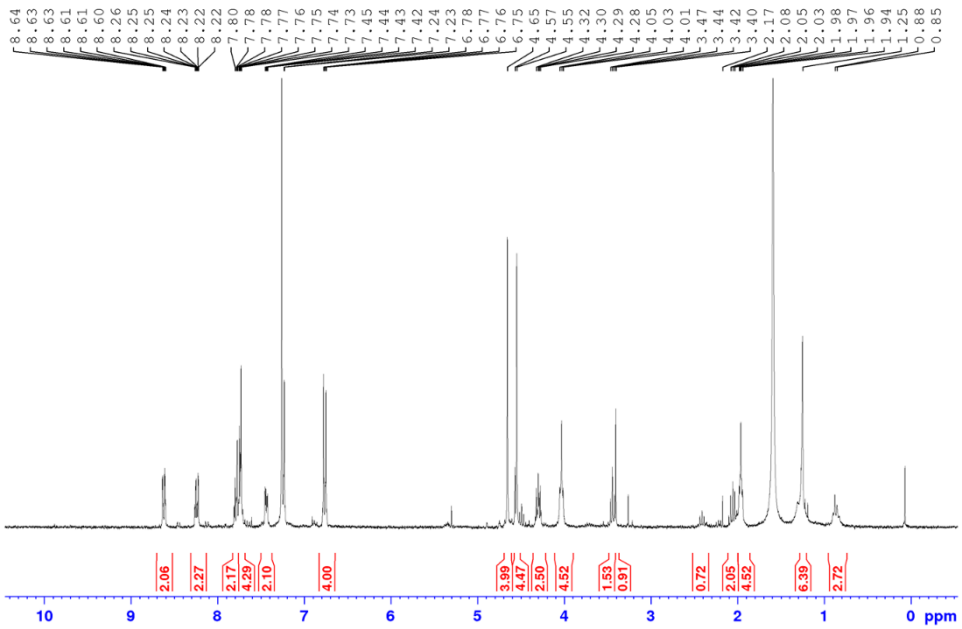

Figure S207. ^{1}H NMR spectrum obtained for the crude product extracted using conditions 1 in $CDCl_3$

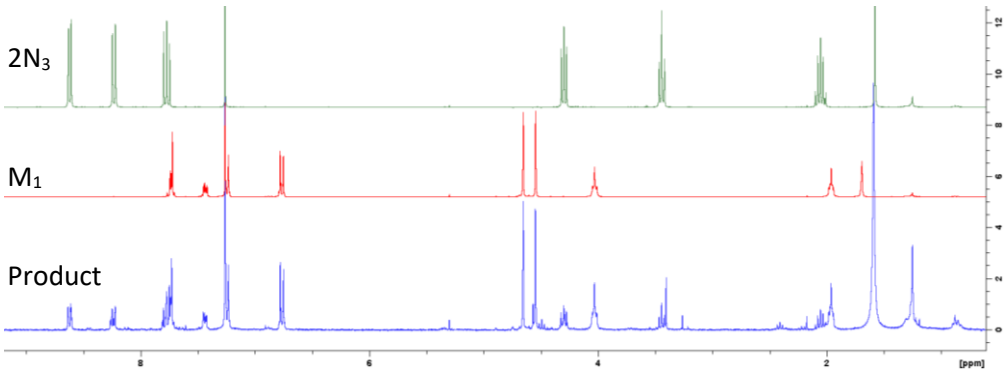

Figure S208. ^{1}H NMR spectrum of the crude product extracted using conditions 1 (blue, bottom) compared to M_1 (red, middle) and $2N_3$ (green, top) in $CDCl_3$

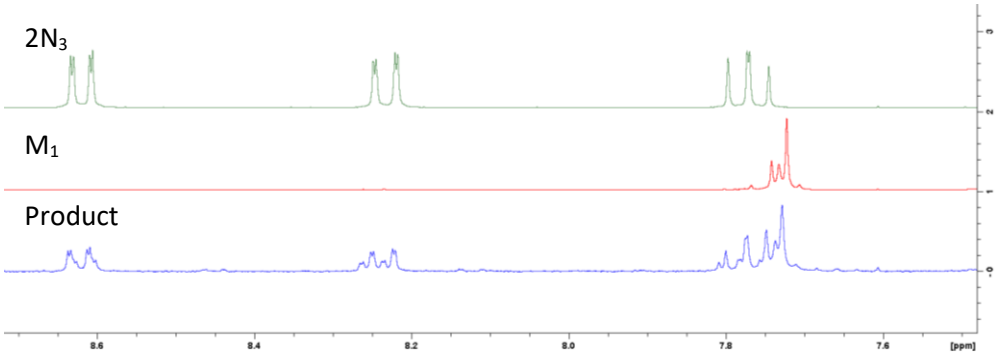

Figure S209. Zoom in on the aromatic region of the ^{1}H NMR spectrum of the crude product extracted using conditions 1 (blue, bottom) compared to M_1 (red, middle) and $2N_3$ (green, top) in $CDCl_3$

Conditions 2:

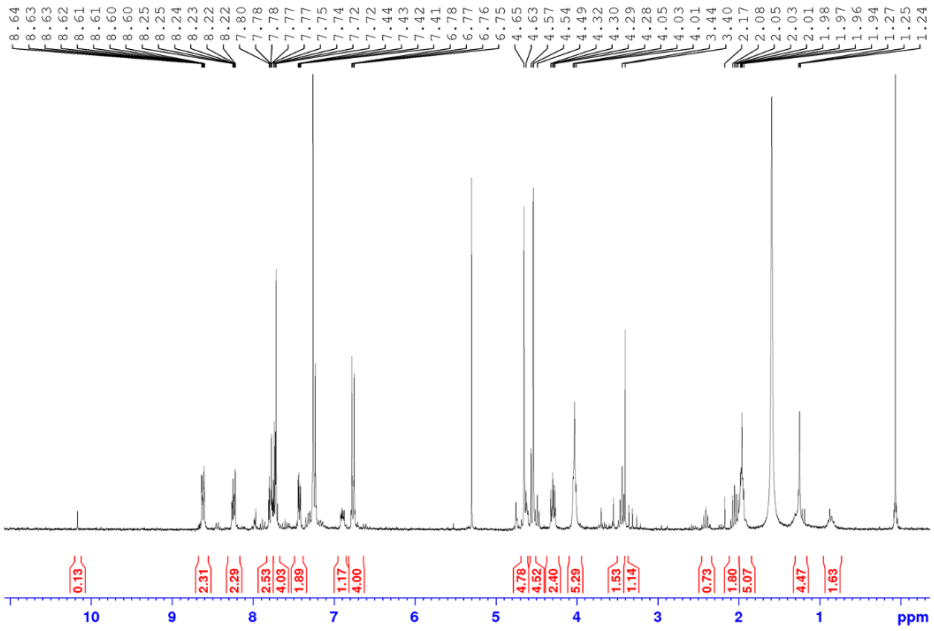

Figure S210. ^{1}H NMR spectrum obtained for the crude product extracted using conditions 2 in $CDCl_3$

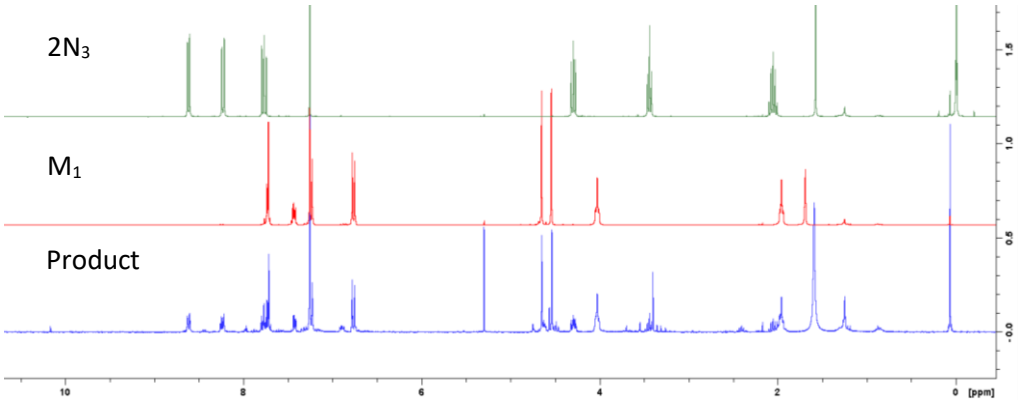

Figure S211. ^{1}H NMR spectrum of the crude product extracted using conditions 2 (blue, bottom) compared to M_1 (red, middle) and $2N_3$ (green, top) in $CDCl_3$

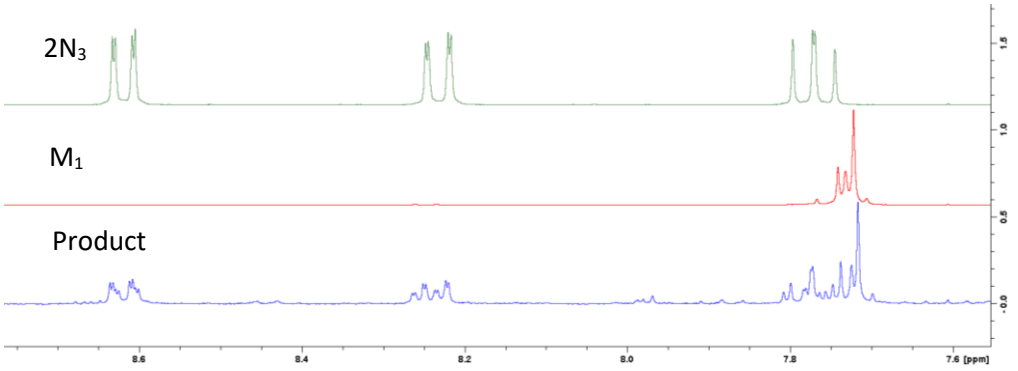

Figure S212. Zoom in on the aromatic region of the ^{1}H NMR spectrum of the crude product extracted using conditions 2 (blue, bottom) compared to M_1 (red, middle) and $2N_3$ (green, top) in $CDCl_3$

Attempt 3

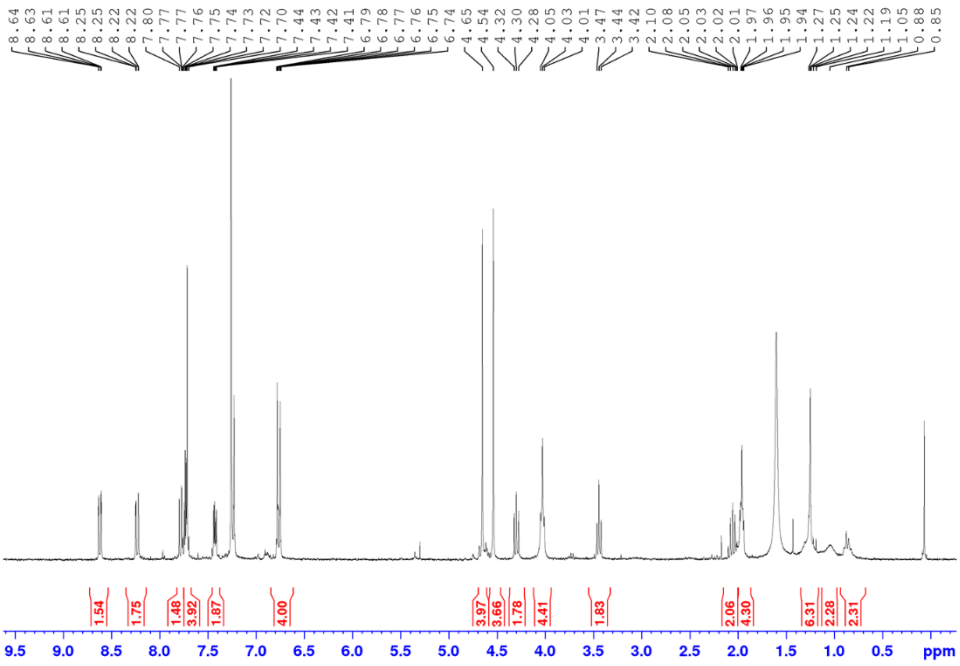

Figure S213. ^{1}H NMR spectrum obtained for the crude product extracted using conditions 3 in $CDCl_3$

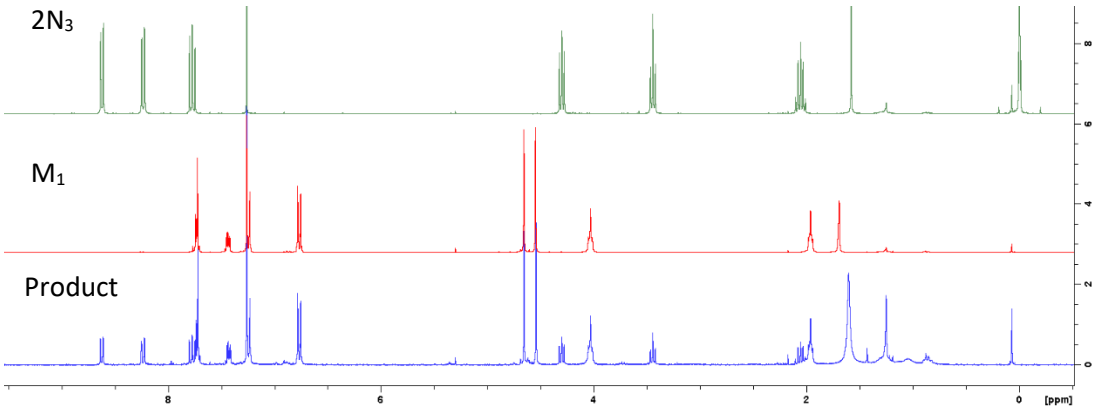

Figure S214. ^{1}H NMR spectrum of the crude product extracted using conditions 3 (blue, bottom) compared to M_1 (red, middle) and $2N_3$ (green, top) in $CDCl_3$

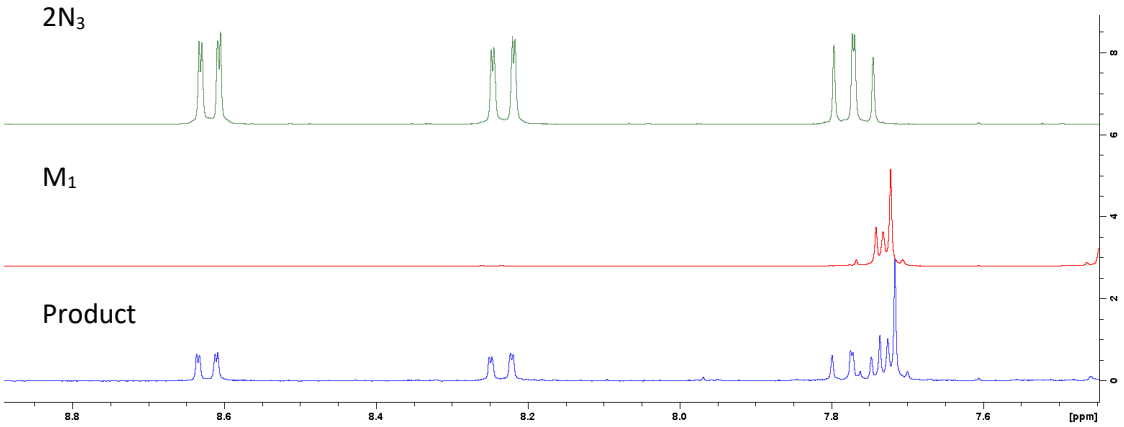

Figure S215. Zoom in on the aromatic region of the ^{1}H NMR spectrum of the crude product extracted using conditions 3 (blue, bottom) compared to M_1 (red, middle) and $2N_3$ (green, top) in $CDCl_3$

Combined ^{1}H NMR spectra of the products from conditions 1, 2 and 3

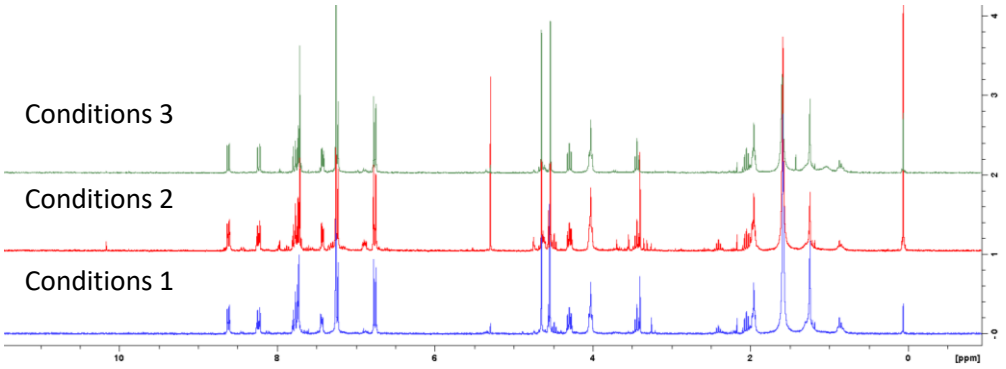

Figure S216. Overlayed ^{1}H NMR spectra of the products obtained from conditions 1 (blue, bottom), 2 (red, middle) and 3 (green, top) in $CDCl_3$

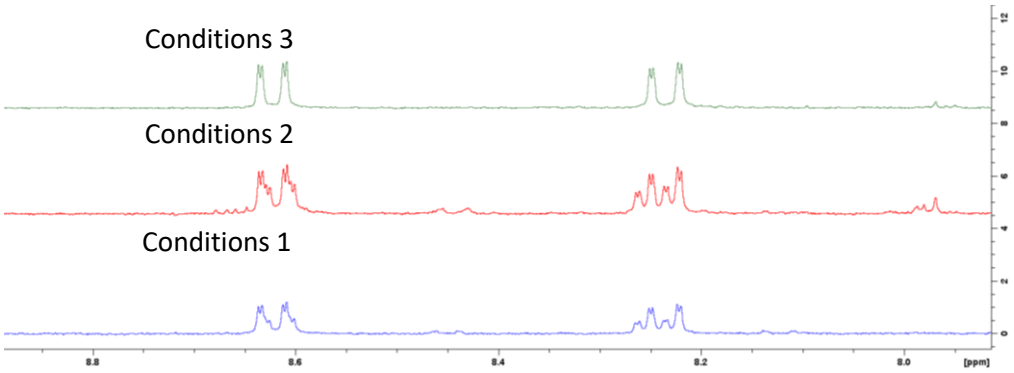

Figure S217. Overlayed ^{1}H NMR spectra of the products obtained from conditions 1 (blue, bottom), 2 (red, middle) and 3 (green, top) in $CDCl_3$ showing the presence of sub-peaks for the naphthalimide protons of conditions 1 and 2

Methyl-protected rotaxanes R_2 – R_4

Rotaxane R_2

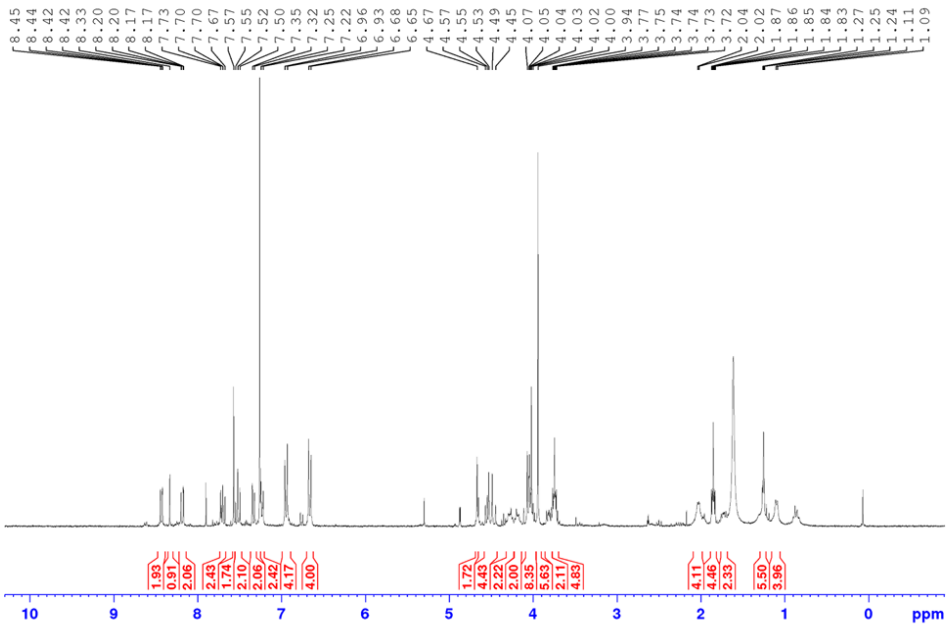

*Figure S218. Full ^{1}H NMR spectrum obtained for **R_2** in $CDCl_3$*

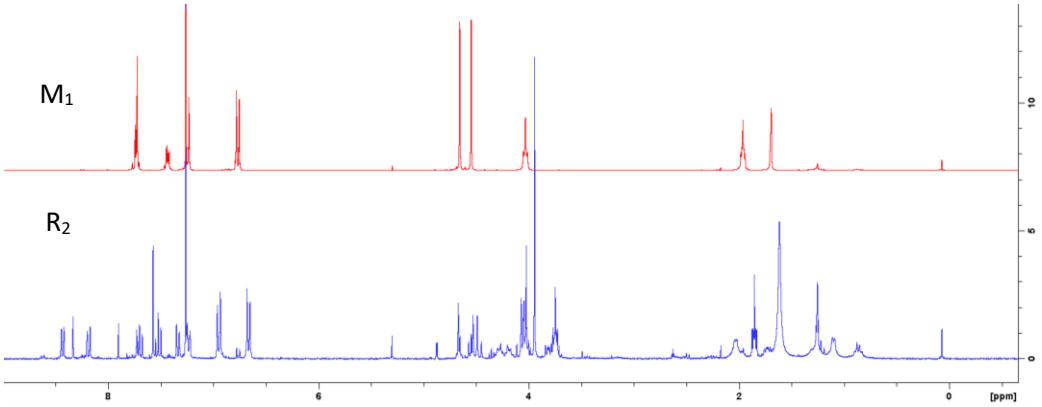

*Figure S219. ^{1}H NMR spectrum of **R_2** (blue, bottom) compared to **M_1** (red, top) in $CDCl_3$*

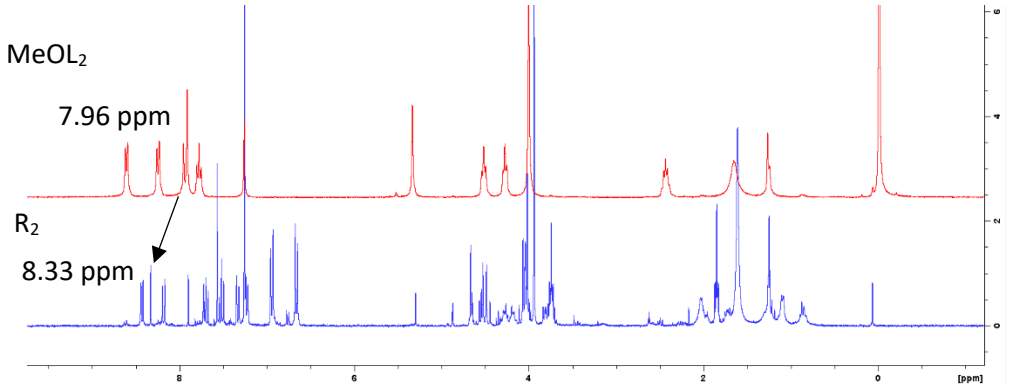

*Figure S220. ^{1}H NMR spectrum of **R_2** (blue, bottom) compared to **$MeOL_2$** (red, top) in $CDCl_3$ showing the downfield shifting of the triazole hydrogen in **R_2** relative to **$MeOL_2$** (free axel)*

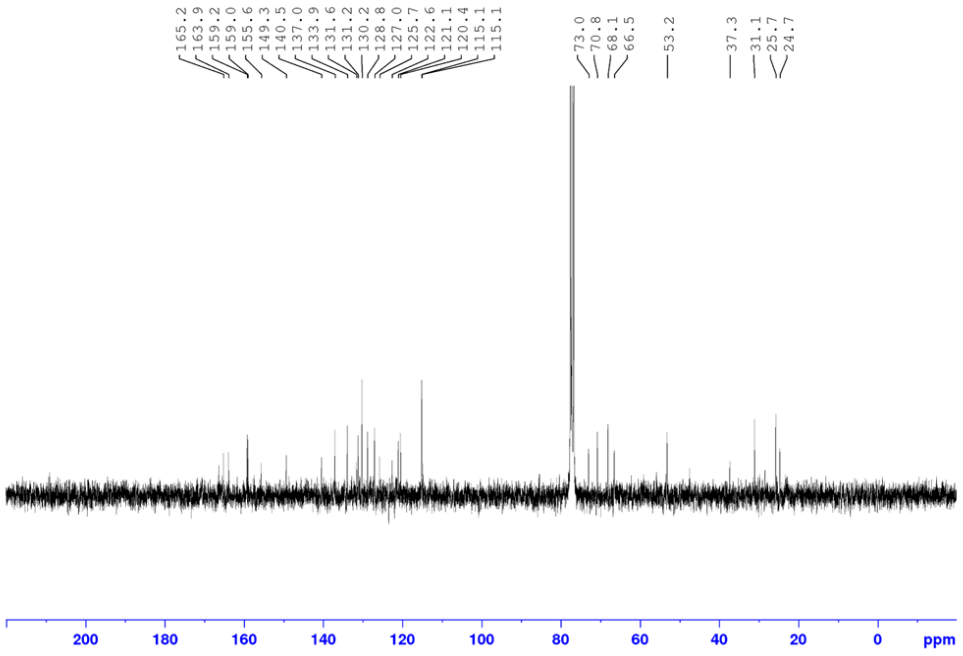

*Figure S221. ^{13}C NMR spectrum of **R₂** in $CDCl_3$*

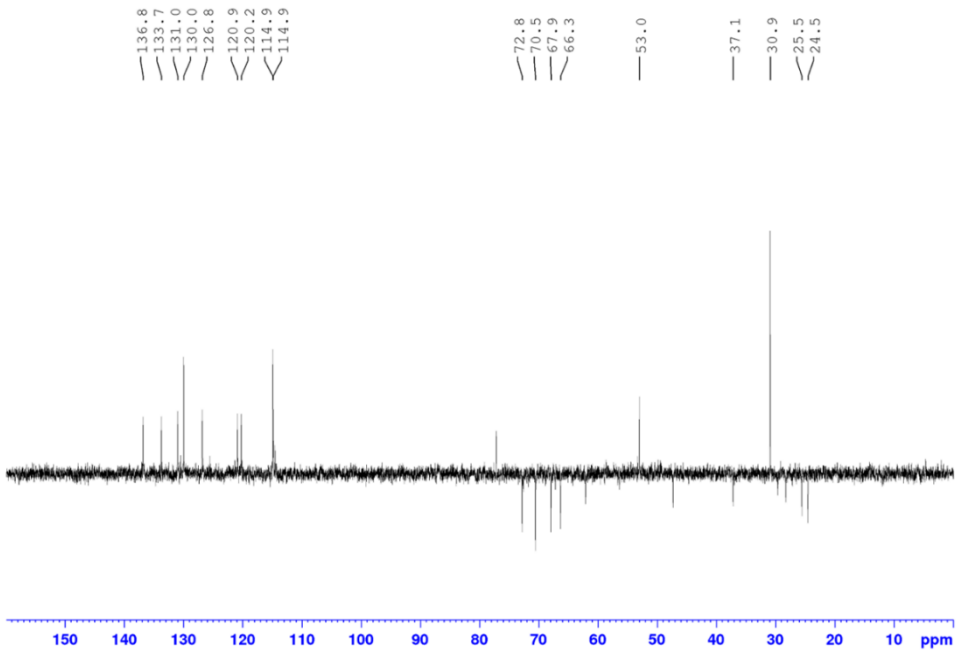

*Figure S222. ^{13}C DEPT spectrum of **R₂** in $CDCl_3$*

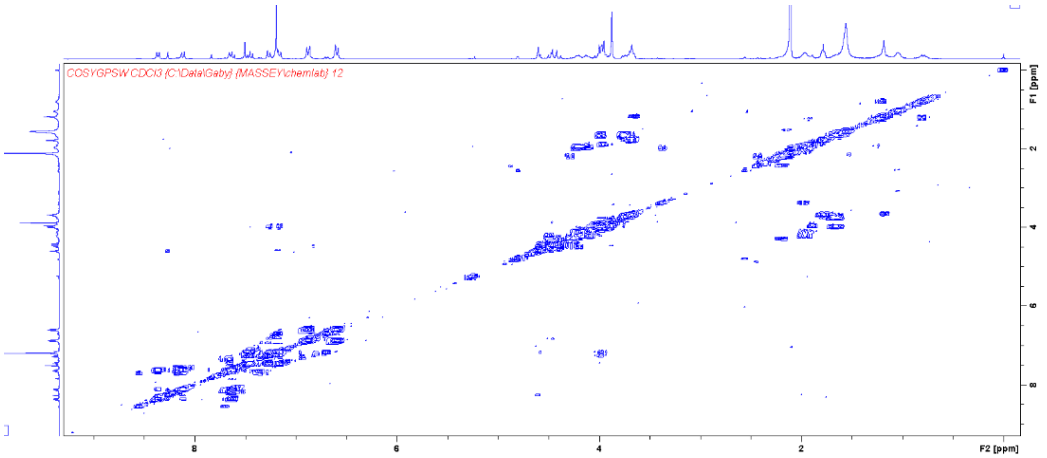

Figure S223. COSY spectrum obtained for ***R2*** *in* $CDCl_3$

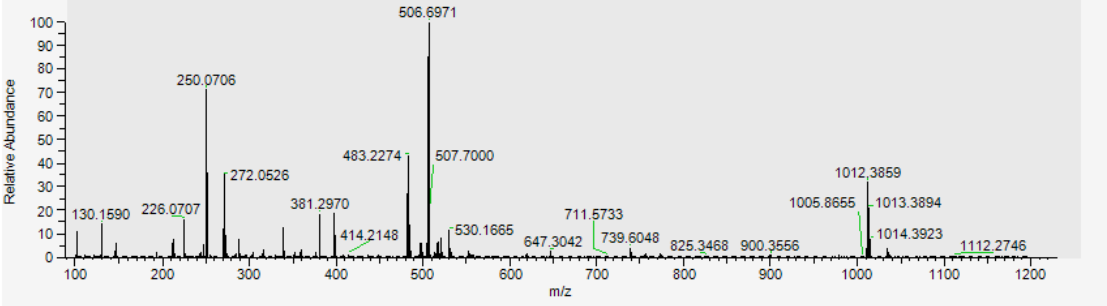

Figure S224. Full HRMS obtained for ***R2***

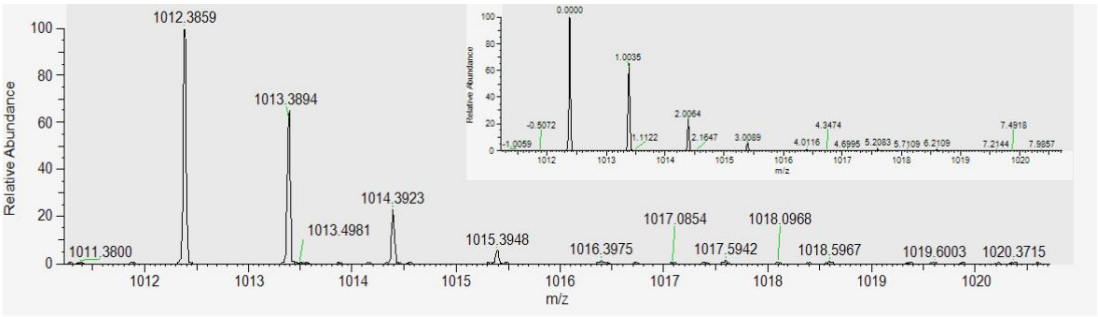

Figure S225. HRMS m/z = 1012.3859 [R_2 *+* H^+*]*$^+$ *(calc. for* $[C_{57}H_{54}N_7O_{11}]^+$*, 1012.3880 g* mol^{-1}*). (Insert) m/z labelled relative to the [*R_2 *+* H^+*]*$^+$ *peak confirming the +1 charge*

Rotaxane R_3

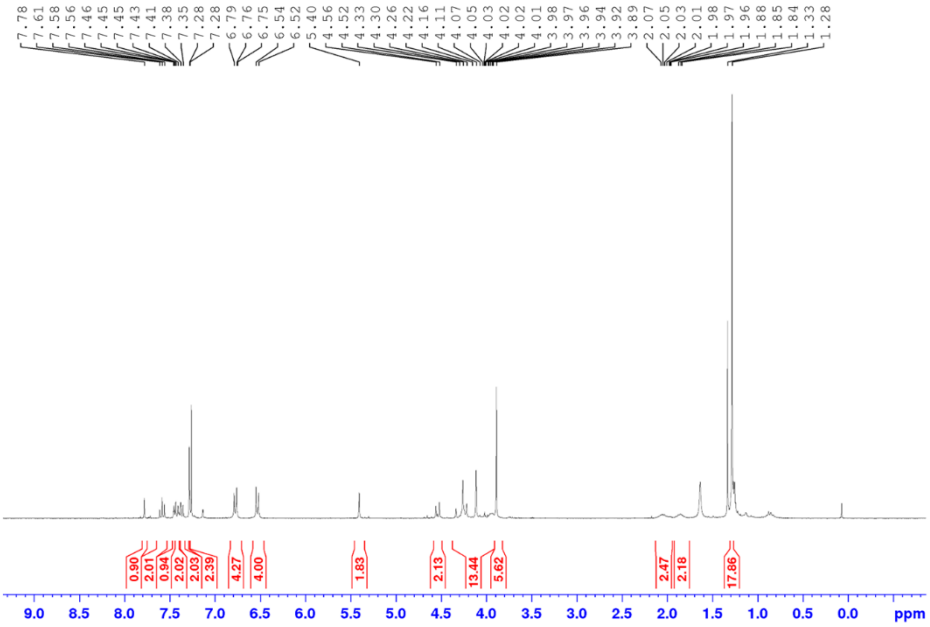

*Figure S226. Full ^{1}H NMR spectrum of **R_3** in $CDCl_3$*

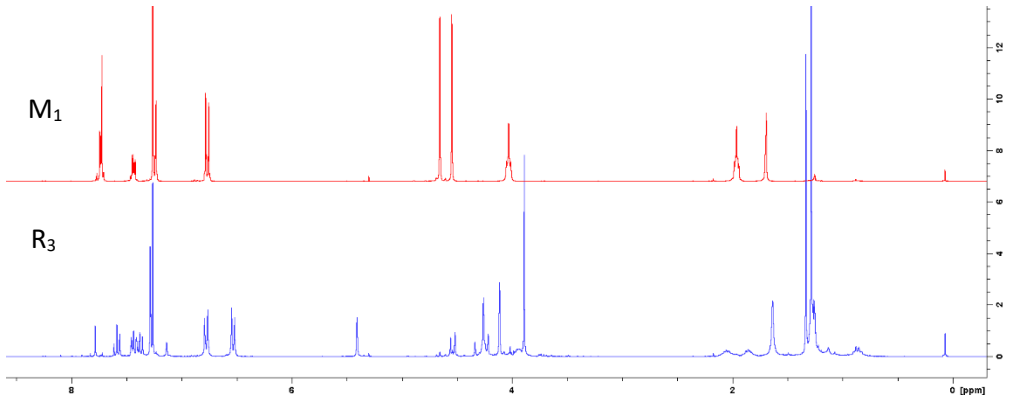

*Figure S227. ^{1}H NMR spectrum of **R_3** (blue, bottom) compared to **M_1** (red, top) in $CDCl_3$*

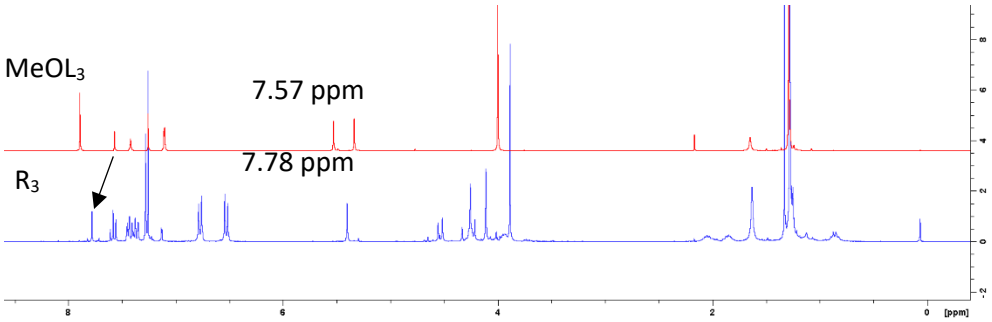

*Figure S228. ^{1}H NMR spectrum of **R_3** (blue, bottom) compared to **$MeOL_3$** (red, top) in $CDCl_3$ showing the downfield shifting of the triazole hydrogen in **R_3** relative to **$MeOL_3$** (free axel)*

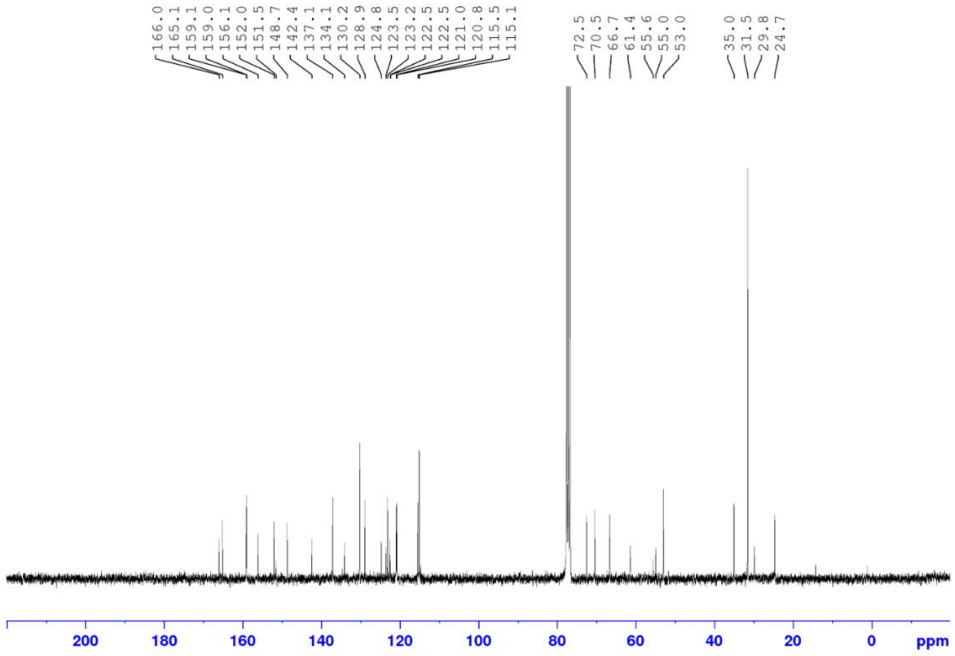

*Figure S229. ^{13}C NMR spectrum of **R₃** in $CDCl_3$*

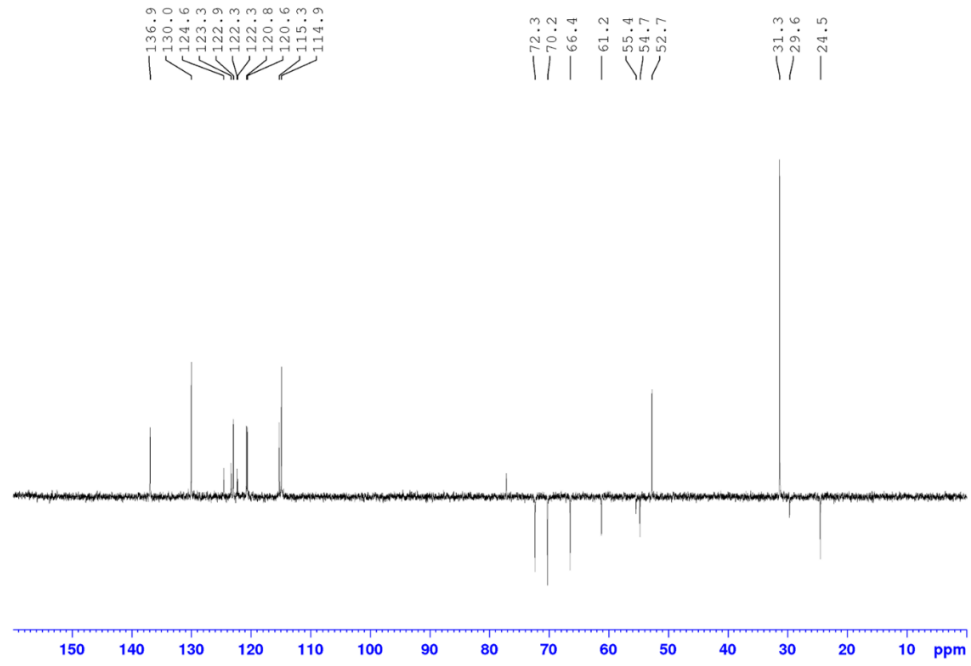

*Figure S230. ^{13}C DEPT spectrum of **R₃** in $CDCl_3$*

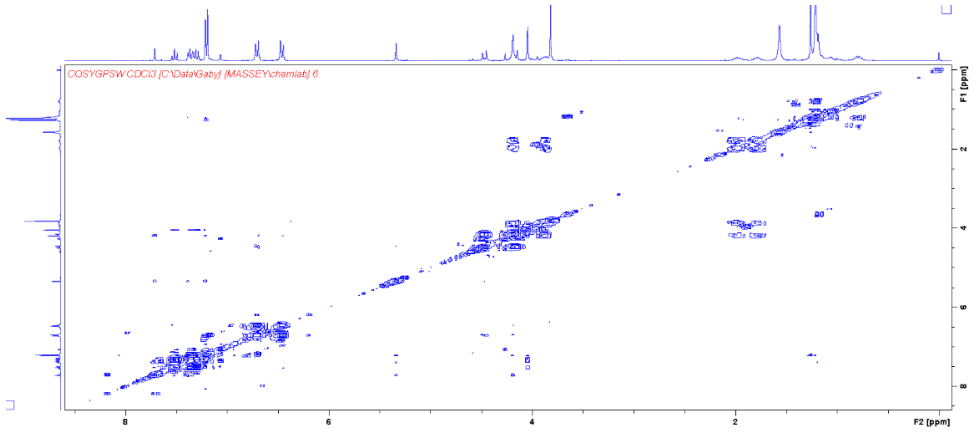

Figure S231. COSY spectrum of ***R₃*** *in $CDCl_3$*

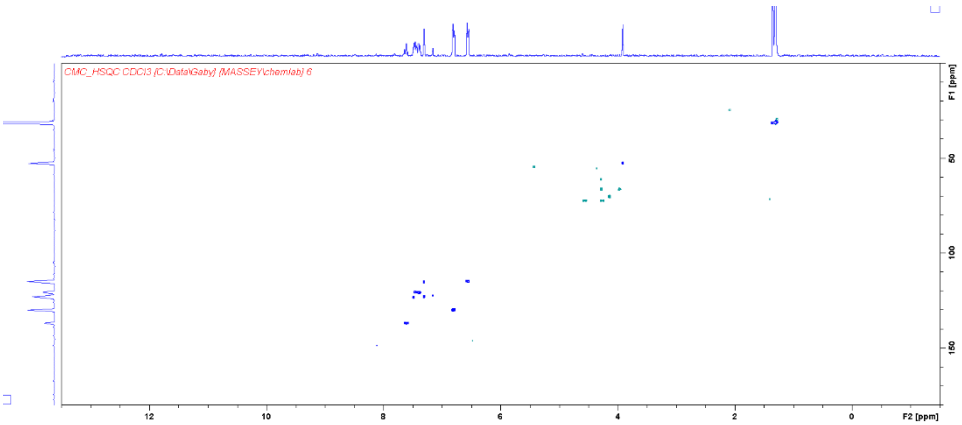

Figure S232. HSQC spectrum of ***R₃*** *in $CDCl_3$*

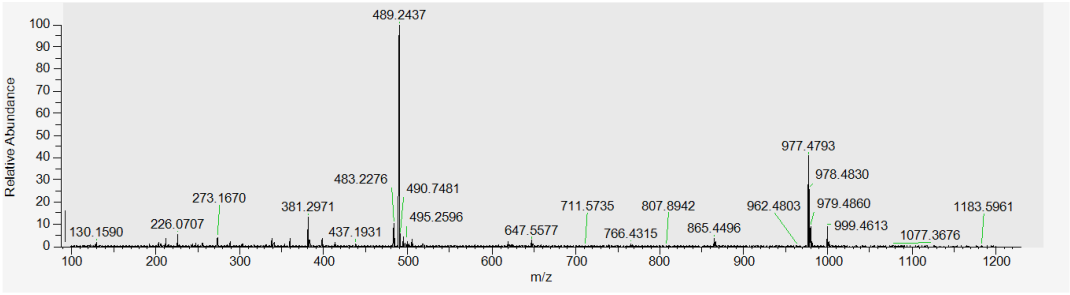

Figure S233. Full HRMS of ***R₃***

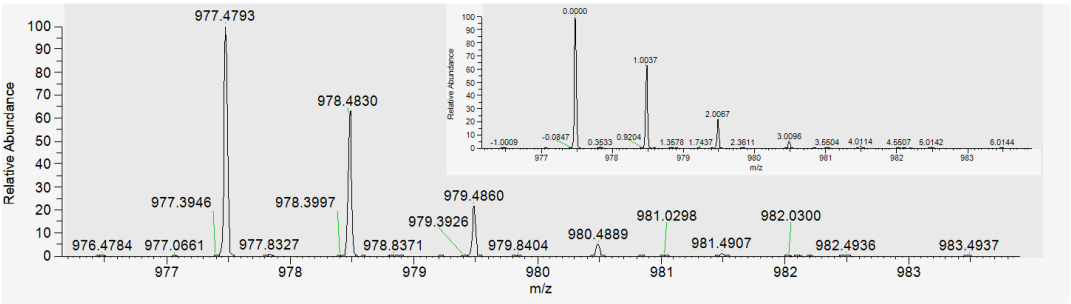

Figure S234. HRMS m/z = 977.4793 $[R_3 + H^+]^+$ (calc. for $[C_{57}H_{65}N_6O_9]^+$, 977.4813 g mol^{-1}). (Insert) m/z labelled relative to the $[R_3 + H^+]^+$ peak confirming the +1 charge

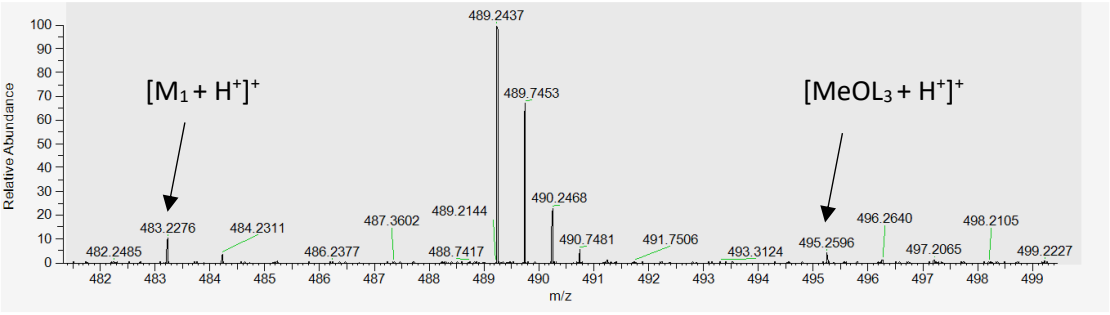

Figure S235. HRMS m/z = 483.2276 $[M_1 + H^+]^+$ (calc. for $[C_{30}H_{31}N_2O_4]^+$, 482.2284 g mol^{-1}) and m/z = 495.2596 $[MeOL_3 + H^+]$ (calc. for $[C_{27}H_{35}N_4O_5]^+$, 495.2607 g mol^{-1})

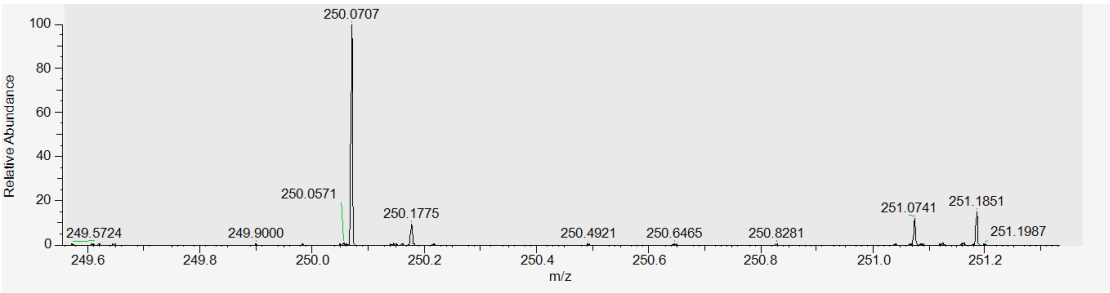

Figure S236. HRMS m/z = 250.0707 $[2 + H^+]^+$ (calc. for $[C_{12}H_{12}NO_5]^+$, 250.0715 g mol^{-1})

Rotaxane R_4

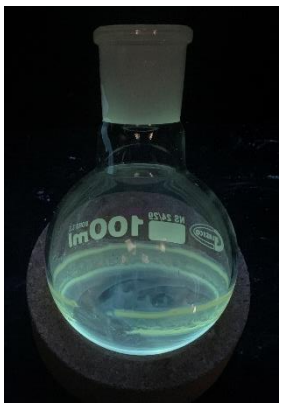

*Figure S237. Crude **R_4** under a long wave UV lamp*

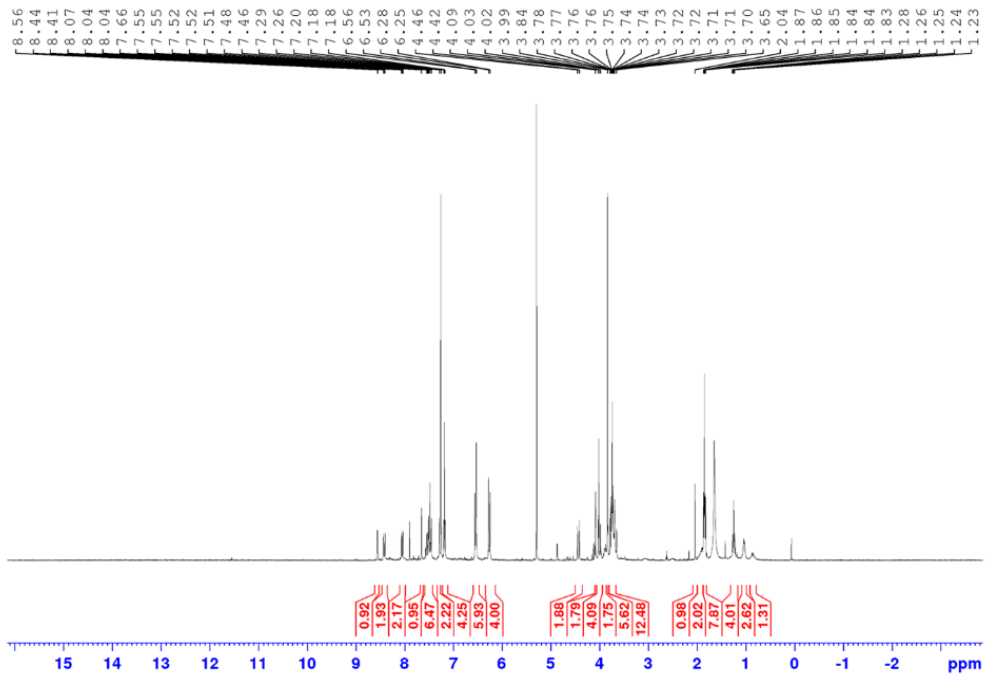

Figure S238. Full [1] H NMR spectrum of ***R₄*** *in $CDCl_3$*

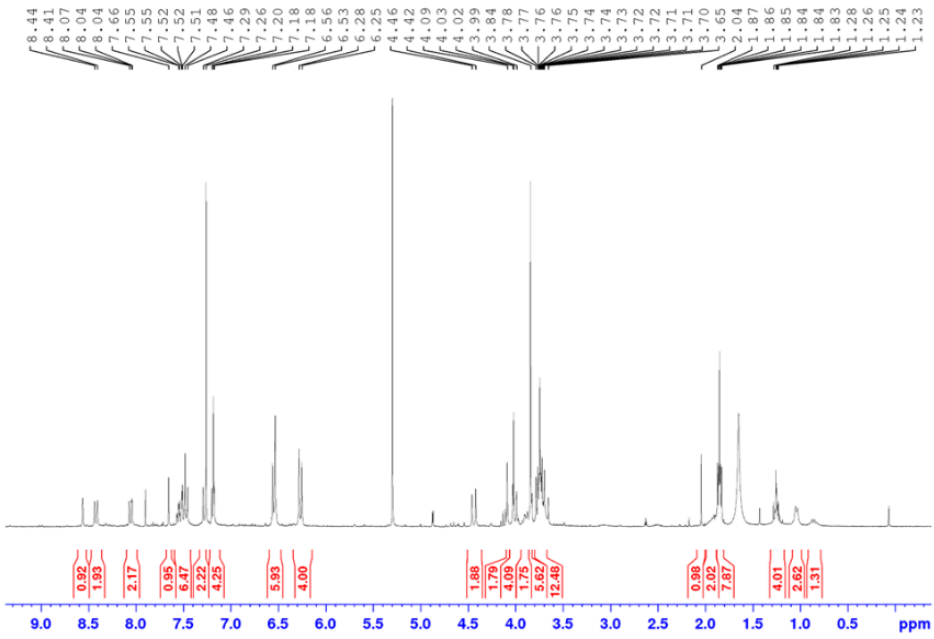

Figure S239. Zoomed in [1]H NMR spectrum of ***R₄*** *in $CDCl_3$*

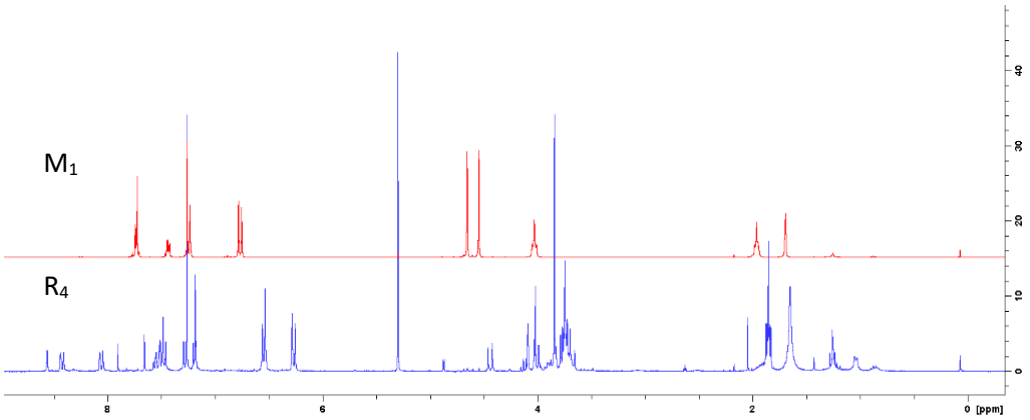

*Figure S240. ^{1}H NMR spectrum of **R4** (blue, bottom) compared to **M1** (red, top) in $CDCl_3$*

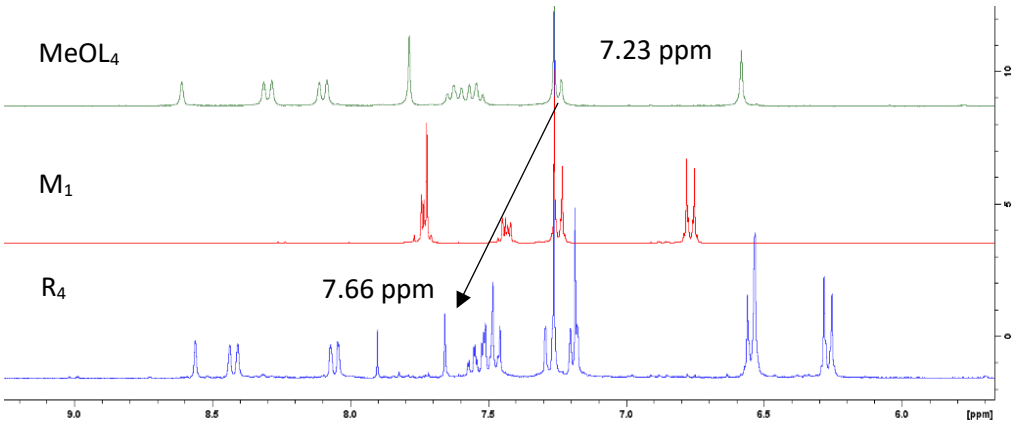

*Figure S241. ^{1}H NMR spectrum of **R4** (blue, bottom) compared to **M1** (red, middle) and **MeOL4** (green, top) in $CDCl_3$ showing the downfield shift of the triazole proton in **R4** compared to **MeOL4** (free axel)*

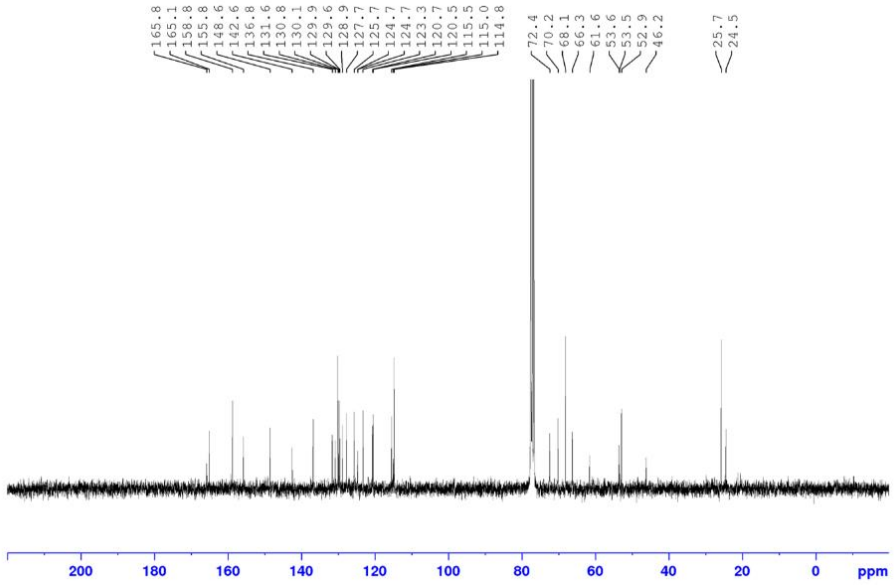

*Figure S242. ^{13}C NMR spectrum of **R4** in CDCl3*

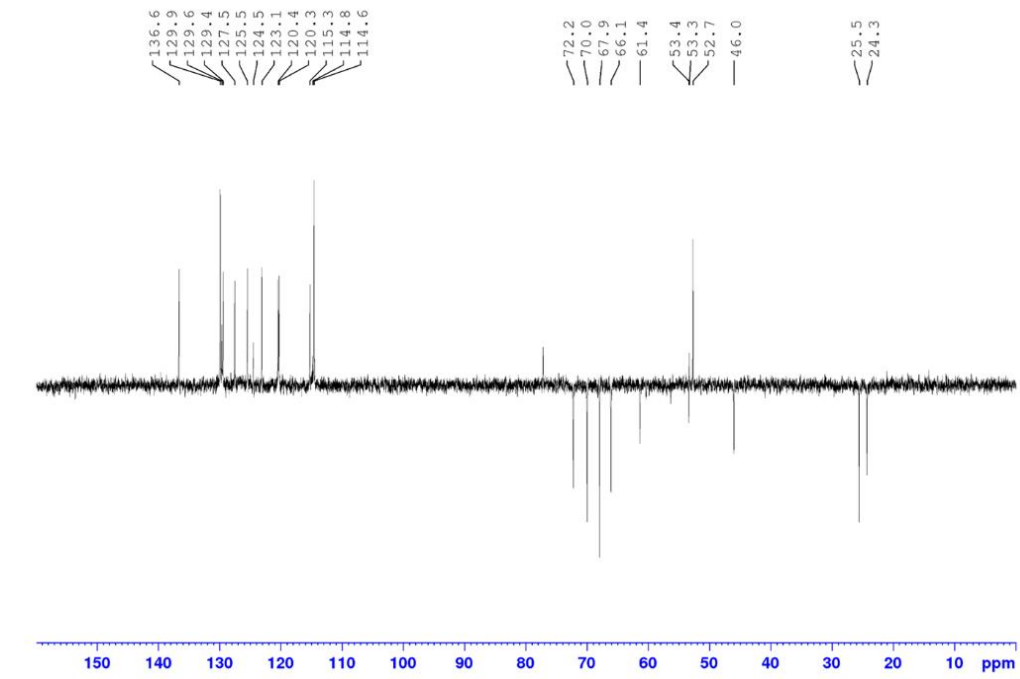

*Figure S243. ^{13}C DEPT spectrum of **R4** in $CDCl_3$*

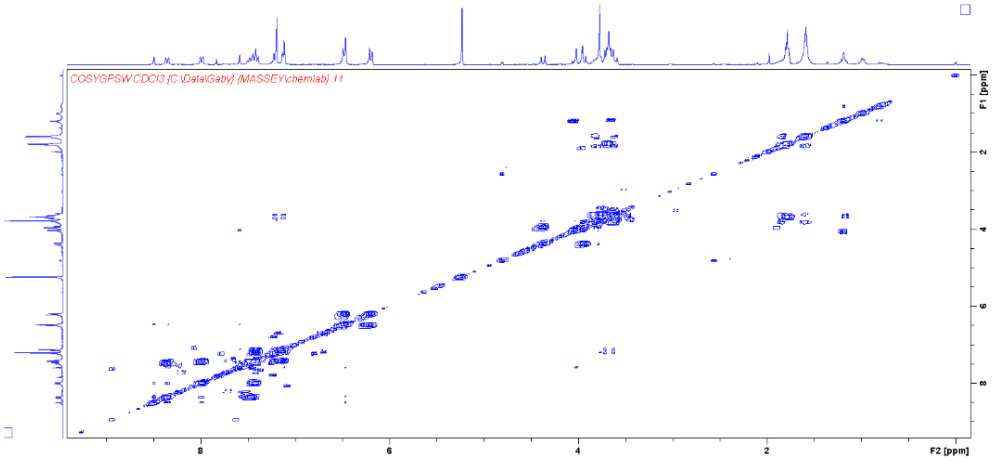

*Figure S244. COSY spectrum of **R4** in $CDCl_3$*

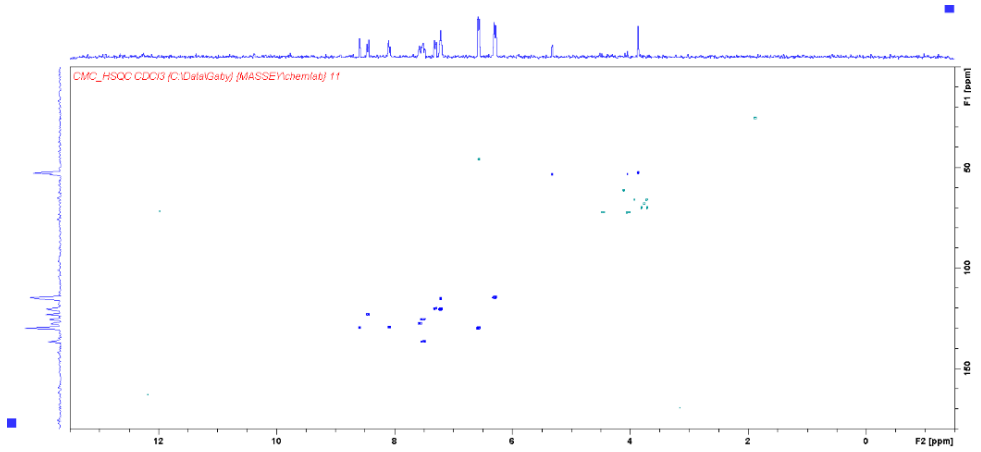

*Figure S245. HSQC spectrum of **R4** in $CDCl_3$*

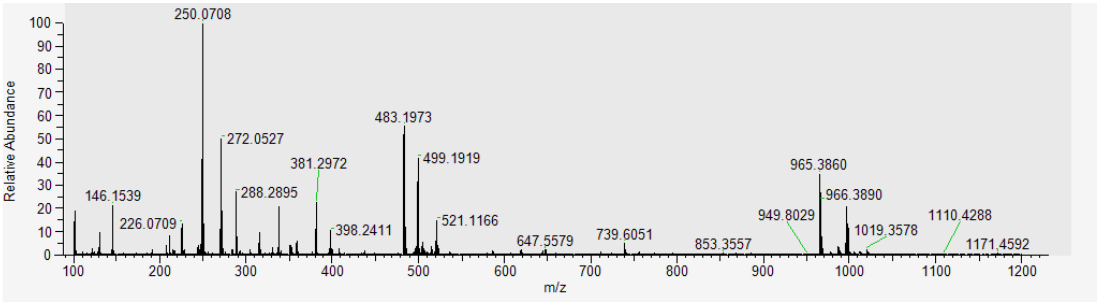

Figure S246. Full HRMS of ***R*****4**

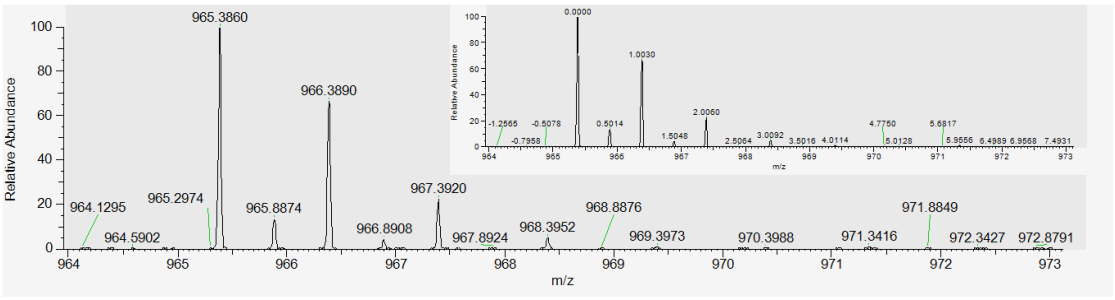

Figure S247. HRMS m/z = 965.3860 [R4 + H+]+ (calc. for [C57H53N6O9]+, 965.3874 g mol-1). (Insert) m/z labelled relative to the [R4 + H+]+ peak confirming the +1 charge

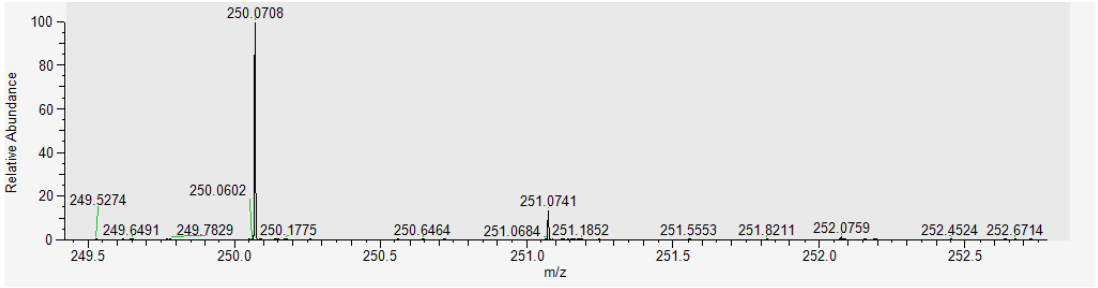

Figure S248. HRMS m/z = 250.0708 [2 + H+]+ (calc. for [C12H12NO5]+, 250.0715 g mol-1)

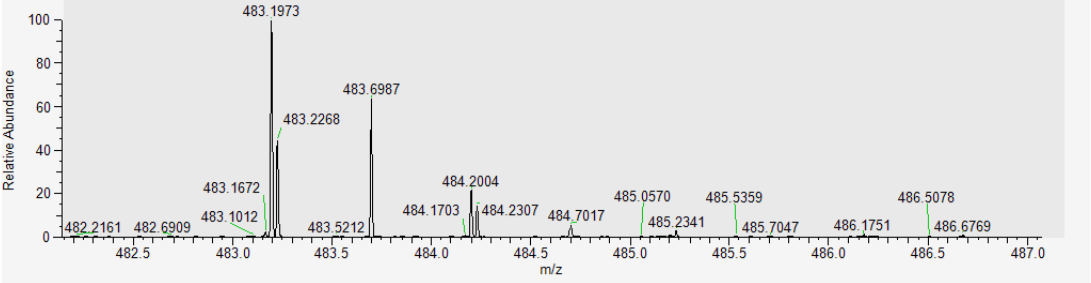

Figure S249. HRMS m/z = 483.1973 [M1 + H+]+ (calc. for [C30H31N2O4]+, 483.2284 g mol-1)

R_3 titrations

To investigate the ability of **R_3** to coordinate with Eu^{3+}, UV/Vis and fluorescence titrations were carried out. A solution of **R_3** dissolved in ACN (1 x 10^{-5} M) was made and to it was added aliquots of $Eu(CF_3SO_3)_3 \cdot 6H_2O$ from a 6.32 x 10^{-5} M solution (depending on the addition amount) in ACN from 0 → 3.37 equivalents. UV/Vis and fluorescence titrations were carried out in duplicate.

R_3 molar absorptivity

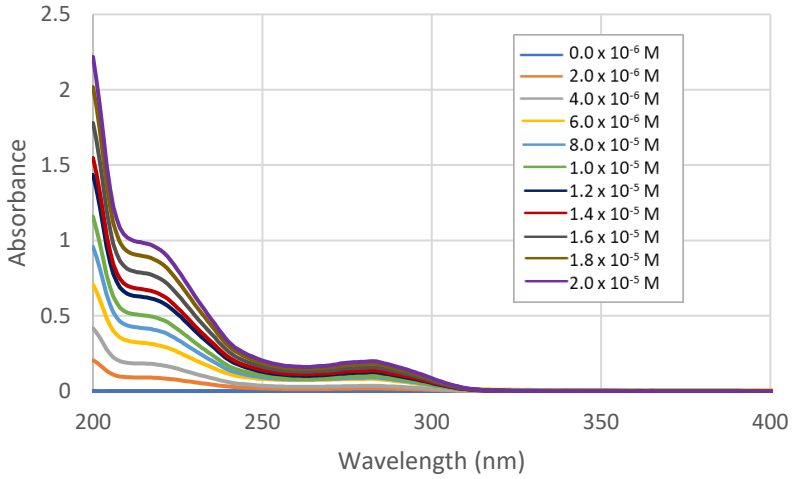

*Figure S250. Absorbance of **R_3** in ACN at increasing concentrations for molar absorptivity calculation*

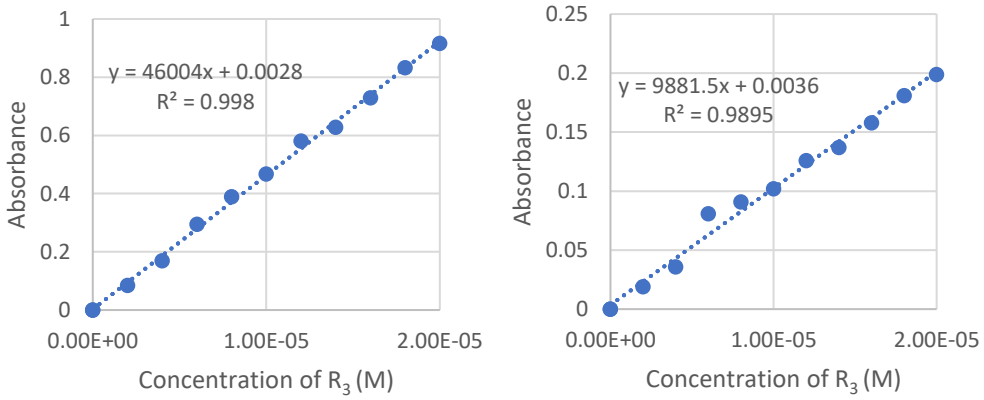

*Figure S251. (Left) Absorbance at 221 nm plotted as a function of **R_3** concentration in ACN. (Right) Absorbance at 283 nm plotted as a function of **R_3** concentration in ACN*

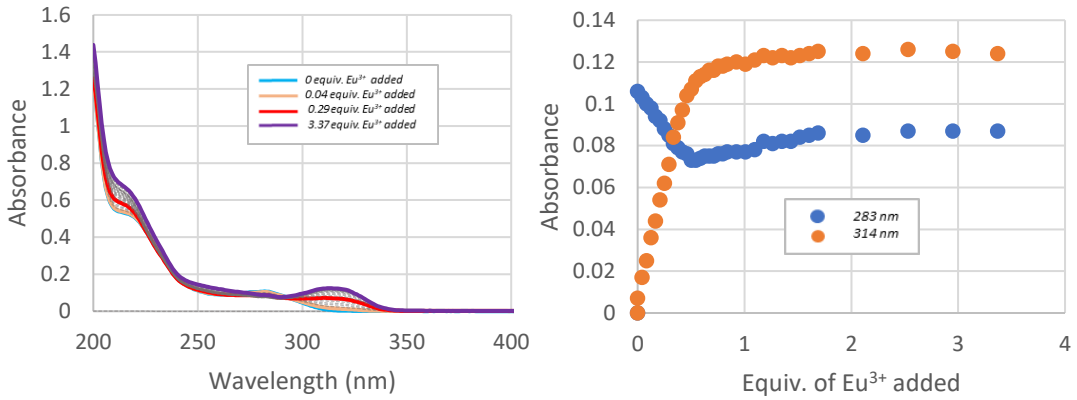

Figure S252. (Left) UV/Vis titration of $\mathbf{R_3}$ *(1 x* 10^{-5} *in ACN) on the stepwise addition of* $Eu(CF_3SO_3)_3 \cdot 6H_2O$ *from 0 → 3.37 equivalents: Run 1. (Right) Plot showing the changes in absorbance values of* $\mathbf{R_3}$ *at 283 nm (blue dots) and 314 nm (orange dots) as a function of equivalents of* Eu^{3+} *added: Run 1.*

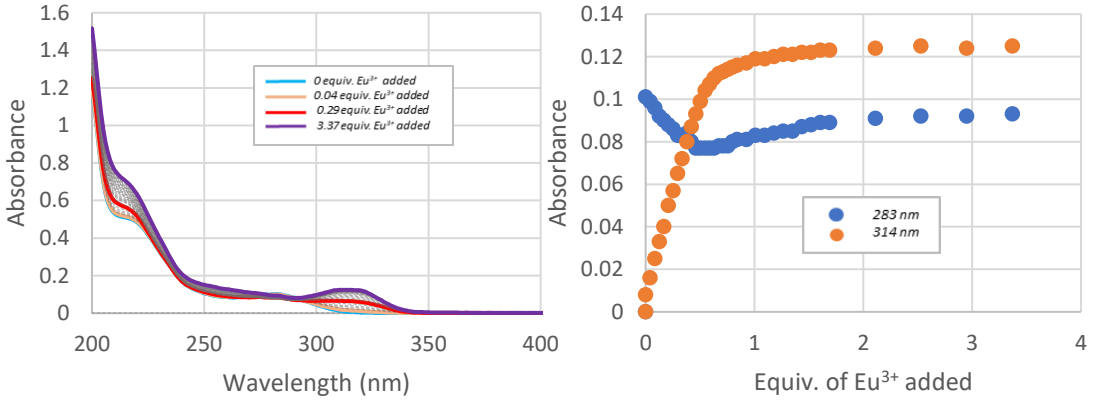

Figure S253. (Left) UV/Vis titration of $\mathbf{R_3}$ *(1 x* 10^{-5} *in ACN) on the stepwise addition of* $Eu(CF_3SO_3)_3 \cdot 6H_2O$ *from 0 → 3.37 equivalents: Run 2. (Right) Plot showing the changes in absorbance values of* $\mathbf{R_3}$ *at 283 nm (blue dots) and 314 nm (orange dots) as a function of equivalents of* Eu^{3+} *added: Run 2.*

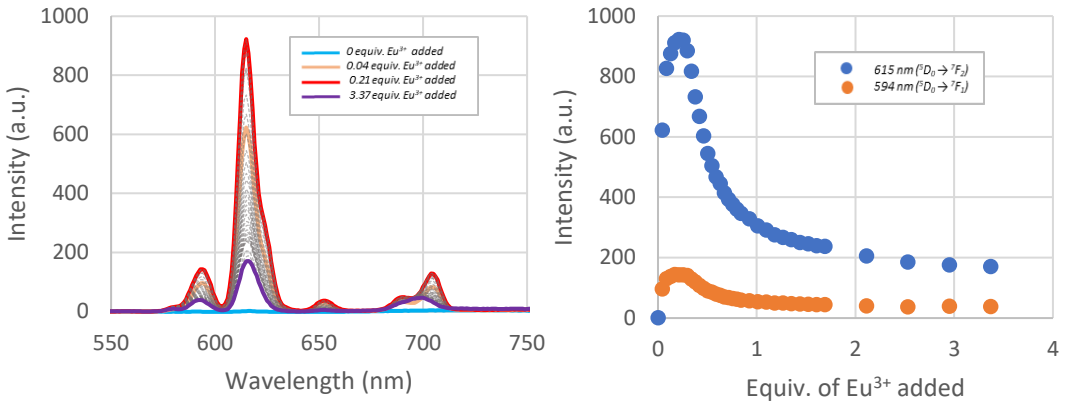

Figure S254. (Left) Fluorescence titration of ***R*****$_3$** *(1 x 10^{-5} M) with Eu(CF$_3$SO$_3$)$_3$·6H$_2$O on excitation at 283 nm: Run 1. (Right) Plot showing the changes in the emission at 615 nm (blue dots) and 594 nm (orange dots) as a function of equivalents of Eu^{3+} added on excitation at 283 nm: Run 1*

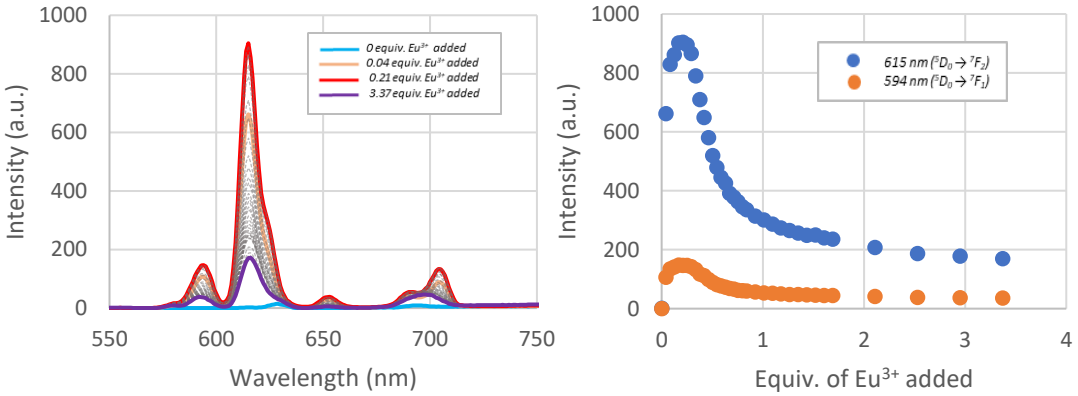

Figure S255. (Left) Fluorescence titration of ***R*****$_3$** *(1 x 10^{-5} M) with Eu(CF$_3$SO$_3$)$_3$·6H$_2$O on excitation at 314 nm: Run 1. (Right) Plot showing the changes in the emission at 615 nm (blue dots) and 594 nm (orange dots) as a function of equivalents of Eu^{3+} added on excitation at 314 nm: Run 1*

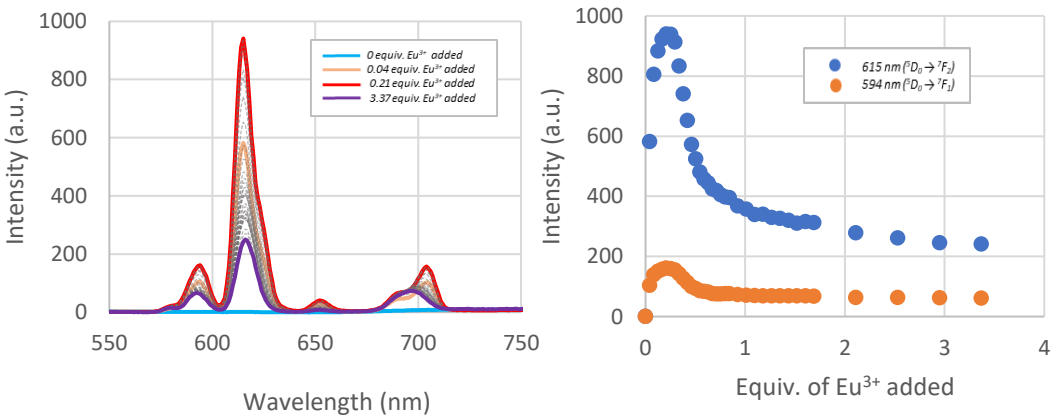

Figure S256. (Left) Fluorescence titration of ***R*****$_3$** *(1 x 10^{-5} M) with Eu(CF$_3$SO$_3$)$_3$·6H$_2$O on excitation at 283 nm: Run 2. (Right) Plot showing the changes in the emission at 615 nm (blue dots) and 594 nm (orange dots) as a function of equivalents of Eu^{3+} added on excitation at 283 nm: Run 2*

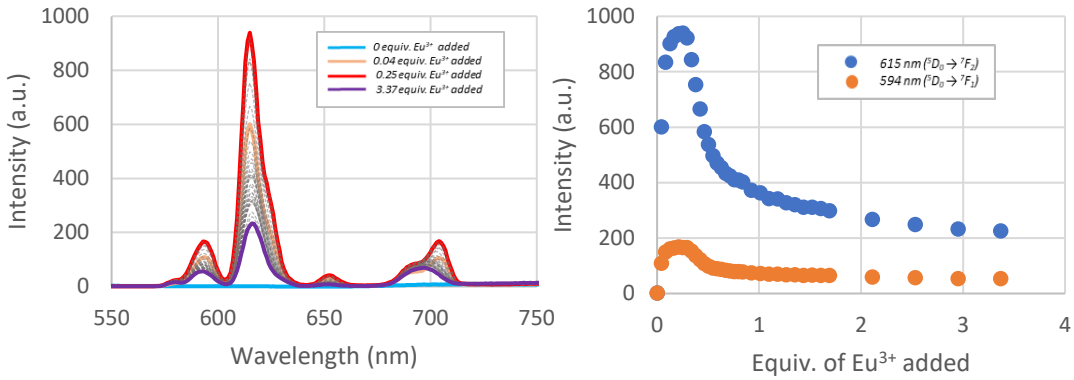

Figure S257. Fluorescence titration of ***R*****$_3$** *(1 x 10^{-5} M) with Eu(CF$_3$SO$_3$)$_3$·6H$_2$O on excitation at 314 nm: Run 2. (Right) Plot showing the changes in the emission at 615 nm (blue dots) and 594 nm (orange dots) as a function of equivalents of Eu^{3+} added on excitation at 314 nm: Run 2*

Amide-protected rotaxanes R$_{2A}$ – R$_{4A}$

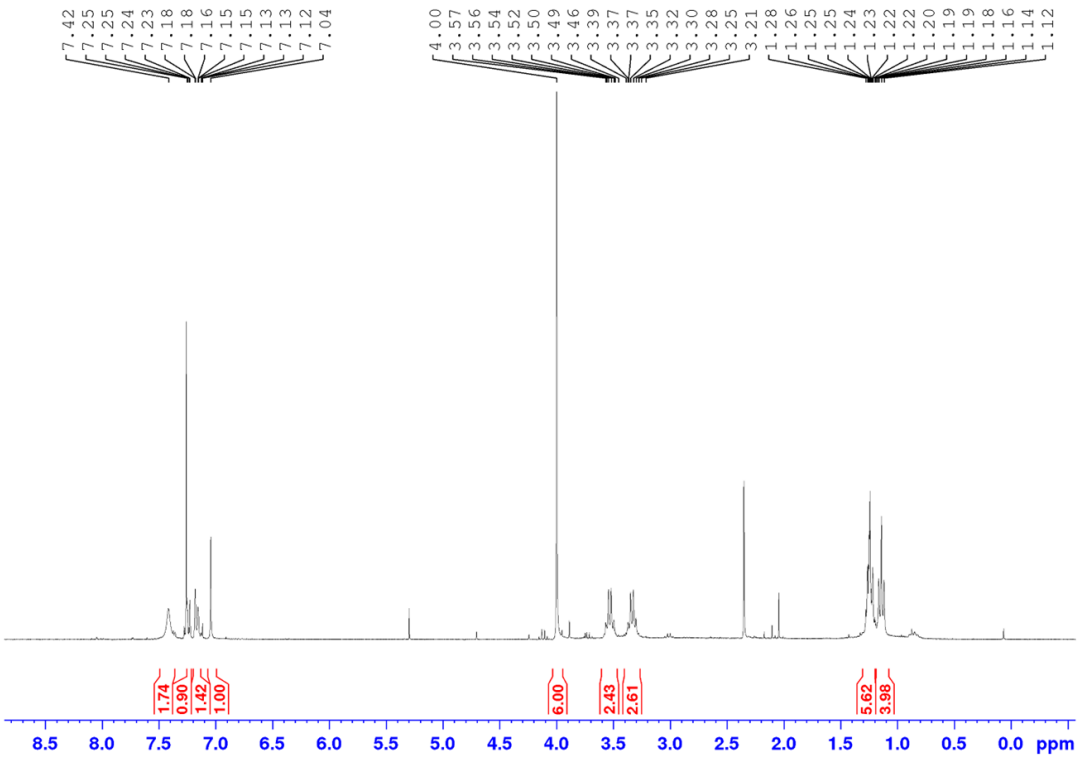

Figure S258. ^{1}H NMR spectrum obtained in CDCl$_3$ for the crude product obtained using method A

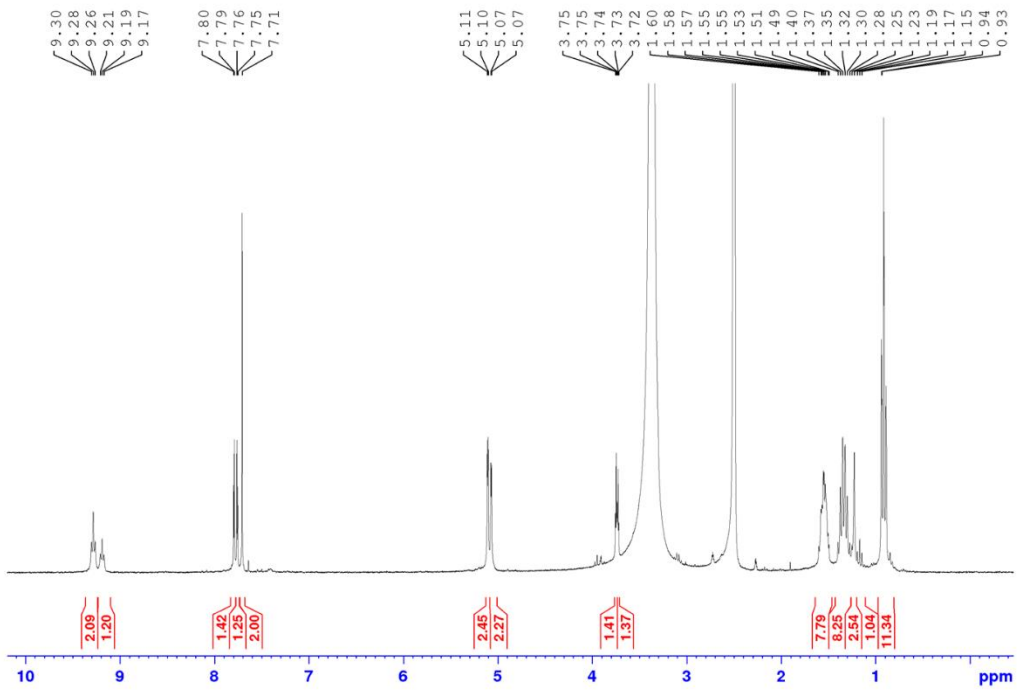

Figure S259. ^{1}H NMR spectrum obtained in DMSO-d_6 for the crude product obtained using method B

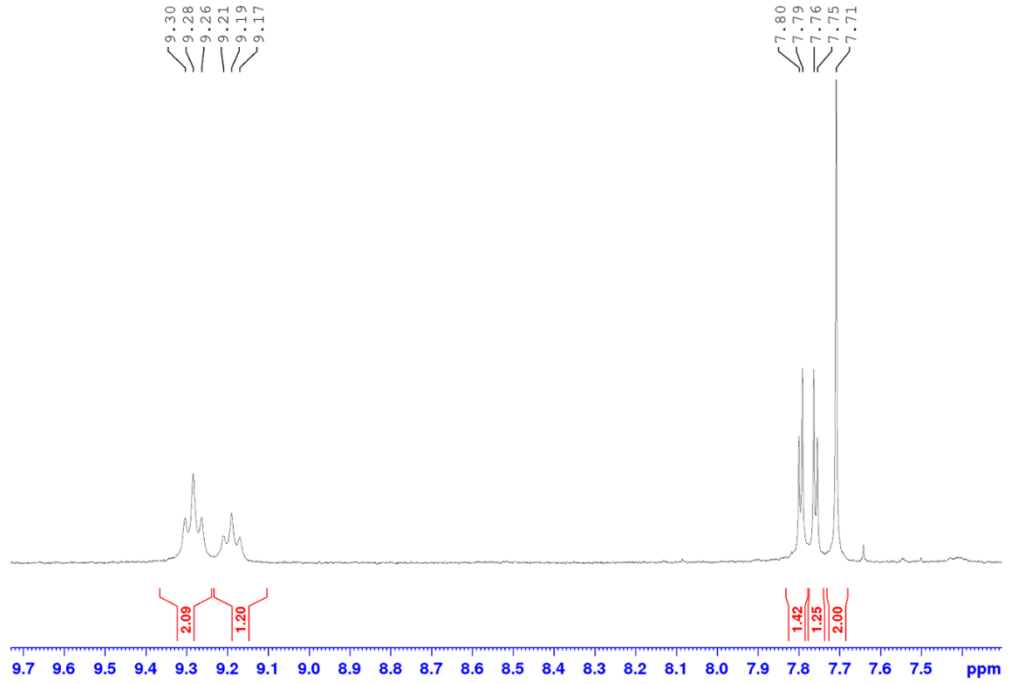

Figure S260. Zoom in on the ^{1}H NMR spectrum obtained in DMSO-d_6 for the crude product obtained using method B showing the amide and pyridyl splitting indicating the presence of $2_{A\text{-}mono}$ and $2_{A\text{-}bis}$

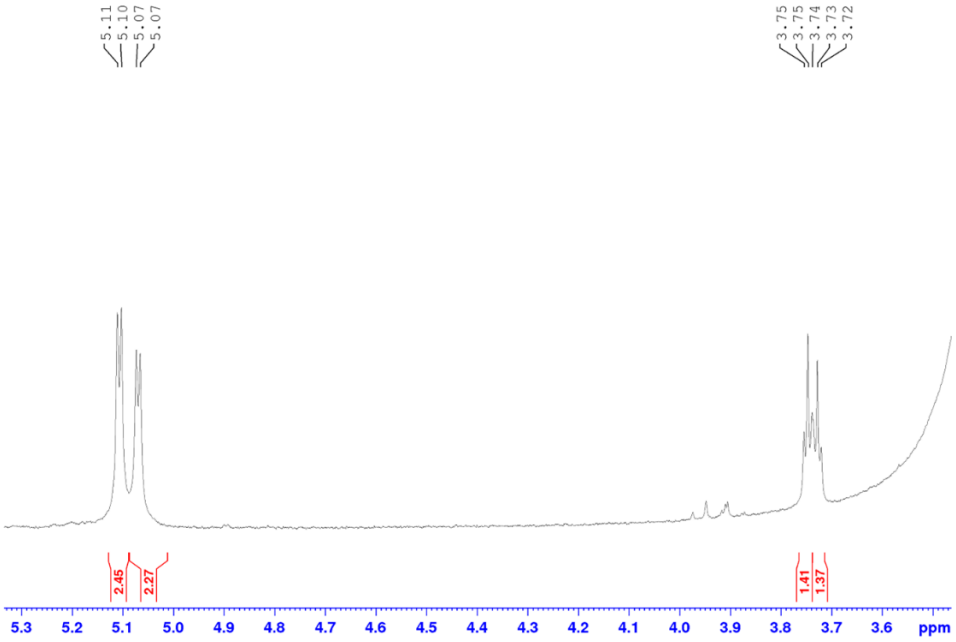

Figure S261. Zoom in on the ^{1}H NMR spectrum obtained in DMSO-d_6 for the crude product obtained using method B showing the CH_2 and alkyne splitting indicating the presence of $2_{A\text{-}mono}$ and $2_{A\text{-}bis}$